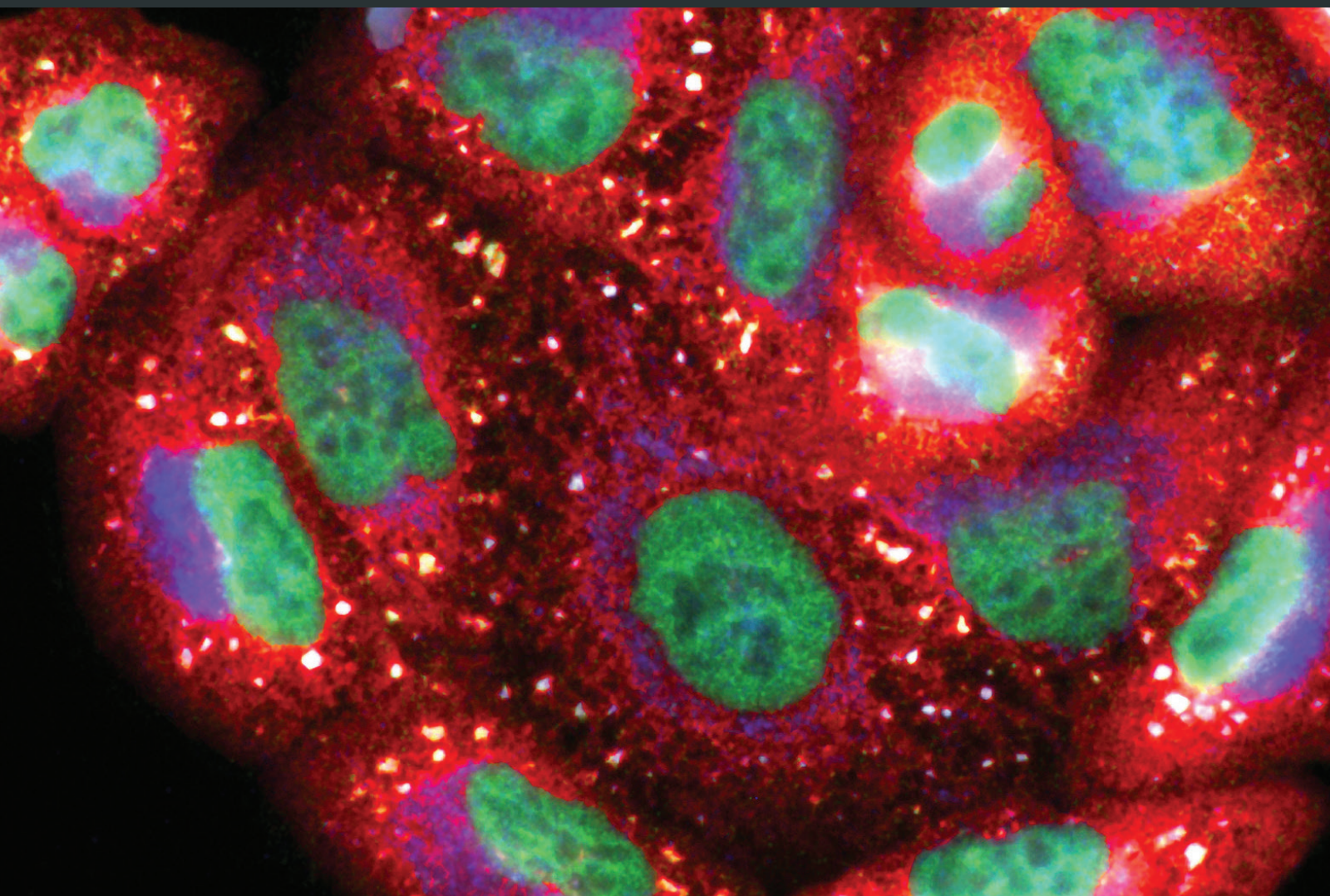# Role of Natural Compounds in Oxidative Stress and Inflammation Linked to Cardiometabolic Disorders: From Biochemical Aspects to Clinical Evidences

Lead Guest Editor: Cristiana Caliceti
Guest Editors: Paola Rizzo and Mariateresa Giuliano

Role of Natural Compounds in Oxidative Stress and Inflammation Linked to Cardiometabolic Disorders: From Biochemical Aspects to Clinical Evidences

Role of Natural Compounds in Oxidative Stress and Inflammation Linked to Cardiometabolic Disorders: From Biochemical Aspects to Clinical Evidences

Lead Guest Editor: Cristiana Caliceti
Guest Editors: Paola Rizzo and Mariateresa Giuliano

Editorial Board

Contents

Editorial

Role of Natural Compounds in Oxidative Stress and Inflammation Linked to Cardiometabolic Disorders: From Biochemical Aspects to Clinical Evidences

Cristiana Caliceti [D],[1] **Paola Rizzo,**[2] **and Mariateresa Giuliano**[3]

[1]*University of Bologna, Bologna, Italy*
[2]*University of Ferrara and GVM Care & Research, Maria Cecilia Hospital, Cotignola, Italy*
[3]*University of Campania, Caserta, Italy*

Correspondence should be addressed to Cristiana Caliceti; cristiana.caliceti@unibo.it

The most cost-effective preventive approach still remains diet and physical activity, also in people without a history of cardiovascular disease. However, lifestyle programs are often difficult to follow for long periods of time, and changes in dietary habits and physical activity sometimes are not enough to reduce risk parameters, such as hypercholesterolemia. In this context, an everyday approach utilizing dietary supplements, nutraceuticals, phytochemicals, and functional foods could improve blood lipid profile in humans and protect cells from oxidative stress and from damage related to inflammatory conditions. Since the prevention of cardiometabolic disorders is a fundamental strategy to decrease hospitalization and the health apparatus costs, a nutraceutical treatment could be, at least in part, a possible weapon to use. In this context, the scientific community has to adequately define the tolerability and safety of dietary supplements, either nutraceuticals or botanicals, as well as understand the precise mechanisms of actions and the risk/benefit ratio related to their assumption.

This special issue offers a selected and articulated overview of the examined topics. It contains seven papers, and the details were listed as follows:

J.-F. Feng et al. explored the therapeutic mechanism of *Dioscorea nipponica* (DN), a medicinal plant used to treat myocardial ischemia (MI), identifying the metabolites generated by intestinal microflora from DN and their cardioprotective efficacy. Results demonstrated that diosgenin, the main metabolite produced by rat intestinal microflora from DN, protects the myocardium against ischemic insult through increasing enzymatic and nonenzymatic antioxidant levels in vivo and by decreasing oxidative stress damage.

J. Tian et al. reviewed the use of herbal medicines for diabetes treatment, to prevent cardiovascular complications. Molecules and signal transduction pathways were critically analyzed, and specific effects of several compounds were highlighted.

Novel pharmacological targets have been investigated by Z. Wang et al. Original data indicated that TRPA1 might be an alternative pharmacological target to mitigate the detrimental cardiac effects induced by doxorubicin. Using an animal model, they demonstrated that blockage of TRPA1 can prevent cardiomyocyte apoptosis, reducing inflammation and oxidative and ER stress.

J. Tian et al. showed that *Ginkgo biloba* leaf extract (GBE) significantly attenuated cardiomyocyte apoptosis, collagen deposition, and inflammation in diabetic mice via inhibition of the p-JNK, CHOP, and caspase-12 pathways, as well as decreasing the serum levels of the proinflammatory cytokines (IL-6, IL-1β, and TNF-α). Blood glucose and lipid profiles were also regulated. These results suggested that GBE might be beneficial in the treatment of diabetic myocardial injury.

K.-H. Cho et al. studied policosanol with in vitro, in vivo (in female subjects), and ex vivo experiments to provide more substantial and concrete data on blood

pressure-lowering effect. They showed that consumption of policosanol for 8 weeks in healthy female subjects lowered blood pressure and CETP activity via elevation of HDL/ apoA-I contents and enhancement of HDL functionalities, including cholesterol efflux and insulin secretion, thus contributing to the prevention of aging-related diseases, hypertension, and stroke.

V. Valli et al. evaluated the changes in the expression of adipogenic markers (C/EBPα, PPARγ variant 1 and variant 2, and GLUT4) in 3T3-L1 murine preadipocytes at four stages of the differentiation process and compared the effectiveness of sulforaphane, genistein, and docosahexaenoic acid in reducing lipid accumulation and modulating C/EBPα, PPARγ1, PPARγ2, and GLUT4 mRNA expression in mature adipocytes, showing that all bioactive compounds suppress adipocyte differentiation. Since obesity is characterized by excess body fat accumulation due to an increase in size and number of differentiated mature adipocytes, these results confirmed that several natural food constituents could be used as important agents in preventing or treating obesity.

N. Calabriso et al. exploited the role of hydroxytyrosol (HT), a well-known olive oil antioxidant on mitochondrial oxidative stress in phorbol myristate acetate- (PMA-) challenged endothelial cells. They observed that HT blunts endothelial dysfunction and pathological angiogenesis by ameliorating mitochondrial function, thus suggesting HT as a potential mitochondria-targeting antioxidant in the inflamed endothelium. The guest editors hope that the information provided in this special issue is useful and offers a scientific profile of the effects of some dietary supplements, nutraceuticals, and phytochemicals on cardiovascular diseases linked to oxidative stress and inflammation.

Finally, we would like to thank the authors for an excellent contribution of their research works, and we also very warmly acknowledged the reviewers for an excellent contribution of their valuable review results.

Cristiana Caliceti
Paola Rizzo
Mariateresa Giuliano

Research Article

Hydroxytyrosol Ameliorates Endothelial Function under Inflammatory Conditions by Preventing Mitochondrial Dysfunction

Nadia Calabriso ⓘ,[1] **Antonio Gnoni** ⓘ,[2] **Eleonora Stanca** ⓘ,[3] **Alessandro Cavallo** ⓘ,[3] **Fabrizio Damiano** ⓘ,[3] **Luisa Siculella** ⓘ,[3] and **Maria Annunziata Carluccio** ⓘ[1]

[1]*National Research Council-Institute of Clinical Physiology, Lecce, Italy*
[2]*Department of Basic Medical Sciences, Neurosciences and Sense Organs, University of Bari "Aldo Moro", Bari, Italy*
[3]*Laboratory of Biochemistry and Molecular Biology, Department of Biological and Environmental Sciences and Technologies,*
University of Salento, Lecce, Italy

Correspondence should be addressed to Luisa Siculella; luisa.siculella@unisalento.it
and Maria Annunziata Carluccio; maria.carluccio@ifc.cnr.it

Mitochondria are fundamental organelles producing energy and reactive oxygen species (ROS); their impaired functions play a key role in endothelial dysfunction. Hydroxytyrosol (HT), a well-known olive oil antioxidant, exerts health benefits against vascular diseases by improving endothelial function. However, the HT role in mitochondrial oxidative stress in endothelial dysfunction is not clear yet. To investigate the HT effects on mitochondrial ROS production in the inflamed endothelium, we used an *in vitro* model of endothelial dysfunction represented by cultured endothelial cells, challenged with phorbol myristate acetate (PMA), an inflammatory, prooxidant, and proangiogenic agent. We found that the pretreatment of endothelial cells with HT (1–$30\,\mu$mol/L) suppressed inflammatory angiogenesis, a crucial aspect of endothelial dysfunction. The HT inhibitory effect is related to reduced mitochondrial superoxide production and lipid peroxidation and to increased superoxide dismutase activity. HT, in a concentration-dependent manner, improved endothelial mitochondrial function by reverting the PMA-induced reduction of mitochondrial membrane potential, ATP synthesis, and ATP5β expression. In PMA-challenged endothelial cells, HT also promoted mitochondrial biogenesis through increased mitochondrial DNA content and expression of peroxisome proliferator-activated receptor gamma coactivator 1-alpha, nuclear respiratory factor-1, and mitochondrial transcription factor A. These results highlight that HT blunts endothelial dysfunction and pathological angiogenesis by ameliorating mitochondrial function, thus suggesting HT as a potential mitochondria-targeting antioxidant in the inflamed endothelium.

1. Introduction

The vascular endothelium is a multifunctional organ critically involved in preserving vascular homeostasis through multiple functions including regulation of vascular tone and barrier, leukocyte trafficking, blood coagulation, nutrient and electrolyte uptake, and neovascularization of hypoxic tissue [1]. Chronic and degenerative diseases, such as cardiovascular diseases, are associated with alterations of endothelial physiological function, a condition termed endothelial dysfunction [2], characterized by reduced nitric oxide and

increased reactive oxygen species (ROS) levels, endothelial inflammatory markers, and aberrant angiogenesis [3, 4]. One of the early manifestations of endothelial dysfunction is the dysregulation of mitochondrial function and biogenesis [5, 6]. Mitochondria, when deregulated, are either a major source or a target of oxidative stress, leading to a vicious circle. Unbalanced and extensive formation of mitochondrial ROS (mtROS) results in oxidative damage to many cellular components; this process in turn accelerates ROS production and generates mitochondrial dysfunction through alterations of mitochondrial membrane potential, ATP production, and

mitochondrial biogenesis [7]. Since increased mtROS production appears to be a key event in altered endothelial functions and inflammatory angiogenesis involved in vascular pathologies [8], identification of mechanisms underlying mitochondrial dysfunction in endothelial cells may contribute to the development of improved approaches for vascular health. There is now a great interest to know whether natural dietary antioxidant compounds, reducing oxidative stress, can safeguard mitochondrial function in the vascular endothelium [9].

Hydroxytyrosol (HT), the major antioxidant phenolic compound present in olives and virgin olive oil, shows beneficial effects on chronic, inflammatory, and degenerative diseases [10, 11]. Most of the health effects of HT studied so far are connected with its ROS-scavenging property and with its ability to activate endogenous antioxidant systems [12–14], to blunt vascular inflammation and to improve endothelial function [15–18]. It has been previously shown that HT counteracted endothelial dysfunction by reducing endothelial inflammatory mediators including endothelial adhesion molecules and inflammatory cytokines [19, 20]. HT also reduced inflammatory angiogenesis, a key pathogenic process in cancer and in the development and vulnerability of atherosclerotic plaque, through inhibition of the proinflammatory enzyme cyclooxygenase-2, prostanoid production, and gelatinases, the matrix-degrading enzymes [21]. These effects were accompanied by a significant reduction in the activation of nuclear factor- (NF-) κB, the redox-sensitive transcription factor, and in the production of intracellular ROS by endothelial NADPH oxidase [21, 22]. However, the potential role of HT in endothelial mtROS production under inflammatory conditions has not been examined yet.

In the present study, we analysed the HT effect on mtROS production and mitochondrial function in inflammatory angiogenesis. To this aim, we utilised a well-known *in vitro* model of human cultured vascular endothelial cells, challenged with phorbol myristate acetate (PMA), an inflammatory, prooxidant, and proangiogenic agent leading to endothelial dysfunction.

In this *in vitro* model, we monitored the HT effects on (i) pathological angiogenesis and mitochondrial oxidative stress; (ii) mitochondrial function by evaluating mitochondrial membrane potential and mitochondrial ATP production; and (iii) mitochondrial biogenesis through mitochondrial DNA content and the expression of factors coordinating the mitochondrial biogenesis, such as peroxisome proliferator-activated receptor gamma coactivator 1-alpha (PGC-1α), nuclear respiratory factor-1 (NRF-1), and mitochondrial transcription factor A (TFAM).

2. Materials and Methods

2.1. Materials.
The materials for cell cultures were obtained from Gibco/BRL. Hydroxytyrosol (HT, 4-(2-hydroxyethyl)-1,2-benzenediol) was obtained from Cayman Chemical (Ann Arbor, MI), and PMA from Sigma-Aldrich (St. Louis, MO). Superoxide-sensitive probe MitoSOX Red, mitochondrial membrane potential probe JC-1, and CM-H2DCFDA

probe were purchased from Molecular Probes. Primary antibodies against β subunit of human ATP synthase (ATP5β), PGC-1α, and NRF-1 and peroxidase-conjugated secondary antibody were purchased from Santa Cruz Biotechnology. Unless otherwise indicated, all other reagents were purchased from Sigma-Aldrich.

2.2. Cell Culture and Treatment.
Human umbilical vein endothelial cells (HUVEC) were harvested, characterized, and maintained as previously described [21]. The human microvascular endothelial cell line (HMEC-1), obtained from Dr. Thomas J. Lawley, was cultured as described [21]. Confluent endothelial cells were shifted to medium supplemented with 3% foetal bovine serum (FBS) and subsequently treated with increasing concentrations of HT (0, 1, 10, and 30 μmol/L) for 1 h and then stimulated with 10 nmol/L PMA. Stock solution of HT (1 mg/mL) was made in absolute ethanol, and stock solution of PMA (300 μmol/L) in DMSO. As a vehicle control, HUVEC were incubated with an appropriate amount of each solvent (<0.025% v/v). The used solvents had no effects on any of the parameters measured. Cellular toxicity was checked by a variety of techniques including cell count, protein content, trypan blue exclusion, and MTT (3-(4,5-dimethylthiazolyl-2)-2,5-diphenyltetrazolium bromide) assays. In preliminary experiments aimed at evaluating phytochemical toxicity, treatment of HUVEC or HMEC-1 with concentrations of HT up to 30 μmol/L for 24 h did not produce any sign of toxicity.

2.3. Detection of Cellular ROS and Mitochondrial Superoxide Production.
Cellular ROS formation was assessed using a carboxy-2′,7′-dichlorofluorescein diacetate (CM-H2DCFDA) probe. CM-H2DCFDA freely permeates the plasma membrane and is hydrolyzed in the cytosol to form the DCFH carboxylate anion [23, 24]. Oxidation results in the formation of fluorescent DCF, which is maximally excited at 495 nm and emitted at 520 nm [24]. HUVEC at confluence were incubated with HT (0, 1, 10, and 30 μmol/L) for 1 h, then loaded with the probe CM-H2DCFDA (10 μmol/L) for 45 min at 37°C, in the dark. Following the incubation, monolayers were gently washed in PBS twice, then stimulated with 10 nmol/L PMA in phenol red-free medium for 0–90 min and monitored by spectrofluorimetric analysis.

Mitochondrial superoxide production was assessed using MitoSOX Red, a mitochondria-targeting fluorescent probe, according to the manufacturer's instructions. MitoSOX Red exhibits fluorescence after oxidation by superoxide anion (excitation 510 nm, emission 580 nm) [25]. HUVEC monolayers were treated with HT (0, 1, 10, and 30 μmol/L) for 1 h, then loaded with the probe MitoSOX Red (5 μmol/L) for 20 min at 37°C in the dark and next stimulated with 10 nmol/L PMA in phenol red-free medium for 0–90 min. MitoSOX Red fluorescence was measured by spectrofluorimetric analysis. Alternatively, for long-term stimulation (10 nmol/L PMA for 16 h), HUVEC were incubated at 37°C in 3% FBS-containing phenol red-free medium in the dark before measurement of MitoSOX Red fluorescence by spectrofluorimetry or by fluorescence microscopy.

2.4. Cell Migration and Tube Formation Assay. HUVEC were cultured in 6-well plates until confluence and then incubated with increasing concentrations of HT (0, 1, 10, and 30 μmol/L) or electron transport chain inhibitors, rotenone or antimycin A (1 μmol/L), for 1 h. Afterwards, a scratch wound was performed with a sterile microtip under standard conditions. After washing with PBS to remove detached cells, a first series of photos were taken by an attached digital output Canon Powershot S50 camera (0 h). Monolayers were then stimulated with 10 nmol/L PMA for 16 h in serum-free medium containing 0.1% human serum albumin, a condition that allows cell survival but not cell proliferation. Monolayers were then washed and again photographed (16 h). Cell repair of the wound was determined by measuring the width (μm) of the denuded area along the scratch (at five different levels) using the Optimas Image analysis software (Media Cybernetics, Pleasanton, CA). The formation of vascular-like structures by endothelial cells was assessed on the growth factor-reduced basement membrane matrix "Matrigel" (11.1 mg/mL; Becton Dickinson Biosciences, Bedford, MA) as previously described [21]. The bottoms of 24-well culture plates were coated with Matrigel (50 μL per well) diluted at 1 : 2 with M199 medium. After gelatination at 37°C for 30 min, gels were overlaid with 500 μL of 2% FBS-containing M199 medium containing 4×10^4 cells per well. The media were supplemented with 10 nmol/L PMA in the absence or presence of 1–30 μmol/L HT or rotenone or antimycin A (1 μmol/L) for 1 h and then incubated for further 16 h at 37°C. Tube formation was monitored by inverted phase-contrast microscopy (Leica, Wetzlar, Germany), and pictures (×100 magnification) were taken by an attached digital output Canon Powershot S50 camera. Tubule branching points were counted in three randomly selected fields per well and were averaged.

2.5. Assessment of Mitochondrial Membrane Potential. Mitochondrial membrane potential (MMP) was assessed as described previously [26] using 5,5′,6,6′-tetrachloro-1,1′, 3,3′-tetraethylbenzimidazol-carbocyanine iodine (JC-1), a cationic dye that exhibits MMP-dependent accumulation and formation of red fluorescent J-aggregates in mitochondria. Each set of samples included a positive control for mitochondrial depolarization (HUVEC or HMEC-1 treated with 1 μmol/L carbonyl cyanide p-(tri-fluromethoxy)phenyl-hydrazone (FCCP)) and hyperpolarization (HUVEC or HMEC-1 treated with 1 μg/mL oligomycin). Fluorescence was determined by a fluorimeter (Fluoroskan II, Labsystem, Helsinki, Finland) using excitation at 488 nm. The JC-1 monomer (green) and the J-aggregates (red) were detected at 530 nm and 590 nm emission, respectively. MMP is evaluated as the red-to-green fluorescence intensity ratio.

2.6. Lipid Peroxidation and Superoxide Dismutase Measurements. The level of cellular lipid peroxidation was determined through the formation of thiobarbituric acid-reactive species (TBARS) as reported in [27] following the method of Esterbauer and Cheeseman [28]. Briefly, malondialdehyde (MDA), a by-product of lipid peroxidation, forms an adduct with thiobarbituric acid (TBA) which

was measured colorimetrically using an MDA equivalent standard. Butylated hydroxytoluene was added to each test sample to prevent further lipid oxidation during sample processing and the TBA reaction. The MDA production, expressed as nmol produced/mg protein, was followed spectrophotometrically at 533 nm. The superoxide dismutase (SOD) activities were determined with the Fluka analytical assay kit using a spectrophotometer Victor™ X (PerkinElmer) at $\lambda = 440$ nm. The Cu/ZnSOD and the mitochondrial MnSOD activities were assayed, without or with KCN (4 mmol/L), using the ability to inhibit the reduction of WST-1 [2-(4-Iodophenyl)-3-(4-nitrophenyl)-5-(2,4-disulfophenyl)-2H-tetrazolium monosodium salt] by superoxide anions generated by the xanthine/xanthine oxidase method. One unit of SOD activity was defined as the amount of the enzyme causing half maximum inhibition of WST-1 reduction.

2.7. Evaluation of the Mitochondrial ATP Synthase Activity. Mitochondrial ATP synthesis was measured spectrophotometrically as described [29]. Briefly, 1×10^6 cells were resuspended in 1 mL of buffer containing 10 mmol/L HEPES (pH 7.4), 150 mmol/L NaCl, 1 mmol/L K-EDTA, 20 mmol/L glucose, 2 mmol/L $MgCl_2$, 5 U/mL hexokinase, 300 μmol/L Ap5A, and 25 mmol/L KH_2PO_4. Endothelial cells were incubated, under stirring for rotation, in the absence or in the presence of oligomycin for 30 minutes. Then, the reaction was stopped with 3% $HClO_4$, and the cells were centrifuged in Eppendorf tubes at 100 ×g for 4 minutes. To the supernatant (500 μL), 500 μL of buffer containing 1 mmol/L $MgCl_2$, 150 mmol/L Tris/HCl (pH 7.4), and 7 U/mL glucose-6-phosphate dehydrogenase was added. The reaction was started by adding 1 mmol/L NADP, and the reduction of the coenzyme was followed spectrophotometrically (Beckman Coulter DU 800), at 360/374 nm with an $\varepsilon = 2.1$ mmol/$L^{-1} \cdot cm^{-1}$.

2.8. Western Blot Analysis. Total cell extract was prepared as previously described [22]. After protein content determination, the cell lysate was separated using NuPAGE Bis-Tris precast 10% polyacrylamide gels under reducing conditions (Invitrogen, Carlsbad, CA, USA). Resolved proteins were transferred onto nitrocellulose sheets (Amersham, Freiburg, Germany), and the resulting membranes were saturated with a 5% blocking agent (Amersham) in Tris-buffered saline (TBS, 20 mmol/L Tris (pH 7.6) and 132 mmol/L NaCl) for 1 h at room temperature. Membranes were then incubated overnight at 4°C with primary antibodies against human ATP5β, PGC-1α, NRF-1, TFAM, and β-actin, followed by a horseradish peroxidase-conjugated secondary antibody. The enhanced chemiluminescence (ECL) method (Amersham) was used to reveal positive bands, according to the manufacturer's instructions. Bands were analysed quantitatively using the Scion Image Alpha 4.0.3.2 software (Scion Corporation).

2.9. Quantitative Reverse Transcription-Polymerase Chain Reaction Analysis. HUVEC were treated with HT (0, 1, 10, and 30 μmol/L) for 1 h and then stimulated with 10 nmol/L PMA for 16 h. Total RNA was isolated by using the TRIzol

TABLE 1: Primer sequence of real-time quantitative PCR.

Gene	Accession number	Primers (sequence 5'–3')	Size (bp)
TNF-α	NM_000594.2	CCTGTGAGGAGGACGAACAT AGGCCCCAGTTTGAATTCTT	240
IL-1β	NM_000576.2	CTGTCCTGCGTGTTGAAAGA AGTTATATCCTGGCCGCCTT	228
VCAM-1	NM_001078.3	CATGGAATTCGAACCCAAAC CCTGGCTCAAGCATGTCATA	140
ICAM-1	NM_000201.2	AGACATAGCCCCACCATGAG CAAGGGTTGGGGTCAGTAGA	190
ATP5β	NM_001686	TGAGGGACTACCACCAATTC TTTCTGGCCTCTAACCAAGC	141
TFAM	NM_001270782.1	CCGAGGTGGTTTTCATCTGT ACGCTGGGCAATTCTTCTAA	147
NRF-1	NM_005011.3	CCGTTGCCCAAGTGAATTAT ACTGTAGCTCCCTGCTGCAT	181
PGC-1α	NM_013261.3	GCTGACAGATGGAGACGTGA TGCATGGTTCTGGGTACTGA	178
36B4	NM_001697.2	TCGACAATGGCAGCATCTAC ATCCGTCTCCACAGACAAGG	191
D-loop	AC_000022.2	GGTTCTTACTTCAGGGCCATC TGACCTTCATGCCTTGACGG	201
Gapdh	NG_007073.2	ATGCCTTCTTGCCTCTTGTC CATGGGTGGAATCATATTGG	245

reagent (Invitrogen) according to the manufacturer's protocol. For quantitative polymerase chain reaction, total RNA (2 μg) was converted into first-strand cDNA by using the High-Capacity cDNA Reverse Transcription Kit (Applied Biosystems, Monza, Italy). The quantitative RT-PCR was performed in the Bio-Rad Biosystems CFX384 Touch Real-Time PCR Detection System, by using SYBR Green PCR Master Mix. The human cDNA fragments were amplified using primers synthesized by Sigma Genosys and reported in Table 1. We explored the expression of the following genes: *ATP5β*, *PGC-1α*, *NRF-1*, *TFAM*, *TNF-α*, *IL-1β*, *VCAM-1*, and *ICAM-1*. The quantifications were performed using the efficiency-adjusted $\Delta\Delta$CT method (CFX Manager), with Gapdh/36B4 as an internal control.

2.10. Determination of the Mitochondrial DNA Copy Number. Total DNA from endothelial cells was obtained by phenol/chloroform extraction. Real-time quantitative PCR (qPCR) was performed to quantify mitochondrial DNA (mtDNA) content. MtDNA level was expressed as the ratio of mtDNA (D-loop) to nuclear DNA (Gapdh) quantity. The primers used for D-loop and Gapdh are reported in Table 1.

2.11. Statistical Analysis. Values were expressed as mean ± SD for the number of experiments indicated in the legends to the figures. Differences between two groups were determined by unpaired Student's *t*-test. Multiple comparisons were performed by one-way analysis of variance (ANOVA), and individual differences were then tested by Fisher's protected least significant difference test, after the demonstration of significant intergroup differences by ANOVA. Differences

between means from at least three independent experiments with $p < 0.05$ were considered statistically significant.

3. Results

3.1. Hydroxytyrosol Inhibits PMA-Induced Angiogenic Response by Reducing Mitochondrial Superoxide Production. In previous studies, we characterized a model of endothelial dysfunction constituted by HUVEC challenged with PMA, an inflammatory and proangiogenic agonist able to induce endothelial activation and inflammatory angiogenesis [20, 21, 30]. In the same works, we have shown that HT reduced endothelial dysfunction [20, 21] by decreasing intracellular oxidative stress and NF-κB activation, a pivotal regulator of inflammatory gene expression.

In the present study, we evaluated the protective effect of HT on endothelial dysfunction by analysing inflammatory and angiogenic response in PMA-triggered endothelial cells (Figure 1). Figure 1 shows that HT (1–30 μmol/L), in a concentration-dependent manner, reduced the expression of the PMA-stimulated inflammatory cytokines, tumor necrosis factor- (TNF-) α and interleukin- (IL-) 1β (Figure 1(a)), as well as the endothelial adhesion molecules, vascular cell adhesion molecule- (VCAM-) 1 and intercellular adhesion molecule- (ICAM-) 1 (Figure 1(b)). Figure 1 also shows that HT pretreatment reduced the PMA-induced angiogenic response (Figures 1(c) and 1(d)). The new vessel formation occurs through a series of steps, including endothelial cell migration and morphological differentiation/reorganization of endothelial cells into a three-dimensional tubular structure [31]. Therefore, we analysed the endothelial cell migration by scratch wound healing and capillary-like tube
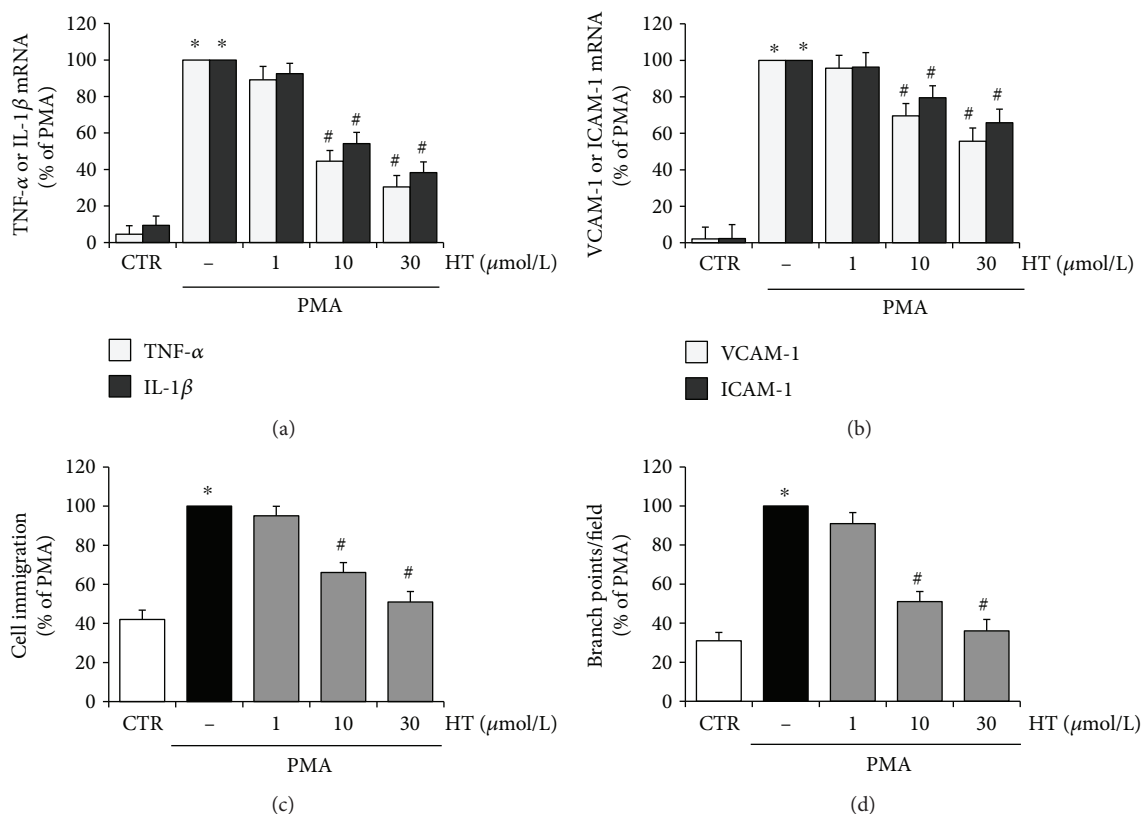
FIGURE 1: HT effects on PMA-induced endothelial dysfunction. HUVEC were pretreated with HT (1–30 μmol/L) or vehicle (control, CTR) for 1 h and stimulated by PMA (10 nmol/L) for 16 h; then, TNF-α and IL-1β (a) or VCAM-1 and ICAM-1 (b) mRNA levels were determined by quantitative RT-PCR. HUVEC were pretreated with HT (1–30 μmol/L) for 1 h; afterwards, a scratch wound was performed and monolayers were stimulated by 10 nmol/L PMA for 16 h. Cell migration was monitored under phase-contrast microscopy and quantified (c). HUVEC were plated onto a 3-dimensional collagen gel (Matrigel) surface, pretreated with HT (1–30 μmol/L), for 1 h, and then stimulated with 10 nmol/L PMA for 16 h. Tube formation was monitored under phase-contrast microscopy and reported as branch points per field (d). $^*p < 0.05$ versus CTR; $^#p < 0.05$ versus PMA alone.

formation by the Matrigel assay. As shown in the bar graph (Figure 1(c)), the HT pretreatment inhibited, in a concentration-dependent manner, the migration of endothelial cells stimulated by PMA. Moreover, HT suppressed the PMA-challenged endothelial angiogenic activity by decreasing the capillary-like tube formation on Matrigel, as documented by the reduced number of branch points, shown in bar graph quantification (Figure 1(d)). The HT inhibitory effects were significantly evident at 10 μmol/L and reached maximum inhibition at 30 μmol/L.

Since increased mtROS production appears to be a critical event in endothelial dysfunction [8], in the present study, we deepened the HT effects on superoxide production and mitochondrial function in inflammatory angiogenesis.

In Figure 2(a), we reported the HT effects on mtROS in PMA-triggered endothelial cells showing that PMA stimulation greatly increased superoxide generation in HUVEC, as evaluated by increased MitoSOX Red fluorescence, resulting from the oxidation of MitoSOX Red by mitochondrial superoxide. HT pretreatment reduced the PMA-induced superoxide production: 10 μmol/L HT decreased superoxide by about 33% and 30 μmol/L HT lowered it to the control levels (Figure 2(a)). The inhibitory effect of HT on PMA-induced mitochondrial superoxide production was confirmed by

fluorescence microscopy imaging (Figure 2(b)). HUVEC challenged with PMA showed bright red fluorescence, which was markedly blunted after HT treatment in a concentration-dependent manner (Figure 2(b)). In addition, we investigated the temporal effects of HT on mtROS production in HUVEC challenged with PMA for short times (0–90 min). Figure 2(c) shows that PMA boosted mtROS already at 30 min. HT at 10 μmol/L, the lowest effective concentration against endothelial inflammation and dysfunction, significantly blunted, at 60 min, MitoSOX Red fluorescence, suggesting an early role of mtROS in PMA-triggered endothelial cells. The kinetics of mtROS production followed a trend similar to that of cytosolic ROS, determined by CM-H2DCFDA fluorescence (Figure 2(d)). In our model system, the levels of nitric oxide, a marker of endothelial dysfunction, were also evaluated. Results showed no difference in nitric oxide levels either after PMA stimulation or after HT treatment (Supplementary Figure 1). These results highlight a crucial role of mtROS both in PMA-induced endothelial dysfunction and in HT protective action.

Noteworthy, the inhibitory actions of HT occurred only under proinflammatory conditions induced by PMA treatment and in the absence of any toxicity as determined by the MTT assay and protein content and cellular counts (data

(a)

(b)

(c)

(d)
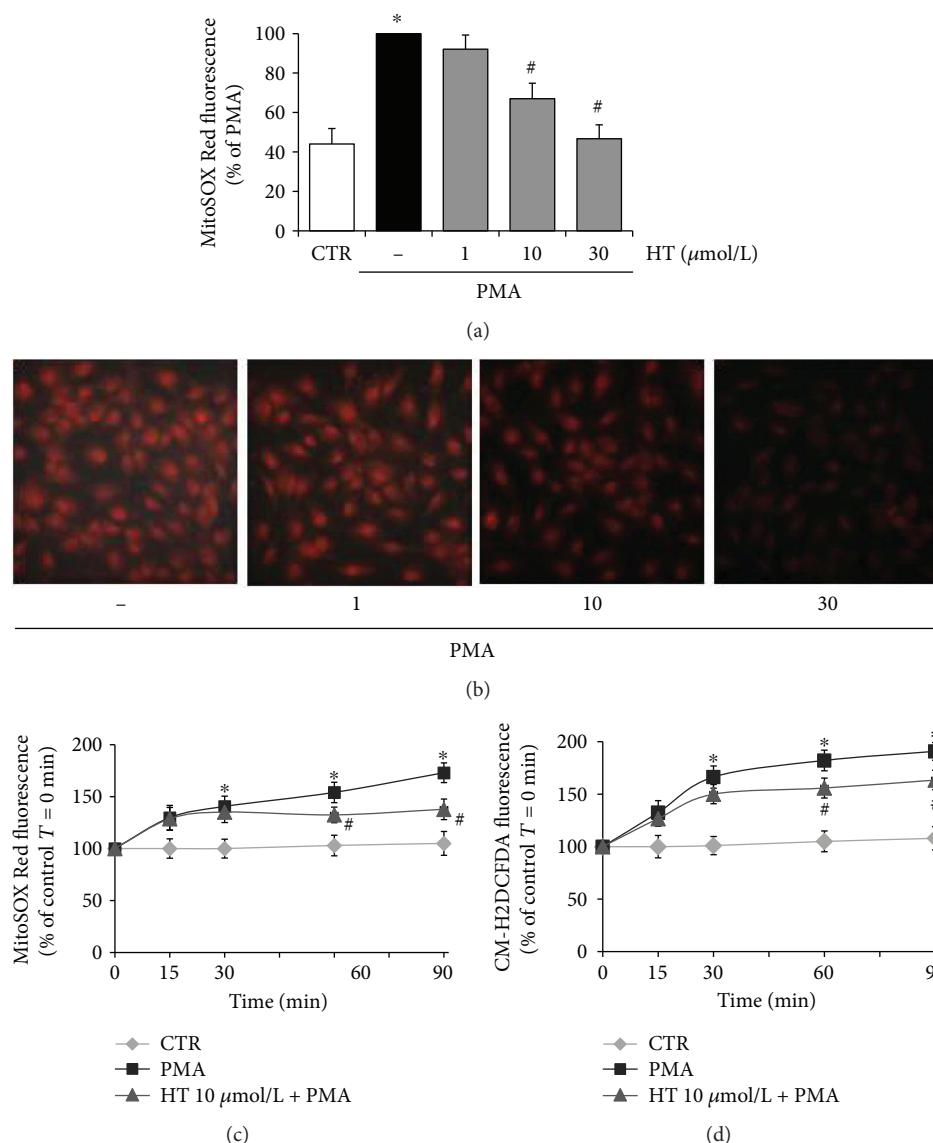
FIGURE 2: Effects of HT on PMA-induced intracellular ROS and mitochondrial superoxide production. HUVEC were pretreated with HT (1–30 μmol/L) or vehicle (control, CTR) for 1 h and loaded by CM-H2DCFDA or MitoSOX Red as described in Materials and Methods, then stimulated with 10 nmol/L PMA for 16 h (a, b) and for the indicated times (c, d), and next fluorescence levels were evaluated by a fluorescence plate reader (a), fluorescence microscope (b), or fluorimeter (c, d). Data represent three independent experiments performed in triplicate and are expressed as means ± SD. $^*p < 0.05$ versus CTR; $^\#p < 0.05$ versus PMA alone.

not shown). Indeed, HT treatment did not display significant effects in HUVEC under basal conditions on mitochondrial ROS production, cell migration, and capillary-like formation (data not shown).

Finally, to analyse the role of superoxide produced by mitochondria in inflammatory angiogenic response, HUVEC were pretreated with rotenone or antimycin A, inhibitors of the mitochondrial complexes I and III, main sites of ROS production in the electron transport chain, respectively. The effects of the two inhibitors on PMA-induced endothelial cell migration and tubule formation were evaluated. As shown in the bar graph (Figure 3(a)) and in representative scratch wound healing images (Figure 3(b)), the pretreatment with rotenone or antimycin A inhibited the migration

of endothelial cells stimulated by PMA. Moreover, both the inhibitors suppressed the PMA-challenged endothelial angiogenic activity by decreasing the capillary-like tube formation on Matrigel, as documented by the reduced number of branch points, shown in representative images (Figure 3(d)) and in bar graph quantification (Figure 3(c)). These inhibitory effects of rotenone or antimycin A point out the key role of mtROS in aberrant angiogenesis under inflammatory conditions. In HUVEC under basal unstimulated conditions, rotenone and antimycin A alone did not cause substantial effects on mtROS production, cell migration, and capillary-like formation.

In addition to macrovascular endothelial cells (HUVEC), microvascular endothelial cells (HMEC-1) were used in

(a)

(b)

(c)

(d)
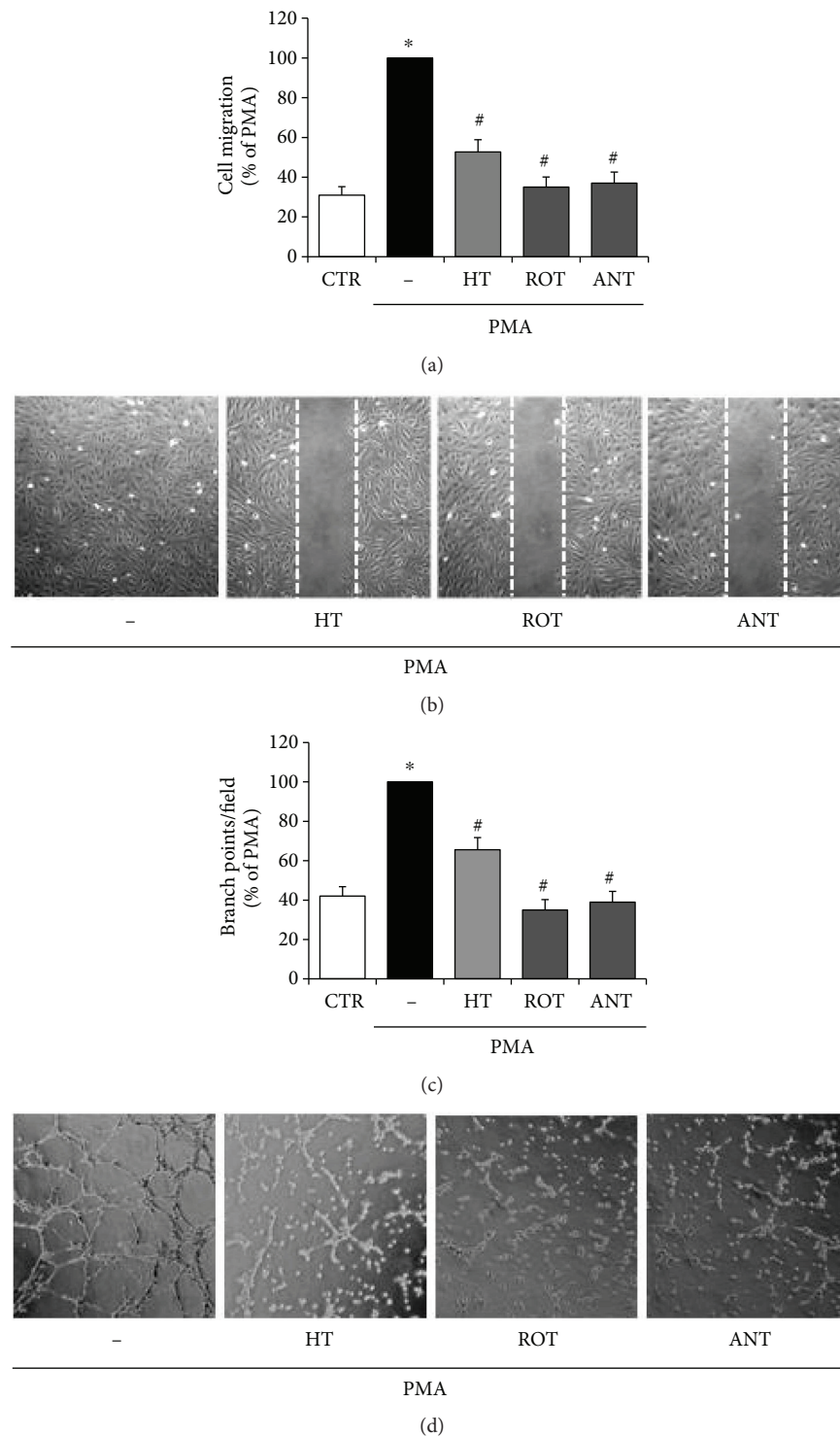
FIGURE 3: HT effects on PMA-induced mitochondrial superoxide production in cell migration and in inflammatory angiogenesis. HUVEC were pretreated with HT ($10\,\mu$mol/L) and rotenone or antimycin A ($1\,\mu$mol/L) for 1 h; afterwards, a scratch wound was performed and monolayers were stimulated by 10 nmol/L PMA for 16 h. Cell migration was quantified and monitored under phase-contrast microscopy (a, b). HUVEC were plated onto a 3-dimensional collagen gel (Matrigel) surface, pretreated with HT ($10\,\mu$mol/L) and rotenone or antimycin A ($1\,\mu$mol/L) for 1 h, and then stimulated with 10 nmol/L PMA for 16 h. Tube formation was monitored under phase-contrast microscopy, photographed, and analysed (c, d). Images are representative of cell migration (b), and capillary-like tube formation is reported as branch points per field (d) in PMA-stimulated endothelial cells (×100 magnification). Data are representative of three independent experiments, expressed as means ± SD, and presented as percentage of PMA-stimulated endothelial cells. Each experiment consisted of four replicates for each condition. $^{*}p < 0.05$ versus CTR; $^{\#}p < 0.05$ versus PMA alone.

(a)

(b)
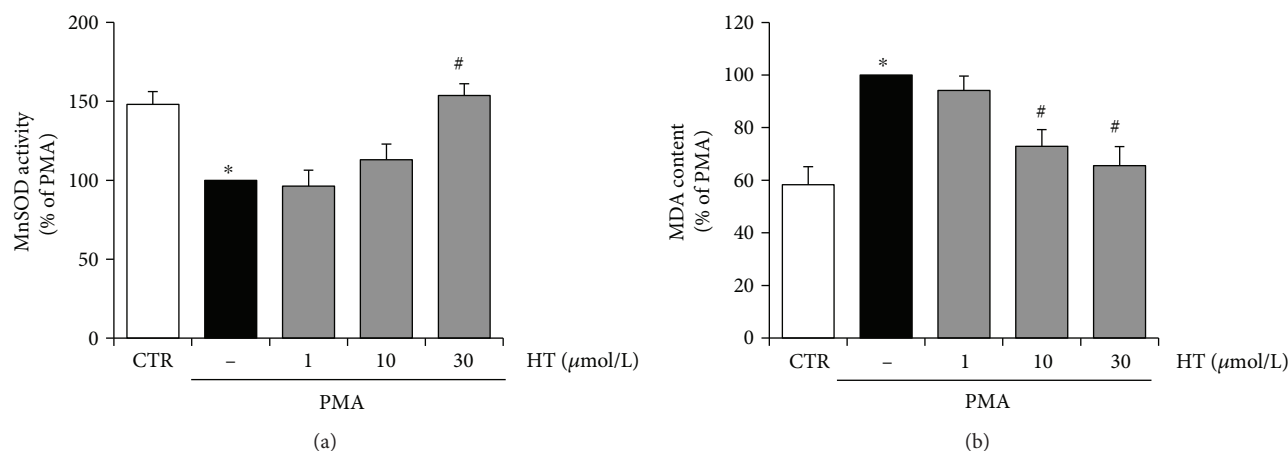
FIGURE 4: HT effects on SOD activity and oxidative damage in stimulated endothelial cells. HUVEC were pretreated with HT (1–30 μmol/L) for 1 h and then stimulated with PMA for further 16 h; afterwards, the activity of MnSOD (a) and lipid peroxidation, followed by MDA production (b), were evaluated. Data are representative of three independent experiments (mean ± SD) and expressed as percentage of PMA-stimulated endothelial cells. $^*p < 0.05$ versus CTR; $^\#p < 0.05$ versus PMA alone.

comparative experiments and similar results were obtained (data not shown).

To further analyse the protective role of HT in endothelial oxidative stress under inflammatory conditions, the HT effects on SOD activities and oxidative damage were examined. We found that PMA reduced MnSOD activity, which was rescued by 30 μmol/L HT pretreatment (Figure 4(a)). The uncontrolled production of cellular ROS induced, among others, direct damages of cellular lipids, the so-called lipid peroxidation, which was assayed by measuring the level of its end product MDA [32]. PMA stimulation increased cellular MDA levels by about 40%, with respect to control unstimulated cells, thus confirming an enhancement of cellular oxidative stress (Figure 4(b)). Pretreatment with HT reduced PMA-induced lipid peroxide production by about 27% at 10 μmol/L and 35% at 30 μmol/L (Figure 4(b)).

The present findings reveal an important role of mtROS in inflammatory angiogenesis and show that HT treatment can improve endothelial function by decreasing mitochondrial superoxide production and oxidative damage.

3.2. Hydroxytyrosol Prevents Mitochondrial Oxidative Dysfunction in the Inflamed Endothelium.
There is increasing evidence that mitochondrial alterations are implicated in vascular endothelial inflammation and angiogenesis [8]. Since mitochondrial membrane potential (MMP) is an important indicator of mitochondrial function in situ, we monitored the MMP in PMA-challenged endothelial cells by using the JC-1 assay. Figure 5(a) shows that PMA stimulation induced a significant MMP decrease, with respect to unstimulated control cells. Pretreatment with HT reverted the PMA-induced depolarization of the mitochondrial membrane with an effect already significant at 10 μmol/L (Figure 5(a)).

MMP drives the synthesis of ATP; therefore, changes in the membrane potential can affect mitochondrial ATP synthesis. We assessed whether in endothelial cells the MMP, reduced by PMA, was connected with changes in mitochondrial ATP synthesis, and we analysed the effects of HT pretreatment. In accordance with MMP alterations (Figure 5(a)), we observed that PMA challenge reduced by about 34% the fraction of ATP produced by endothelial mitochondrial FoF1-ATP synthase (Figure 5(b)). In detail, in unstimulated endothelial cells, the amount of ATP synthesized by the FoF1-ATP synthase was 10.3 ± 1.3 nmol of ATP formed/min/1 × 10^6 cells; meanwhile, in PMA-challenged cells, it was lowered to 6.8 ± 1.1 nmol of ATP formed/min/1 × 10^6 cells. HT pretreatment reverted the PMA-reduced mitochondrial ATP production in a concentration-dependent manner, increasing it by about 35% versus PMA at 10 μmol/L HT and reaching the control values at 30 μmol/L HT. Since it is well known that the activity of ATP synthase is influenced by the expression of the enzyme catalytic subunit ATP5β, we investigated the ATP5β protein and mRNA levels. We found that PMA significantly reduced the expression of ATP5β protein in endothelial cells, while HT pretreatment reverted PMA-reduced ATP5β expression already at 10 μmol/L HT and caused a further increase in the protein content at 30 μmol/L HT (Figure 5(c)). Consistently with ATP5β protein levels, the ATP5β mRNA abundance significantly decreased following PMA stimulation with respect to unstimulated control cells, while preincubation with 10 μmol/L HT reverted PMA-reduced ATP5β mRNA amount to the unstimulated control level (Figure 5(d)).

These results highlight that HT treatment was able to improve endothelial mitochondrial function under inflammatory conditions, by counteracting the decrease in MMP as well as in ATP synthesis and ATP5β expression.

3.3. Hydroxytyrosol Promotes Mitochondrial Biogenesis in the Inflamed Endothelium.
To determine whether in PMA-challenged endothelial cells the observed improvement in mitochondrial function promoted by HT was associated with increased mitochondrial biogenesis, the mtDNA content and the expression of PGC-1α, NRF-1, and TFAM, which play a pivotal role in this process, were investigated. Western blotting analysis and real-time qRT-PCR revealed that the

(a)

(b)

(c)

(d)
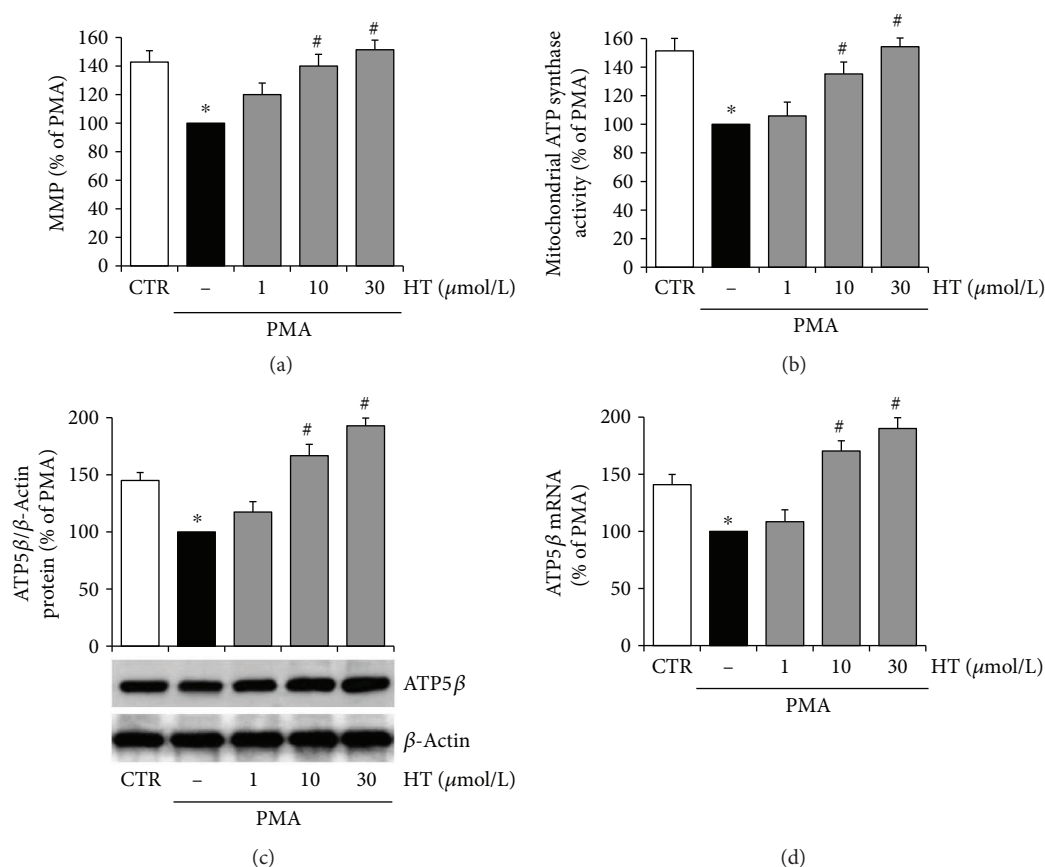
FIGURE 5: HT improves mitochondrial function in PMA-stimulated endothelial cells. HUVEC were pretreated with HT (1–30 μmol/L) for 1 h and then stimulated with PMA (10 nmol/L) for further 16 h. After treatments, MMP was assayed by using JC-1 staining and evaluated by using a fluorescence plate reader (a). Mitochondrial oligomycin-sensitive ATP synthesis was measured in endothelial cells incubated in the absence (−) or in the presence of HT (1–30 μmol/L) (b). The expression of β subunit of ATP synthase was evaluated at protein (c) and mRNA levels (d) by Western blotting or quantitative RT-PCR, respectively. ATP5β protein expression was normalized to β-actin, and ATP5β mRNA amount was normalized to Gapdh mRNA. Data are representative of four independent experiments (mean ± SD), each consisting of four replicates for each condition, and expressed as percentage of PMA-stimulated endothelial cells. $^*p < 0.05$ versus CTR; $^\#p < 0.05$ versus PMA alone.

expression of the mitochondrial biogenesis factors, PGC-1α and NRF-1, was significantly reduced by PMA treatment (Figures 6(a) and 6(b)). HT preincubation reverted the PMA-reduced expression of NRF-1 and PGC-1 with a significant effect at 10 μmol/L, at both protein (Figure 6(a)) and mRNA levels (Figure 6(b)). PMA significantly reduced also the abundance of TFAM mRNA, which was increased by HT treatment (Figure 6(c)). Finally, the mtDNA copy number, which is a critical determinant of overall mitochondrial health, was analysed. To this aim, mtDNA and nuclear DNA (nDNA) were measured by real-time qPCR. The mtDNA copy number was expressed as the ratio of mtDNA (D-loop) to nDNA (Gapdh). PMA stimulation of endothelial cells decreased the mtDNA copy number with respect to unstimulated control cells. HT treatment reverted the PMA reduction of the mtDNA copy number already at 10 μmol/L with a further increase at 30 μmol/L (Figure 6(d)).

The present findings unveil that HT can improve endothelial function by promoting mitochondrial biogenesis under inflammatory conditions.

4. Discussion

HT, the major phenolic compound present in olives and virgin olive oil, exerts anti-inflammatory and antiangiogenic function through inhibition of intracellular ROS levels and NF-κB activation in the inflamed endothelium [20, 21]. However, the role of HT in mtROS production in inflammatory angiogenic response has not been to date clarified.

In the present study, we show that the endothelial protective effect of HT occurs by inhibiting the expression of inflammatory cytokines and endothelial adhesion molecules and that HT prevents inflammatory angiogenesis by reducing mitochondrial superoxide production and by improving mitochondrial function and biogenesis.

At low concentrations, ROS could behave as proangiogenic signalling molecules in endothelial cells, but at elevated levels, ROS could cause endothelial cell dysfunction and pathological angiogenesis [33–35]. In vascular endothelial cells, mitochondria, far from being simply ATP-producing organelles, also play a key role in cell signalling through

(a)

(b)

(c)

(d)
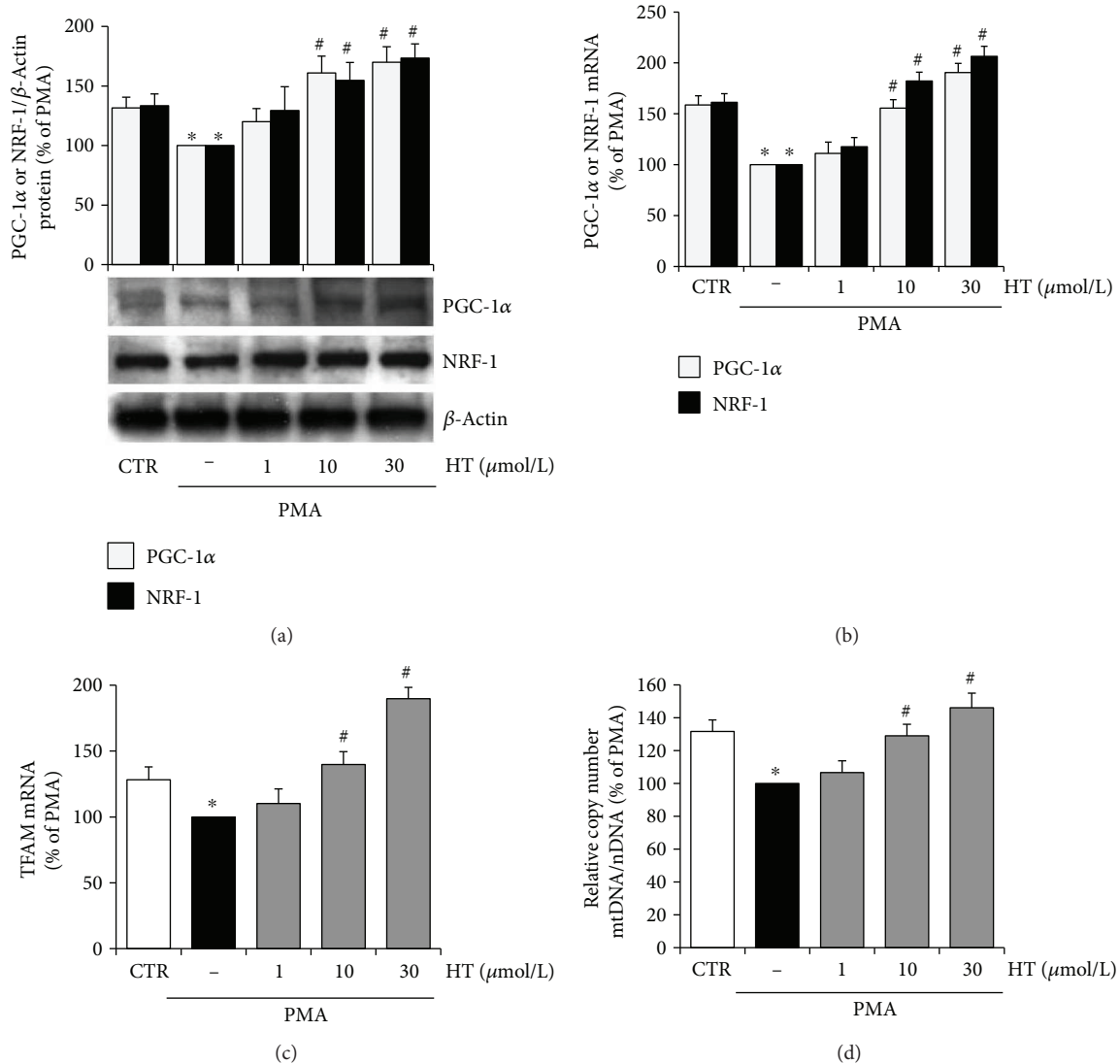
FIGURE 6: HT increases mitochondrial biogenesis in stimulated endothelial cells. HUVEC were pretreated with HT (1–30 μmol/L) for 1 h and then stimulated with PMA for further 16 h. The expression of mitochondrial biogenesis factors was evaluated by Western blotting (a), and the corresponding mRNA levels were assessed by quantitative RT-PCR (b, c). DNA was isolated, and quantitative real-time PCR was used to determine nuclear DNA (nDNA) and mitochondrial DNA (mtDNA) contents. The mtDNA content was expressed as the ratio of the mtDNA copy number to the nDNA copy number (mtDNA/nDNA) (d). Data are representative of four independent experiments (mean ± SD) and expressed as percentage of PMA-stimulated endothelial cells. $^*p < 0.05$ versus CTR; $^\#p < 0.05$ versus PMA alone.

mtROS production [36, 37]. High levels of mtROS alter normal ROS signalling and mitochondrial functions leading to endothelial dysfunction and ultimately to the development of cardiovascular disease [38]. In vascular endothelial cells, the mitochondrial electron transport chain represents one of the major sites of ROS production. Although most electrons through the chain redox gradient reach at the end complex IV, they prematurely can react with oxygen, at the level of complexes I and III, to form superoxide [39]. In this study, we found that PMA induced aberrant angiogenesis, as shown by increased endothelial cell migration and tubule-like structure formation. The inflammatory angiogenic response triggered by PMA occurred through mechanisms that determine an increase in mtROS production.

Indeed, PMA-induced endothelial migration and capillary morphogenesis were suppressed by preincubation with rotenone and antimycin A, inhibitors of the electron transport chain, respectively, at the level of mitochondrial complexes I and III, major sources of mtROS. In our model system, mtROS were boosted already at 30 min after PMA stimulation and their levels remained high after 16 h, suggesting mtROS as an initial and late player in PMA-induced endothelial dysfunction. Our results are in accordance with previous findings by Joo et al. [40] who reported that Mito-TEMPO, a specific mitochondrial antioxidant, inhibited the PMA-stimulated expression of endothelial adhesion molecules, implying an important role of mtROS in endothelial inflammation. About the role of HT in PMA-induced

superoxide, we found that HT pretreatment decreased, in a concentration-dependent manner, superoxide production as well as membrane lipid peroxidation. Overall, our findings point out the key role of mtROS overproduction in aberrant inflammatory angiogenesis and suggest that the HT antiangiogenic effect could be ascribed to its protective action on endothelial mitochondria. It should be remarked that endothelial superoxide can be detoxified through the action of the mitochondrial MnSOD, a matrix-abundant and highly efficient enzyme that can convert superoxide to hydrogen peroxide, which is the more stable and less reactive form than superoxide [41]. Here, we found, in agreement with the reduced superoxide levels, that HT increased MnSOD activity in PMA-triggered endothelial cells. This result is in accordance with previous data showing HT effects on the activation and expression of several cytoprotective enzymes [12–14].

The primary function of mitochondria is to generate ATP by the oxidative process. ATP synthesis is driven via the transfer of electrons through complexes I to IV, generating a concentration gradient of protons across the inner mitochondrial membrane thus maintaining membrane potential. During stress conditions, electron transport and ATP synthesis often fail leading to the accumulation of ROS and mitochondrial dysfunction, along with a significant reduction of oxidative phosphorylation efficiency, due to membrane potential breakdown, ATP depletion, and uncoupled oxidative phosphorylation [42]. We found that associated with an overproduction of mtROS, PMA significantly reduced MMP as well as mitochondrial ATP synthesis in endothelial cells. The reduced production of mitochondrial ATP by PMA would seem in contrast with its proangiogenic action, since angiogenesis is a highly energetic process. However, our findings are in agreement with reports showing that the inhibition of mitochondrial ATP synthesis does not impair endothelial vessel sprouting [43] but has a critical role as a stress sensor in the dysfunctional endothelium [38]. According to decreased overproduction of mtROS, HT pretreatment attenuated the PMA-induced mitochondrial membrane depolarization in endothelial cells, and it recovered the lowered ATP levels by inducing FoF1-ATP synthase activity and the expression of catalytic subunit, ATP5β. These results highlight that HT can protect the endothelium against inflammation-induced injury, improving mitochondrial function and preventing mtROS overproduction.

To deepen the mechanisms of action underlying the HT endothelial mitochondrial protection, we studied the effects of HT on mitochondrial biogenesis, which has recently emerged as a potential therapeutic target to improve endothelial function [38]. Mitochondrial biogenesis is a highly regulated process requiring replication of mtDNA and expression of nuclear and mitochondrial genes [44–46]. The primary role is performed by PGC-1α, which activates NRF-1 to coordinate expression of nuclear genes required for biogenesis [47, 48]. PGC-1α also activates TFAM that is responsible for the transcriptional control of mtDNA [49]. It has been established that the increased expression of these factors modulates mitochondrial biogenesis in endothelial cells and plays a pivotal role in optimizing cellular

mitochondrial function [50]. Our findings reveal that PMA decreased mitochondrial biogenesis by reducing the expression of PGC-1α, NRF-1, and TFAM as well as by decreasing the mtDNA copy number. The reduction of PMA-induced mitochondrial biogenesis is in accordance with the decreased ATP5β expression and mitochondrial ATP production. HT pretreatment restored PMA-reduced mitochondrial biogenesis, enhancing mtDNA content and PGC-1α, NRF-1, and TFAM expression. In line with this, HT also increased ATP5β expression and mitochondrial ATP production, resulting in an improved mitochondrial performance in endothelial cells under inflammatory conditions. Our observations are in agreement with previous *in vitro* findings about the HT ability to activate PGC-1α and to induce mitochondrial biogenesis in 3T3-L1 murine adipocytes and in ARPE-19 human retinal pigment epithelial cells [14, 51, 52]. Multiple lines of evidence have shown a multifactorial protection of PGC-1α in vascular health [46]. Vascular risk factors including hyperglycaemia significantly decrease PGC-1α protein expression and reduce the mitochondrial number as shown in the retina of diabetic patients and in retinal endothelial cells treated with high glucose [53, 54]. PGC-1α overexpression decreased endothelial inflammatory response [55], whereas PGC-1α-deficient mice displayed increased inflammatory markers in atherosclerotic plaques [56]. Moreover, PGC-1α can protect the endothelium through the inhibition of the redox-sensitive transcription factor NF-κB, a crucial regulator of inflammation and endothelial dysfunction [55]. The increased PGC-1α expression by HT, shown in this study, is in accordance with previous findings, which indicate that HT reduced inflammatory angiogenesis by suppressing the activation of NF-κB [20, 21]. Moreover, our findings further support other studies regarding the role of natural bioactive compounds as molecules capable of modulating mitochondrial biogenesis, MMP, mitochondrial electron transport chain, and ATP synthesis as well as mitochondrial oxidative status in endothelial cells [9, 33, 50, 57–59]. Noteworthy, HT protective effects were observed to occur at micromolar concentrations, which are physiologically relevant and nutritionally achievable, as HT is well absorbed in the small intestine and metabolized in the body after intake of virgin olive oil and/or olives [60].

Taken together, these results indicate that HT could represent a mitochondria-targeting antioxidant nutrient in endothelial cells under inflammatory conditions, having a beneficial impact at a mitochondrial level by preventing the oxidative stress and improving the mitochondrial function and biogenesis (Figure 7).

5. Conclusion

This study demonstrates, for the first time, that HT can counteract inflammatory angiogenesis through the improvement of endothelial mitochondrial function and biogenesis. These properties point out HT as a mitochondrial nutrient targeting the inflamed endothelium and provide a new mechanism of action by which HT could prevent chronic degenerative pathologies, including cardiovascular diseases.
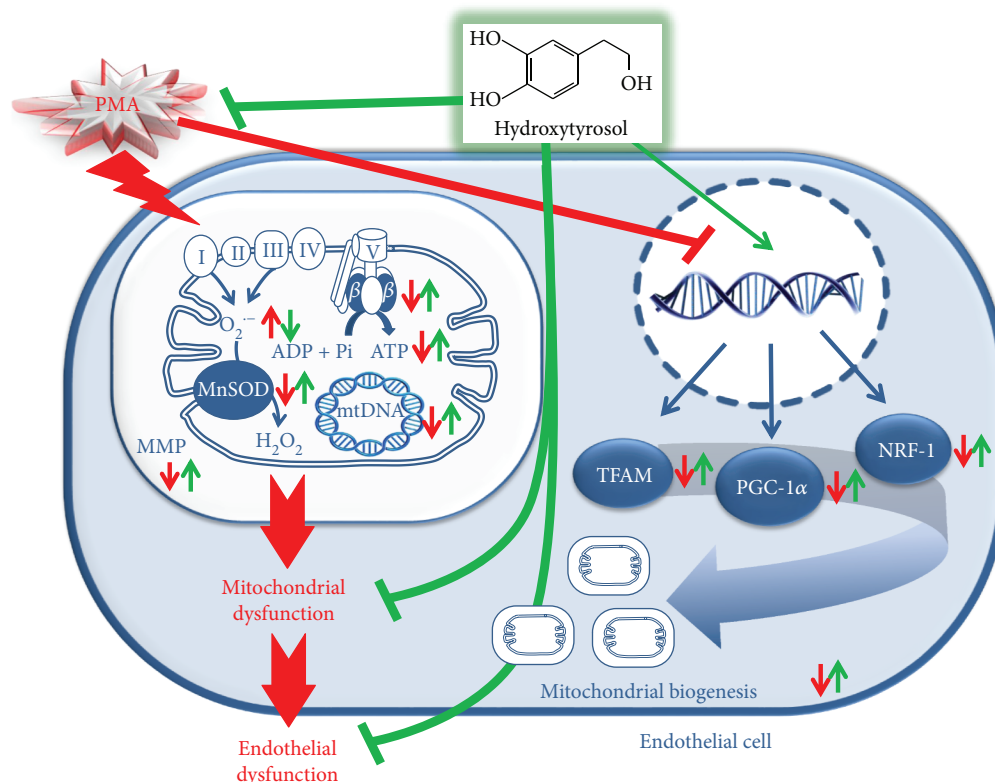
FIGURE 7: A schematic illustration of the molecular mechanism underlying HT protective effects on mitochondrial function in PMA-stimulated endothelial cells. Red line indicates PMA action, green line indicates HT effect, up arrow indicates upregulation, and down arrow indicates downregulation.

Conflicts of Interest

The authors declare that they have no conflicts of interest.

Acknowledgments

Supplementary Materials

Supplementary material includes the experimental procedure to detect nitric oxide levels, and the Supplementary Figure 1 shows the HT effects on PMA-induced nitric oxide production. Supplementary Figure 1: HT effects on PMA-induced nitric oxide production. HUVEC were pretreated with HT (1–30 μmol/L) or vehicle (control, CTR) for 1 h and stimulated by PMA (10 nmol/L) for 16 h; then, nitric oxide was quantified as its stable oxidation product, nitrite, in the supernatant, by using the nitrite assay kit. Data represent three independent experiments, and they are expressed as means ± SD. *(Supplementary Materials)*

References

[1] M. Potente, H. Gerhardt, and P. Carmeliet, "Basic and therapeutic aspects of angiogenesis," *Cell*, vol. 146, no. 6, pp. 873–887, 2011.

[2] J. Davignon and P. Ganz, "Role of endothelial dysfunction in atherosclerosis," *Circulation*, vol. 109, no. 23, Supplement 1, pp. III27–III32, 2004.

[3] M. Feletou and P. M. Vanhoutte, "Endothelial dysfunction: a multifaceted disorder (the Wiggers Award Lecture)," *American Journal of Physiology Heart and Circulatory Physiology*, vol. 291, no. 3, pp. H985–H1002, 2006.

[4] P. Carmeliet and R. K. Jain, "Molecular mechanisms and clinical applications of angiogenesis," *Nature*, vol. 473, no. 7347, pp. 298–307, 2011.

[5] S. M. Davidson and M. R. Duchen, "Endothelial mitochondria: contributing to vascular function and disease," *Circulation Research*, vol. 100, no. 8, pp. 1128–1141, 2007.

[6] S. Dikalov, "Cross talk between mitochondria and NADPH oxidases," *Free Radical Biology & Medicine*, vol. 51, no. 7, pp. 1289–1301, 2011.

[7] A. Szewczyk, W. Jarmuszkiewicz, A. Koziel et al., "Mitochondrial mechanisms of endothelial dysfunction," *Pharmacological Reports*, vol. 67, no. 4, pp. 704–710, 2015.

[8] E. Yu, J. Mercer, and M. Bennett, "Mitochondria in vascular disease," *Cardiovascular Research*, vol. 95, no. 2, pp. 173–182, 2012.

[9] C. Sandoval-Acuna, J. Ferreira, and H. Speisky, "Polyphenols and mitochondria: an update on their increasingly emerging ROS-scavenging independent actions," *Archives of Biochemistry and Biophysics*, vol. 559, pp. 75–90, 2014.

[10] S. Martin-Pelaez, M. I. Covas, M. Fito, A. Kusar, and I. Pravst, "Health effects of olive oil polyphenols: recent advances and possibilities for the use of health claims," *Molecular Nutrition & Food Research*, vol. 57, no. 5, pp. 760–771, 2013.

[11] P. Priore, A. Cavallo, A. Gnoni, F. Damiano, G. V. Gnoni, and L. Siculella, "Modulation of hepatic lipid metabolism by olive oil and its phenols in nonalcoholic fatty liver disease," *IUBMB Life*, vol. 67, no. 1, pp. 9–17, 2015.

[12] H. Zrelli, M. Matsuoka, S. Kitazaki et al., "Hydroxytyrosol induces proliferation and cytoprotection against oxidative injury in vascular endothelial cells: role of Nrf2 activation and HO-1 induction," *Journal of Agricultural and Food Chemistry*, vol. 59, no. 9, pp. 4473–4482, 2011.

[13] H. Zrelli, M. Matsuoka, S. Kitazaki, M. Zarrouk, and H. Miyazaki, "Hydroxytyrosol reduces intracellular reactive oxygen species levels in vascular endothelial cells by upregulating catalase expression through the AMPK–FOXO3a pathway," *European Journal of Pharmacology*, vol. 660, no. 2-3, pp. 275–282, 2011.

[14] L. Zhu, Z. Liu, Z. Feng et al., "Hydroxytyrosol protects against oxidative damage by simultaneous activation of mitochondrial biogenesis and phase II detoxifying enzyme systems in retinal pigment epithelial cells," *The Journal of Nutritional Biochemistry*, vol. 21, no. 11, pp. 1089–1098, 2010.

[15] J. S. Perona, R. Cabello-Moruno, and V. Ruiz-Gutierrez, "The role of virgin olive oil components in the modulation of endothelial function," *The Journal of Nutritional Biochemistry*, vol. 17, no. 7, pp. 429–445, 2006.

[16] C. E. Storniolo, J. Rosello-Catafau, X. Pinto, M. T. Mitjavila, and J. J. Moreno, "Polyphenol fraction of extra virgin olive oil protects against endothelial dysfunction induced by high glucose and free fatty acids through modulation of nitric oxide and endothelin-1," *Redox Biology*, vol. 2, pp. 971–977, 2014.

[17] S. Lamy, A. Ben Saad, A. Zgheib, and B. Annabi, "Olive oil compounds inhibit the paracrine regulation of TNF-α-induced endothelial cell migration through reduced glioblastoma cell cyclooxygenase-2 expression," *The Journal of Nutritional Biochemistry*, vol. 27, pp. 136–145, 2016.

[18] M. Dell'Agli, R. Fagnani, N. Mitro et al., "Minor components of olive oil modulate proatherogenic adhesion molecules involved in endothelial activation," *Journal of Agricultural and Food Chemistry*, vol. 54, no. 9, pp. 3259–3264, 2006.

[19] M. A. Carluccio, M. A. Ancora, M. Massaro et al., "Homocysteine induces VCAM-1 gene expression through NF-kappaB and NAD(P)H oxidase activation: protective role of Mediterranean diet polyphenolic antioxidants," *American Journal of Physiology Heart and Circulatory Physiology*, vol. 293, no. 4, pp. H2344–H2354, 2007.

[20] M. A. Carluccio, L. Siculella, M. A. Ancora et al., "Olive oil and red wine antioxidant polyphenols inhibit endothelial activation: antiatherogenic properties of Mediterranean diet phytochemicals," *Arteriosclerosis, Thrombosis, and Vascular Biology*, vol. 23, no. 4, pp. 622–629, 2003.

[21] E. Scoditti, N. Calabriso, M. Massaro et al., "Mediterranean diet polyphenols reduce inflammatory angiogenesis through MMP-9 and COX-2 inhibition in human vascular endothelial cells: a potentially protective mechanism in atherosclerotic vascular disease and cancer," *Archives of Biochemistry and Biophysics*, vol. 527, no. 2, pp. 81–89, 2012.

[22] N. Calabriso, M. Massaro, E. Scoditti et al., "Extra virgin olive oil rich in polyphenols modulates VEGF-induced angiogenic responses by preventing NADPH oxidase activity and expression," *The Journal of Nutritional Biochemistry*, vol. 28, pp. 19–29, 2016.

[23] A. Gomes, E. Fernandes, and J. L. Lima, "Fluorescence probes used for detection of reactive oxygen species," *Journal of Biochemical and Biophysical Methods*, vol. 65, no. 2-3, pp. 45–80, 2005.

[24] B. Kalyanaraman, V. Darley-Usmar, K. J. Davies et al., "Measuring reactive oxygen and nitrogen species with fluorescent probes: challenges and limitations," *Free Radical Biology & Medicine*, vol. 52, no. 1, pp. 1–6, 2012.

[25] K. M. Robinson, M. S. Janes, and J. S. Beckman, "The selective detection of mitochondrial superoxide by live cell imaging," *Nature Protocols*, vol. 3, no. 6, pp. 941–947, 2008.

[26] G. Nowak, "Protein kinase C-α and ERK1/2 mediate mitochondrial dysfunction, decreases in active Na$^+$ transport, and cisplatin-induced apoptosis in renal cells," *Journal of Biological Chemistry*, vol. 277, no. 45, pp. 43377–43388, 2002.

[27] V. Senatore, E. Cione, A. Gnoni, and G. Genchi, "Retinoylation reactions are inversely related to the cardiolipin level in testes mitochondria from hypothyroid rats," *Journal of Bioenergetics and Biomembranes*, vol. 42, no. 4, pp. 321–328, 2010.

[28] H. Esterbauer and K. H. Cheeseman, "Determination of aldehydic lipid peroxidation products: malonaldehyde and 4-hydroxynonenal," *Methods in Enzymology*, vol. 186, pp. 407–421, 1990.

[29] F. Taurino, C. Giannoccaro, A. M. Sardanelli et al., "Function and expression study uncovered hepatocyte plasma membrane ecto-ATP synthase as a novel player in liver regeneration," *Biochemical Journal*, vol. 473, no. 16, pp. 2519–2530, 2016.

[30] N. Calabriso, M. Massaro, E. Scoditti et al., "Red grape skin polyphenols blunt matrix metalloproteinase-2 and -9 activity and expression in cell models of vascular inflammation: protective role in degenerative and inflammatory diseases," *Molecules*, vol. 21, no. 12, 2016.

[31] S. Liekens, E. De Clercq, and J. Neyts, "Angiogenesis: regulators and clinical applications," *Biochemical Pharmacology*, vol. 61, no. 3, pp. 253–270, 2001.

[32] A. Ayala, M. F. Munoz, and S. Arguelles, "Lipid peroxidation: production, metabolism, and signaling mechanisms of malondialdehyde and 4-hydroxy-2-nonenal," *Oxidative Medicine and Cellular Longevity*, vol. 2014, Article ID 360438, 31 pages, 2014.

[33] L. Duluc, C. Jacques, R. Soleti, F. Iacobazzi, G. Simard, and R. Andriantsitohaina, "Modulation of mitochondrial capacity and angiogenesis by red wine polyphenols *via* estrogen receptor, NADPH oxidase and nitric oxide synthase pathways," *The International Journal of Biochemistry & Cell Biology*, vol. 45, no. 4, pp. 783–791, 2013.

[34] Y. W. Kim and T. V. Byzova, "Oxidative stress in angiogenesis and vascular disease," *Blood*, vol. 123, no. 5, pp. 625–631, 2014.

[35] M. Schieber and N. S. Chandel, "ROS function in redox signaling and oxidative stress," *Current Biology*, vol. 24, no. 10, pp. R453–R462, 2014.

[36] S. W. Ballinger, "Mitochondrial dysfunction in cardiovascular disease," *Free Radical Biology & Medicine*, vol. 38, no. 10, pp. 1278–1295, 2005.

[37] P. Puddu, G. M. Puddu, L. Galletti, E. Cravero, and A. Muscari, "Mitochondrial dysfunction as an initiating event in atherogenesis: a plausible hypothesis," *Cardiology*, vol. 103, no. 3, pp. 137–141, 2005.

[38] X. Q. Tang, Y. X. Luo, H. Z. Chen, and D. P. Liu, "Mitochondria, endothelial cell function, and vascular diseases," *Frontiers in Physiology*, vol. 5, 2014.

[39] P. Dromparis and E. D. Michelakis, "Mitochondria in vascular health and disease," *Annual Review of Physiology*, vol. 75, no. 1, pp. 95–126, 2013.

[40] H. K. Joo, Y. R. Lee, G. Kang et al., "The 18-kDa translocator protein inhibits vascular cell adhesion molecule-1 expression via inhibition of mitochondrial reactive oxygen species," *Molecules and Cells*, vol. 38, no. 12, pp. 1064–1070, 2015.

[41] A. Okado-Matsumoto and I. Fridovich, "Subcellular distribution of superoxide dismutases (SOD) in rat liver: Cu,Zn-SOD in mitochondria," *Journal of Biological Chemistry*, vol. 276, no. 42, pp. 38388–38393, 2001.

[42] D. X. Zhang and D. D. Gutterman, "Mitochondrial reactive oxygen species-mediated signaling in endothelial cells," *American Journal Physiology Heart and Circulatory Physiology*, vol. 292, no. 5, pp. H2023–H2031, 2007.

[43] R. Missiaen, F. Morales-Rodriguez, G. Eelen, and P. Carmeliet, "Targeting endothelial metabolism for anti-angiogenesis therapy: a pharmacological perspective," *Vascular Pharmacology*, vol. 90, pp. 8–18, 2017.

[44] R. C. Scarpulla, "Nuclear control of respiratory gene expression in mammalian cells," *Journal of Cellular Biochemistry*, vol. 97, no. 4, pp. 673–683, 2006.

[45] R. Mangiullo, A. Gnoni, F. Damiano et al., "3,5-diiodo-L-thyronine upregulates rat-liver mitochondrial F_oF_1-ATP synthase by GA-binding protein/nuclear respiratory factor-2," *Biochimica et Biophysica Acta (BBA) - Bioenergetics*, vol. 1797, no. 2, pp. 233–240, 2010.

[46] R. C. Scarpulla, "Metabolic control of mitochondrial biogenesis through the PGC-1 family regulatory network," *Biochimica et Biophysica Acta (BBA) - Molecular Cell Research*, vol. 1813, no. 7, pp. 1269–1278, 2011.

[47] I. S. Patten and Z. Arany, "PGC-1 coactivators in the cardiovascular system," *Trends in Endocrinology & Metabolism*, vol. 23, no. 2, pp. 90–97, 2012.

[48] T. Wenz, "Regulation of mitochondrial biogenesis and PGC-1α under cellular stress," *Mitochondrion*, vol. 13, no. 2, pp. 134–142, 2013.

[49] D. P. Kelly and R. C. Scarpulla, "Transcriptional regulatory circuits controlling mitochondrial biogenesis and function," *Genes & Development*, vol. 18, no. 4, pp. 357–368, 2004.

[50] A. Csiszar, N. Labinskyy, J. T. Pinto et al., "Resveratrol induces mitochondrial biogenesis in endothelial cells," *American Journal of Physiology Heart and Circulatory Physiology*, vol. 297, no. 1, pp. H13–H20, 2009.

[51] Z. Liu, L. Sun, L. Zhu et al., "Hydroxytyrosol protects retinal pigment epithelial cells from acrolein-induced oxidative stress and mitochondrial dysfunction," *Journal of Neurochemistry*, vol. 103, no. 6, pp. 2690–2700, 2007.

[52] J. Gao, X. Zou, L. Yang, Z. H. Feng, and J. K. Liu, "Hydroxytyrosol protects against acrolein induced preosteoblast cell toxicity: involvement of Nrf2/Keap1 pathway," *Journal of Functional Foods*, vol. 19, pp. 28–38, 2015.

[53] Z. Zheng, H. Chen, H. Wang et al., "Improvement of retinal vascular injury in diabetic rats by statins is associated with the inhibition of mitochondrial reactive oxygen species pathway mediated by peroxisome proliferator-activated receptor gamma coactivator 1alpha," *Diabetes*, vol. 59, no. 9, pp. 2315–2325, 2010.

[54] J. M. Santos, S. Tewari, A. F. Goldberg, and R. A. Kowluru, "Mitochondrial biogenesis and the development of diabetic retinopathy," *Free Radical Biology & Medicine*, vol. 51, no. 10, pp. 1849–1860, 2011.

[55] H. J. Kim, K. G. Park, E. K. Yoo et al., "Effects of PGC-1α on TNF-α-induced MCP-1 and VCAM-1 expression and NF-κB activation in human aortic smooth muscle and endothelial cells," *Antioxidants & Redox Signaling*, vol. 9, no. 3, pp. 301–307, 2007.

[56] S. Stein, C. Lohmann, C. Handschin et al., "ApoE−/− PGC-1α−/− mice display reduced IL-18 levels and do not develop enhanced atherosclerosis," *PLoS One*, vol. 5, no. 10, article e13539, 2010.

[57] S. Davinelli, N. Sapere, M. Visentin, D. Zella, and G. Scapagnini, "Enhancement of mitochondrial biogenesis with polyphenols: combined effects of resveratrol and equol in human endothelial cells," *Immunity & Ageing*, vol. 10, no. 1, p. 28, 2013.

[58] L. Duluc, C. Jacques, R. Soleti, R. Andriantsitohaina, and G. Simard, "Delphinidin inhibits VEGF induced-mitochondrial biogenesis and Akt activation in endothelial cells," *The International Journal of Biochemistry & Cell Biology*, vol. 53, pp. 9–14, 2014.

[59] S. S. Xing, X. Y. Yang, W. J. Li et al., "Salidroside stimulates mitochondrial biogenesis and protects against H_2O_2-induced endothelial dysfunction," *Oxidative Medicine and Cellular Longevity*, vol. 2014, Article ID 904834, 13 pages, 2014.

[60] M. I. Covas, K. de la Torre, M. Farre-Albaladejo et al., "Postprandial LDL phenolic content and LDL oxidation are modulated by olive oil phenolic compounds in humans," *Free Radical Biology & Medicine*, vol. 40, no. 4, pp. 608–616, 2006.

Research Article

Consumption of Cuban Policosanol Improves Blood Pressure and Lipid Profile via Enhancement of HDL Functionality in Healthy Women Subjects: Randomized, Double-Blinded, and Placebo-Controlled Study

Kyung-Hyun Cho [ID],[1,2,3] **Suk-Jeong Kim**,[1,2,3] **Dhananjay Yadav** [ID],[1,2,3] **Jae-Yong Kim**,[1] **and Jae-Ryong Kim**[4]

[1]Department of Medical Biotechnology, Yeungnam University, Gyeongsan 712-749, Republic of Korea
[2]Research Institute of Protein Sensor, Yeungnam University, Gyeongsan 712-749, Republic of Korea
[3]LipoLab, Yeungnam University, Gyeongsan 712-749, Republic of Korea
[4]Department of Biochemistry and Molecular Biology, Smart-Aging Convergence Research Center, College of Medicine, Yeungnam University, Daegu 705-717, Republic of Korea

Correspondence should be addressed to Kyung-Hyun Cho; chok@yu.ac.kr

Policosanol has been reported to improve blood pressure, lipid profile, and HDL functionality via inhibition of cholesteryl ester transfer protein (CETP) both *in vitro* and *in vivo* in zebrafish and human models. However, there are limited reports and randomized, double-blinded trials on policosanol that could advocate the blood pressure-lowering effect in prehypertensive participants. Therefore, we performed *in vitro*, *in vivo*, and ex vivo experiments to provide more substantial and concrete data on the blood pressure-lowering effect of policosanol. Consumption of policosanol for 8 weeks enhanced plasma antioxidant activity. In the policosanol group, plasma total cholesterol (TC) and triglyceride (TG) levels were reduced up to 20% and 14%, respectively, and HDL-C level was elevated up to 1.3-fold compared to that at week 0. TG/HDL-C and cholesteryl ester transfer protein (CETP) activities were reduced up to 36% and 20%, respectively. Uptake of oxidized LDL in macrophages was reduced as oxidized species levels were reduced, and HDL_2-associated paraoxonase activities were enhanced by 60% compared to those at week 0. Encapsulation of policosanol into reconstituted HDL (PCO-rHDL) enhanced cholesterol efflux activity and insulin secretion capacity. In conclusion, consumption of policosanol for 8 weeks in healthy female subjects resulted in lowered blood pressure and CETP activity via elevation of HDL/apoA-I contents and enhancement of HDL functionalities, including cholesterol efflux and insulin secretion. These functional enhancements of HDL can contribute to the prevention of aging-related diseases, hypertension, and stroke.

1. Introduction

It is well known that elevation of serum HDL-C levels is an effective strategy for suppressing the incidence of aging-related diseases such as cardiovascular disease (CVD), diabetes, and Alzheimer's disease [1]. In addition to HDL-C quantity, it has been firmly established that HDL quality and functionality are more important in the suppression of aging-related diseases [2]. However, there has been no strategy involving the use of dietary foods or medicines in the elevation of HDL-C quantity and enhancement of HDL functionality except for aerobic exercise [3]. As a functional food, Cuban policosanol (PCO) was reported to elevate HDL-C levels in hypercholesterolemic

rabbits and humans as well as reduce LDL-C levels and oxidation [4–6].

Policosanol enhances the beneficial functions of HDL and maximizes its antioxidant, antiglycation, and antiatherosclerotic activities along with inhibition of CETP activity [7–9]. These results suggest an association between policosanol activity and HDL functionality for enhancement of longevity. Reconstituted HDL (rHDL) containing policosanol (PCO-rHDL) was shown to induce upregulation of tissue regeneration activity in a zebrafish model [7] along with a lipid-lowering effect [8]. However, until now, the basic mechanism of policosanol has not been fully elucidated. One problematic hurdle preventing any investigation into the physiological functions of policosanol is its water insolubility in enzyme assay, cell-based assay, and *in vivo* animal systems. To overcome this, a policosanol mixture was assimilated into reconstituted HDL with apoA-I in order to investigate the physiological functions of policosanol in lipoprotein metabolism [7]. Policosanol in rHDL has potent antioxidant, antiglycation, and CETP inhibitory activities as well as tissue regeneration activity, especially upon integration into HDL. The physiological effect of policosanol was investigated in brain cells (neuroglioma) and hypercholesterolemic zebrafish. Nine weeks of policosanol consumption resulted in decreased serum TC and TG levels, increased HDL-C levels via CETP activity inhibition, and amelioration of fatty liver [8]. Kaup et al. previously reported that Egyptian rice bran extract, which is enriched with policosanol and γ-oryzanol, has an antidiabetic effect in rats [10].

We recently reported that daily consumption of policosanol by young smoker (YS, $n = 7$) and middle-aged male participants (MN, $n = 11$) for 8 weeks resulted in a lowering of systolic blood pressure up to 4%. The serum TG levels exhibited a reduction up to 28 and 26% from the baseline values in the young nonsmoker (YN, $n = 7$) and middle-aged participants. Nonetheless, the percentage of HDL-C in total cholesterol was elevated in all male participants (YN, 36%; YS, 35%; MN, 8%) after 8 weeks of policosanol consumption [9]. Nonetheless, our previous report was a pilot study in a different group of participants and needed a more specific data that may suggest the efficacy of policosanol on blood pressure. Moreover, the study lacks an appropriate control.

Although there have been many conflict data and arguments about the cholesterol-lowering efficacy of policosanol [11, 12], a recent meta-analysis [13] of randomized controlled trials from 22 studies including 1886 subjects concluded that policosanol could significantly reduce total cholesterol and LDL-C and increase HDL-C. In spite of many reports having examined the efficacy of policosanol in human subjects and animal models, there has been no *in vitro* or *in vivo* study on HDL functionality such as enhancement of cholesterol efflux and antioxidant ability with individually purified lipoprotein by sequential density gradient ultracentrifugation rather than concentration measured in the serum sample. Therefore, we tested the physiological effects of policosanol consumption on blood pressure and HDL functionality in healthy Korean female subjects.

2. Materials and Methods

2.1. Policosanol and Encapsulation. Policosanol tablet (10 mg) was obtained from Rainbow & Nature Pty, Ltd (Thornleigh, NSW, Australia). Policosanol (sugar cane wax alcohol, SCWA) contains several alcohol chains of various lengths. Contents of higher aliphatic alcohols were >90%. The individual alcohols present in policosanol are 1-tetracosanol ($C_{24}H_{49}OH$; molecular weight (MW): 354.7 mμ) ≤2%, 1-hexacosanol ($C_{26}H_{53}OH$; MW: 382.4 mμ) ≤4.5–10%, 1-heptacosanol ($C_{27}H_{55}OH$; MW: 396.4 mμ) ≤5%, 1-octacosanol ($C_{28}H_{57}OH$; MW: 410.5 mμ) ≤60–70%, 1-nonacosanol ($C_{29}H_{59}OH$; MW: 424.8 mμ) ≤2%, 1-triacontanol ($C_{30}H_{61}OH$; MW: 438.5 mμ) ≤10–15%, 1-dotriacontanol ($C_{32}H_{65}OH$; MW: 466.5 mμ) ≤3–8%, and 1-tetratriacontanol ($C_{34}H_{69}OH$; MW: 494.5 mμ) ≤2%.

To overcome the insolubility of policosanol in aqueous isotonic buffer, we synthesized rHDL-containing PCO (PCO-rHDL). A rHDL-containing policosanol was synthesized according to our previous report [7] by the sodium cholate dialysis method using initial molar ratios of 95 : 5 : 1 for POPC : cholesterol : apoA-I containing 0.5 μg, 2.5 μg, or 5 μg of policosanol.

2.2. Participants. We recruited healthy female volunteers who had prehypertension (systolic 120–139 mmHg, diastolic 80–89 mmHg). All volunteers were prescreened for eligibility for the following inclusion criteria: age 18–65 years who had prehypertension without any known endocrinological disorder. Heavy alcohol consumers (>30 g EtOH/day) and those who consumed any prescribed drugs for hyperlipidemia, diabetes mellitus, or hypertension were excluded. All subjects had unremarkable medical records without prohibited drug use or history of systemic diseases. On the first visit day, all participants casted dice for randomized grouping. The description of the study is shown in Figure 1, and the recruited participants consumed policosanol for 8 weeks. We analyzed serum parameters from all participants who consumed policosanol daily (10 mg tablet) or placebo for 8 weeks. Informed consent was obtained from all participants prior to commencement of the study, and the Institutional Review Board at Yeungnam University (Gyeongsan, South Korea) approved the protocol (IRB no. 7002016-A-2016-021).

2.3. Study Design. This study was a double-blinded, randomized, and placebo-controlled trial with 8-week treatment periods. Subjects were instructed to take one tablet containing policosanol (10 mg of sugar cane wax alcohol) or placebo consisting of a dextrin and lactose mixture, manufactured in Cosmax Bio Inc. (Jecheon, Korea), per day. Other ingredients to make tablet are corn starch, cellulose, gelatin, stearic acid, and so on. All ingredients, the manufacturing process, and the facility were approved by Korean FDA.

All participants were instructed to avoid excess alcohol drinking (less than 30 g of EtOH per day). They were also instructed to avoid vigorous exercise (less than 30 min per day at 60–80% maximum capacity). If subjects had a

Flow diagram of subjects include in the study
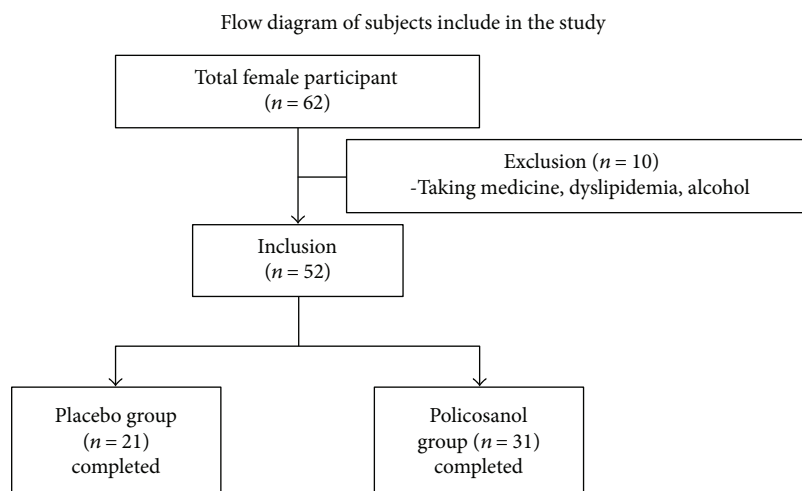
FIGURE 1: Design of study and participants. Inclusion criteria were normolipidemic, normoglycemic, and healthy subjects. Exclusion criteria were heavy alcohol drinkers (30 g > day of EtOH), patients with endocrinological disorders, and those taking hyperlipidemic medicine.

sedentary lifestyle before enrollment, we recommended them to maintain their lifestyle during the consumption period to avoid bias due to excess exercise.

2.4. Anthropometric Analysis. Height, body weight, body mass index (BMI), total body fat (%), total body fat mass (kg), and visceral fat mass (kg) of each participants were measured at the same time of the day at 4-week intervals using an X-Scan Plus II body composition analyzer (Jawon Medical, Gyeongsan, Korea).

2.5. Measurement of Blood Pressure. Blood pressure was measured each visit for three times, and the average was recorded at 4-week intervals using three methods. First, we used a digital blood pressure monitor (Omron HBP-9020, Kyoto, Japan). Second, a pulse wave analyzer, SphygmoCor system (AtCor Medical, Sydney, Australia), was used to measure brachial and aortic artery blood pressure. Third, a mercury sphygmomanometer was used for manual measurement by a licensed technician.

To diagnose hypertension, three different methods were employed in the current study to measure blood pressure based on the brachial and radial arteries. However, there exists a discrepancy in blood pressure measurement among these devices [14]. Instruments such as the Omron digital blood pressure device and mercury sphygmomanometer are commonly used in hospitals to estimate blood pressure. However, in epidemiological studies, focusing on central aortic blood pressure is advisable due to its various advantages over traditional blood pressure measurements. Aortic blood pressure is the pressure exerted on the heart and brain and is dissimilar to blood pressure in the limbs such as the arms. Central aortic blood pressure is more accurate and standardized for the diagnosis and management of hypertension compared to blood pressure measurements based on brachial arteries [15]. In comparing their predictive values for cardiovascular mortality, central blood pressure was shown to be better than brachial blood pressure [16]. Brown reported that measurement of blood pressure using

a mercury sphygmomanometer or Omron digital machine is based on the brachial artery, which has a structure that is reportedly unaffected by hypertension [17]. To overcome these limitations, this study used three different types of methods for measuring blood pressure.

2.6. Measurement of Augmentation Index and Augmentation Pressure. Augmentation index, which is the difference between the second and first systolic peaks expressed as a percentage of the pulse pressure, is a measure of systemic arterial stiffness and wave reflection, as described previously [18]. A licensed technician trained in the technique and blinded to the characteristics of each subject performed measurements of augmentation pressure and augmentation index.

2.7. Plasma Analysis. Blood was obtained from the subjects following overnight fasting. Blood was collected using a vacutainer (BD Biosciences, Franklin Lakes, NJ, USA) containing EDTA (final concentration of 1 mM) at weeks 0 and 8 during intake of policosanol. Plasma was isolated by low-speed centrifugation (3000g) and stored at −80°C until analysis. To analyze plasma, total cholesterol (TC), triglyceride (TG), high-density lipoprotein cholesterol (HDL-C), glucose, uric acid, aspartate aminotransferase (AST), and alanine aminotransferase (ALT) levels were measured using commercially available kits (Cleantech TS-S; Wako Pure Chemical, Osaka, Japan). Plasma aldosterone levels was measured by radioimmunoassay (RIA) using the instrument 1470-Gamma Counter (PerkinElmer) via Seegene Medical Foundation (Seoul, Korea).

2.8. Ferric Reducing Ability of Plasma Assay. The ferric reducing ability of plasma (FRAP) was determined using the method described by Benzie and Strain [19]. The antioxidant activities of individual HDL fractions (20 μg each in PBS) were estimated by measuring increases in absorbance induced by generated ferrous ions.

2.9. Characterization of Lipoproteins. Very low-density lipoprotein (VLDL, $d < 1.019$ g/mL), low-density lipoprotein

(LDL, $1.019 < d < 1.063$), high-density lipoprotein$_2$ (HDL$_2$, $1.063 < d < 1.125$), and high-density lipoprotein$_3$ (HDL$_3$, $1.125 < d < 1.225$) were isolated from the individual plasma of each group via sequential ultracentrifugation [20], and the density was adjusted by addition of NaCl and NaBr in accordance with standard protocols. Samples were centrifuged for 22 hr at 10°C and 100,000g using a Himac CP100NX (Hitachi, Tokyo, Japan) at the Instrumental Analysis Center of Yeungnam University. To measure lipoproteins, total cholesterol (TC) and triglyceride (TG) levels were analyzed using commercially available kits (Cleantech TS-S; Wako Pure Chemical, Osaka, Japan). Protein concentrations of lipoproteins were calculated via Lowry protein assay, as modified by Markwell et al. [21].

To estimate the degree of oxidation in lipoprotein, the concentration of oxidized species in lipoproteins was determined by the thiobarbituric acid reactive substance (TBARS) assay method using malondialdehyde as a standard [22]. To differentiate the extent of glycation between the groups, advanced glycation end products (AGEs) in lipoproteins were determined from reading fluorometric intensities at 370 nm (excitation) and 440 nm (emission), as described previously [23], using a spectrofluorometer LS55 (PerkinElmer, Shelton, CT, USA) with the WinLab software package (version 4.0).

2.10. Cholesteryl Ester Transfer Protein Assay. A rHDL-containing apoA-I and cholesteryl oleate were synthesized in accordance with the method described by Cho [24] using trace amounts of [^{3}H]-cholesteryl oleate (TRK886, 3.5 μCi/mg of apoA-I; GE Healthcare). Briefly, lipids (POPC, cold cholesteryl oleate, and [^{3}H]-cholesteryl oleate) were mixed in a glass vial and gently vortexed, followed by drying under a N$_2$ gas stream at 37°C. After drying, the lipids were dispersed by addition of TBS with slight agitation. Phospholipid bilayer formation was facilitated by addition of sodium cholate and apoA-I. After extensive dialysis for 24 hr to remove cholate, [^{3}H]-CE-rHDL was recovered and characterized by scintillation counting and protein determination.

[^{3}H]-CE-rHDL was immobilized using CNBr-activated Sepharose 4B resin (Amersham Biosciences) for easy separation after the reaction, in accordance with the manufacturer's instructions. CE transfer reaction was performed in 300 μL reaction mixtures containing human serum (20 μL) or HDL$_3$ (20 μL, 2 mg/mL) as a cholesteryl ester transfer protein (CETP) source, [^{3}H]-rHDL-agarose (20 μL, 0.25 mg/mL) as a CE donor, and human LDL (20 μL, 0.25 mg/mL) as a CE acceptor. After incubation at 37°C, the reaction was halted via brief centrifugation (10,000g) for 3 min at 4°C. The supernatant containing the CE acceptor (150 μL) was then subjected to scintillation counting, and percentage transfer of [^{3}H]-CE from [^{3}H]-rHDL to LDL was calculated.

2.11. Paraoxonase Assay. Paraoxonase-1 (PON-1) activity was determined by measuring the initial velocity of *p*-nitrophenol production at 37°C based on its absorbance at 405 nm (microplate reader, Bio-Rad model 680; Bio-Rad, Hercules, CA, USA), as described previously [25] with slight

modification [26]. Prior to the measurement, HDL was thoroughly dialyzed against PBS to eliminate EDTA.

2.12. LDL Oxidation. Oxidized LDL (oxLDL) was obtained by incubation of the LDL fraction with CuSO$_4$ (final concentration of 10 μM) for 4 hr at 37°C. oxLDL was then filtered through a 0.22 μm filter (Millex; Millipore, Bedford, MA) and measured by thiobarbituric acid reactive substances (TBARS) assay to determine the extent of oxidation [22].

2.13. Phagocytosis of LDL into Macrophages. THP-1 cells, a human monocytic cell line, were obtained from the American Type Culture Collection (ATCC, TIB-202™, Manassas, VA, USA) and maintained in RPMI 1640 medium (HyClone, Logan, UT) supplemented with 10% fetal bovine serum until needed. Cells below 20 passages were incubated in medium containing phorbol 12-myristate 13-acetate (PMA, 150 nM) in 24-well plates for 48 hr at 37°C in a humidified incubator (5% CO$_2$, 95% air) in order to induce differentiation into macrophages. Differentiated and adherent macrophages were then rinsed with warm PBS, followed by incubation with 450 μL of fresh RPMI 1640 medium containing 0.1% FBS and 50 μg of each LDL (1 mg of protein/mL in PBS) for 48 hr at 37°C in a humidified incubator. After incubation, cells were washed with PBS three times and then fixed in 4% paraformaldehyde for 10 min. Next, fixed cells were stained with Oil Red O staining solution (0.67%) and washed with distilled water. THP-1 macrophage-derived foam cells were then observed and photographed using a Nikon Eclipse TE2000 microscope (Tokyo, Japan) at 400x magnification, as in our previous report [27]. Cell medium (0.2 mL) was then analyzed by the TBARS assay to evaluate changes in the levels of oxidized species using a malondialdehyde (MDA) standard.

2.14. Antiatherogenic Activity of HDL$_3$. Differentiated and adherent macrophages were then washed with warm PBS and incubated with 400 μL of fresh RPMI 1640 medium containing 0.1% fetal bovine serum, 50 μg of oxLDL (1 mg of protein/mL in PBS), and 30 μg of HDL$_3$ (2 mg of protein/mL in PBS) from each group for 48 hr at 37°C in a humidified incubator. After incubation, cells were stained with Oil Red O solution (0.67%) to visualize the amount of lipid species in cells. THP-1 macrophage-derived foam cells were then observed and photographed using a Nikon Eclipse TE2000 microscope (Tokyo, Japan) at 400x magnification. Quantification area was carried out via computer-assisted morphometry using Image-Pro Plus software (version 4.5.1.22, Media Cybernetics, Bethesda, MD).

2.15. In Vitro Cholesterol Efflux. THP-1 cells were incubated in medium containing phorbol 12-myristate 13-acetate (PMA, 150 nM) on a plate for 48 hr at 37°C in a humidified incubator to induce differentiation into macrophages. The macrophages were treated with radiolabeled cholesterol (0.1 μCi of [^{3}H]-cholesterol) in RPMI 1640 medium (HyClone, Logan, UT) containing 1% fetal bovine serum (HyClone, Logan, UT) per well (0.5 mL) for 48 hr. The medium containing the isotope was saved and replaced with fresh media containing 0.3 mM 8-(4-chlorophenylthio)-

cyclic adenosine monophosphate (cAMP, Cat. No. C3912, Sigma-Aldrich, St. Louis, MO) for upregulation of cellular cholesterol pump (adenosine triphosphate- (ATP-) binding cassette (ABC) transporter-1, ABCA-1) for 18 hr. After removal of media containing cAMP, human HDL_3 (28 μg of apoA-I) or rHDL containing policosanol was added and incubated with serum-free media (0.5 mL) for 24 hr. Subsequently, the cell medium (0.5 mL) in individual wells was collected in a 1.7 mL tube. Cells were rinsed with PBS three times and dissolved in 0.2 mL of RIPA buffer (50 mM Tris-HCl [pH 8.0], 150 mM NaCl, 5 mM EDTA [pH 8.0], 1% NP-40, 0.5% sodium deoxycholate, and 0.1% sodium dodecyl sulfate) for cell lysis. An aliquot of the cell lysate (0.1 mL) was mixed with scintillation cocktail (3 mL) to quantify the isotope amount of cholesterol taken up into cells. After scintillation counting of [^{3}H]-cholesterol in cells and medium, the amount of effluxed cholesterol from cells was calculated using the following formula [28]:

$$\%Cholesterol\ efflux = \frac{(media\ counts \times dilution\ factor)}{(media\ count \times dilution\ factor) + (cell\ lysis\ count \times dilution\ factor)} \times 100,$$

$$\%Net\ efflux = \%cholesterol\ efflux\ (with\ HDL_3) - \%blank\ efflux\ (without\ HDL_3). \tag{1}$$

2.16. ELISA and Western Blot. To evaluate CETP activity in plasma, each well of a polystyrene microplate (no. 3590; Corning Inc., Corning, NY, USA) was coated with anti-human CETP rabbit antibody (ab19012; Abcam, Cambridge, UK) at a concentration of 0.25 μg/mL and incubated overnight at 4°C. Equally, diluted serum samples were incubated for 2 hr at room temperature. After extensive washing, anti-human CETP mouse antibody (ab2726; Abcam, 1 μg/mL) was treated and incubated for 2 hr at room temperature. To develop the color reaction, anti-mouse IgG antibody (ab6728; Abcam, 0.5 μg/mL conjugated with horseradish peroxidase) was added. For color development, 3,3′,5,5′ tetramethylbenzidine (TMB) substrate solution (Cat. No. 555214; BD Biosciences, Franklin Lakes, NJ, USA) was treated and quantified using a VICTOR X4 microplate reader (Perkin Elmer, Waltham, MA).

Apolipoprotein/lipoprotein constitution was compared via sodium dodecyl sulfate-polyacrylamide gel electrophoresis (SDS-PAGE) with identical protein loading quantities (5 μg of total protein per lane) from cell lysate via immunodetection. Anti-human apoA-I antibody (ab7613), anti-ABCA1 antibody (ab24261), and anti-GAPDH antibody (ab6672) were purchased from Abcam (Cambridge, UK). The relative band intensities were compared via band scanning using a Gel Doc® XR (Bio-Rad, Hercules, CA) with Quantity One software, version 4.5.2. We used simple basic steps to measure the band intensity by densitometry analysis. Blot images are imported into the Quantity One software, and then the contrast was adjusted in such a manner that the bands were clearly noticeable on the blot image. The area around each band was selected; further, the background intensity was subtracted from the blot image. The bands were then outlined by drawing a boundary around it; band intensities were exported in excel format for further analysis.

2.17. Insulin Secretion Assay. A rat insulinoma cell line (INS-1), kindly provided by K-C. Won (Department of Internal Medicine, College of Medicine, Yeungnam University), was maintained at 37°C in RPMI 1640 medium (Gibco BRL, Grand Island, NY, USA) containing 11.1 mmol/L of glucose and 2 mmol/L of L-glutamine. The medium was supplemented with 10% FBS, 1 mmol/L of pyruvate, 10 mmol/L of HEPES, 50 μmol/L of β-mercaptoethanol, 100 units/mL of penicillin, and 100 μg/mL of streptomycin (INS-1 medium), as in our previous report [29]. INS-1 cells were incubated at 37°C in the presence or absence of PCO-rHDL or plasma HDL. Incubations were carried out under low (final concentration of 2.8 mM) or high glucose concentration (final concentration of 25 mM) in culture medium, as previously reported [30]. After incubation, insulin secretion was determined using a radioimmunoassay kit (rat insulin RI-13K; Millipore, Billerica, MA, USA), according to the manufacturer's recommendation.

2.18. Electron Microscopy. Transmitted electron microscopy (TEM) was performed with a Hitachi electron microscope (model H-7600; Ibaraki, Japan) operated at 80 kV, as in our previous reports [31]. VLDL, LDL, and HDL were negatively stained with 1% sodium phosphotungstate (pH 7.4) with a final apolipoprotein concentration of 0.3 mg/mL in TBS.

2.19. Data Analysis. All data are expressed as the mean ± SD from the three independent experiments with duplicate samples. Data comparisons were carried out by Student's *t*-test using the SPSS program (version 14.0; SPSS Inc., Chicago, IL, USA). The differences between the means were assessed using Duncan's multiple-range test. Statistical significance was defined as $p < 0.05$.

3. Results

3.1. Changes in Body Composition. After 8 weeks of policosanol consumption, both groups had the same BMI. However, total body fat mass decreased up to 12% in the policosanol group, whereas the control group showed almost no change in body fat mass, as shown in Table 1. For fat distribution, visceral fat mass was reduced more than subcutaneous fat mass up to 20% in the policosanol group.

3.2. Blood Pressure. Based on the three measurements, the policosanol group showed significantly reduced average

TABLE 1: Change of blood pressure and plasma profile after 8 weeks consumption.

Age	Placebo (n = 21) 31 ± 16		Policosanol (n = 31) 31 ± 15	
	Week 0	Week 8	Week 0	Week 8
Body composition				
BMI	21 ± 3	21 ± 3	21 ± 4	21 ± 4
Total body fat (kg)	13.5 ± 3	13.1 ± 3	15.2 ± 4	13.8 ± 4*
Percentage of body fat (%)	24 ± 5	23 ± 6	25 ± 6	23 ± 5
Subcutaneous fat (kg)	11.9 ± 2.1	11.7 ± 2.4	13.6 ± 3.3	12.5 ± 3.0
Visceral fat (kg)	1.3 ± 0.4	1.4 ± 0.4	1.5 ± 0.5	1.2 ± 0.4*
Blood pressure (mmHg)				
SphygmoCor XCEL				
Systolic	133 ± 14	126 ± 8	131 ± 10	118 ± 14
Diastolic	87 ± 10	85 ± 8	82 ± 9	75 ± 7
Omron blood pressure monitor				
Systolic	131 ± 16	129 ± 9	130 ± 10	119 ± 8
Diastolic	86 ± 11	85 ± 7	83 ± 8	67 ± 7*
Mercury sphygmomanometer				
Systolic	131 ± 9	125 ± 8	129 ± 8	116 ± 12*
Diastolic	84 ± 6	83 ± 5	84 ± 8	72 ± 8*
Average blood pressure				
Systolic	132 ± 12	127 ± 7	130 ± 7	117 ± 14*
Diastolic	86 ± 9	84 ± 6	83 ± 8	72 ± 8*
Augmentation index (AI)	17 ± 3	16 ± 3	16 ± 3	7 ± 1*
Augmentation pressure (AP)	7 ± 1	5 ± 1	7 ± 2	2 ± 0*
Plasma profile				
TC (mg/dL)	195 ± 22	201 ± 21	180 ± 14	146 ± 10*
TG (mg/dL)	84 ± 17	92 ± 20	83 ± 16	72 ± 12*
HDL-C (mg/dL)	42 ± 3	45 ± 4	42 ± 4	53 ± 8**
%HDL-C	21 ± 3	22 ± 3	23 ± 2	36 ± 4**
TG/HDL-C	2.0 ± 0.6	2.1 ± 0.6	2.0 ± 0.2	1.4 ± 0.1*
Calculated LDL-C (mg/dL)	138 ± 22	137 ± 20	125 ± 11	81 ± 7*
Glucose (mg/dL)	87 ± 5	89 ± 5	91 ± 6	83 ± 5
CETP activity (% CE transfer)	38 ± 4	40 ± 4	39 ± 5	31 ± 4*
CETP amount (μg/mL)	1.9 ± 0.2	1.9 ± 0.2	2.0 ± 0.2	1.5 ± 0.1
Uric acid (mg/dL)	6.7 ± 1.4	6.5 ± 2.4	6.6 ± 0.8	5.3 ± 1.2*
Aldosterone (ng/dL)	19 ± 7	25 ± 8	38 ± 10	23 ± 6*

AU: arbitrary unit; BP: blood pressure; BMI: body mass index; CETP: cholesteryl ester transfer protein; HDL-C: high-density lipoprotein cholesterol; TC: total cholesterol; TG: triglyceride; *$p < 0.05$; versus 0–8 weeks in each group.

systolic and diastolic blood pressure levels up to 10% and 14%, respectively, whereas the control group showed similar blood pressure levels during 8 weeks of consumption. The policosanol group showed a significant reduction of augmentation index (AI) and augmentation pressure (AP) up to 57% and 72%, respectively, whereas the control group showed no change after consumption (Table 1).

3.3. *Plasma Lipid Profile and CETP Activity.* As shown in Table 1, the policosanol group showed 19% and 14% reductions in TC and TG levels, respectively, at week 8 compared with week 0, whereas the control group showed no difference. Plasma HDL-C level and percentage of HDL-C in TC were significantly elevated in the policosanol group up to 1.3-fold and 1.6-fold, respectively, compared with those at week 0. Furthermore, the calculated ratio of the TG/HDL-C level in the policosanol group was reduced to 1.4 after 8 weeks, whereas the control group showed no change (around 2.1). The calculated LDL-C level was also reduced in the policosanol group by 35%, whereas the control group showed no change. Before policosanol consumption (at week 0), all groups showed relatively high CETP activity (around 38%
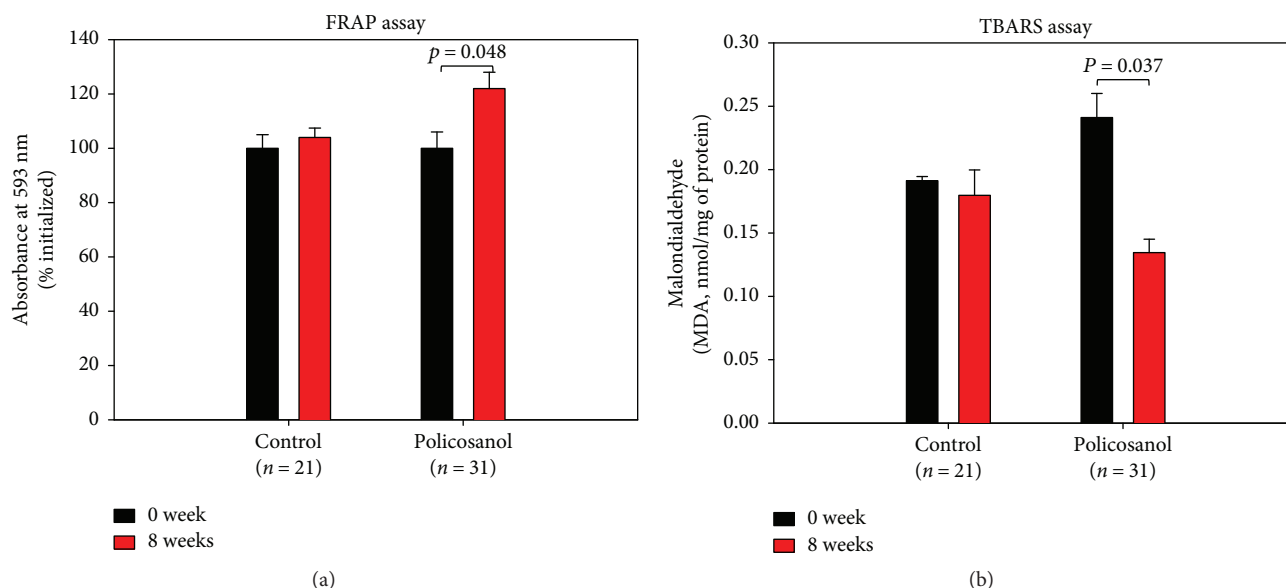
FIGURE 2: Changes in antioxidant ability and extent of oxidized species in serum upon policosanol consumption (bar represents the standard deviation of the mean). (a) Ferric ion reduction ability of serum (0.05 mL). (b) Determination of oxidized species using the thiobarbituric acid reactive substance method in serum (0.1 mL).

CE transfer). After 8 weeks, the policosanol group showed a significant reduction in CETP activity (around 31% CE transfer), whereas the control group showed no change. In addition, the serum CETP amount was reduced in the policosanol group up to 25% compared with that at week 0, whereas the placebo group showed no change. There was no significant change in glucose level in both groups from weeks 0 to 8. Uric acid and aldosterone levels were significantly reduced in the participants who consumed policosanol for 8 weeks (10 mg per day). However, there were no significant changes in uric acid and aldosterone in the placebo group after 8 weeks.

3.4. Serum Antioxidant Activity.
The ferric ion reduction ability of plasma was elevated by 22% in the policosanol group after 8 weeks of consumption, as shown in Figure 2(a), whereas the control group showed no difference over 8 weeks. Malondialdehyde content also significantly decreased up to 50% after 8 weeks of policosanol consumption compared with that at week 0 (Figure 2(b)). The serum uric acid level was reduced by 20% in the policosanol group after 8 weeks of consumption, whereas the control group showed no change (Table 1).

3.5. Antioxidative Extent of Lipoproteins.
After 8 weeks of policosanol consumption, LDL from the policosanol group showed slower electromobility following cupric ion-mediated oxidation and agarose electrophoresis, as shown in Figure 3(a), whereas LDL from the control group showed faster electromobility. Without cupric ion treatment, all LDL showed similar electromobility, although LDL from the policosanol group after 8 weeks showed the slowest electromobility suggesting less production of negatively charged molecules and less fragmentation of apoB in LDL. However, the oxidized LDL moved faster to the cathode position

because of the high negative charge and fragmentation of apoB (Figure 3(a)). Quantification of oxidized species using the TBARS method revealed that the policosanol group showed a significantly reduced malondialdehyde (MDA) content (up to 30% less) after 8 weeks, whereas the control group showed no change (Figure 3(b)). After policosanol consumption, PON activities for HDL_2 and HDL_3 in the policosanol group were elevated by 14% and 38%, respectively, compared to those of the control group, as shown in Figure 4.

3.6. Glycation Extent of Lipoproteins.
After 8 weeks of policosanol consumption, the policosanol group showed a significantly lowered glycation extent in all lipoprotein fractions, as shown in Figure 5(a). For VLDL and LDL, the policosanol group showed 43% and 39% less production of advanced glycation end products (AGEs) compared to the control group. For HDL_2 and HDL_3, the policosanol group showed 25% and 38% less production of AGEs, respectively, than the control group.

Protein content was detected in lipoprotein species, as shown in Figure 5(b). For VLDL, the policosanol group showed 20% less protein content than the control group did, whereas protein content in LDL was similar between the groups. However, protein contents in HDL_2 and HDL_3 increased in the policosanol group by 1.3- and 1.2-fold, respectively, compared to the control.

3.7. Enhanced Antiatherosclerotic Activity of HDL_3 in Policosanol Group.
As shown in Figures 6(a) and 6(b), oxLDL was easily taken up into macrophages, as evidenced by Oil Red O staining, and HDL_3 from the control group resulted in 30% inhibition of phagocytosis. Interestingly, HDL_3 from the policosanol group resulted in 70% reduction of phagocytosis, which was 2.4-fold greater than that of the control

(a)

(b)
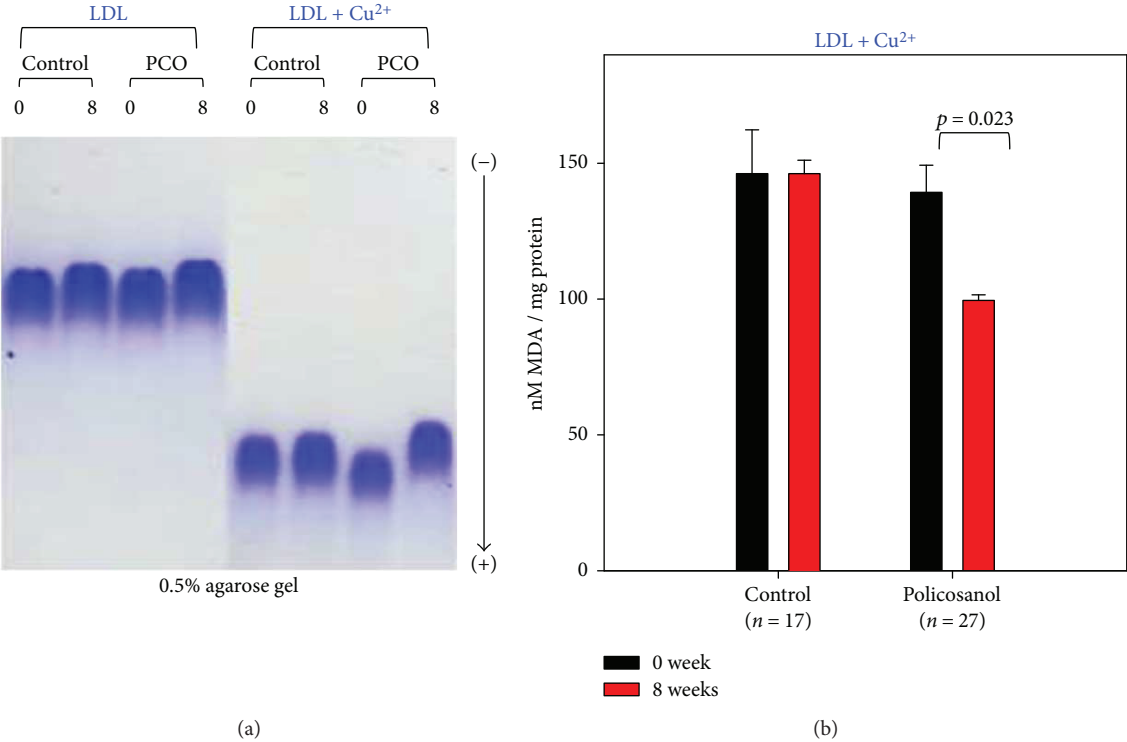
Figure 3: Comparison of LDL oxidation extent during policosanol consumption. (a) Comparison of electromobility of LDL between weeks 0 and 8 with or without cupric ion on a 0.5% agarose gel. (b) Determination of oxidized species using the thiobarbituric acid reactive substance method in LDL (1 mg of protein) in native state at weeks 0 and 8 (bar represents the standard deviation of the mean).

(a) HDL$_2$-PON

(b) HDL$_3$-PON
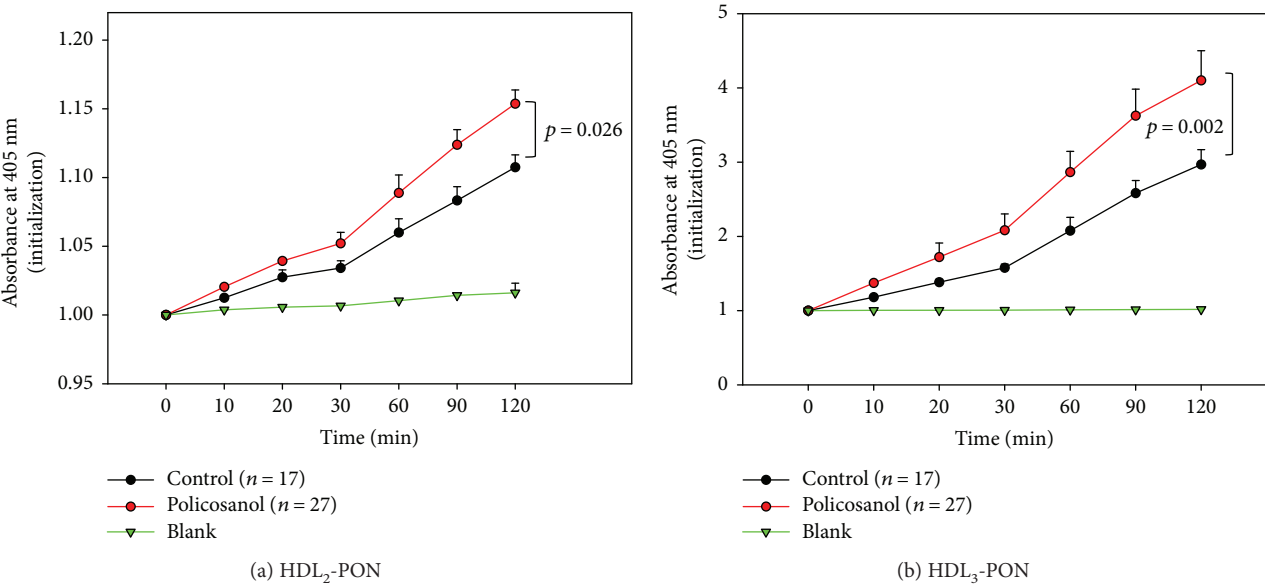
Figure 4: Changes in activity of paraoxonase in HDL at 8 weeks after policosanol consumption. Error bars indicate the SD from three independent experiments with duplicate samples. (a) Equally diluted HDL$_2$ (20 mL, 2 mg/mL) was added to 230 mL of paraoxon-ethyl (Sigma Cat. No. D-9286) containing solution (90 mM Tris-HCl/3.6 mM NaCl/2 mM CaCl$_2$ [pH 8.5]). (b) Equally diluted HDL$_3$ (20 mL, 2 mg/mL) was added to 230 mL of paraoxon-ethyl (Sigma Cat. No. D-9286) containing solution (90 mM Tris-HCl/3.6 mM NaCl/2 mM CaCl$_2$ (pH 8.5)) (bar represents the standard deviation of the mean).

group. Quantification of oxidized species in cell culture media showed that oxLDL treatment resulted in the highest level of MDA (around 4.5 μM) in media. HDL$_3$ from the

policosanol group resulted in the lowest MDA level (around 2.1 μM) in media, whereas control cells showed a 2.9 μM MDA level (Figure 6(c)).
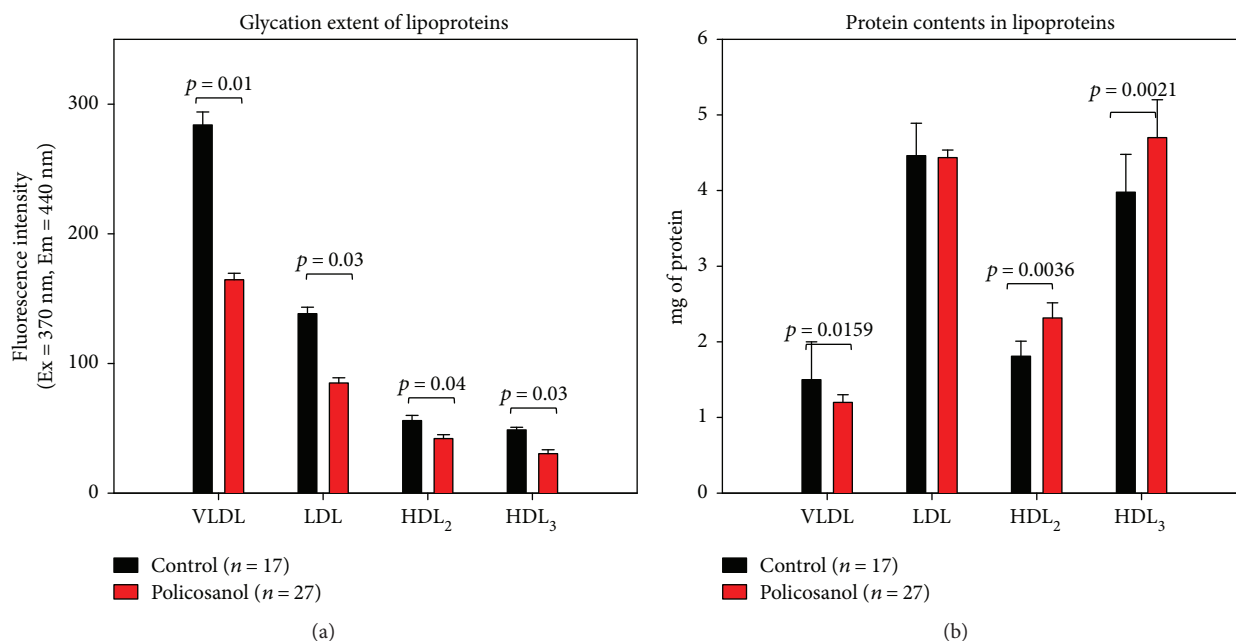
FIGURE 5: Glycation extent and total amounts of proteins in lipoproteins between groups after 8 weeks of policosanol consumption. (a) Fluorometric determination (Ex = 370 nm, Em = 440 nm) of glycation extent (bar represents the standard deviation). (b) Protein determination of individual lipoproteins (bar represents the standard deviation).

3.8. HDL Particle Size and Number. TEM image analysis revealed that the control and policosanol groups showed similar particle size after 8 weeks (photos of Figure 7). However, the particle number was significantly elevated up to 1.5-fold in the PCO group compared to the control group (graphs of Figure 7).

3.9. Insulin Secretion. Under basal and high glucose conditions (final concentrations of 2.8 and 25 mM in media), HDL_2 from the control group induced 5% and 8% insulin secretion over 8 weeks in rat insulinoma cells (INS-1), as shown in Figure 8. HDL_2 from the policosanol group caused a significant increase in insulin secretion under basal glucose and high glucose conditions compared to that at week 0.

HDL_3 from the policosanol group showed a significant enhancement of insulin secretion. In particular, HDL_3 from the policosanol group caused a 14% increase in secretion compared to that at week 0 under high glucose conditions. Additionally, HDL_3 from the policosanol group caused a 5% increase in secretion compared to that at week 0 under basal glucose conditions. Moreover, there was no significant difference observed in insulin secretion in control groups under basal and high glucose conditions.

3.10. Enhanced Cholesterol Efflux by rHDL-Containing Policosanol. As shown in Supplementary Figure 1A, cholesterol efflux activity increased from 24% to 29% as the policosanol content of rHDL significantly increased from 0.5 to 2.5 μg in the presence of the same amount of rHDL ($p = 0.03$, under 56 μg of apoA-I). Although there was no significant change ($p = 0.06$), 2.5 μg of policosanol in the presence of a lower amount of rHDL (28 μg of apoA-I) more strongly enhanced cholesterol efflux

activity than did 0.5 μg of policosanol in the same amount of rHDL (28 μg of apoA-I). However, 0.5 μg of policosanol adequately enhanced cholesterol efflux activity compared with apoA-I alone, and a greater amount of policosanol (2.5 μg) treatment resulted in a higher cholesterol efflux activity with the same amount of apoA-I in rHDL.

In addition to efflux activity, immunodetection revealed that uptake of apoA-I into macrophages was more facilitated (up to 60%) as policosanol content increased with the same amount of apoA-I regardless of cAMP treatment, as shown in Supplementary Figure 1B. The expression level of ABCA1 also increased up to 2-fold upon PCO-rHDL treatment, especially in the presence of cAMP, whereas GAPDH expression as a loading control (total 10 μg of protein from cell lysate) had no effect.

3.11. Improved Insulin Secretion by Policosanol. Rat INS-1 cells were incubated with rHDL-containing policosanol under basal (2.8 mM glucose in culture medium) and high glucose conditions (25 mM glucose). After 48 hr of incubation, rHDL-treated cells had insulin secretion levels of 20 ± 2 and 39 ± 4 ng/mL under basal and high glucose conditions, respectively (Supplementary Figure 2). In contrast, cells treated with PCO-rHDL containing 28 μg of apoA-I and policosanol (from 2.5 to 5 μg) showed elevated insulin secretion levels up to 90 and 98 ng/mL, respectively. Cells treated with PCO-rHDL containing 56 μg of apoA-I and policosanol (from 2.5 to 5 μg) showed elevated insulin secretion levels up to 116 and 127 ng/mL under basal and high glucose conditions, respectively. In the presence of the same amount of apoA-I, insulin secretion was elevated up to 1.4-fold depending on the policosanol content in rHDL (Supplementary Figure 2).

(a) THP-1 cell (oxLDL + HDL$_3$)

(b)

(c)
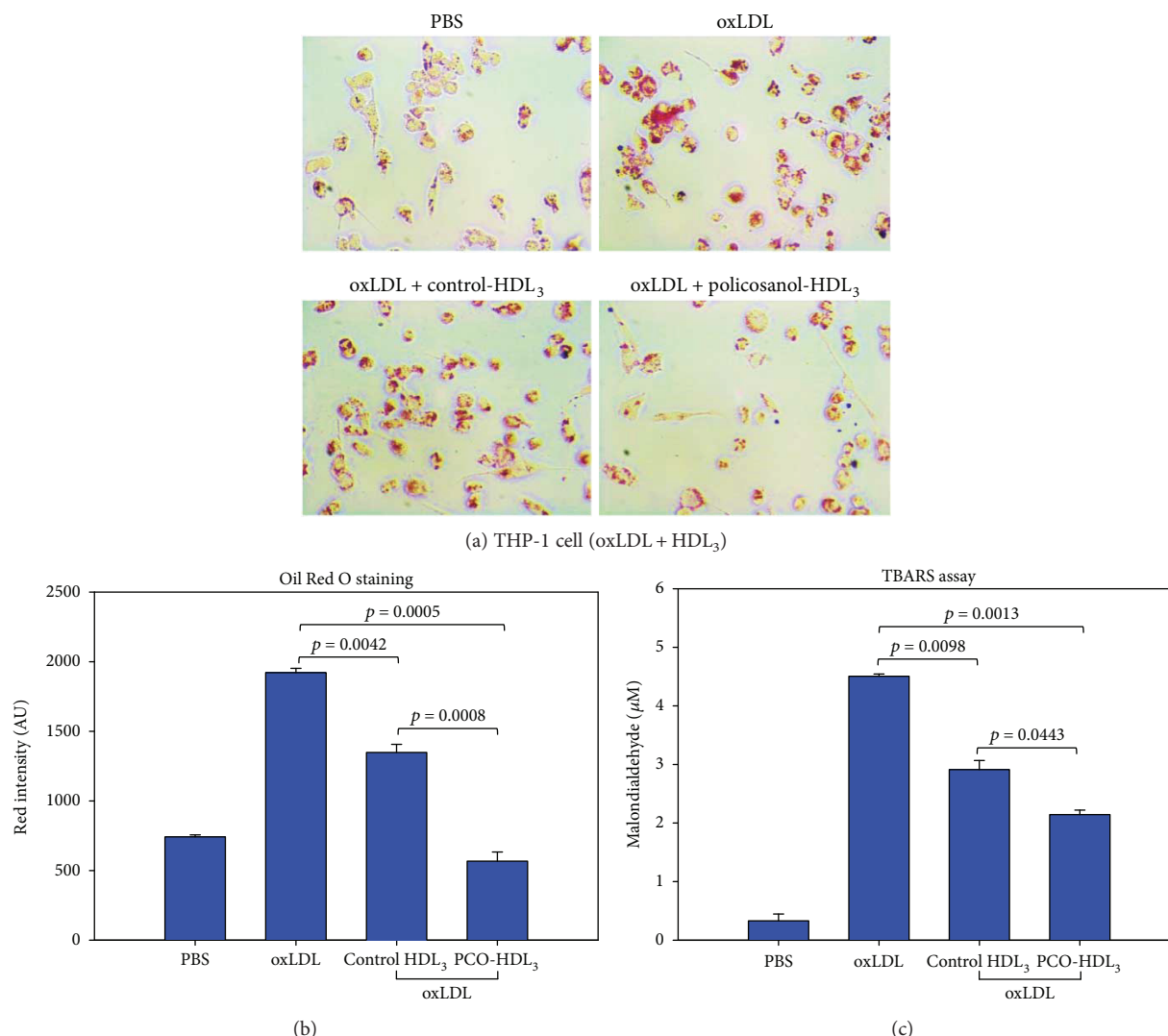
FIGURE 6: Comparison of oxLDL uptake into macrophages in the presence of HDL$_3$ from each group. (a) Inhibition of oxLDL phagocytosis by HDL from each group, as visualized by Oil Red O staining. (b) Quantification of Oil Red O-stained area by computer-assisted morphometry. (c) Quantification of oxidized species in cell culture media using the TBARS method.

4. Discussion

In the current study, 8 weeks of policosanol consumption resulted in a reduction in blood pressure and visceral fat amount in healthy female subjects with prehypertension. The lowering effects of policosanol on blood pressure were accompanied by lowering of serum total cholesterol and triglyceride levels as well as increased HDL-C levels via inhibition of serum CETP activity (Table 1). One of the interesting findings of this study is that policosanol could enhance cholesterol efflux in a dose-dependent manner by stimulating the expression of ABCA-1 (Supplementary Figure 1). Cholesterol efflux is a key feature of HDL that exerts regression activity via removal of cholesterol from atherosclerotic plaques in the reverse cholesterol transport pathway. It has been reported that efflux activity is mainly dependent on the configuration of apoA-I [32]. Therefore, the current finding shows that policosanol enhanced cholesterol efflux synergistically with apoA-I. It has been

suggested that the apoA-I configuration in discoidal HDL may be important for the recognition of cellular proteins as well as for interactions with specific lipid domains of the cell membrane. Our group previously reported that encapsulation of policosanol in rHDL caused a reduction in α-helix content in apoA-I along with an increased exposure of Trp residues [7]. These configurational changes might increase the affinity between apoA-I and the lipid domain of ABCA-1 for enhancement of cholesterol efflux.

Native apoA-I and HDL can stimulate insulin secretion [33] and exert antidiabetic activity, whereas modified apoA-I/HDL cannot. Native reconstituted HDL also displayed insulin secretion activity along with a wound-healing effect. Many studies on patients have reported that policosanol has efficacy in the treatment of hyperlipidemia, diabetes, and hypertension [34, 35], although the detailed molecular mechanism has not been elucidated. As there has been almost no study on the effects of policosanol on healthy subjects with hyperlipidemia and hypertension, this study

(a)

(b)

(c)
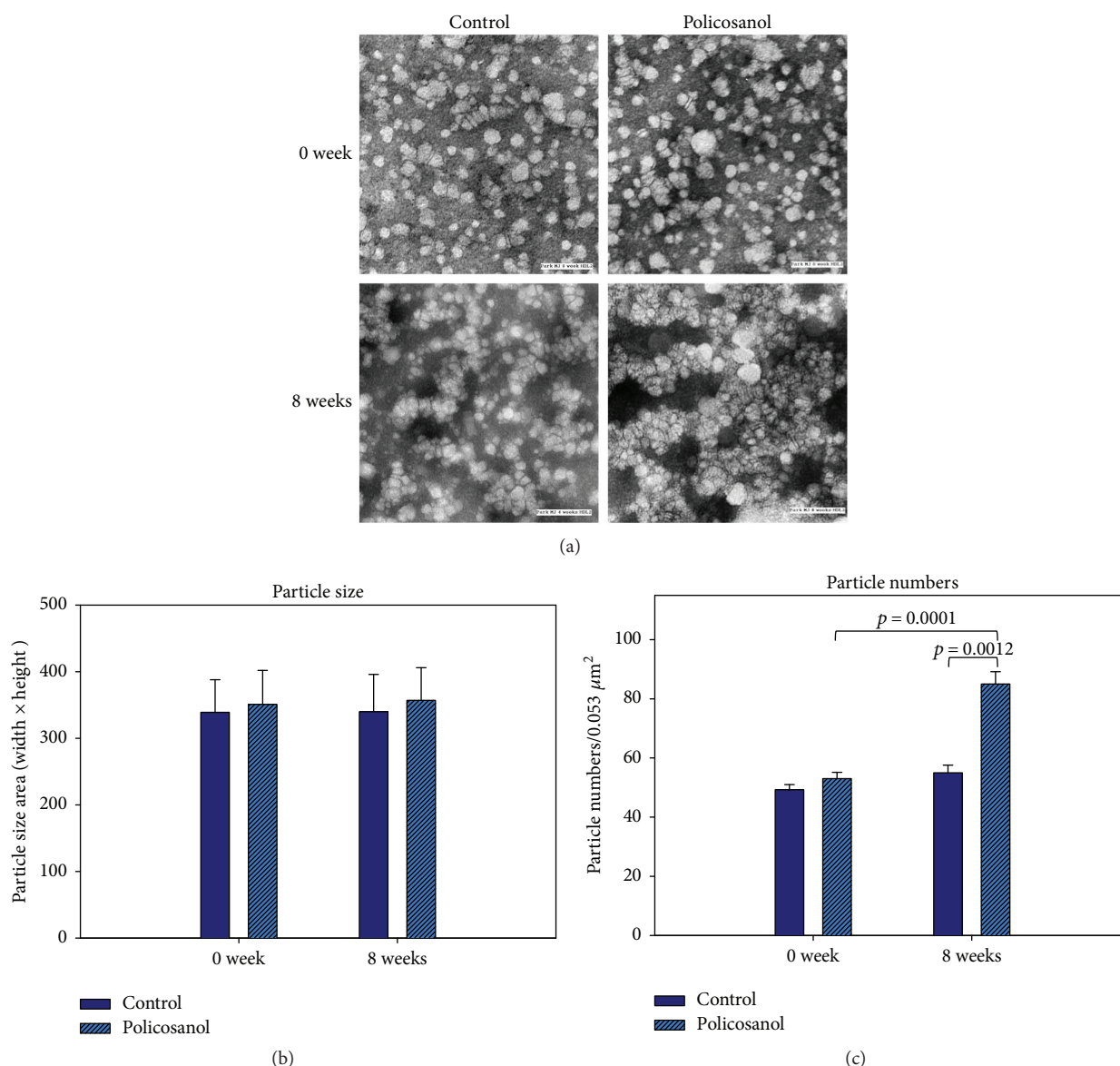
FIGURE 7: Electron microscopic observation of HDL_2. (a) Illustrative image of negatively stained high-density lipoprotein 2 (HDL2) from control and policosanol group (electron microscopy). All micrographs are shown at a magnification of 40,000x. Scale bar corresponds to 100 nm. (b) Graphs show measured width and length from 20 particles of HDL. (c) Histogram shows calculated particle numbers per $0.053\,\mu m^2$ area.

investigated the efficacy of policosanol in ordinary and healthy subjects with prehypertension.

A recent paper reported that hexacosanol reduces plasma and hepatic cholesterol by activation of adenosine $5'$-monophosphate- (AMP-) activated protein kinase (AMPK) and suppression of sterol regulatory element-binding protein-2 in HepG2 and C57BL/6J mice [36]. It has been well known that AMPK activation activities were correlated with increased export of cholesterol and excretion of cholesterol [37]. Recently, AMPK activation enhances anti-atherogenic effects of HDL with slightly lowering serum total cholesterol and body weight in $apoE^{-/-}$ mice [38]. Taken together, these papers make agreement that policosanol can enhance HDL functionality via AMPK activation and CETP inhibition.

CETP is an atherogenic factor, which is capable of degenerating HDL functionality and composition. Elevated CETP activity is associated with increased serum TG and TG-enriched LDL levels. We previously reported that policosanol can potently inhibit human CETP *in vitro* [7, 8], similar to MK-0859 (anacetrapib), a CETP inhibitor from Merck (Kenilworth, NJ, USA). Supplementation with policosanol was previously shown to cause significant reduction of CETP activity in zebrafish plasma [8] and human plasma, especially in young and middle-aged healthy male subjects [9]. In the current report, female subjects also showed significant reduction of CETP activity and amount (25%) in serum upon policosanol consumption. It has been well established that impairment of HDL functionality in patients with rheumatoid arthritis is associated with elevation of CETP activity
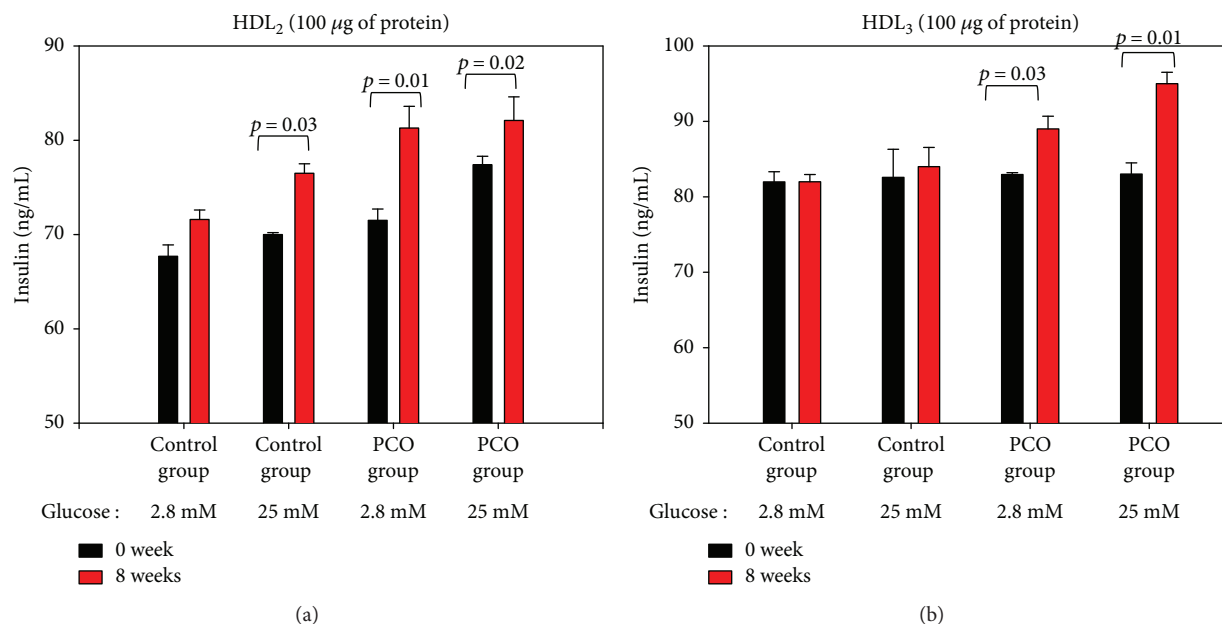
FIGURE 8: Insulin secretion activity of HDL from each group after 8 weeks of policosanol consumption. Rat insulinoma cells (INS-1) were incubated for 2 hr in the presence of HDL_2 and HDL_3 (final 100 μg of protein) at different glucose concentrations (final concentration of 2.8 or 25 mM in culture medium). Insulin levels in medium were quantified using a radioimmunoassay kit. Results are expressed as the mean ± standard deviation (SD) from three independent experiments with duplicate samples.

and expression, as in our recent report [39]. Especially in an autoimmune disease state, such as rheumatoid arthritis, arterial stiffness was shown to be positively correlated with elevation of CETP activity [40]. Furthermore, CETP inhibition might be connected to lower visceral fat and antiobesity effect. Since higher CETP activity explains lower HDL-C in obese subjects, it has been suggested that plasma CETP levels may be regulated by the degree of total body fat accumulation [41].

The lipid profile most associated with exacerbation of metabolic syndrome is high TG levels, whereas low HDL-C levels are associated with high risk of insulin resistance [42] and systemic inflammation due to high visceral fat mass [43]. Policosanol consumption reduced the TG/HDL-C ratio and visceral fat amount (Table 1). In the current study, reduction of serum TG level was correlated with reduction of visceral fat mass in the policosanol group, and a Taiwanese study revealed that the serum TG level independently contributes to visceral fat amount [44]. Reduction of serum TG level could cause reduction of visceral fat mass. Nonobese patients with polycystic ovary syndrome show significantly higher serum TG and lower HDL-C levels along with 1.7-fold increased visceral fat thickness [45] despite having normal BMI levels. It has been suggested that visceral fat thickness is negatively correlated with HDL-C level and positively correlated with serum TG level [46]. Further, the TG/HDL ratio can be a predictive marker for the success of antidiabetic medications following weight loss [47].

Systolic and diastolic blood pressures are positively correlated with visceral fat accumulation in premenopausal subjects [48]. These results are in good agreement with our previous report in which male subjects showed reduction of visceral fat mass and blood pressure after 8 weeks of policosanol

consumption [9]. Nevertheless, the previous report involved many limitations such as small sample size, weak study design (absence of randomized, double-blinded, and placebo-control), and diagnostic method of blood pressure.

Interestingly, antioxidant ability in plasma was elevated while oxidation of LDL was reduced upon policosanol consumption. PCO-rHDL also showed antioxidant ability against cupric ion treatment, as in our previous report [7, 8]. Resistance of LDL oxidation to cupric ion (Figure 3) is associated with enhancement of HDL-associated paraoxonase activity (Figure 4). Higher paraoxonase activity is also associated with protection of LDL oxidation from lipid peroxidation [49]. The glycation extent of each lipoprotein fraction was reduced by policosanol consumption (Figure 5(a)), although protein content was similar to or higher than that of the control. The antiglycation effect of policosanol consumption (Figure 5) is well correlated with our previous report [7] that PCO-rHDL shows an inhibitory effect *in vitro* against fructose-mediated glycation of HDL. The antiglycation effect is known to be associated with vasorelaxation via improvement of atrial stiffness since AGEs are a proven marker of CVD, diabetes, and hypertension [50]. From a study with Chinese subjects, plasma AGE concentration was found to be positively correlated with pulse wave velocity from the carotid to femoral arteries [51]. More interestingly, the serum TG level was elevated under conditions of high plasma AGE content.

Interestingly, HDL functionality and particle numbers were elevated by policosanol, which is a new finding since there are no agents known to enhance apoA-I expression and HDL quality except curcumin [52]. Although several nutraceuticals have been reported to induce lipid-lowering [53] and arterial hypertension [54], the beneficial

functions of lipid-free apoA-I and HDL can be impaired by oxidation and glycation, resulting in amyloid formation and aggregation [55, 56].

PCO-rHDL was taken up more by macrophages via upregulation of ABC-A1 (Supplementary Figure 1). Since dysfunction of ABCA1 is associated with a significant reduction in serum HDL levels, cholesterol efflux ability is positively correlated with apoA-I expression. A few angiotensin receptor blockers such as telmisartan and candesartan are known to interact with ABC transporters [57, 58]. Our current results suggest that policosanol might regulate the expression of apolipoproteins and transporters, which are involved in reverse cholesterol transport. Apart from the functionality of HDL-C and structural changes in lipoproteins, we determine the levels of uric acid and aldosterone levels in both groups. Previous studies have linked the elevation of these biomarkers in blood which may increase the risk of causing hypertension [59–61]. These reports suggested a plausible role of biomarker uric acid and aldosterone levels. Hence, we examine the concentration of these biomarkers before and after policosanol consumption. Our results have demonstrated that the levels of uric acid and aldosterone were significantly reduced after consumption of policosanol for 8 weeks. We did not find any significant difference in the levels of these biomarkers in the placebo group. Clinically, these results imply that enhancement of HDL functionality is well correlated with improvement of blood pressure and visceral fat mass. These results are in good agreement with our previous report in which male subjects showed a reduction of visceral fat mass and blood pressure after 8 weeks of policosanol consumption [9]. The novelty of this study was the study design, notably participant's number, use of placebo group, recruitment of prehypertensive participants (SBP 120–139 mmHg, DBP 80–89 mmHg), three devices used to measuring blood pressure, and homogenous data with a considerable time period of therapy of policosanol. Additionally, this study measured the important biomarkers such as renin and aldosterone, which are previously known parameters that could associate with increased risk of hypertension and CVD. Therefore, the study result could determine the appropriateness and authenticity with respect to the study design, recruitment, and number of participants used in this study.

5. Conclusions

The present study tested the effects of policosanol on biomarkers of HDL functionality, including cellular cholesterol efflux, insulin secretion, CETP activity, paraoxonase activity, and apoA-I level, after 8 weeks of policosanol consumption. Improvement of HDL functionality was associated with lowered blood pressure and inhibition of CETP activity in female prehypertension subjects.

Abbreviations

BP: blood pressure
BMI: body mass index
CETP: cholesteryl ester transfer protein
TC: total cholesterol
TG: triglyceride
TP: total protein
HDL-C: high-density lipoprotein-cholesterol
HDL: high-density lipoprotein
LDL: low-density lipoprotein
VLDL: very low-density lipoprotein.

Disclosure

An earlier version of the paper has been presented in the 6th International Congress on Lipid & Atherosclerosis (ICoLA 2017).

Conflicts of Interest

The authors declare no conflict of interests.

Authors' Contributions

Suk-Jeong Kim and Dhananjay Yadav performed the experiments. Jae-Yong Kim and Jae-Ryong Kim analyzed the data; Kyung-Hyun Cho wrote the manuscript and supervised all research for this study.

Acknowledgments

Supplementary Materials

Supplementary Figure 1: (A) cholesterol efflux activity of rHDL-containing apoA-I and policosanol. Macrophages were treated with radiolabeled cholesterol. The isotope amount of cholesterol taken up into cells was quantified, as detailed in the text; (B) immunodetection of apoA-I and ABCA-1 in cell lysate after treatment with rHDL. BI: band intensity. Supplementary Figure 2: insulin secretion activity of rHDL-containing policosanol. Rat insulinoma cells (INS-1) were incubated for 2 hr in the presence of rHDL with or without policosanol (final concentration of 2.5–5 mg in media) at different glucose concentrations (final concentration of 2.8 or 25 mM in culture medium). Insulin levels in medium were quantified using a radioimmunoassay kit. Results are expressed as the mean ± standard deviation (SD) from three independent experiments with duplicate samples. (Supplementary Materials)

References

[1] K.-A. Rye, C. A. Bursill, G. Lambert, F. Tabet, and P. J. Barter, "The metabolism and anti-atherogenic properties of HDL," Journal of Lipid Research, vol. 50, Supplement, pp. S195–S200, 2009.

[2] K.-H. Cho, "Biomedicinal implications of high-density lipoprotein: its composition, structure, functions, and clinical applications," *BMB Reports*, vol. 42, no. 7, pp. 393–400, 2009.

[3] S. Dragan, C. Serban, and M. Banach, "Can we change the functionality of HDL cholesterol with nonpharmacological and pharmacological agents?," *Current Medicinal Chemistry*, vol. 21, no. 25, pp. 2927–2946, 2014.

[4] I. Gouni-Berthold and H. K. Berthold, "Policosanol: clinical pharmacology and therapeutic significance of a new lipid-lowering agent," *American Heart Journal*, vol. 143, no. 2, pp. 356–365, 2002.

[5] S. Fernández, M. Rosa, R. Gamez et al., "A pharmacological surveillance study of the tolerability of policosanol in the elderly population," *The American Journal of Geriatric Pharmacotherapy*, vol. 2, no. 4, pp. 219–229, 2004.

[6] M. Janikula, "Policosanol: a new treatment for cardiovascular disease? (Policosanol)," *Alternative Medicine Review*, vol. 7, no. 3, pp. 203–217, 2002.

[7] S.-M. Lim, J.-A. Yoo, E.-Y. Lee, and K.-H. Cho, "Enhancement of high-density lipoprotein cholesterol functions by encapsulation of policosanol exerts anti-senescence and tissue regeneration effects via improvement of anti-glycation, anti-apoptosis, and cholesteryl ester transfer inhibition," *Rejuvenation Research*, vol. 19, no. 1, pp. 59–70, 2016.

[8] E.-Y. Lee, J.-A. Yoo, S.-M. Lim, and K.-H. Cho, "Anti-aging and tissue regeneration ability of policosanol along with lipid-lowering effect in hyperlipidemic zebrafish via enhancement of high-density lipoprotein functionality," *Rejuvenation Research*, vol. 19, no. 2, pp. 149–158, 2016.

[9] J.-Y. Kim, S.-M. Kim, S.-J. Kim, E.-Y. Lee, J.-R. Kim, and K.-H. Cho, "Consumption of policosanol enhances HDL functionality via CETP inhibition and reduces blood pressure and visceral fat in young and middle-aged subjects," *International Journal of Molecular Medicine*, vol. 39, no. 4, pp. 889–899, 2017.

[10] R. M. Kaup, M. T. Khayyal, and E. J. Verspohl, "Antidiabetic effects of a standardized Egyptian rice bran extract," *Phytotherapy Research*, vol. 27, no. 2, pp. 264–271, 2013.

[11] H. K. Berthold, S. Unverdorben, R. Degenhardt, M. Bulitta, and I. Gouni-Berthold, "Effect of policosanol on lipid levels among patients with hypercholesterolemia or combined hyperlipidemia: a randomized controlled trial," *JAMA*, vol. 295, no. 19, pp. 2262–2269, 2006.

[12] F. Francini-Pesenti, D. Beltramolli, S. Dall'Acqua, and F. Brocadello, "Effect of sugar cane policosanol on lipid profile in primary hypercholesterolemia," *Phytotherapy Research*, vol. 22, no. 3, pp. 318–322, 2008.

[13] J. Gong, X. Qin, F. Yuan et al., "Efficacy and safety of sugarcane policosanol on dyslipidemia: a meta-analysis of randomized controlled trials," *Molecular Nutrition & Food Research*, vol. 62, no. 1, 2018.

[14] W. Li, X. Wang, L. Lu, and H. Li, "Discrepancy of blood pressure between the brachial artery and radial artery," *World Journal of Emergency Medicine*, vol. 4, no. 4, pp. 294–297, 2013.

[15] J. E. Sharman and S. Laurent, "Central blood pressure in the management of hypertension: soon reaching the goal?," *Journal of Human Hypertension*, vol. 27, no. 7, pp. 405–411, 2013.

[16] S.-L. Chen, F.-F. Zhang, J. Xu et al., "Pulmonary artery denervation to treat pulmonary arterial hypertension: the single-center, prospective, first-in-man PADN-1 study (first-in-man pulmonary artery denervation for treatment of pulmonary artery hypertension)," *Journal of the American College of Cardiology*, vol. 62, no. 12, pp. 1092–1100, 2013.

[17] Yasmin and M. J. Brown, "Similarities and differences between augmentation index and pulse wave velocity in the assessment of arterial stiffness," *QJM*, vol. 92, no. 10, pp. 595–600, 1999.

[18] M. Butlin and A. Qasem, "Large artery stiffness assessment using SphygmoCor technology," *Pulse*, vol. 4, no. 4, pp. 180–192, 2017.

[19] I. F. F. Benzie and J. J. Strain, "The ferric reducing ability of plasma (FRAP) as a measure of "antioxidant power": the FRAP assay," *Analytical Biochemistry*, vol. 239, no. 1, pp. 70–76, 1996.

[20] R. J. Havel, H. A. Eder, and J. H. Bragdon, "The distribution and chemical composition of ultracentrifugally separated lipoproteins in human serum," *The Journal of Clinical Investigation*, vol. 34, no. 9, pp. 1345–1353, 1955.

[21] M. A. K. Markwell, S. M. Haas, L. L. Bieber, and N. E. Tolbert, "A modification of the Lowry procedure to simplify protein determination in membrane and lipoprotein samples," *Analytical Biochemistry*, vol. 87, no. 1, pp. 206–210, 1978.

[22] M. S. Blois, "Antioxidant determinations by the use of a stable free radical," *Nature*, vol. 181, no. 4617, pp. 1199-1200, 1958.

[23] J. D. McPherson, B. H. Shilton, and D. J. Walton, "Role of fructose in glycation and cross-linking of proteins," *Biochemistry*, vol. 27, no. 6, pp. 1901–1907, 1988.

[24] K.-H. Cho, "Synthesis of reconstituted high density lipoprotein (rHDL) containing apoA-I and apoC-III: the functional role of apoC-III in rHDL," *Molecules and Cells*, vol. 27, no. 3, pp. 291–297, 2009.

[25] H. W. Eckerson, C. M. Wyte, and B. La Du, "The human serum paraoxonase/arylesterase polymorphism," *American Journal of Human Genetics*, vol. 35, no. 6, pp. 1126–1138, 1983.

[26] K.-H. Park, D.-G. Shin, J.-R. Kim, J.-H. Hong, and K.-H. Cho, "The functional and compositional properties of lipoproteins are altered in patients with metabolic syndrome with increased cholesteryl ester transfer protein activity," *International Journal of Molecular Medicine*, vol. 25, no. 1, pp. 129–136, 2010.

[27] K.-H. Park, W. Jang, K.-Y. Kim, J.-R. Kim, and K.-H. Cho, "Fructated apolipoprotein A-I showed severe structural modification and loss of beneficial functions in lipid-free and lipid-bound state with acceleration of atherosclerosis and senescence," *Biochemical and Biophysical Research Communications*, vol. 392, no. 3, pp. 295–300, 2010.

[28] B. F. Asztalos, M. de la Llera-Moya, G. E. Dallal, K. V. Horvath, E. J. Schaefer, and G. H. Rothblat, "Differential effects of HDL subpopulations on cellular ABCA1- and SR-BI-mediated cholesterol efflux," *Journal of Lipid Research*, vol. 46, no. 10, pp. 2246–2253, 2005.

[29] K.-H. Park, J.-Y. Kim, I. Choi, J.-R. Kim, K. C. Won, and K.-H. Cho, "Fructated apolipoprotein A-I exacerbates cellular senescence in human umbilical vein endothelial cells accompanied by impaired insulin secretion activity and embryo toxicity," *Biochemistry and Cell Biology*, vol. 94, no. 4, pp. 337–345, 2016.

[30] J.-H. Yoon and K.-H. Cho, "A point mutant of apolipoprotein A-I (V156K) showed enhancement of cellular insulin secretion and potent activity of facultative regeneration in zebrafish," *Rejuvenation Research*, vol. 15, no. 3, pp. 313–321, 2012.

[31] H. H. Lee, J. E. Park, I. H. Choi, and K. H. Cho, "Enhanced functional and structural properties of high-density lipoproteins

from runners and wrestlers compared to throwers and lifters," *BMB Reports*, vol. 42, no. 9, pp. 605–610, 2009.

[32] L. Á. Cuellar, E. D. Prieto, L. V. Cabaleiro, and H. A. Garda, "Apolipoprotein A-I configuration and cell cholesterol efflux activity of discoidal lipoproteins depend on the reconstitution process," *Biochimica et Biophysica Acta (BBA) - Molecular and Cell Biology of Lipids*, vol. 1841, no. 1, pp. 180–189, 2014.

[33] A. von Eckardstein and C. Widmann, "High-density lipoprotein, beta cells, and diabetes," *Cardiovascular Research*, vol. 103, no. 3, pp. 384–394, 2014.

[34] O. Torres, A. J. Agramonte, J. Illnait, R. M. Ferreiro, L. Fernandez, and J. C. Fernandez, "Treatment of hypercholesterolemia in NIDDM with policosanol," *Diabetes Care*, vol. 18, no. 3, pp. 393–397, 1995.

[35] K. Xu, X. Liu, Y. Li et al., "Safety and efficacy of policosanol in patients with high on-treatment platelet reactivity after drug-eluting stent implantation: two-year follow-up results," *Cardiovascular Therapeutics*, vol. 34, no. 5, pp. 337–342, 2016.

[36] J. H. Lee, Y. Jia, T. T. Thach et al., "Hexacosanol reduces plasma and hepatic cholesterol by activation of AMP-activated protein kinase and suppression of sterol regulatory element-binding protein-2 in HepG2 and C57BL/6J mice," *Nutrition Research*, vol. 43, pp. 89–99, 2017.

[37] M. D. Fullerton, R. J. Ford, C. P. McGregor et al., "Salicylate improves macrophage cholesterol homeostasis via activation of Ampk," *Journal of Lipid Research*, vol. 56, no. 5, pp. 1025–1033, 2015.

[38] A. Ma, J. Wang, L. Yang, Y. An, and H. Zhu, "AMPK activation enhances the anti-atherogenic effects of high density lipoproteins in apoE$^{-/-}$ mice," *Journal of Lipid Research*, vol. 58, no. 8, pp. 1536–1547, 2017.

[39] J.-Y. Kim, E.-Y. Lee, J. K. Park, Y. W. Song, J.-R. Kim, and K.-H. Cho, "Patients with rheumatoid arthritis show altered lipoprotein profiles with dysfunctional high-density lipoproteins that can exacerbate inflammatory and atherogenic process," *PLoS One*, vol. 11, no. 10, article e0164564, 2016.

[40] E. Botta, T. Meroño, C. Saucedo et al., "Associations between disease activity, markers of HDL functionality and arterial stiffness in patients with rheumatoid arthritis," *Atherosclerosis*, vol. 251, pp. 438–444, 2016.

[41] T. Arai, S. Yamashita, K.-i. Hirano et al., "Increased plasma cholesteryl ester transfer protein in obese subjects. A possible mechanism for the reduction of serum HDL cholesterol levels in obesity," *Arteriosclerosis, Thrombosis, and Vascular Biology*, vol. 14, no. 7, pp. 1129–1136, 1994.

[42] M. Zhou, L. Zhu, X. Cui et al., "The triglyceride to high-density lipoprotein cholesterol (TG/HDL-C) ratio as a predictor of insulin resistance but not of β cell function in a Chinese population with different glucose tolerance status," *Lipids in Health and Disease*, vol. 15, no. 1, p. 104, 2016.

[43] L. Catrysse and G. van Loo, "Inflammation and the metabolic syndrome: the tissue-specific functions of NF-κB," *Trends in Cell Biology*, vol. 27, no. 6, pp. 417–429, 2017.

[44] C. Y. Huang, H. L. Huang, K. C. Yang et al., "Serum triglyceride levels independently contribute to the estimation of visceral fat amount among nondiabetic obese adults," *Medicine*, vol. 94, no. 23, article e965, 2015.

[45] B. Yildirim, N. Sabir, and B. Kaleli, "Relation of intra-abdominal fat distribution to metabolic disorders in nonobese patients with polycystic ovary syndrome," *Fertility and Sterility*, vol. 79, no. 6, pp. 1358–1364, 2003.

[46] Y. Matsuzawa, I. Shimomura, T. Nakamura, Y. Keno, K. Kotani, and K. Tokunaga, "Pathophysiology and pathogenesis of visceral fat obesity," *Obesity Research*, vol. 3, no. S2, pp. 187s–194s, 1995.

[47] G. P. S. Shantha, A. A. Kumar, S. Kahan, P. K. Irukulla, and L. J. Cheskin, "Triglyceride/HDL ratio as a screening tool for predicting success at reducing anti-diabetic medications following weight loss," *PLoS One*, vol. 8, no. 7, article e69285, 2013.

[48] H. Kanai, Y. Matsuzawa, K. Kotani et al., "Close correlation of intra-abdominal fat accumulation to hypertension in obese women," *Hypertension*, vol. 16, no. 5, pp. 484–490, 1990.

[49] K. R. Feingold and C. Grunfeld, "Effect of inflammation on HDL structure and function," *Current Opinion in Lipidology*, vol. 27, no. 5, pp. 521–530, 2016.

[50] M. McNulty, A. Mahmud, and J. Feely, "Advanced glycation end-products and arterial stiffness in hypertension," *American Journal of Hypertension*, vol. 20, no. 3, pp. 242–247, 2007.

[51] C. Y. Liu, Q. F. Huang, Y. B. Cheng et al., "A comparative study on skin and plasma advanced glycation end products and their associations with arterial stiffness," *Pulse*, vol. 4, no. 4, pp. 208–218, 2017.

[52] S. Ganjali, C. N. Blesso, M. Banach, M. Pirro, M. Majeed, and A. Sahebkar, "Effects of curcumin on HDL functionality," *Pharmacological Research*, vol. 119, pp. 208–218, 2017.

[53] A. F. G. Cicero, A. Colletti, G. Bajraktari et al., "Lipid-lowering nutraceuticals in clinical practice: position paper from an International Lipid Expert Panel," *Nutrition Reviews*, vol. 75, no. 9, pp. 731–767, 2017.

[54] C. Serban, A. Sahebkar, S. Ursoniu, F. Andrica, and M. Banach, "Effect of sour tea (Hibiscus sabdariffa L.) on arterial hypertension: a systematic review and meta-analysis of randomized controlled trials," *Journal of Hypertension*, vol. 33, no. 6, pp. 1119–1127, 2015.

[55] C. L. Teoh, M. D. W. Griffin, and G. J. Howlett, "Apolipoproteins and amyloid fibril formation in atherosclerosis," *Protein & Cell*, vol. 2, no. 2, pp. 116–127, 2011.

[56] M. Das, C. J. Wilson, X. Mei, T. E. Wales, J. R. Engen, and O. Gursky, "Structural stability and local dynamics in disease-causing mutants of human apolipoprotein A-I: what makes the protein amyloidogenic?," *Journal of Molecular Biology*, vol. 428, no. 2, pp. 449–462, 2016.

[57] N. Ishiguro, K. Maeda, A. Saito et al., "Establishment of a set of double transfectants coexpressing organic anion transporting polypeptide 1B3 and hepatic efflux transporters for the characterization of the hepatobiliary transport of telmisartan acylglucuronide," *Drug Metabolism and Disposition*, vol. 36, no. 4, pp. 796–805, 2008.

[58] J. Weiss, A. Sauer, N. Divac et al., "Interaction of angiotensin receptor type 1 blockers with ATP-binding cassette transporters," *Biopharmaceutics & Drug Disposition*, vol. 31, no. 2-3, pp. 150–161, 2010.

[59] T. S. Perlstein, O. Gumieniak, G. H. Williams et al., "Uric acid and the development of hypertension: the normative aging study," *Hypertension*, vol. 48, no. 6, pp. 1031–1036, 2006.

[60] I. Saito, T. Saruta, K. Kondo et al., "Serum uric acid and the renin-angiotensin system in hypertension," *Journal of the American Geriatrics Society*, vol. 26, no. 6, pp. 241–247, 1978.

[61] V. Xanthakis and R. S. Vasan, "Aldosterone and the risk of hypertension," *Current Hypertension Reports*, vol. 15, no. 2, pp. 102–107, 2013.

Research Article

Inhibition of TRPA1 Attenuates Doxorubicin-Induced Acute Cardiotoxicity by Suppressing Oxidative Stress, the Inflammatory Response, and Endoplasmic Reticulum Stress

Zhen Wang,[1,2,3] **Menglong Wang,**[1,2,3] **Jianfang Liu,**[1,2,3] **Jing Ye,**[1,2,3] **Huimin Jiang,**[1,2,3] **Yao Xu,**[1,2,3] **Di Ye,**[1,2,3] **and Jun Wan** [ID][1,2,3]

[1]*Department of Cardiology, Renmin Hospital of Wuhan University, Wuhan 430060, China*
[2]*Cardiovascular Research Institute, Wuhan University, Wuhan 430060, China*
[3]*Hubei Key Laboratory of Cardiology, Wuhan 430060, China*

Correspondence should be addressed to Jun Wan; wanjun1963@126.com

The transient receptor potential ankyrin 1 (TRPA1) channel is expressed in cardiomyocytes and involved in many cardiovascular diseases. However, the expression and function of TRPA1 in doxorubicin- (Dox-) induced acute cardiotoxicity have not been elucidated. This study aimed at investigating whether blocking the TRPA1 channel with the specific inhibitor HC-030031 (HC) attenuates Dox-induced cardiac injury. The animals were randomly divided into four groups: control, HC, Dox, and Dox + HC. Echocardiography was used to evaluate cardiac function, and the heart was removed for molecular experiments. The results showed that the expression of TRPA1 was increased in the heart after Dox treatment. Cardiac dysfunction and increased serum CK-MB and LDH levels were induced by Dox, but these effects were attenuated by HC treatment. In addition, HC mitigated Dox-induced oxidative stress, as evidenced by the decreased MDA level and increased GSH level and SOD activity in the Dox + HC group. Meanwhile, HC treatment lowered the levels of the proinflammatory cytokines IL-1β, IL-6, IL-17, and TNF-α induced by Dox. Furthermore, HC treatment mitigated endoplasmic reticulum (ER) stress and cardiomyocyte apoptosis induced by Dox. These results indicated that inhibition of TRPA1 could prevent Dox-induced cardiomyocyte apoptosis in mice by inhibiting oxidative stress, inflammation, and ER stress.

1. Introduction

Doxorubicin (Dox), an anthracycline anticancer drug, is one of the most preferred agents for the treatment of different malignant tumors, including leukemia, lymphomas, breast cancer, and ovarian cancer. However, its application is hampered due to a significant dose-dependent cardiotoxicity manifested by cardiomyopathy and congestive heart failure [1, 2]. A recent study reported that 21% of patients developed chemotherapy-related cardiotoxicity after Dox administration [3]. Therefore, considerable efforts have been made to identify an effective therapeutic target for mitigating Dox-induced cardiac damage.

Transient receptor potential (TRP) channels are nonselective cation channels that mediate sensory transduction and respond to various stimuli. The 28 mammalian TRP channels can be grouped into six subfamilies based on sequence homology. Among them, TRPA1 is predominantly expressed in nociceptive neurons and is also expressed at high levels in the heart, lung, skeletal muscle, skin, and vascular endothelial cells [4, 5]. It is well established that oxidative stress metabolites, such as reactive oxygen species (ROS) and specific metabolites of lipid peroxidation, are endogenous agonists of TRPA1 [6]. Takahashi et al. demonstrated that TRPA1 directly detects molecular oxygen and plays a pivotal role in maintaining oxygen homeostasis [7].

In addition, mounting evidence suggests that TRPA1 may be a key gatekeeper in detecting stimuli and regulating the inflammatory response [8, 9].

Accumulating evidence indicates the important role of TRPA1 in the pathophysiology of cardiac disease [10]. TRPA1 activators given prophylactically could reduce the infarct size in a rat model of myocardial ischemia-reperfusion injury [11]. However, the role of TRPA1 in Dox-induced cardiotoxicity is still unknown. In the present study, we clearly show that the inhibition of TRPA1 ameliorated Dox-induced cardiomyocyte apoptosis and cardiac dysfunction, which correlated with decreases in oxidative stress products, proinflammatory cytokine levels, and endoplasmic reticulum (ER) stress.

2. Materials and Methods

2.1. Animals. All procedures involving animals were conducted in compliance with the National Institutes of Health (NIH) Guide for the Care and Use of Laboratory Animals and were approved by the Ethics Committee for Animal Research of Wuhan University (Wuhan, China). Male C57BL/6J mice, aged 6–8 weeks and weighing 23–25 g, were obtained from Vital River Laboratory Animal Technology Co. Ltd. (Beijing, China). Mice were acclimatized for 7 days before assignment to their experimental groups and housed in a light-controlled room (12 h light/dark cycle) with free access to standard chow and water. The animals ($n = 80$) were randomly divided into four treatment groups of 20 mice each: control (CTRL), HC-030031 (HC), Dox, and Dox + HC. The CTRL and HC alone groups received an equivalent volume of placebo or HC orally for ten consecutive days. Dox-treated mice were injected with a single dose of Dox dissolved in normal saline (20 mg/kg i.p.) at day 5. Mice in the Dox + HC group were pretreated with HC (10 mg/kg) for 5 days by gavage and then treated for 5 additional days after the injection of Dox.

2.2. Echocardiography. Echocardiography was performed in anesthetized (1.5–2% isoflurane) mice using a Mylab30CV ultrasound (Biosound Esaote Inc.) equipped with a 10 MHz linear array ultrasound transducer. The left ventricle (LV) was assessed in both parasternal long-axis and short-axis views. End-systole and end-diastole were defined as the phases in which the smallest and largest areas of the LV were obtained, respectively. LV ejection fraction (EF) and LV fractional shortening (FS) were measured via LV M-mode tracing with a sweep speed of 50 mm/s at the midpapillary muscle level.

2.3. Biochemical Determination. Blood was collected, and the serum was separated by centrifugation. Serum concentrations of creatine kinase isoenzymes (CK-MB) and lactate dehydrogenase (LDH) in different treatment groups were measured by an automatic biochemical analyzer (ADVIA® 2400, Siemens Ltd., China).

2.4. Oxidative Stress Detection. At the end of the experiment, the cardiac tissues were removed and washed in ice-cold phosphate-buffered saline. The cardiac tissues (30 mg) were added to 300 μl of phosphate-buffered saline, ground into homogenates, and centrifuged at 3000 rpm at 4°C for 15 min to collect the supernatant. The activities of superoxide dismutase 1 (SOD) and the content of malondialdehyde (MDA) and glutathione (GSH) were detected by commercially available kits purchased from Nanjing Jiancheng Bioengineering Institute (Nanjing, China).

2.5. Histological Analysis. Hearts were arrested in diastole with 10% potassium chloride solution, fixed by perfusion with 10% paraformaldehyde, and embedded in paraffin. Subsequently, heart paraffin blocks were transversely sectioned at 4-5 μm, stained with hematoxylin, and eosin (H&E) for histopathology, and then visualized by light microscopy.

2.6. Western Blot. Protein was extracted from left ventricular tissue, and the protein concentration was assessed using a BCA protein assay kit (23,227, Thermo Fisher Scientific, Waltham, MA, USA). Protein (50 μg) was separated by 10% sodium dodecyl sulfate-polyacrylamide gel electrophoresis (SDS-PAGE), transferred onto polyvinylidene fluoride membranes (IPFL00010, Millipore, Billerica, MA, USA), and incubated with different primary antibodies. The following primary antibodies were used: TRPA1 (1 : 1000 dilution, NOVUS), GAPDH (1 : 1000 dilution, Cell Signaling Technology), cleaved caspase-3 (1 : 1000 dilution, Cell Signaling Technology), Bax (1 : 1000 dilution, Cell Signaling Technology), Bcl-2 (1 : 1000 dilution, Cell Signaling Technology), Phospho-NF-κB p65 (1 : 1000 dilution, Cell Signaling Technology), CHOP (1 : 1000 dilution, Cell Signaling Technology), Phospho-eIF2α (1 : 1000 dilution, Cell Signaling Technology), caspase-12 (1 : 1000 dilution, Cell Signaling Technology), NF-κB p65 (1 : 1000 dilution, Bioworld), Nox2 (1 : 200 dilution, Santa Cruz Biotechnology), Nox4 (1 : 200 dilution, Santa Cruz Biotechnology), GRP78 (1 : 200 dilution, Santa Cruz Biotechnology), ATF-6α (1 : 200 dilution, Santa Cruz Biotechnology), and XBP-1 (1 : 200 dilution, Santa Cruz Biotechnology). The secondary antibody, goat anti-rabbit IgG (926–32,211; LI-COR), was incubated with the membrane for 1 h. The bands were visualized using a two-colored infrared imaging system (Odyssey; LI-COR) to quantify protein expression. The protein expression levels were normalized to GAPDH levels.

2.7. Real-Time Polymerase Chain Reaction Analysis. RNA was collected from LV tissue using TRIzol (15596026; Invitrogen Life Technologies, Carlsbad, CA, USA). cDNA was synthesized from 2 g of RNA from each group using oligo (DT) primers and the Transcriptor First Strand cDNA Synthesis Kit (04896866001; Roche). Quantitative analysis was conducted using a LightCycler 480 and SYBR Green Master Mix (04707516001; Roche). All details about the primers are presented in Table 1.

2.8. Statistical Analysis. Data are presented as the mean ± S.D. Comparisons between groups were made using analysis of variance (ANOVA), followed by Dunnett's test or Tukey's test. Differences with a P value less than 0.05 were considered significant.

TABLE 1: Primers for quantitative polymerase chain reaction.

Gene	Forward primer (5′-3′)	Reverse primer (5′-3′)
TRPA1	GTCCAGGGCGTTGTCTATCG	CGTGATGCAGAGGACAGAGAT
IL-1β	GGGCCTCAAAGGAAAGAATC	TACCAGTTGGGGAACTCTGC
IL-6	CCAAGAGGTGAGTGCTTCCC	CTGTTGTTCAGACTCTCTCCCT
IL-17	TTTAACTCCCTTGGCGCAAAA	CTTTCCCTCCGCATTGACAC
TNF-α	GACGTGGAACTGGCAGAAGAG	TTGGTGGTTTGTGAGTGTGAG
GAPDH	AACTTTGGCATTGTGGAAGG	CACATTGGGGGTAGGAACAC
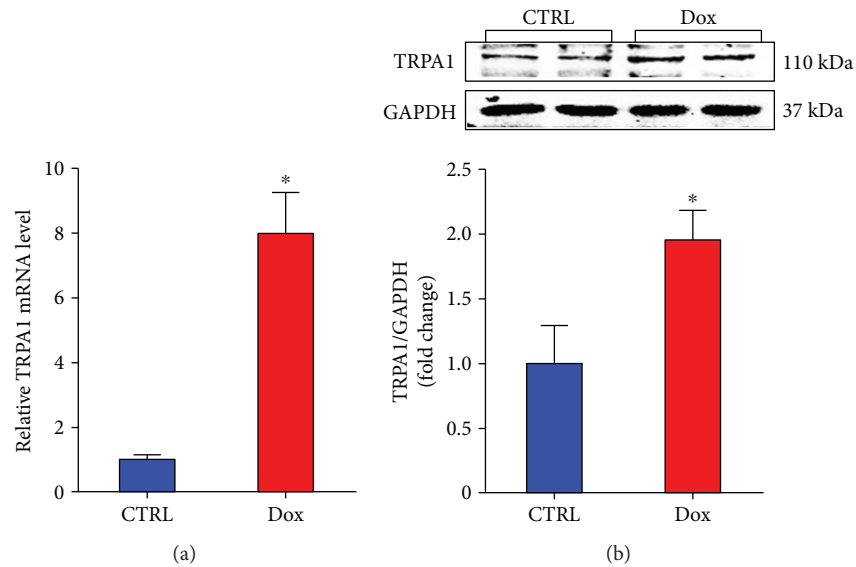
FIGURE 1: Dox treatment increases TRPA1 expression in heart tissue. (a) The relative mRNA levels of TRPA1 in the left ventricle of mice from the indicated groups. (b). Representative Western blot bands and quantitative results of protein levels of TRPA1 in Dox-induced cardiac injury. ($n = 6$). $^*P < 0.05$ versus CTRL.

3. Results

3.1. Dox Treatment Increases Cardiac TRPA1 Expression.
To investigate the potential role of TRPA1 in the development of Dox-induced myocardial lesions, we first examined the expression of TRPA1 in the heart after Dox treatment. The RT-PCR results showed that Dox treatment enhanced myocardial TRPA1 mRNA levels (Figure 1(a)). Then, western blot results showed the same trend for TRPA1 expression in the Dox-treated heart (Figure 1(b)). These results suggested that TRPA1 expression is induced by Dox treatment and that TRPA1 may be involved in Dox-induced cardiotoxicity.

3.2. Inhibition of TRPA1 Ameliorates Cardiac Dysfunction in Mice Treated with Dox.
To explore the potential function of TRPA1 in Dox-induced cardiotoxicity, the TRPA1-specific inhibitor HC was applied for 5 days before and after Dox treatment. We first evaluated the body weight (BW) and heart weight (HW) of mice in each group. Compared to control mice, mice treated with Dox showed a decrease in BW and HW (Figures 2(a)-2(b)). However, HC treatment did not improve the decreased BW and HW induced by Dox. The expression of serum enzymes such as CK-MB and LDH,

which reflect cardiac injuries, was significantly increased after the administration of Dox (Figures 2(c)-2(d)). Interestingly, the administration of HC significantly decreased the level of serum enzymes, indicating attenuated cardiotoxicity. In addition, the decreased cardiac ejection fraction (EF) and fractional shortening (FS) in the Dox group were significantly improved by HC treatment (Figures 2(e)-2(f)). Histological examination revealed increased vacuolar and myofibrillar disorganization in Dox-treated mice, and these effects were significantly ameliorated in the Dox +HC group (Figure 2(g)). The HC alone group did not show any significant changes in any of these markers compared to the control group (Figures 2(a)–2(g)).

3.3. Inhibition of TRPA1 Protects against Dox-Induced Oxidative Stress in Cardiac Tissue.
Dox treatment caused a significant reduction in the activities of SOD and GSH and an increase in the levels of MDA compared with the control group (Figures 3(a)–3(c)). However, HC treatment significantly decreased MDA levels and restored SOD activity and GSH antioxidant levels compared with the Dox-treated mice (Figures 3(a)–3(c)). Furthermore, the expression of Nox2

(a)

(b)

(c)

(d)

(e)

(f)

CTRL   HC   Dox   Dox + HC

(g)
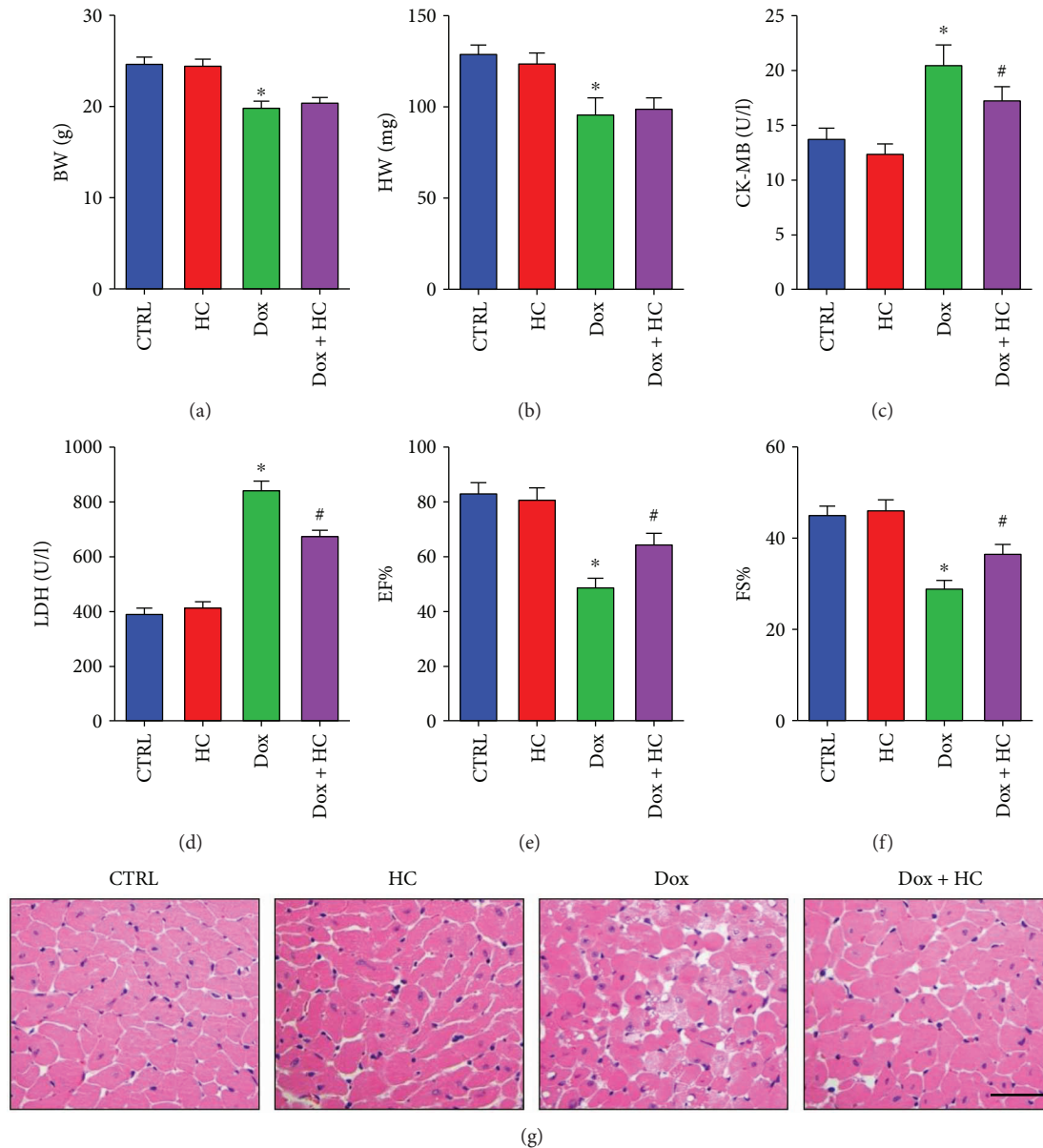
FIGURE 2: Inhibition of TRPA1 ameliorates cardiac function in mice treated with Dox. (a, b) The body weight (BW) and heart weight (HW) in different groups ($n = 10$). (c, d) The serum levels of cardiotoxicity markers, including creatine kinase isoenzymes (CK-MB) and lactate dehydrogenase (LDH) ($n = 6$). (e, f) The echocardiographic parameters in different groups ($n = 8$). (g) The pathological structure indicated by HE staining (scale bar, 50 μm) ($n = 6$). *$P < 0.05$ compared with the CTRL group. #$P < 0.05$ compared with the Dox group. EF: ejection fraction; FS: fractional shortening.

and Nox4, which are important generators of ROS, was lower in the Dox + HC group compared with the Dox group (Figure 3(d)). These findings indicate that HC treatment decreases the cardiac oxidative stress induced by Dox.

3.4. Inhibition of TRPA1 Reduces Dox-Induced Inflammation in Cardiac Tissue.
As shown in Figure 4, the expression in the heart of proinflammatory cytokines, including IL-1β, IL-6, IL-17, and TNF-α, was significantly increased by Dox (Figure 4(a)). Conversely, significant reductions in IL-1β, IL-6, IL-17, and TNF-α were observed in the Dox + HC group compared with the Dox group (Figure 4(a)). In

addition, the inhibitory effects of HC on inflammation were further confirmed by western blot results showing that HC reduced NF-κB signaling (Figure 4(b)). These results demonstrate that HC protects against heart injury by inhibiting inflammatory responses.

3.5. Inhibition of TRPA1 Attenuates Dox-Induced ER Stress.
Emerging evidence suggests that ER stress plays a crucial role in Dox-induced cardiotoxicity [12, 13]. Thus, we investigated whether the cardioprotective effects of HC against Dox-induced cardiotoxicity are associated with decreased ER stress. The results showed that HC treatment suppressed

(a)

(b)

(c)

(d)
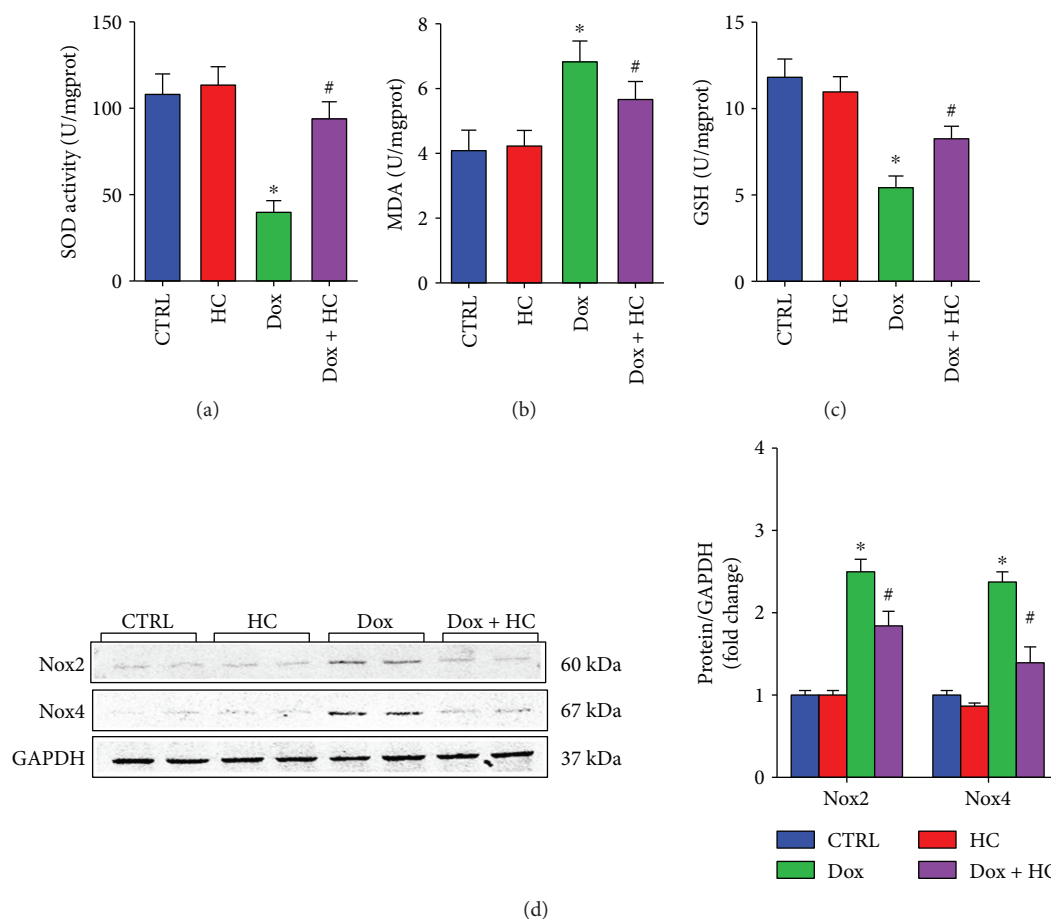
FIGURE 3: Inhibition of TRPA1 protects against Dox-induced oxidative stress. The serum levels of superoxide dismutase (SOD) (a), malondialdehyde (MDA) (b), and glutathione (GSH) ($n = 6$) (c). (d) Western blots showing the protein levels of Nox2 and Nox4 in different groups ($n = 6$). $^*P < 0.05$ compared with the CTRL group, $^\#P < 0.05$ compared with the Dox group.

the expression of glucose-regulated protein 78 (GRP78), an important marker indicating the severity of ER stress. In addition, we found that Dox induction increased the levels of C/EBP homologous protein (CHOP) and cleaved caspase-12, important mediators of ER stress-induced apoptosis, and this induction was attenuated by HC treatment. Furthermore, the activation of ER stress signaling pathways was inhibited by HC treatment, as evidenced by the decreased expression of activating transcription factor 6 (ATF6), eukaryotic translation initiation factor 2α (eIF2α), and X-box binding protein 1 (XBP-1) in the Dox + HC group (Figure 5). These results indicate that HC treatment attenuates the ER stress induced by Dox.

3.6. Inhibition of TRPA1 Attenuates Dox-Induced Cardiomyocyte Apoptosis. It is well known that apoptosis is involved in Dox-induced cardiotoxicity [14, 15]. We evaluated the severity of apoptosis and identified the potential signaling pathways related to apoptosis in the heart. The levels of Bax and cleaved caspase-3 in myocardial tissue were upregulated in the Dox group compared with the control group (Figure 6). By contrast, the expression level of Bcl-2 was significantly lower in the Dox group than in the control group. The HC alone group did not show any significant

changes in any of these markers compared to the control group (Figure 6). However, HC treatment significantly attenuated the increased Bax and cleaved caspase-3 levels and improved the expression of Bcl-2 after Dox treatment. These findings demonstrate that HC can decrease Dox-induced cardiomyocyte apoptosis.

4. Discussion

Cardiotoxicity is induced by a single intraperitoneal injection of Dox (20 mg/kg) in mice, which triggers the development of cardiac dysfunction and congestive heart failure [16, 17]. The present study demonstrated the potential role of TRPA1 in Dox-induced cardiotoxicity and elucidated the potential underlying molecular mechanisms. First, we observed that the expression level of TRPA1 was upregulated in the heart after Dox treatment. Moreover, we demonstrated that inhibition of TRPA1 with the specific inhibitor HC ameliorated Dox-induced cardiac injuries, as evidenced by attenuated heart dysfunction, structural damage, oxidative stress, inflammatory response, and ER stress. More importantly, Dox-induced cardiomyocyte apoptosis was attenuated by HC treatment. These findings imply that the inhibition of

(a)

(b)
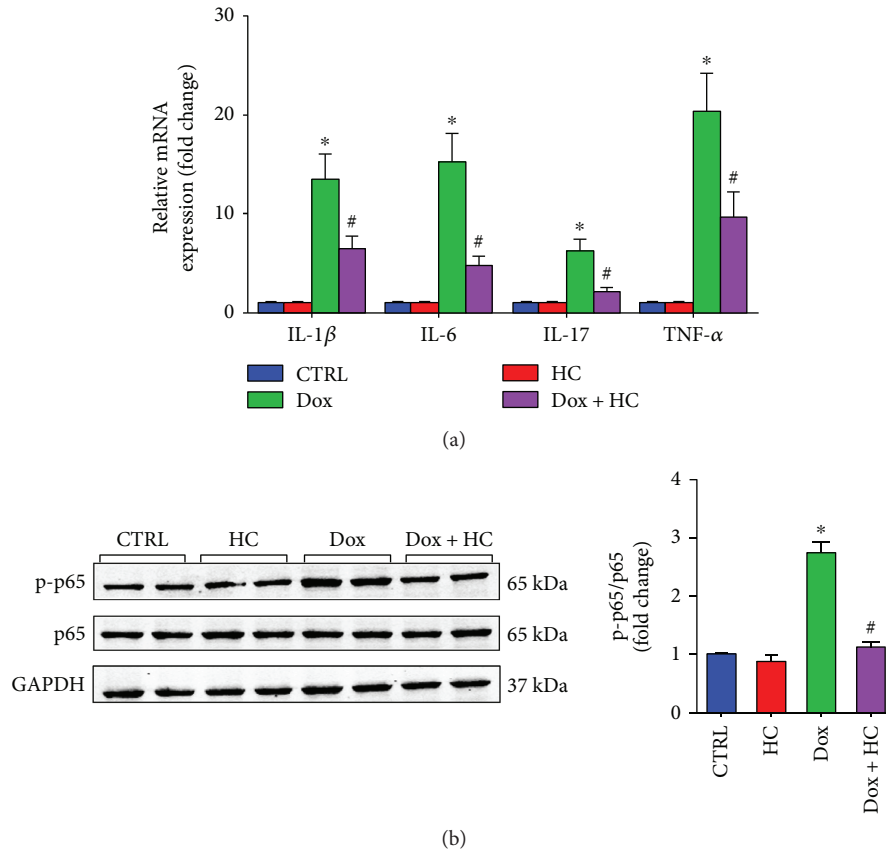
FIGURE 4: Inhibition of TRPA1 protects against Dox-induced inflammatory in cardiac tissue. (a) The mRNA expression of inflammatory cytokines, including Il-1β, IL-6, IL-17, and TNF-α, in different groups ($n = 6$). (b) Western blot analysis of p65 and p-p65 in different groups ($n = 6$). $^{*}P < 0.05$ compared with the CTRL group, $^{\#}P < 0.05$ compared with the Dox group.

(a)

(b)
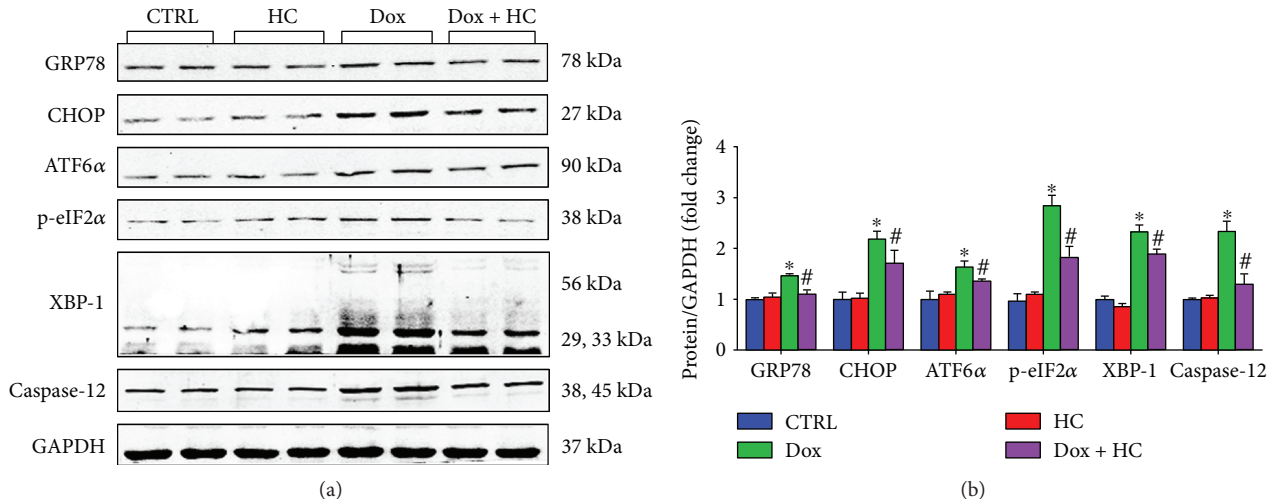
FIGURE 5: Inhibition of TRPA1 attenuates Dox-induced ER stress. Representative western blots (a) and quantitative results (b) showing the expression of glucose-regulated protein 78 (GRP78), C/EBP homologous protein (CHOP), activating transcription factor 6 (ATF6), eukaryotic translation initiation factor 2 (p-eIF2), X-box binding protein 1 (XBP-1), and caspase-12 in different groups ($n = 6$). $^{*}P < 0.05$ compared with the CTRL group, $^{\#}P < 0.05$ compared with the Dox group.

TRPA1 could effectively attenuate the progression of Dox-induced cardiotoxicity.

Redox homeostasis, which depends on the fine balance between enzymatic cascades, serves a pivotal role in adaptive responses under stress conditions. However, uncontrolled accumulation of reactive oxygen species (ROS), a state known as oxidative stress, occurs during tissue damage and impaired cell function [18, 19]. It is well established that

(a)

(b)
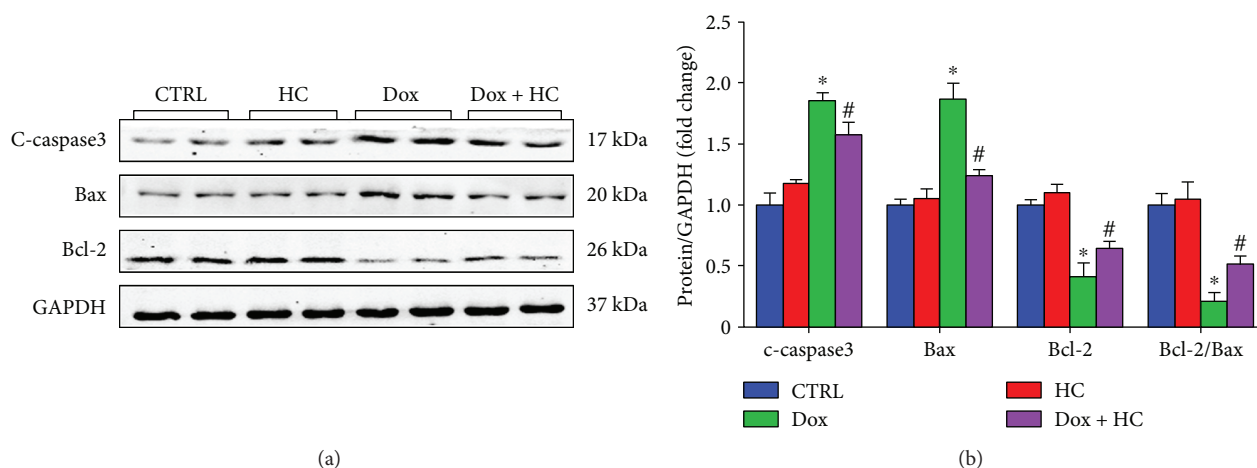
FIGURE 6: Inhibition of TRPA1 attenuates Dox-induced cardiomyocyte apoptosis. Representative western blots (a) and quantitative results (b) showing the expression of c-caspase-3, Bax, and Bcl-2 in different groups ($n = 6$). $^*P < 0.05$ compared with the CTRL group, $^\#P < 0.05$ compared with the Dox group.

TRPA1 acts as a polymodal nociceptor and molecular integrator of cellular stressors, including ROS and reactive nitrogen species (RNS) [20]. Genetic deletion of TRPA1, or the blockade of its activation with a selective antagonist, abrogated trigeminal neuropathic pain and oxidative stress [21].

In the present study, the levels of myocardium biomarkers, including lipid peroxidation products (MDA) and antioxidant enzymes (SOD and GSH), were used to estimate oxidative stress. The administration of Dox significantly increased MDA levels, reduced the activity of SOD, and reduced GSH content in the heart. Interestingly, HC treatment reduced the extent of Dox-induced oxidative stress by increasing SOD activity and MDA levels and decreasing GSH levels. Furthermore, previous studies reported that Dox could induce the production of ROS via activation of the NADPH oxidase pathway [22]. Zhao et al. found that Nox2 deficiency protected mice against cardiac injury and apoptosis after Dox treatment [23]. Consistent with these studies, we found that the expression of Nox2 and Nox4, the pivotal NADPH oxidase subunit, was upregulated after Dox administration. However, treatment with HC inhibited the oxidative stress, possibly by downregulating the expression of Nox2 and Nox4 in the heart.

The inflammatory process is absolutely essential for defense privilege that intended to eliminate or neutralize invading pathogens, clear damaged tissues, and promote their repair, but the termination of the response is of equal importance. Failure to control inflammation can lead to immunopathology, such as systemic inflammation leading to organ dysfunction and death. In previous research, TRPA1 emerged as a key regulator of sensory neuropeptide release and acute neurogenic inflammation. However, there is accumulating evidence for a link between TRPA1 and immunoinflammatory processes. In the cornea following a chemical injury, the absence of TRPA1 or TRPA1 antagonist treatment suppressed inflammation and fibrosis by decreasing levels of IL-6, TGF-β1, and vascular endothelial growth factor [24]. Similarly, loss of TRPA1 restrained neutrophil infiltration and proinflammatory cytokines, mainly IL-1β,

produced by monosodium urate. These reports highlight the potential for anti-inflammatory signaling via alternative mechanisms targeting TRPA1 [25]. Besides its direct deleterious effect, Dox can also induce inflammatory responses via enhanced expression and release of proinflammatory cytokines [26, 27]. It has been demonstrated that Dox treatment induces the release of proinflammatory cytokines, such as TNF-α, via the activation of NF-κB in the heart [28]. Studies demonstrated that the inhibition of TRPA1 results in a relevant reduction of the proinflammatory cytokines IL-1β and TNF-α in cystic fibrosis patients [29]. Similarly, our results indicated that Dox treatment provokes a series of inflammatory responses and increases the expression levels of inflammatory cytokines, which lead to the deterioration of myocardial function. Inhibition of TRPA1 significantly reduced the expression of proinflammatory cytokines, such as IL-1β, IL-6, IL-17, and TNF-α and suppressed the expression of NF-κB. This study indicates that the anti-inflammatory consequences of TRPA1 inhibition may partly contribute to the potential cardioprotective effect against Dox-induced cardiotoxicity.

To further investigate the potential mechanisms behind TRPA1-mediated Dox-induced cardiotoxicity in the heart, we examined the level of ER stress that plays a pivotal role in the development of heart failure [30, 31]. Consistent with previous reports, ER stress-related proteins were enhanced in Dox-treated mice. Many studies have demonstrated that Dox promotes the endoplasmic reticulum-initiated apoptotic response by activating the expression of proapoptotic factors and inhibiting the expression of antiapoptotic factors [32]. As a specific proapoptotic pathway, ER stress can activate the CHOP and caspase-12 pathways and thereby mediate apoptosis [33]. In our study, HC treatment attenuated the expression of CHOP and caspase-12, leading to decreased myocardial apoptosis and ameliorated cardiac dysfunction. Furthermore, many studies have demonstrated that CHOP can also directly regulate apoptosis factors such as Bax, Bcl-2, and cleaved caspase-3, which are key determinants of cell death [34]. Our data also support this hypothesis, since HC

treatment significantly increased the expression of Bcl-2 and decreased the expression of Bax and cleaved caspase-3.

In conclusion, our study indicates that the inhibition of TRPA1 could protect the heart from Dox-induced cardio-myocyte apoptosis and cardiac dysfunction by inhibiting oxidative stress, inflammatory responses, and ER stress. These findings suggest that TRPA1 could be a potential therapeutic target for the treatment of cardiotoxicity caused by Dox.

Conflicts of Interest

The authors have no conflict of interests to disclose.

Authors' Contributions

Zhen Wang, Menglong Wang, and Jianfang Liu contributed equally to this work.

Acknowledgments

References

[1] P. Vejpongsa and E. T. H. Yeh, "Prevention of anthracycline-induced cardiotoxicity: challenges and opportunities," *Journal of the American College of Cardiology*, vol. 64, no. 9, pp. 938–945, 2014.

[2] I. Fernandez-Ruiz, "Cardioprotection: cardiotoxicity of anti-cancer therapy," *Nature Reviews Cardiology*, vol. 13, no. 4, p. 183, 2016.

[3] H. Sawaya, I. A. Sebag, J. C. Plana et al., "Early detection and prediction of cardiotoxicity in chemotherapy-treated patients," *The American Journal of Cardiology*, vol. 107, no. 9, pp. 1375–1380, 2011.

[4] B. Nilius, G. Appendino, and G. Owsianik, "The transient receptor potential channel TRPA1: from gene to pathophysiology," *Pflügers Archiv*, vol. 464, no. 5, pp. 425–458, 2012.

[5] S. R. Andrei, P. Sinharoy, I. N. Bratz, and D. S. Damron, "TRPA1 is functionally co-expressed with TRPV1 in cardiac muscle: co-localization at z-discs, costameres and intercalated discs," *Channels*, vol. 10, no. 5, pp. 395–409, 2016.

[6] D. A. Andersson, C. Gentry, S. Mossand, and S. Bevan, "Transient receptor potential A1 is a sensory receptor for multiple products of oxidative stress," *The Journal of Neuroscience*, vol. 28, no. 10, pp. 2485–2494, 2008.

[7] N. Takahashi, T. Kuwaki, S. Kiyonaka et al., "TRPA1 underlies a sensing mechanism for O_2," *Nature Chemical Biology*, vol. 7, no. 10, pp. 701–711, 2011.

[8] D. M. Bautista, S. E. Jordt, T. Nikai et al., "TRPA1 mediates the inflammatory actions of environmental irritants and proalgesic agents," *Cell*, vol. 124, no. 6, pp. 1269–1282, 2006.

[9] D. M. Bautista, M. Pellegrino, and M. Tsunozaki, "TRPA1: a gatekeeper for inflammation," *Annual Review of Physiology*, vol. 75, no. 1, pp. 181–200, 2013.

[10] J. V. Bodkin and S. D. Brain, "Transient receptor potential ankyrin 1: emerging pharmacology and indications for cardiovascular biology," *Acta Physiologica*, vol. 203, no. 1, pp. 87–98, 2011.

[11] Y. Lu, H. Piplani, S. L. McAllister, C. M. Hurt, and E. R. Gross, "Transient receptor potential ankyrin 1 activation within the cardiac myocyte limits ischemia–reperfusion injury in rodents," *Anesthesiology*, vol. 125, no. 6, pp. 1171–1180, 2016.

[12] H. Y. Fu, S. Sanada, T. Matsuzaki et al., "Chemical endoplasmic reticulum chaperone alleviates doxorubicin-induced cardiac dysfunction," *Circulation Research*, vol. 118, no. 5, pp. 798–809, 2016.

[13] R. C. Chen, G. B. Sun, J. X. Ye, J. Wang, M. D. Zhang, and X. B. Sun, "Salvianolic acid B attenuates doxorubicin-induced ER stress by inhibiting TRPC3 and TRPC6 mediated Ca^{2+} overload in rat cardiomyocytes," *Toxicology Letters*, vol. 276, pp. 21–30, 2017.

[14] L. Wang, T.-P. Zhang, Y. Zhang et al., "Protection against doxorubicin-induced myocardial dysfunction in mice by cardiac-specific expression of carboxyl terminus of hsp70-interacting protein," *Scientific Reports*, vol. 6, no. 1, p. 28399, 2016.

[15] M. U. Rehman, M. Tahir, A. Q. Khan et al., "D-limonene suppresses doxorubicin-induced oxidative stress and inflammation via repression of COX-2, iNOS, and NFκB in kidneys of Wistar rats," *Experimental Biology and Medicine.*, vol. 239, no. 4, pp. 465–476, 2014.

[16] K. Li, R. Y. Sung, W. Z. Huang et al., "Thrombopoietin protects against in vitro and in vivo cardiotoxicity induced by doxorubicin," *Circulation*, vol. 113, no. 18, pp. 2211–2220, 2006.

[17] M. Kobayashi, F. Usui, T. Karasawa et al., "NLRP3 deficiency reduces macrophage interleukin-10 production and enhances the susceptibility to doxorubicin-induced cardiotoxicity," *Scientific Reports*, vol. 6, no. 1, p. 26489, 2016.

[18] M. Schieber and N. S. Chandel, "ROS function in redox signaling and oxidative stress," *Current Biology*, vol. 24, no. 10, pp. R453–R462, 2014.

[19] B. Halliwell, "Free radicals and antioxidants: updating a personal view," *Nutrition Reviews*, vol. 70, no. 5, pp. 257–265, 2012.

[20] N. Takahashi and Y. Mori, "TRP channels as sensors and signal integrators of redox status changes," *Frontiers in Pharmacology*, vol. 2, p. 58, 2011.

[21] G. Trevisan, S. Benemei, S. Materazzi et al., "TRPA1 mediates trigeminal neuropathic pain in mice downstream of monocytes/macrophages and oxidative stress," *Brain*, vol. 139, no. 5, pp. 1361–1377, 2016.

[22] L. Wojnowski, B. Kulle, M. Schirmer et al., "NAD(P)H oxidase and multidrug resistance protein genetic polymorphisms are associated with doxorubicin-induced cardiotoxicity," *Circulation*, vol. 112, no. 24, pp. 3754–3762, 2005.

[23] Y. Zhao, D. McLaughlin, E. Robinson et al., "Nox2 NADPH oxidase promotes pathologic cardiac remodeling associated with doxorubicin chemotherapy," *Cancer Research*, vol. 70, no. 22, pp. 9287–9297, 2010.

[24] Y. Okada, K. Shirai, P. S. Reinach et al., "TRPA1 is required for TGF-β signaling and its loss blocks inflammatory fibrosis in mouse corneal stroma," *Laboratory Investigation*, vol. 94, no. 9, pp. 1030–1041, 2014.

[25] G. Trevisan, C. Hoffmeister, M. F. Rossato et al., "TRPA1 receptor stimulation by hydrogen peroxide is critical to trigger hyperalgesia and inflammation in a model of acute gout," *Free Radical Biology & Medicine*, vol. 72, pp. 200–209, 2014.

[26] M. Pecoraro, M. Del Pizzo, S. Marzocco et al., "Inflammatory mediators in a short-time mouse model of doxorubicin-induced cardiotoxicity," *Toxicology and Applied Pharmacology*, vol. 293, pp. 44–52, 2016.

[27] Z. Q. Wang, M. T. Chen, R. Zhang, Y. Zhang, W. Li, and Y. G. Li, "Docosahexaenoic acid attenuates doxorubicin-induced cytotoxicity and inflammation by suppressing NF-κB/iNOS/NO signaling pathway activation in H9C2 cardiac cells," *Journal of Cardiovascular Pharmacology*, vol. 67, no. 4, pp. 283–289, 2016.

[28] E. T. Abd, R. H. Mohamed, H. F. Pasha, and H. R. Abdel-Aziz, "Catechin protects against oxidative stress and inflammatory-mediated cardiotoxicity in adriamycin-treated rats," *Clinical and Experimental Medicine*, vol. 12, no. 4, pp. 233–240, 2012.

[29] P. Prandini, F. De Logu, C. Fusi et al., "Transient receptor potential ankyrin 1 channels modulate inflammatory response in respiratory cells from patients with cystic fibrosis," *American Journal of Respiratory Cell and Molecular Biology*, vol. 55, no. 5, pp. 645–656, 2016.

[30] T. Minamino, I. Komuro, and M. Kitakaze, "Endoplasmic reticulum stress as a therapeutic target in cardiovascular disease," *Circulation Research*, vol. 107, no. 9, pp. 1071–1082, 2010.

[31] T. Minamino and M. Kitakaze, "ER stress in cardiovascular disease," *Journal of Molecular and Cellular Cardiology*, vol. 48, no. 6, pp. 1105–1110, 2010.

[32] C. C. Chua, J. Gao, Y. S. Ho et al., "Over-expression of a modified bifunctional apoptosis regulator protects against cardiac injury and doxorubicin-induced cardiotoxicity in transgenic mice," *Cardiovascular Research*, vol. 81, no. 1, pp. 20–27, 2009.

[33] I. Tabas and D. Ron, "Integrating the mechanisms of apoptosis induced by endoplasmic reticulum stress," *Nature Cell Biology*, vol. 13, no. 3, pp. 184–190, 2011.

[34] H. Y. Fu, K.-i. Okada, Y. Liao et al., "Ablation of C/EBP homologous protein attenuates endoplasmic reticulum–mediated apoptosis and cardiac dysfunction induced by pressure overload," *Circulation*, vol. 122, no. 4, pp. 361–369, 2010.

Research Article

Ginkgo biloba Leaf Extract Protects against Myocardial Injury via Attenuation of Endoplasmic Reticulum Stress in Streptozotocin-Induced Diabetic ApoE$^{-/-}$ Mice

Jinfan Tian [1,2] **Yanfei Liu** [3,4] **Yue Liu** [3] **Keji Chen,** [3] **and Shuzheng Lyu** [1,2]

^{1}*Department of Cardiology, Beijing Anzhen Hospital, Capital Medical University, Beijing 100029, China*
^{2}*Beijing Institute of Heart, Lung and Blood Vessel Diseases, Beijing 100029, China*
^{3}*Cardiovascular Disease Center, Xiyuan Hospital, China Academy of Chinese Medical Sciences, Beijing 100091, China*
^{4}*Graduate School, Beijing University of Chinese Medicine, Beijing 100029, China*

Correspondence should be addressed to Yue Liu; liuyueheart@hotmail.com and Shuzheng Lyu; shuzheng@medmail.com.cn

Diabetes was induced in high-fat diet-fed ApoE$^{-/-}$ mice via administration of low-dose streptozotocin (STZ) for five days. Mice were then treated with GBE (200 or 400 mg/kg) by gastric gavage daily for 12 weeks. Mice in the untreated diabetic group received saline instead, and nondiabetic C57BL/6J mice served as controls. Collagen I and III mRNA expression was measured by real-time PCR. TNF-α, IL-1β mRNA levels, and NF-κB expression were determined to analyze intramyocardial inflammation. Hallmarks of endoplasmic reticulum stress- (ERS-) related apoptosis pathways, including phosphorylated c-Jun N-terminal kinase (p-JNK), C/EBP homologous protein (CHOP), caspase-12, and cleaved caspase-3, were analyzed by Western blotting. Diabetic ApoE$^{-/-}$ myocardial injury was associated with increased cardiomyocyte apoptosis (increased expression of p-JNK, CHOP, caspase-12, and cleaved caspase-3), interstitial fibrosis (increased mRNA levels of collagen I and III), and inflammation (increased mRNA levels of TNF-α and IL-1β, and NF-κB expression). GBE at 200 and 400 mg/kg/day significantly attenuated cardiomyocyte apoptosis, collagen deposition, and inflammation in diabetic mice via inhibition of the p-JNK, CHOP, and caspase-12 pathways. Serum levels of the proinflammatory cytokines (IL-6, IL-1β, and TNF-α), blood glucose, and lipid profiles were also regulated by GBE treatment. GBE might be beneficial in the treatment of diabetic myocardial injury.

1. Introduction

Diabetic cardiomyopathy (DCM), one of the leading cardiovascular complications of diabetes, ultimately leads to heart failure, which increases the mortality among diabetes patients. Diabetic myocardial injuries, including cardiomyocyte apoptosis, myocardial fibrosis, and intramyocardial inflammation, are important pathological characteristics of DCM. Diabetes-induced cardiomyocyte apoptosis often occurs concomitantly with interstitial collagen deposition and myofiber disarray [1]. In addition, accumulating evidence has shown that substrate metabolic alteration,

oxidative stress, and chronic inflammation contribute to DCM and diabetic myocardial injury [2, 3].

Endoplasmic reticulum stress (ERS) plays a critical role in the development of diabetic myocardial injury because the sustained and uncorrected unfolded protein response (UPR) could induce cell death [4]. The UPR is mediated by three pathways, the inositol-requiring kinase-1 (IRE1), protein kinase R-like ER kinase (PERK), and activating transcription factor 6 (ATF6) pathways. ERS-mediated cell death involves activation of c-Jun N-terminal kinase (JNK), C/EBP homologous protein (CHOP), and caspase-12, which consequently activates caspase-3.
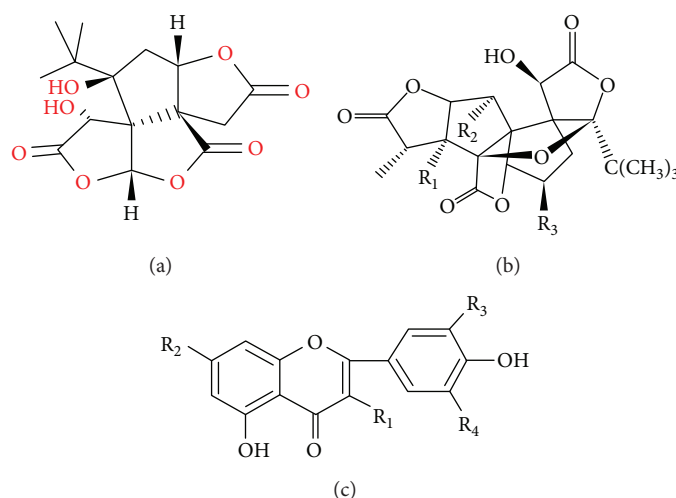
(a)

(b)

(c)

FIGURE 1: Chemical structures of the constituents of GBE. (a) Bilobalide, (b) ginkgolide, and (c) ginkgo flavonol glycosides.

IRE1 and JNK activation may result in the upregulation of nuclear factor kappa-B (NF-κB) expression via phosphorylation of IkB kinase (IKK) [5, 6]. Upregulation of NF-κB expression leads to increased production of proinflammatory cytokines, such as tumor necrosis factor-α (TNF-α), interleukin-1β (IL-1β), and IL-6, which contribute to cardiomyocyte apoptosis and myocardial fibrosis [7].

Recently, herbal treatment of diabetic myocardial injury has gained much attention. *Ginkgo biloba* leaves have been used as a traditional herbal medicine for hundreds of years in China. The major components of *Ginkgo biloba* leaf extract (GBE) include two active substances, namely, terpenoids (including ginkgolides and bilobalide) and flavonoids (Figure 1). GBE was shown to exhibit antioxidant, free radical scavenging and membrane-stabilizing activities, which contributed to its beneficial effects in ischemia/reperfusion injury in a diabetic rat myocardium [8]. In addition, it showed anti-inflammatory and antioxidant effects in the pancreas of streptozotocin- (STZ-) induced diabetic animals [9, 10]. Moreover, GBE enhanced insulin sensitivity and prevented insulin resistance by increasing insulin-induced Akt phosphorylation and insulin receptor substrate 1 expression [11]. GBE was also shown to ameliorate diabetic nephropathy in STZ-induced diabetic rats [12].

Currently, few studies have investigated the potential use of GBE for the treatment of diabetic myocardial injury. In the present study, we aimed to investigate whether GBE could protect against diabetic myocardial injury and elucidate the underlying mechanisms.

2. Materials and Methods

2.1. Drugs. GBE powders and atorvastatin were purchased from Beijing Handian Pharmaceutical Co. Ltd. and Pfizer Pharmaceutical Co. Ltd., respectively. GBE used in the present study contains 44.9% ginkgo flavonoids, 6.3% terpenoids, and <1 ppm ginkgo acid.

2.2. Experimental Animals. Male ApoE$^{-/-}$ mice, aged 6-7 weeks and weighing 19–21 g (C57BL/6J background,

introduced from Jackson Laboratory of USA by Peking University Health Science Center Laboratory Animal Science Department; quality certification number SCXK (Beijing) 2016-0012), were used in this study. The rearing condition of the mice was grade 2. Mice were maintained under controlled conditions (room temperature, 22–24°C; relative humidity, 50%; and lights on; from 7:00 to 19:00). The experimental protocol was approved by the institutional animal care and use committee of Xiyuan Hospital, China Academy of Chinese Medical Sciences. Animal experiments were carried out in accordance with the Guide for the Care and Use of Laboratory Animals published by the US National Institutes of Health.

2.3. Experimental Protocol. ApoE$^{-/-}$ mice were fed with a high-fat diet (basic diet, 78.85%; fat, 21%; and cholesterol, 0.15%) for four weeks before diabetes was induced by intraperitoneal injection of 50 mg/kg/day STZ (Sigma) diluted with citrate buffer (pH 4.5; final concentration, 1%) for five consecutive days, as described in a previous study [13]. Mice exhibiting plasma glucose levels > 12 mmol/L were considered diabetic and were used in the study ($n = 58$) [13, 14]. The diabetic mice were then treated with atorvastatin [15, 16] (10 mg/kg/day, intragastric (i.g.), $n = 14$), GBE at a low dose (200 mg/kg/day, i.g., $n = 16$), or GBE at a high dose (400 mg/kg/day, i.g., $n = 17$). The doses of GBE were selected based on previous studies [17, 18]. Diabetic mice treated with equal volumes of saline served as the untreated diabetic group ($n = 11$). All ApoE$^{-/-}$ mice were maintained on a high-fat diet and sacrificed after 12-week treatment. C58BL/6J mice ($n = 20$) served as the control group. The study timeline is shown in Figure 2.

2.4. Body Weight and Plasma Glucose Changes. The body weight and fasting plasma glucose levels were measured before the initial GBE dose and every four weeks thereafter. Plasma samples were collected by the cutting tail method, and the plasma glucose levels were measured using a glucometer (Roche).
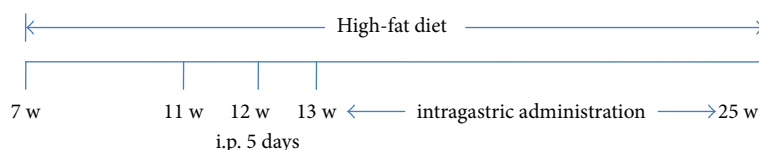
Figure 2: Timeline of the experimental protocol *in vivo*.

2.5. Tissue Preparation and Histological Examination.

All animals were euthanized, and the heart samples were collected before they were perfused with heparin saline. The specimens were transversely cut and fixed with 4% paraformaldehyde for 24 h. They were then embedded in paraffin and cut into 5 μm thick sections for hematoxylin/eosin and Masson's staining. Immunohistochemical staining of cleaved caspase-3 was also performed (rabbit polyclonal anti-cleaved caspase-3, CST, 1 : 200 dilution). Immunohistochemical semiquantitative analysis was conducted on microscopic images using Image-pro plus 6.0 software (Media Cybernetics Inc., Rockville, MD, USA) under 200x magnification. The positive expression of cleaved caspase-3 was represented by integral optical density (IOD).

2.6. Western Blot Analysis.

The heart tissues were removed from liquid nitrogen, weighed, and homogenized in radioimmunoprecipitation assay (RIPA) lysis buffer. Protein concentration was determined using the bicinchoninic acid method. Equal amounts of protein (40 μg) from each sample were separated by sodium dodecyl sulfate-polyacrylamide gel electrophoresis (SDS-PAGE) and transferred onto a nitrocellulose membrane. Nonspecific sites were blocked by incubating the membranes with 5% nonfat milk and 0.2% tween 20 in Tris-buffered saline for 2 h at room temperature. After washing, the membranes were incubated overnight at 4°C with the following primary antibodies: anti-CHOP (CST2895S, 1 : 2000), anti-JNK (CST9252S, 1 : 2000), anti-p-JNK (CST9251S, 1 : 1000), anti-caspase-12 (CST2202S, 1 : 1000), anti-cleaved caspase-3 (CST9664S, 1 : 1000), and anti-NF-κB (Abcam 86299, 1 : 2000). The membranes were washed with TBS-T and incubated with horseradish peroxidase- (HRP-) conjugated secondary antibodies. Then, the membrane was assayed using an enhanced chemiluminescence system. Glyceraldehyde 3-phosphate dehydrogenase (GAPDH) was used to ensure equal sample loading. The expression levels of CHOP, caspase-12, cleaved caspase-3, and NF-κB were adjusted for GAPDH, and the values were normalized over the untreated diabetic group. The expression levels of p-JNK were adjusted for total JNK and then normalized over the untreated diabetic group.

2.7. Quantitative Real-Time PCR.

Real-time polymerase chain reaction (PCR) was performed to determine the mRNA expression of collagen I and III, TNF-α, and IL-1β. GAPDH was used as an internal control. The primer sequences were as follows: collagen I, 5′-TGGAAACCCGAGGTATGCTT-3′ (forward) and 5′-CATTGCATTGCACGTCATCG-3′ (reverse);

collagen III, 5′-ACTGGTGAACGTGGCTCTAA-3′ (forward) and 5′-AACCTGGAGGACCTGGATTG-3′ (reverse); TNF-α, 5′-CTCATGCACCACCATCAAGG-3′ (forward) and 5′-ACCTGACCACTCTCCCTTTG-3′ (reverse); IL-1β, 5′-GAAGAAGAGCCCATCCTCTG-3′ (forward) and 5′-TCATCTCGGAGCCTGTAGTG-3′ (reverse); and GAPDH, 5′-TGCCCCCATGTTTGTGATG-3′ (forward) and 5′-TGTGGTCATGAGCCCTTCC-3′(reverse). Relative mRNA level was normalized over the untreated diabetic group. All experiments were repeated for at least three times.

2.8. Serum Lipid Profile and Glucose Analysis.

At the end of the 12-week period, all mice were fasted overnight before they were sacrificed, and blood samples were collected and centrifuged at 3000 rpm for 10 min. Serum glucose, high-density lipoprotein cholesterol (HDL-c), total cholesterol (TC), triglycerides (TG), and low-density lipoprotein cholesterol (LDL-c) levels were determined using an automated system.

2.9. Measurement of Serum Inflammatory Cytokine Levels.

Serum levels of inflammatory cytokines (IL-6, IL-1β, and TNF-α) were measured using commercially available ELISA kits, purchased from Beijing Fang Cheng Jia Hong Technology Co. Ltd. (catalog numbers FU-X0850, FU-X0840, and FU-X1059, resp.). The serum was collected as previously described. Five serial dilutions of the standard were prepared according to the manufacturer's instructions. Blank and sample wells were set, respectively. Sample diluent (40 μL) was added to the sample wells in the precoated ELISA plates, followed by the addition of the samples (10 μL). After sealing the plates with a closure plate membrane, they were incubated for 30 min at 37°C. HRP-conjugated reagent (50 μL) was added to all wells, except for the blank well. After incubation at 37°C, the liquid in the wells was removed, and the plate was washed with a wash liquid. Chromogen solution A (50 μL) and chromogen solution B (50 μL) were added to each well. The plates were incubated in dark at 37°C for 15 min. The blank well was considered zero, and the absorbance of each well was measured at 450 nm within 15 min after adding the stop solution.

2.10. Statistical Analysis.

SPSS 17.0 was used for statistical analyses. The data were presented as the means ± standard deviation ($\bar{x} \pm s$). One-way analysis of variance (ANOVA) was used to perform comparisons among group means, and the least significant difference (LSD) test was used for multiple comparisons between the untreated diabetic group and other groups. $P < 0.05$ was considered statistically significant. GraphPad Prism 5.0 software was used for graphical presentation.

3. Results

3.1. Body Weight and Plasma Glucose Levels. STZ resulted in a significant increase in plasma glucose levels, compared to those in the control group (14.8 ± 2.2 versus 5.3 ± 0.8 mmol/L, $P < 0.01$). At the end of the 12-week gavage, the untreated diabetic mice showed severe hyperglycemia compared to the control group (23.4 ± 6.4 versus 7.5 ± 1.0 mmol/L, $P < 0.01$). GBE treatment at 200 and 400 mg/kg/day suppressed the plasma glucose levels; however, only high-dose GBE resulted in a statistically significant difference (low-dose GBE group versus untreated diabetic group, 18.8 ± 6.5 mmol/L versus 23.4 ± 6.4 mmol/L, $P = 0.06$; high-dose GBE group versus untreated diabetic group, 15.3 ± 7.1 mmol/L versus 23.4 ± 6.4 mmol/L, $P = 0.01$).

There was a significant weight loss in the diabetic mice compared to those in the control group (22.37 ± 11.67 versus 26.58 ± 11.56 g, $P < 0.01$). Body weight loss was associated with hyperglycemia and polyuria. Body weight of mice in the untreated diabetic group was significantly lower than that in the control group at the end of the study course (30.01 ± 1.35 versus 26.38 ± 22.72 g, $P < 0.01$). Atorvastatin and GBE treatment did not affect the body weight in diabetic mice.

3.2. Effect of GBE on Serum Lipid and Glucose Profiles. Serum lipid and blood glucose levels were measured before the mice were sacrificed. LDL-c, TC, TG, and blood glucose levels significantly increased in the untreated diabetic group, compared to those in the control group. Atorvastatin and GBE (200 and 400 mg/kg/day) significantly decreased LDL-c, TC, and TG levels ($P < 0.01$, Figures 3(a)–3(c)). GBE at 200 mg/kg/day lowered the serum glucose levels, compared to those in the untreated diabetic group ($P < 0.05$, Figure 3(e)). There were no significant differences in HDL-c levels among the control, untreated diabetic, atorvastatin, low-dose GBE, and high-dose GBE groups (Figure 3(d)).

3.3. Effect of GBE on Serum Inflammatory Cytokine Levels. The levels of serum inflammatory cytokines, including IL-6, IL-1β, and TNF-α, significantly increased in the diabetic mice, compared to the control mice. GBE (200 and 400 mg/kg/day) significantly decreased serum IL-1β, TNF-α, and IL-6 levels. Moreover, high-dose GBE (400 mg/kg/day) resulted in lower levels of inflammatory cytokines, compared to those administered with low-dose GBE ($P < 0.01$, Figures 4(a)–4(c)).

3.4. Effect of GBE on the Histomorphology of Diabetic Hearts. Similar to the findings reported by Ahmed et al. [19], H&E staining showed diffuse disruption of the myocardium, with a fragmented and feathery appearance of DCM. Fibroblasts and inflammatory cells infiltrated the untreated diabetic myocardium, whereas atorvastatin and GBE treatment alleviated their infiltration (Figure 5(a)). In addition, Masson's staining showed that GBE treatment blunted the total cardiac collagen content (Figure 5(b)).

Immunostaining showed that cleaved caspase-3 expression significantly increased in the untreated diabetic mice, compared to that in the control group, whereas atorvastatin and GBE at 200 and 400 mg/kg/day significantly decreased

the expression of cleaved caspase-3 ($P < 0.05$, Figures 5(c) and 5(d)). The difference between low-dose and high-dose GBE was not statistically significant.

3.5. Effect of GBE on mRNA Levels of Collagen I and III. Collagen I and III mRNA levels increased in the untreated diabetic mice. Atorvastatin and GBE (200 and 400 mg/kg/day) treatment resulted in a statistically significant decrease in collagen I and III mRNA levels ($P < 0.05$, Figures 6(a) and 6(b)). There was no significant difference between low-dose and high-dose GBE.

3.6. Effect of GBE on Intramyocardial Inflammation. NF-κB plays a crucial role in the regulation of intramyocardial inflammation in the development of DCM. The untreated diabetic mice displayed increased expression of NF-κB. Atorvastatin and GBE significantly decreased the expression of NF-κB ($P < 0.05$, Figures 7(a) and 7(b)). TNF-α and IL-1β mRNA levels increased in the untreated diabetic mice; however, GBE treatment at doses of 200 and 400 mg/kg/day significantly inhibited the STZ-induced increase in TNF-α and IL-1β mRNA levels ($P < 0.05$, Figures 7(c) and 7(d)). The difference between the findings for low-dose and high-dose GBE was not statistically significant.

3.7. Effect of GBE on Hallmarks of ERS-Associated Apoptosis. Western blot analysis showed that the expression of the hallmarks of ERS-associated apoptosis, including p-JNK, CHOP, caspase-12, and cleaved caspase-3, significantly increased in the myocardium of diabetic mice, compared to those in the normal control group. This suggested that the p-JNK, CHOP, and caspase-12 cascades were activated in the diabetic myocardium. Atorvastatin and GBE (200 and 400 mg/kg/day) significantly decreased the expression of p-JNK, CHOP, caspase-12, and cleaved caspase-3 ($P < 0.05$, Figures 8(a)–8(h)). There were no statistical differences between the low-dose and high-dose GBE.

4. Discussion

Diabetes mellitus is a worldwide metabolic disease responsible for increased morbidity and mortality. Patients with diabetes mellitus are at a high risk of cardiovascular diseases, such as atherosclerosis and DCM, which are comorbidities of diabetes mellitus [20]. STZ has been frequently used to induce diabetes in experimental animals because of its toxic effects on the pancreatic β-cells and its potential to induce oxidative stress [21]. Hence, in the present study, we established a diabetic myocardial injury ApoE$^{-/-}$ mouse model by STZ injection combined with a high-fat diet, as previously described [22, 23]. Although it was not able to distinguish between hyperlipidemia- and diabetes-induced myocardial injury, this study aimed to investigate whether GBE attenuated diabetic myocardial injury in ApoE$^{-/-}$ mice, thus providing potential evidence for the treatment of diabetes patients with DCM and atherosclerosis as comorbidities. We found that collagen I and III mRNA expression was elevated in diabetic mice. TNF-α and IL-1β mRNA levels, which represent intramyocardial inflammation, increased in a diabetic heart owing to increased NF-κB activation.

(a)

(b)

(c)

(d)

(e)
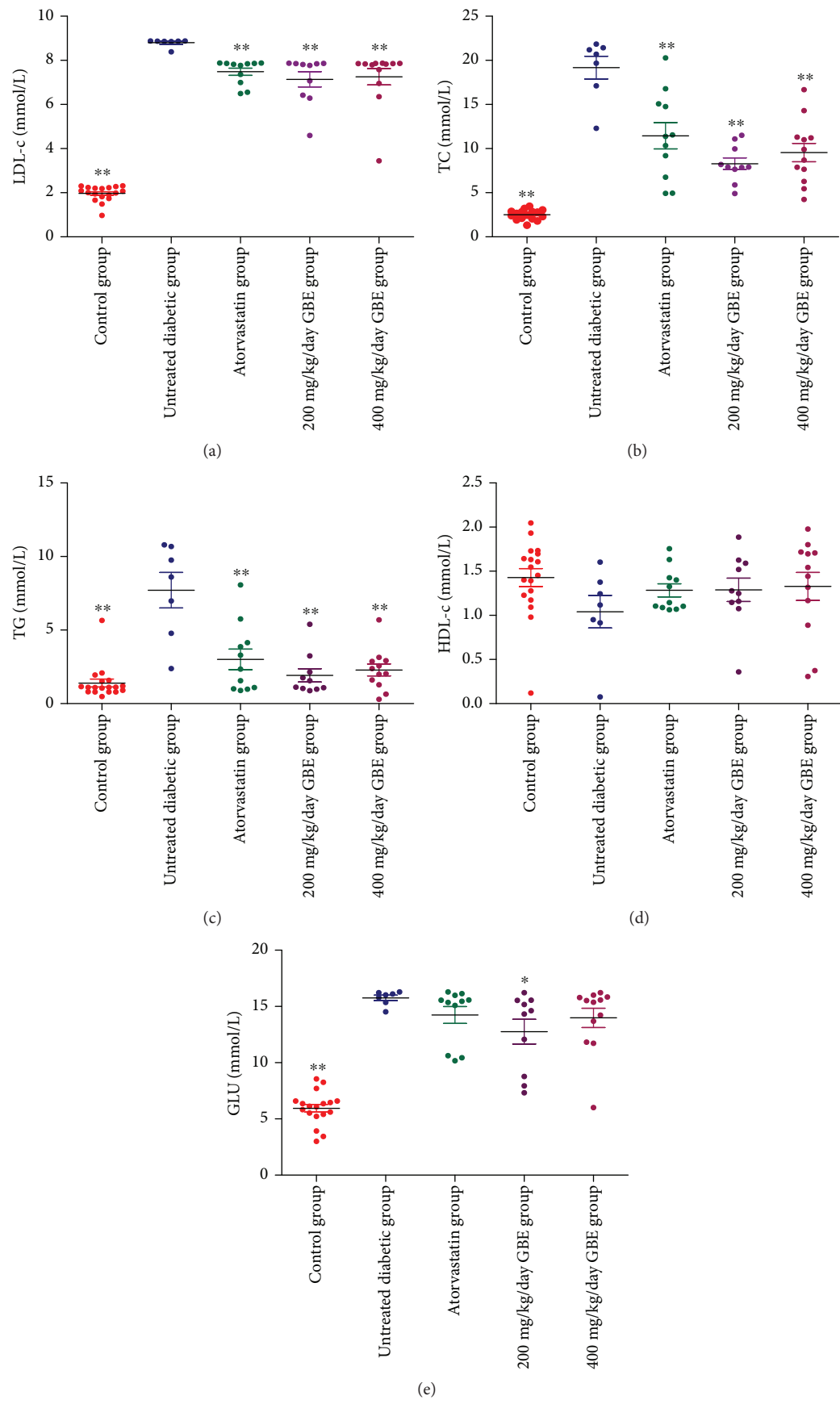
Figure 3: Serum lipid profiles and glucose levels. $^*P < 0.05$ and $^{**}P < 0.01$ versus the untreated diabetic group.

(a)

(b)

(c)
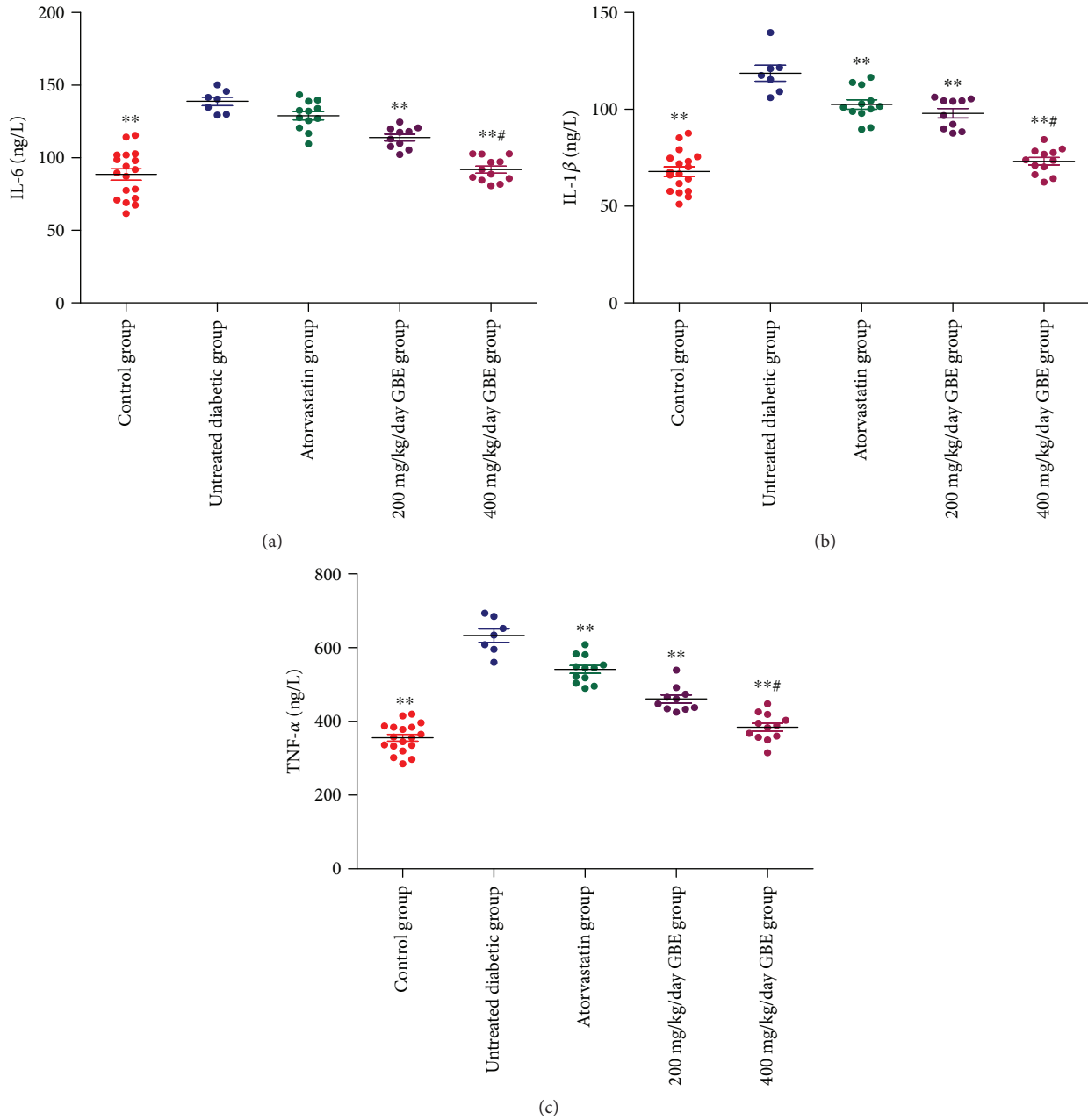
FIGURE 4: Serum proinflammatory cytokines determined by ELISA. $^{**}P < 0.01$ versus the untreated diabetic group; $^{#}P < 0.01$ versus the 200 mg/kg/day GBE group.

Additionally, hallmarks of ERS-related apoptosis, including p-JNK, CHOP, caspase-12, and cleaved caspase-3, were upregulated in the diabetic heart. These indicated that interstitial collagen deposition, ERS-related apoptosis, and NF-κB-mediated inflammation were induced in diabetic ApoE$^{-/-}$ mice. Consistent with the results of previous studies [15, 16, 19, 24], atorvastatin treatment improved the histological abnormalities, fibrosis, and apoptosis of cardiomyocytes via inhibition of NF-κB-induced inflammation and cleaved caspase-3-mediated apoptosis in the diabetic heart. To our knowledge, the present study is the first study to show that traditional Chinese medicine, GBE, could protect against diabetic myocardial injury, particularly apoptosis,

myocardial fibrosis, and NF-κB-mediated inflammation via inhibition of ERS-related apoptosis, as evidenced by the decrease in p-JNK, caspase-12, and cleaved caspase-3 expression. Furthermore, GBE regulated the lipid profile and blood glucose levels.

Cell death, including necrosis and apoptosis, in response to hyperglycemia has been defined as one of the important pathophysiological features of diabetic myocardial injury [1]. Cardiomyocyte loss, myocardial fibrosis, and inflammation result in myocardial remolding that leads to compromised cardiac function. In line with the results of previous studies, the present study showed that hyperglycemia triggered apoptosis of cardiomyocytes. The UPR is an adaptive

(a)

(b)

(c)
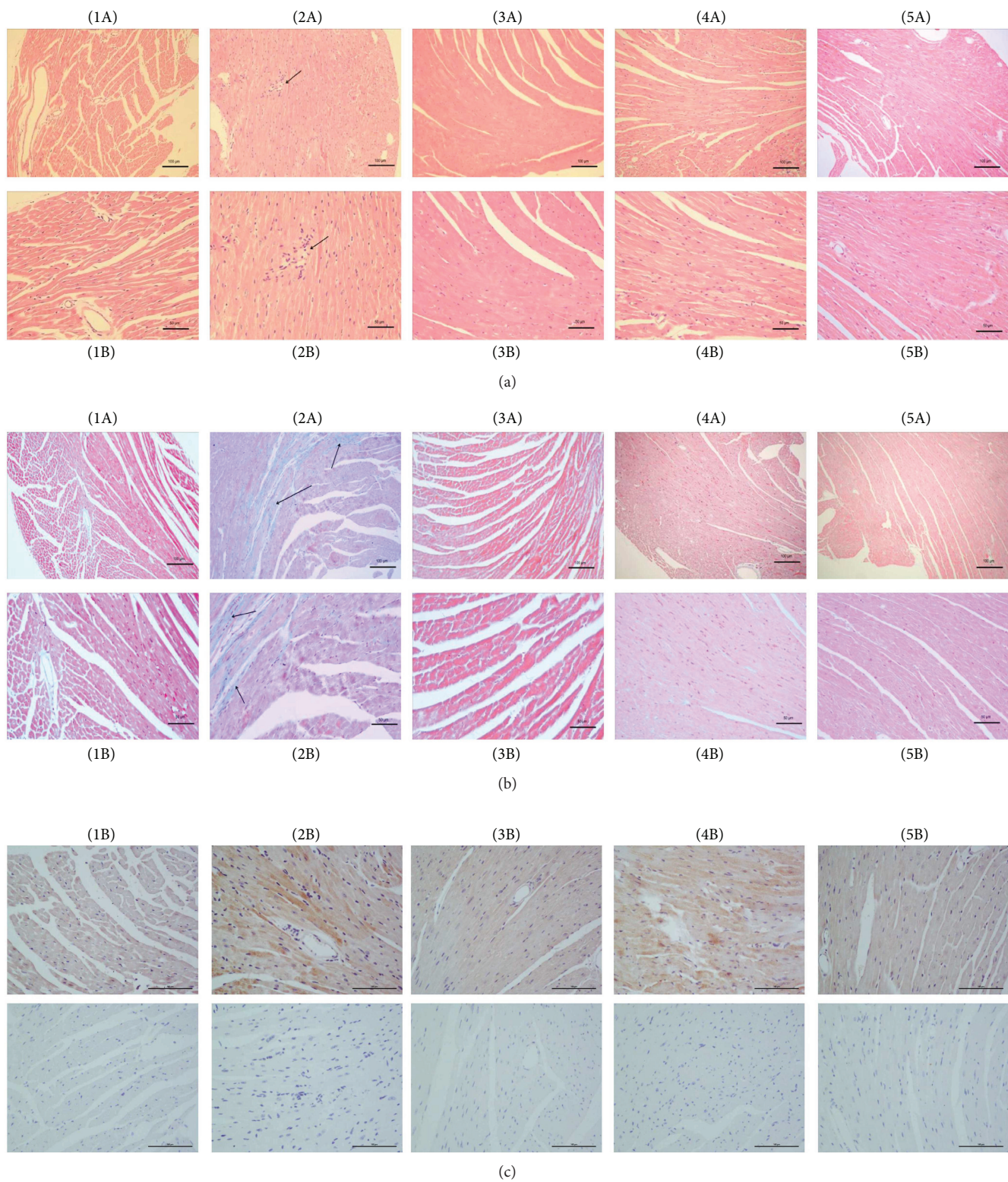
Figure 5: Continued.

(d)
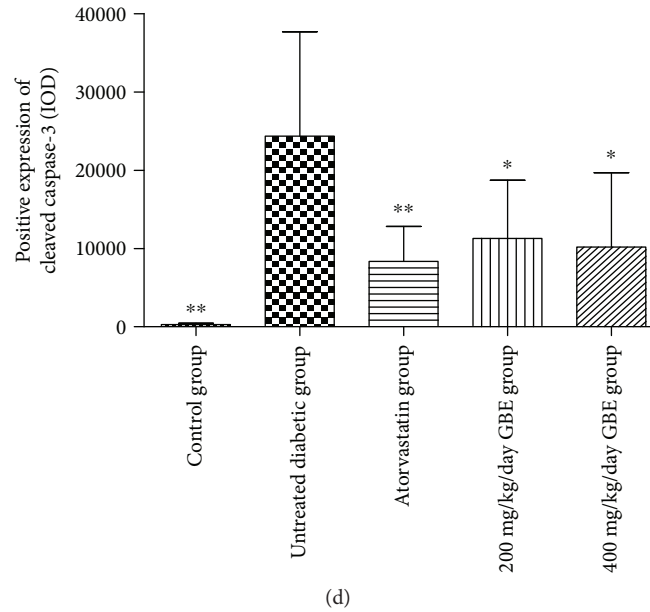
FIGURE 5: Effects of GBE on the cardiac histomorphological changes in diabetic ApoE$^{-/-}$ mice. (a) H&E staining of cross-sectional tissue slices of the myocardium. (b) Masson's staining of collagen in the myocardium. The blue area against the red represents collagen deposition. Arrows indicate interstitial fibers. (c, d) Immunostaining of cleaved caspase-3. The brown-yellow area represents the positive expression of cleaved caspase-3. Images of the samples incubated only with the secondary antibody were provided correspondingly. (1A, 1B) Control group; (2A, 2B) untreated diabetic group; (3A, 3B) atorvastatin group; (4A, 4B) 200 mg/kg/day GBE group; and (5A, 5B) 400 mg/kg/day GBE group. (A) 100x magnification; (B) 200x magnification. $^*P < 0.05$ and $^{**}P < 0.01$ versus the untreated diabetic group.

(a)

(b)
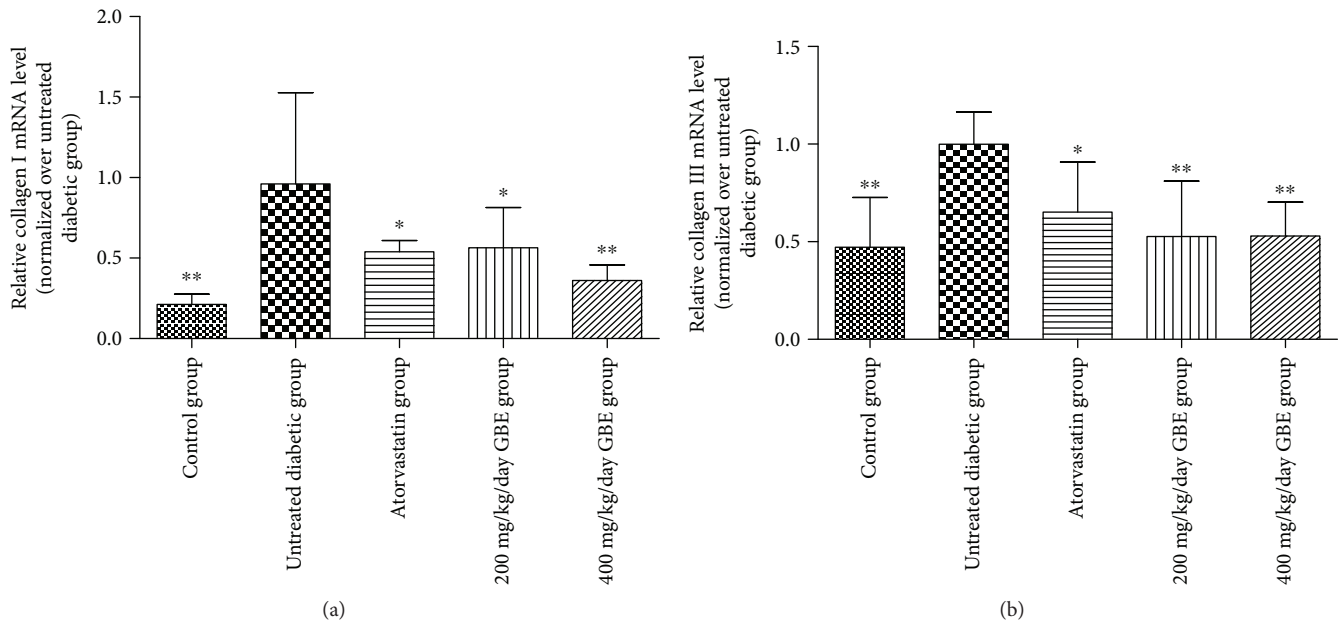
FIGURE 6: Relative mRNA expression of collagen I and III (normalized over the untreated diabetic group). $^*P < 0.05$ and $^{**}P < 0.01$ versus the untreated diabetic group.

process to restore the normal ER function. However, the excess and prolonged UPR in hyperglycemic conditions induces cardiomyocyte apoptosis. Three proapoptotic pathways are associated with ERS [4]. The first apoptotic pathway involves activation of JNK by the IRE-1-tumor necrosis factor receptor-associated factor 2- (TRAF2-) apoptosis signal-regulating kinase-1 (ASK1) complex. The second

apoptotic pathway is the caspase-12 pathway in rodents. Clustering of caspase-12 in the endoplasmic reticulum membranes may be attributable to TRAF2 recruitment by activated IRE-1 and PERK [25]. Activated caspase-12 translocates from the ER to the cytosol, where it cleaves procaspase 9, and subsequently activates the downstream effector caspase-3. CHOP, which is regulated by IRE1,
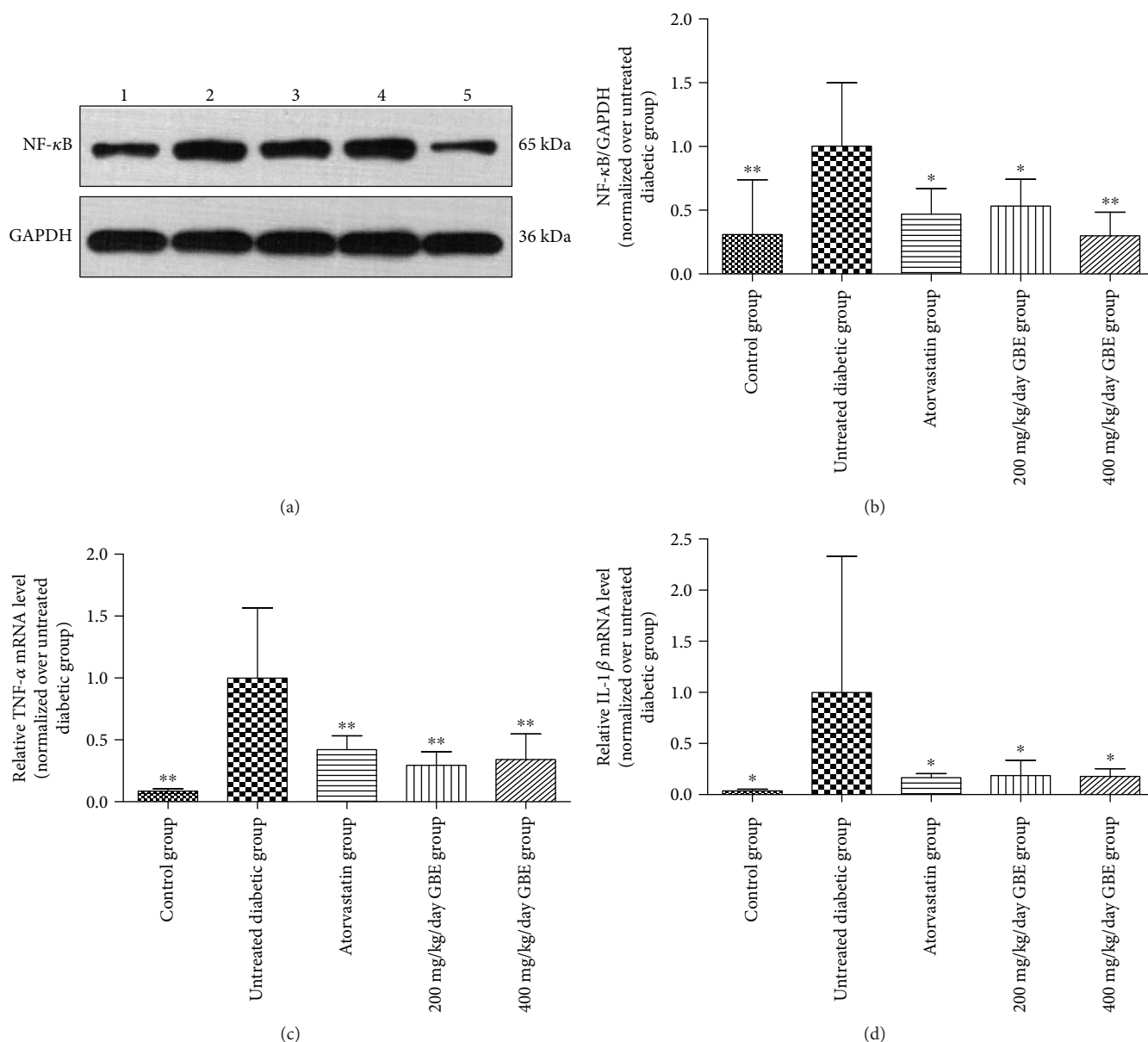
FIGURE 7: Effects of GBE on NF-κB-mediated intramyocardial inflammation. (a, b) NF-κB expression was determined by Western blotting. (c, d) Relative mRNA expression of TNF-α and IL-1β measured by real-time PCR. $^*P < 0.05$ and $^{**}P < 0.01$ versus the untreated diabetic group.

ATF6, and particularly PERK, is the third proapoptotic pathway related to ERS. Caspase-12 and CHOP are considered specific apoptotic pathways associated with ERS [26]. The present study showed that the three proapoptotic pathways related to ERS were upregulated in the untreated diabetic ApoE$^{-/-}$ mice, accompanied by increased expression of cleaved caspase-3, an effector of caspase-12. Our findings are consistent with the results of Zhang et al. [4], who showed that both the mRNA and protein levels of caspase-12 and CHOP were upregulated in STZ-induced diabetic rats. Taken together, ERS plays an important role in diabetic myocardial injury [27].

An earlier study conducted by Fitzl et al. [28] showed that EGb761, a standard GBE, attenuated the decrease in the volume fraction of myofibrils. According to Qiao et al. [17], GBE could attenuate ischemia/reperfusion-induced cardiac myocyte apoptosis by inhibiting cytochrome c release from the mitochondria and blocking the activation of caspase-3. The present study revealed that GBE downregulated the expression of p-JNK, CHOP, caspase-12, and cleaved caspase-3, indicating that GBE exerted antiapoptotic effects by attenuating ERS.

It has been reported that the IRE1α and PERK pathways of the UPR could trigger the NF-κB-mediated inflammatory pathway by phosphorylation of IKK; in addition, the ATF6 pathway is linked to NF-κB activation, suggesting that the three pathways of the UPR could activate this inflammatory cascade [5, 6, 29]. Nuclear translocation of NF-κB results in

(a)

(b)

(c)

(d)

(e)

(f)
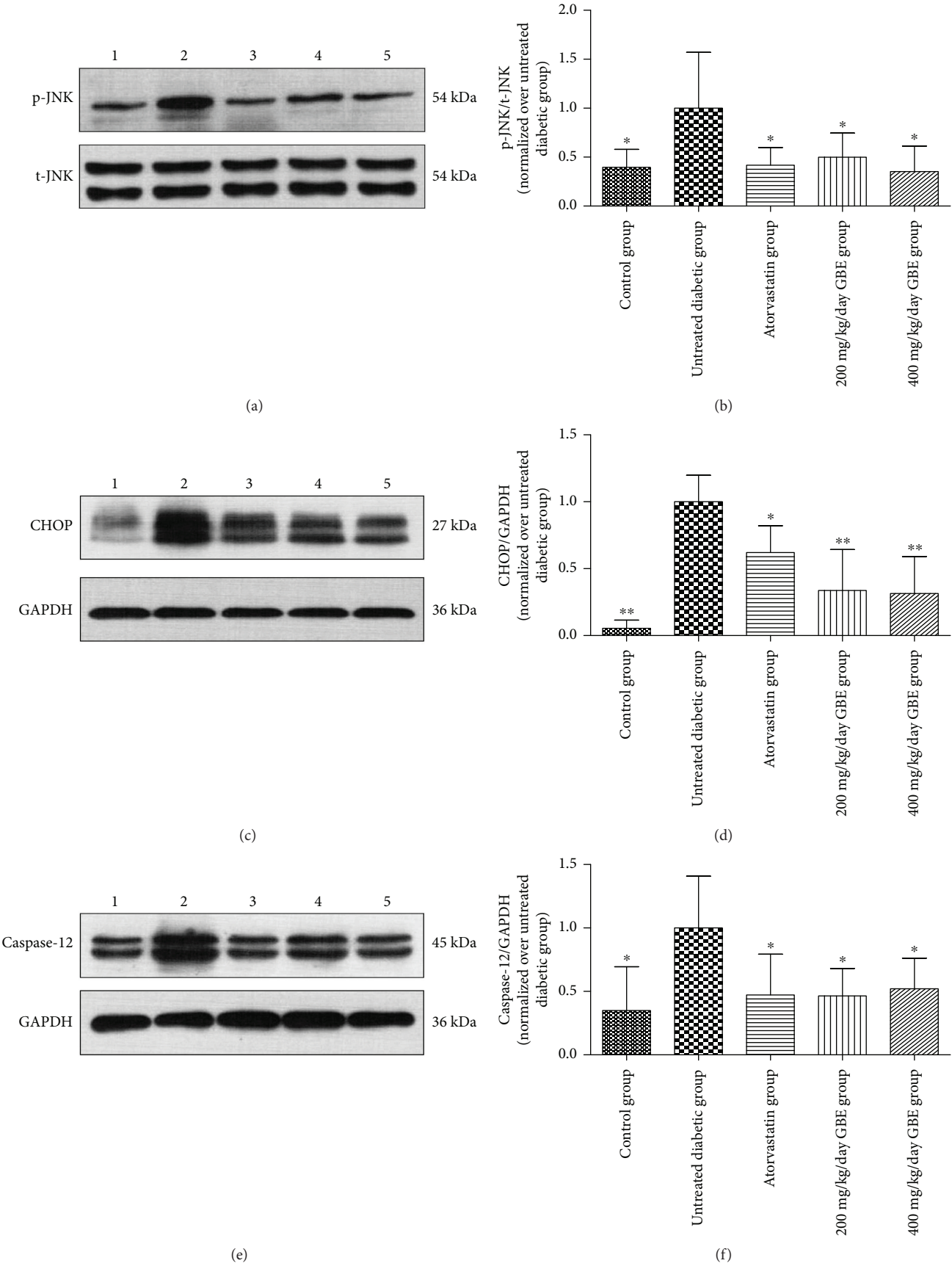
Figure 8: Continued.

(g)

(h)
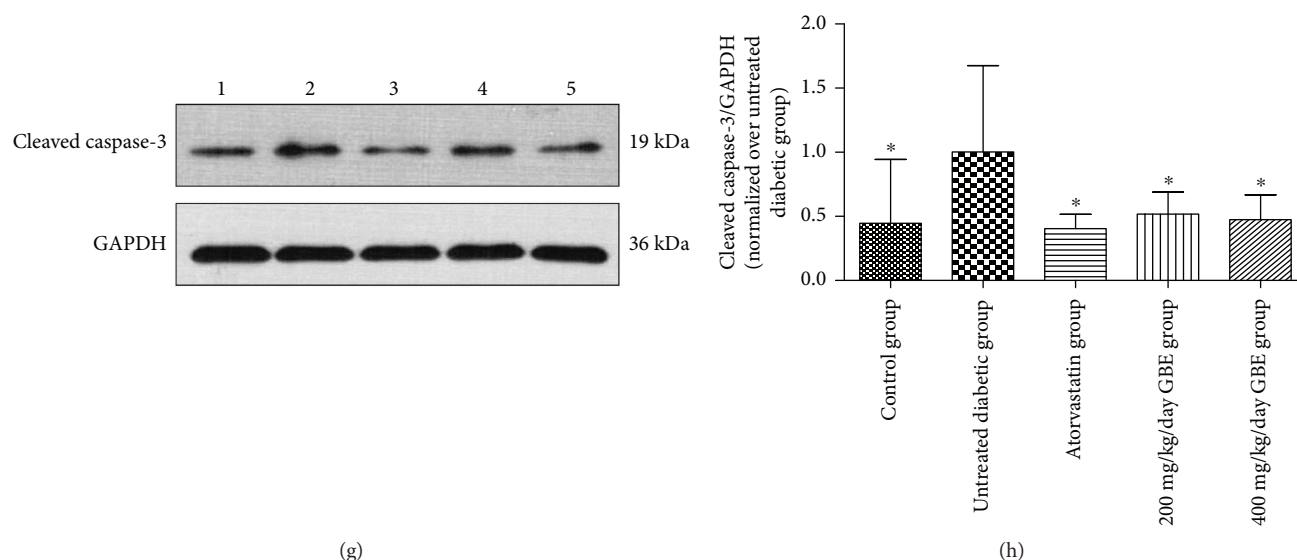
FIGURE 8: Effects of GBE on ERS-related apoptosis hallmark expression. Expression levels of p-JNK/JNK, CHOP, caspase-12, and cleaved caspase-3 were determined by Western blotting. The expression levels of CHOP, caspase-12, and cleaved caspase-3, were adjusted for GAPDH, and the expression of p-JNK was adjusted for total JNK. These values were normalized over the untreated diabetic group. (a, b) Expression levels of p-JNK/JNK; (c, d) expression of CHOP; (e, f) expression of caspase-12; and (g, h) expression of cleaved caspase-3. $^*P < 0.05$ and $^{**}P < 0.01$ versus the untreated diabetic group. 1: control group; 2: untreated group; 3: atorvastatin group; 4: 200 mg/kg/day GBE group; and 5: 400 mg/kg/day GBE group.
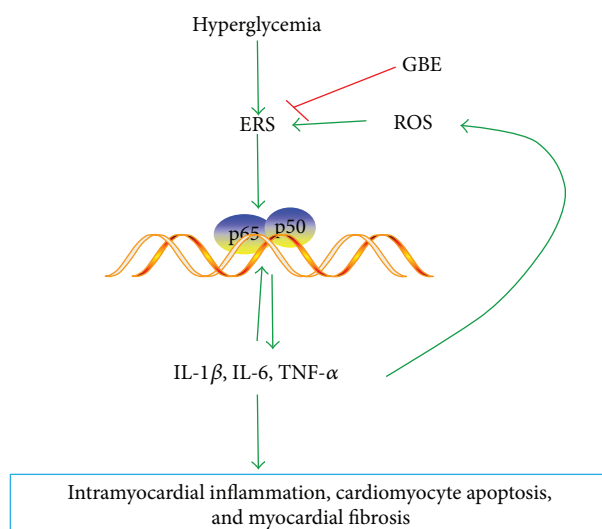
FIGURE 9: Mechanism underlying the protective effects of GBE against myocardial injury induced by hyperglycemia. The three pathways of UPR could activate NF-κB by phosphorylation of IKK, promoting the production of inflammation cytokines. TNF-α activates NF-κB in the presence of ROS in a positive feedback loop, resulting in the generation of more inflammatory cytokines, leading to intramyocardial inflammation, cardiomyocyte apoptosis, and myocardial fibrosis. GBE attenuated diabetic myocardial injury via blocking ERS. ROS: reactive oxygen species.

increased expression of the downstream proinflammatory cytokines, including IL-6, IL-1β, and TNF-α. IL-1β and TNF-α further activate ERS (a positive loop), resulting in a more potent inflammatory response, myocardial interstitial fibrosis, and cardiomyocyte apoptosis. TNF-α promotes reactive oxygen species (ROS) production and inflammation [30] and mediates JNK activation leading to caspase-3 activation and cardiac cell apoptosis [14]. Therefore, inflammation

can also induce ERS [31] (Figure 9). In the present study, GBE decreased collagen type I and III mRNA levels and interstitial collagen deposition, as revealed by Masson's staining. The increase in TNF-α and IL-1β mRNA levels in the diabetic heart was inhibited by GBE at 200 and 400 mg/kg/day. This was associated with reduced NF-κB expression. Collectively, our findings suggest that GBE attenuated interstitial fibrosis via inhibition of inflammation and ERS, as well

as owing to its direct radical scavenging activity and ability to inhibit the opening of the mPTP channel [32]. Although it was not possible to establish whether GBE directly attenuated ERS or acted via modulation of inflammation, it was definite that GBE blocked the positive loop of ERS and inflammation via attenuation of ERS (Figure 9).

In the present study, we observed that GBE at 200 and 400 mg/kg/day decreased plasma glucose levels at the end of the study period. GBE at 200 mg/kg/day decreased the serum glucose level before the mice were sacrificed; additionally, GBE at 400 mg/kg/day could decrease the serum glucose levels; however, it did not reach statistical significance. Cheng et al. [9] showed that GBE restored the activities of antioxidant enzymes, including superoxide dismutase (SOD), catalase (CAT), and glutathione peroxidase (GSH-Px) in the liver and pancreas of STZ-induced diabetic rats. Other studies showed that GBE could alleviate STZ-induced pancreatic damage in mice via inhibition of pancreatic inflammation and expression of proinflammatory cytokines, such as IL-1β, TNF-α, and IL-6 [10, 33]. The decrease in the serum levels of IL-6, IL-1β, and TNF-α by GBE treatment in our study suggested that the hypoglycemic effects were partly attributable to the inhibition of inflammation.

In the present study, STZ-induced diabetic ApoE$^{-/-}$ mice displayed severe hyperlipidemia, characterized by elevated serum LDL-c, TC, and TG levels, which were reversed by GBE administration, suggesting that GBE could lower lipid levels in diabetic settings. Zhang et al. [34] reported that GBE exhibited multidirectional lipid-lowering effects in rats, including reduction of cholesterol absorption, inactivation of 3-hydroxy-3-methylglutaryl-coenzyme A (HMG-COA), and favorable regulation of the profiles of essential polyunsaturated fatty acids. Yao et al. [35] showed that GBE at doses of 48 and 96 mg/kg/day normalized ethanol-induced dysregulation of the lipid profiles in rats. According to the study conducted by Cheng et al. [9], the lipid-lowering effects were probably attributed to the improvement of insulin resistance.

In conclusion, GBE attenuated diabetic myocardial injuries, including cardiomyocyte apoptosis, interstitial fibrosis, and intramyocardial inflammation in ApoE$^{-/-}$ diabetic mice by inhibiting ERS. Interestingly, in the present study, the cardioprotective effects of GBE in diabetic conditions were not dose-dependent, which might be because at doses of 200–400 mg/kg/day, the anti-inflammatory and antiapoptotic efficacy of GBE reached a plateau.

Conflicts of Interest

The authors declare that there is no conflict of interest regarding the publication of this article.

Authors' Contributions

Yue Liu and Shuzheng Lyu conceived the topic, drafted the paper together, and are the corresponding authors. Jinfan Tian searched the literature and wrote the manuscript with Yanfei Liu. Keji Chen helped to draft the manuscript. All authors read and approved the final manuscript.

References

[1] K. Huynh, B. C. Bernardo, J. R. McMullen, and R. H. Ritchie, "Diabetic cardiomyopathy: mechanisms and new treatment strategies targeting antioxidant signaling pathways," *Pharmacology & Therapeutics*, vol. 142, no. 3, pp. 375–415, 2014.

[2] X. Palomer, L. Salvadó, E. Barroso, and M. Vázquez-Carrera, "An overview of the crosstalk between inflammatory processes and metabolic dysregulation during diabetic cardiomyopathy," *International Journal of Cardiology*, vol. 168, no. 4, pp. 3160–3172, 2013.

[3] I. Falcão-Pires and A. F. Leite-Moreira, "Diabetic cardiomyopathy: understanding the molecular and cellular basis to progress in diagnosis and treatment," *Heart Failure Reviews*, vol. 17, no. 3, pp. 325–344, 2012.

[4] Z. Li, T. Zhang, H. Dai et al., "Endoplasmic reticulum stress is involved in myocardial apoptosis of streptozocin-induced diabetic rats," *The Journal of Endocrinology*, vol. 196, no. 3, pp. 565–572, 2008.

[5] S. Papa, F. Zazzeroni, C. G. Pham, C. Bubici, and G. Franzoso, "Linking JNK signaling to NF-κB: a key to survival," *Journal of Cell Science*, vol. 117, no. 22, pp. 5197–5208, 2004.

[6] J. Su, L. Zhou, X. Kong et al., "Endoplasmic reticulum is at the crossroads of autophagy, inflammation, and apoptosis signaling pathways and participates in the pathogenesis of diabetes mellitus," *Journal of Diabetes Research*, vol. 2013, Article ID 193461, 6 pages, 2013.

[7] H. L. Wen, Z. S. Liang, R. Zhang, and K. Yang, "Anti-inflammatory effects of triptolide improve left ventricular function in a rat model of diabetic cardiomyopathy," *Cardiovascular Diabetology*, vol. 12, no. 1, p. 50, 2013.

[8] A. Tosaki, T. Pali, and M. T. Droy-Lefaix, "Effects of *Ginkgo biloba* extract and preconditioning on the diabetic rat myocardium," *Diabetologia*, vol. 39, no. 11, pp. 1255–1262, 1996.

[9] D. Cheng, B. Liang, and Y. Li, "Antihyperglycemic effect of *Ginkgo biloba* extract in streptozotocin-induced diabetes in rats," *BioMed Research International*, vol. 2013, Article ID 162724, 7 pages, 2013.

[10] K. J. Rhee, C. G. Lee, S. W. Kim, D. H. Gim, H. C. Kim, and B. D. Jung, "Extract of *Ginkgo biloba* ameliorates streptozotocin-induced type 1 diabetes mellitus and high-fat diet-induced type 2 diabetes mellitus in mice," *International Journal of Medical Sciences*, vol. 12, no. 12, pp. 987–994, 2015.

[11] R. M. Banin, B. K. S. Hirata, I. S. Andrade et al., "Beneficial effects of *Ginkgo biloba* extract on insulin signaling cascade, dyslipidemia, and body adiposity of diet-induced obese rats," *Brazilian Journal of Medical and Biological Research*, vol. 47, no. 9, pp. 780–788, 2014.

[12] Q. Lu, X. X. Yin, J. Y. Wang, Y. Y. Gao, and Y. M. Pan, "Effects of *Ginkgo biloba* on prevention of development of

experimental diabetic nephropathy in rats," *Acta Pharmacologica Sinica*, vol. 28, no. 6, pp. 818–828, 2007.

[13] M. Geoffrion, X. Du, Z. Irshad et al., "Differential effects of glyoxalase 1 overexpression on diabetic atherosclerosis and renal dysfunction in streptozotocin-treated, apolipoprotein E-deficient mice," *Physiological Reports*, vol. 2, no. 6, article e12043, 2014.

[14] Y. Pan, Y. Wang, Y. Zhao et al., "Inhibition of JNK phosphorylation by a novel curcumin analog prevents high glucose–induced inflammation and apoptosis in cardiomyocytes and the development of diabetic cardiomyopathy," *Diabetes*, vol. 63, no. 10, pp. 3497–3511, 2014.

[15] X.-m. Ren, G.-f. Zuo, W. Wu et al., "Atorvastatin alleviates experimental diabetic cardiomyopathy by regulating the GSK-3β-PP2Ac-NF-κB signaling Axis," *PLoS One*, vol. 11, no. 11, article e0166740, 2016.

[16] J. Quidgley, N. Cruz, and M. J. Crespo, "Atorvastatin improves systolic function, but does not prevent the development of dilated cardiomyopathy in streptozotocin-induced diabetic rats," *Therapeutic Advances in Cardiovascular Disease*, vol. 8, no. 4, pp. 133–144, 2014.

[17] Z. Y. Qiao, J. H. Huang, J. W. Ma et al., "*Ginkgo biloba* extract reducing myocardium cells apoptosis by regulating apoptotic related proteins expression in myocardium tissues," *Molecular Biology Reports*, vol. 41, no. 1, pp. 347–353, 2014.

[18] Y. Liu, Y. F. Liu, J. F. Tian, C. G. Fu, and K. J. Cheng, "The effect and mechanism of extract of *Ginkgo biloba* (EGb) on cardiovascular protection on the rat model of type 2 diabetes after myocardial infarction," *Chinese Journal of Integrated Traditional and Western Medicine*, vol. 37, no. 9, pp. 1100–1104, 2017.

[19] A. A. M. Abdel-Hamid and A. E.-D. L. Firgany, "Atorvastatin alleviates experimental diabetic cardiomyopathy by suppressing apoptosis and oxidative stress," *Journal of Molecular Histology*, vol. 46, no. 4-5, pp. 337–345, 2015.

[20] C. Packard and A. G. Olsson, "Management of hypercholesterolaemia in the patient with diabetes," *International Journal of Clinical Practice Supplement*, vol. 130, pp. 27–32, 2002.

[21] K. K. Wu and Y. Huan, "Diabetic atherosclerosis mouse models," *Atherosclerosis*, vol. 191, no. 2, pp. 241–249, 2007.

[22] R. Huang, Z. Shi, L. Chen, Y. Zhang, J. Li, and Y. An, "Rutin alleviates diabetic cardiomyopathy and improves cardiac function in diabetic ApoEknockout mice," *European Journal of Pharmacology*, vol. 814, pp. 151–160, 2017.

[23] W. Li, Q. Fang, P. Zhong et al., "EGFR inhibition blocks palmitic acid-induced inflammation in cardiomyocytes and prevents hyperlipidemia-induced cardiac injury in mice," *Scientific Reports*, vol. 6, no. 1, article 24580, 2016.

[24] S. Van Linthout, A. Riad, N. Dhayat et al., "Anti-inflammatory effects of atorvastatin improve left ventricular function in experimental diabetic cardiomyopathy," *Diabetologia*, vol. 50, no. 9, pp. 1977–1986, 2007.

[25] T. Yoneda, K. Imaizumi, K. Oono et al., "Activation of caspase-12, an endoplastic reticulum (ER) resident caspase, through tumor necrosis factor receptor-associated factor 2-dependent mechanism in response to the ER stress," *The Journal of Biological Chemistry*, vol. 276, no. 17, pp. 13935–13940, 2001.

[26] N. Morishima, K. Nakanishi, H. Takenouchi, T. Shibata, and Y. Yasuhiko, "An endoplasmic reticulum stress-specific caspase cascade in apoptosis. Cytochrome *c*-independent activation of caspase-9 by caspase-12," *The Journal of Biological Chemistry*, vol. 277, no. 37, pp. 34287–34294, 2002.

[27] J. Xu, Q. Zhou, W. Xu, and L. Cai, "Endoplasmic reticulum stress and diabetic cardiomyopathy," *Experimental Diabetes Research*, vol. 2012, Article ID 827971, 12 pages, 2012.

[28] G. Fitzl, R. Martin, D. Dettmer, V. Hermsdorf, H. Drews, and K. Welt, "Protective effects of *Gingko biloba* extract EGb 761 on myocardium of experimentally diabetic rats: I: ultrastructural and biochemical investigation on cardiomyocytes," *Experimental and Toxicologic Pathology*, vol. 51, no. 3, pp. 189–198, 1999.

[29] H. Yamazaki, N. Hiramatsu, K. Hayakawa et al., "Activation of the Akt-NF-κB pathway by subtilase cytotoxin through the ATF6 branch of the unfolded protein response," *The Journal of Immunology*, vol. 183, no. 2, pp. 1480–1487, 2009.

[30] J. J. Kim, S. B. Lee, J. K. Park, and Y. D. Yoo, "TNF-α-induced ROS production triggering apoptosis is directly linked to Romo1 and Bcl-X$_L$," *Cell Death & Differentiation*, vol. 17, no. 9, pp. 1420–1434, 2010.

[31] S. Z. Hasnain, R. Lourie, I. Das, A. C.-H. Chen, and M. A. McGuckin, "The interplay between endoplasmic reticulum stress and inflammation," *Immunology & Cell Biology*, vol. 90, no. 3, pp. 260–270, 2012.

[32] A. S. Saini, R. Taliyan, and P. L. Sharma, "Protective effect and mechanism of *Ginkgo biloba* extract-EGb 761 on STZ-induced diabetic cardiomyopathy in rats," *Pharmacognosy Magazine*, vol. 10, no. 38, pp. 172–178, 2014.

[33] C. C. Chen, A. N. Chiang, H. N. Liu, and Y. T. Chang, "EGb-761 prevents ultraviolet B-induced photoaging via inactivation of mitogen-activated protein kinases and proinflammatory cytokine expression," *Journal of Dermatological Science*, vol. 75, no. 1, pp. 55–62, 2014.

[34] Q. Zhang, G.-J. Wang, J.-Y. A et al., "Application of GC/MS-based metabonomic profiling in studying the lipid-regulating effects of *Ginkgo biloba* extract on diet-induced hyperlipidemia in rats," *Acta Pharmacologica Sinica*, vol. 30, no. 12, pp. 1674–1687, 2009.

[35] P. Yao, F. Song, K. Li et al., "*Ginkgo biloba* extract prevents ethanol induced dyslipidemia," *The American Journal of Chinese Medicine*, vol. 35, no. 4, pp. 643–652, 2007.

Research Article

Modulation of Adipocyte Differentiation and Proadipogenic Gene Expression by Sulforaphane, Genistein, and Docosahexaenoic Acid as a First Step to Counteract Obesity

Veronica Valli,[1] Katharina Heilmann,[2] Francesca Danesi ⓘ,[1] Alessandra Bordoni ⓘ,[1] and Clarissa Gerhäuser[2]

[1]*Department of Agri-Food Science and Technology (DISTAL), University of Bologna, Piazza Goidanich 60, 47521 Cesena, Italy*
[2]*German Cancer Research Center (DKFZ), Division of Epigenomics and Cancer Risk Factors, Im Neuenheimer Feld 280, 69121 Heidelberg, Germany*

Correspondence should be addressed to Alessandra Bordoni; alessandra.bordoni@unibo.it

Obesity is characterized by excess body fat accumulation due to an increase in the size and number of differentiated mature adipocytes. Adipocyte differentiation is regulated by genetic and environmental factors, and its inhibition could represent a strategy for obesity prevention and treatment. The current study was designed with two aims: (i) to evaluate the changes in the expression of adipogenic markers (C/EBPα, PPARγ variant 1 and variant 2, and GLUT4) in 3T3-L1 murine preadipocytes at four stages of the differentiation process and (ii) to compare the effectiveness of sulforaphane, genistein, and docosahexaenoic acid in reducing lipid accumulation and modulating C/EBPα, PPARγ1, PPARγ2, and GLUT4 mRNA expression in mature adipocytes. All bioactive compounds were shown to suppress adipocyte differentiation, although with different effectiveness. These results set the stage for further studies considering natural food constituents as important agents in preventing or treating obesity.

1. Introduction

Obesity is the main dysfunction of adipose tissue and is associated with premature death and the development of chronic diseases such as cardiovascular diseases (CVD), type 2 diabetes, hypertension, and certain cancers [1]. In particular, a chronic inflammation in the absence of overt infection or autoimmune process is a puzzling phenomenon linked to obesity [2].

Environment, lifestyle, and genetic susceptibility certainly contribute to the increased risk of obesity, one of the easiest to be recognized and the most difficult to treat medical conditions [3]. Antiobesity drugs lack physiology specificity and have side effects [4].

Obesity is characterized by an excess accumulation of white adipose mass, resulting from both the increase in adipocyte cell size and the development of mature cells from undifferentiated precursors. Particularly, de novo generation of fat cells plays a key role in the development of obesity.

Discovering compounds able to regulate the size, number, and function of adipocytes and understanding their mechanisms of action could greatly contribute to obesity prevention and treatment. In this light, natural compounds represent a potential novel strategy, already exploited for preventing other metabolic disorders [5]. Bioactive compounds have been shown to exert specific effects on the biochemical and metabolic functions of adipocytes [6–8], in particular inhibition of preadipocyte differentiation, lipolysis stimulation, and induction of apoptosis of existing adipocytes [9], therefore contributing to a possible decrease in adipose tissue mass [10].

The aim of the current study was to compare the antiadipogenic effect of three bioactive compounds, namely, docosahexaenoic acid (DHA), genistein (GEN), and sulforaphane (SFN). DHA (C22:6 n-3) is an n-3 polyunsaturated fatty acid

(PUFA) abundant in fatty fish. It is considered effective in the prevention of many chronic diseases, mainly CVD [11]. GEN (4,5,7-trihydroxyisoflavone), the most abundant isoflavone found in soybeans, has received particular attention for its structural similarity to estrogen and its high affinity to the estrogen receptor. It is a well-known antioxidant, chemopreventive, and anti-inflammatory agent [12, 13]. SFN, an isothiocyanate compound, is a constituent of cruciferous vegetables such as broccoli sprouts, Brussels sprouts, and cabbage. SFN is known to have antioxidant, immunomodulatory, anticancer, and antidiabetic properties [14, 15].

In some previous earlier studies [16–19], all tested bioactive compounds have been shown to be antiadipogenic in the 3T3-L1 cell line. Notwithstanding, to our knowledge, their effectiveness has never been compared in the same experimental conditions. Although *in vitro* studies always need confirmation *in vivo*, the selection of the most active bioactive could be useful to formulate functional foods contributing to the development of new strategies to prevent obesity.

3T3-L1 cells constitute the most frequently used preadipocyte model, sharing many properties with normal adipocytes [20]. Their differentiation into mature adipocytes involves the exposure of a confluent, quiescent population of cells to a variety of effectors that activate a complex cascade of genes [21].

It is well documented that adipogenesis is finely controlled by key transcription factors such as peroxisome proliferator-activated receptor-γ (PPARγ) and CCAAT-enhancer-binding protein-α (C/EBPα). PPARγ and C/EBPα regulate the expression of various genes involved in lipogenesis, lipolysis, and insulin sensitivity, such as the one encoding for glucose transporter type 4 (GLUT4) [22, 23]. In the first part of the study, changes in the expression of PPARγ, C/EBPα, and GLUT4 genes were evaluated in the murine 3T3-L1 cell line at various stages of the differentiation process.

In the second part of the study, preadipocytes were supplemented during and after differentiation with DHA, GEN, and SFN, and both lipid accumulation and the mRNA expression of PPARγ, C/EBPα, and GLUT4 were evaluated to evidence and compare their potential inhibitory activity on adipogenesis.

2. Materials and Methods

Dulbecco's modified Eagle's medium (DMEM)/F12 GlutaMAX I was purchased from Invitrogen (Darmstadt, Germany), donor bovine serum (DBS) was from Gibco Life Technologies (Darmstadt, Germany), fetal bovine serum (FBS GOLD) was from PAA Laboratories (Pasching, Austria), and TRIzol Reagent was from Ambion, Life Technologies (Darmstadt, Germany). All other chemicals were purchased from Sigma-Aldrich (Schnelldorf, Germany) and were of the highest analytical grade.

2.1. Cell Culture and Differentiation. 3T3-L1 mouse preadipocytes were obtained from the American Type Culture Collection (ATCC) and maintained at 37°C in a humidified atmosphere containing 95% air and 5% CO_2; preadipocytes

were subcultured every three days when 80% confluent or less into a new $175 \, cm^2$ flask. Cells were cultured in DMEM/F12 GlutaMAX I with the addition of D-glucose (3151 mg/L f.c.) (GM) containing 10% DBS and 1% penicillin/streptomycin (PS). Cells were seeded in 12-well plates or a $25 \, cm^2$ flask at a concentration of 50,000 cells/mL. Three days after seeding, cells were stimulated to differentiate with GM supplemented with 10% FBS, 1% PS, insulin (10 μg/mL), dexamethasone (1 μM), isobutylmethylxanthine (0.2 mM), and rosiglitazone (10 μM) (differentiation medium). After further 3 days (differentiation), cells were maintained in GM with FBS, PS, and insulin (postdifferentiation medium) for another 5 days (postdifferentiation) when approximately 90% of the cells displayed the characteristic lipid-filled adipocyte phenotype.

2.2. Bioactive Supplementation. DHA, GEN, and SFN were added to the differentiation and postdifferentiation medium at three different final concentrations (10, 25, or 50 μM). The SRB assay was performed in preliminary experiments, evidencing no cytotoxicity for any of the tested concentrations of each bioactive.

The treatment with bioactives began three days after seeding and lasted until the end of postdifferentiation (eleven days from seeding). All bioactive compounds were purchased from Sigma-Aldrich (Schnelldorf, Germany). Each compound was dissolved in dimethyl sulfoxide (DMSO). Unsupplemented control cells (CTR) received a corresponding amount of DMSO (<0.5% final concentration). The medium was changed every two days during postdifferentiation.

2.3. Lipid Staining. The effect of the bioactive compounds on adipogenesis was evaluated morphologically by staining accumulated lipids with Oil Red O [24] as previously described [25]. Briefly, cells were fixed with 4% formalin solution in phosphate-buffered saline (PBS) for two hours, washed with water, rinsed with isopropanol 60%, and stained with Oil Red O for 30 minutes at room temperature. After washing with distilled water for 3 times, the lipid droplets were quantified by dissolving Oil Red O in isopropanol 100% and measuring the optical density at 500 nm.

The lowest bioactive concentrations able to influence lipid accumulation (10 μM GEN, 10 μM SFN, 25 μM DHA) were then used in gene expression experiments.

2.4. Gene Expression Analysis. Unsupplemented, control cells were collected at four different steps of the differentiation protocol: one day after seeding (T1); three days after seeding (postconfluent cells), before the beginning of differentiation (T2); six days after seeding (end of the differentiation), before the addition of the postdifferentiation medium (T3); and eleven days after seeding, at the end of postdifferentiation (T4). Cells were collected at the different time points, and total RNA was extracted as described below.

In experiments evaluating bioactives' effect, 10 μM GEN, 10 μM SFN, or 25 μM DHA was added to the differentiation and postdifferentiation media as described above. At the end

TABLE 1: Primer sequences used in qPCR.

Gene	Forward primer	Reverse primer	Probe number
Target genes			
PPARγ1	GAAAGACAACGGACAAATCACC	GGGGGTGATATGTTTGAACTTG	7
PPARγ2	TGCTGTTATGGGTGAAACTCTG	CTGTGTCAACCATGGTAATTTCTT	2
C/EBPα	AAACAACGCAACGTGGAGA	GCGGTCATTGTCACTGGTC	67
GLUT4	GACGGACACTCCATCTGTTG	GCCACGATGGAGACATAGC	5
Reference genes			
ACTB	GTGGGAGAGCAAGGAAGAGA	CACTCTTGGCCCAGTCTACG	56
HPRT1	TCCTCCTCAGACCGCTTTT	CCTGGTTCATCATCGCTAATC	95
TBP	CGGTCGCGTCATTTCTC	GGGTTATCTTCACACACCATGA	107

of the postdifferentiation period (T4), cells were collected, and total RNA was extracted with TRIzol Reagent following the manufacturer's protocol. Contaminating DNA was eliminated by DNase treatment (DNA-free Kit from Ambion, Life Technologies, Darmstadt, Germany). RNA quantity and quality, respectively, were assessed by spectrophotometric analyses at 260/230 nm using a NanoDrop ND-2000 spectrophotometer (Thermo Fisher Scientific, Wilmington, DE, USA) and by the microfluidics-based Bioanalyzer platform with an RNA Nano 6000 Chip (Agilent Technology, Waldbronn, Germany).

cDNA was synthesized from 0.5 μg or 1 μg of DNase-treated total RNA using SuperScript II reverse transcriptase (Invitrogen, Darmstadt, Germany) according to the manufacturer's instructions. Quantitative real-time PCR (qPCR) was performed using the Universal ProbeLibrary system (Roche, Mannheim, Germany) on a Roche LightCycler 480 real-time PCR system (Roche, Mannheim, Germany). The cycling program for analysis was 15 min at 95°C followed by 45 cycles of 10 s at 95°C, 20 s at 55°C, and 10 s at 72°C with the primer pairs and the respective monocolor hydrolysis probes indicated in Table 1. The expression levels of target mRNAs were normalized to three reference genes: β-actin (ACTB), hypoxanthine phosphoribosyltransferase 1 (HPRT1), and TATA-box-binding protein (TBP).

2.5. Statistical Analysis. Gene expression data were analyzed using DataAssist software version 3.01 (Applied Biosystems, Foster City, CA, USA) and expressed as the mean fold change in relative expression compared with the untreated control cells, which were normalized to one. Average fold change and standard deviation (SD) were obtained from three biological replicate samples per condition.

All data were analyzed by one-way ANOVA, followed by Dunnett's or Tukey's tests. Statistical analysis of the data was performed using the GraphPad Prism 5 software (San Diego, CA, USA).

3. Results

3.1. Characterization of Preadipocyte Differentiation. During differentiation (T1–T4), preadipocytes acquired the characteristics of mature adipocytes. At three days after

seeding (T2), nondifferentiated cells showed typical fibroblastoid morphology, while at the end of the differentiation process (T4), cells had abundant intracytoplasmic lipid accumulation, showing typical white adipocyte morphology (Figure 1).

To characterize the differentiation process, PPARγ1, PPARγ2, C/EBPα, and GLUT4 gene expression was evaluated at four different stages of adipocyte differentiation: one day after seeding (T1), three days after seeding (T2), at the end of the differentiation (T3), and at the end of postdifferentiation (T4).

The expression of selected genes was very low and similar at T1 and T2, while it significantly increased at T3. For all analyzed genes, a prominent increase in mRNA levels was observed in mature adipocytes (T4) (Figure 2).

3.2. Effects of Bioactive Compound Supplementation. The antiadipogenic potential of DHA, GEN, and SFN was first investigated evaluating their influence on lipid accumulation. Preadipocytes were supplemented with different concentrations (10, 25, and 50 μM) of the test compounds during the differentiation and postdifferentiation periods, as described above, and lipid accumulation was detected by Oil Red O staining. All bioactive compounds markedly reduced lipid droplet formation compared to controls. GEN and SFN were effective at the lowest concentration used for supplementation (10 μM), while a higher DHA concentration (25 μM) was required to reduce lipid accumulation (Figure 3).

The lowest bioactive concentrations causing a significant decrease in lipid accumulation were used to verify the modification in the mRNA levels of the adipogenesis marker genes after differentiation.

At T4, all bioactive compounds significantly reduced the transcript levels of PPARγ1, PPARγ2, C/EBPα, and GLUT4. The effect of GEN and SFN on PPARγ and GLUT4 expression appeared stronger than the DHA effect did (Figure 4).

4. Discussion

Adipose tissue has an important function in the energy balance by regulating lipid metabolism, glucose homeostasis,

(a)　　　　　　　　　　　　　　　　(b)　　　　　　　　　　　　　　　　(c)
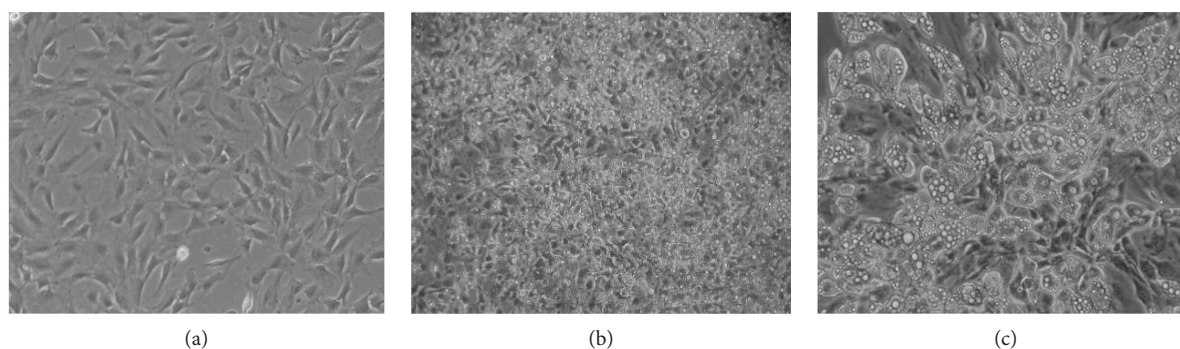
FIGURE 1: Morphological changes among (a) preadipocytes three days after seeding (T2), (b) adipocytes at the end of the differentiation (T3), and (c) adipocytes at the end of postdifferentiation (T4). Images showing different cell morphologies were captured at the different steps using a Leica DM IL microscope (Wetzlar, Germany), with 10x magnification.
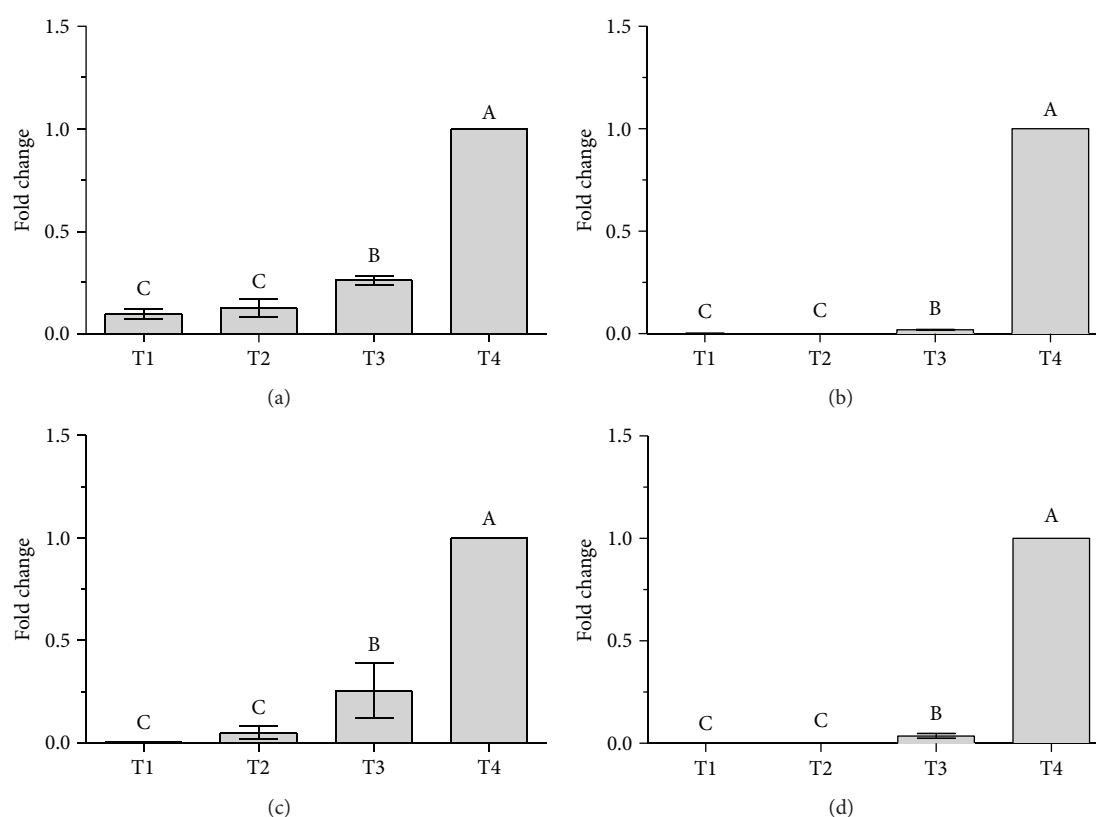
FIGURE 2: (a) PPARγ1, (b) PPARγ2, (c) C/EBPα, and (d) GLUT4 mRNA expression at 4 different stages of adipocyte differentiation. T1: one day after seeding; T2: three days after seeding, before the beginning of differentiation; T3: at the end of the differentiation, before the addition of the postdifferentiation medium; T4: at the end of postdifferentiation (mature adipocytes). Data are expressed as the mean fold change relative to the mature cells (T4), normalized to one. Statistical analysis was by one-way ANOVA ($p < 0.001$ for all panels) followed by Tukey's HSD test. The expression is significantly different between groups marked with different letters (at least $p < 0.05$).

and adipokine secretion. Thus, its dysfunction is critical in developing metabolic diseases [26]. Indeed, the incidence of metabolic syndrome, a combination of cardiometabolic risk determinants, is increasing worldwide largely as a consequence of the continued obesity epidemic [27].

In general, obesity is related to the extent of adipocyte differentiation, intracellular lipid accumulation, and lipolysis [17]. The process of adipocyte differentiation requires

the activation of numerous transcription factors which are in charge of the coordinated induction and silencing of more than 2000 genes [28]. Several transcriptional regulators, including C/EBP and PPARγ, play a pivotal role in this process.

The master regulator PPARγ is both necessary and sufficient for adipogenesis [29, 30]. PPARγ has two isoforms, the ubiquitary PPARγ1 and the adipose tissue-specific PPARγ2.
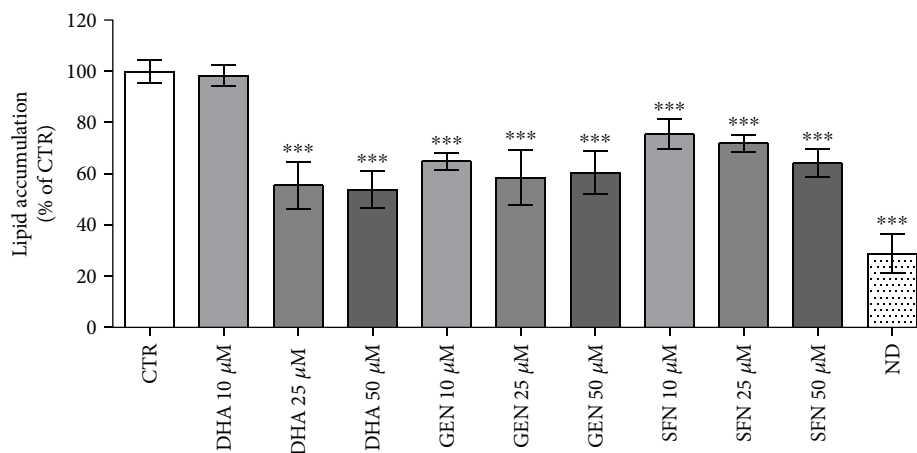
FIGURE 3: Lipid accumulation in supplemented and control cells. Data are expressed as a percentage relative to unsupplemented control cells (CTR), assigned as 100%. Statistical analysis was performed by one-way ANOVA ($p < 0.001$) followed by Dunnett's test: $***p < 0.001$ versus CTR. ND: nondifferentiated cells, before the beginning of the differentiation process.

(a)

(b)

(c)

(d)
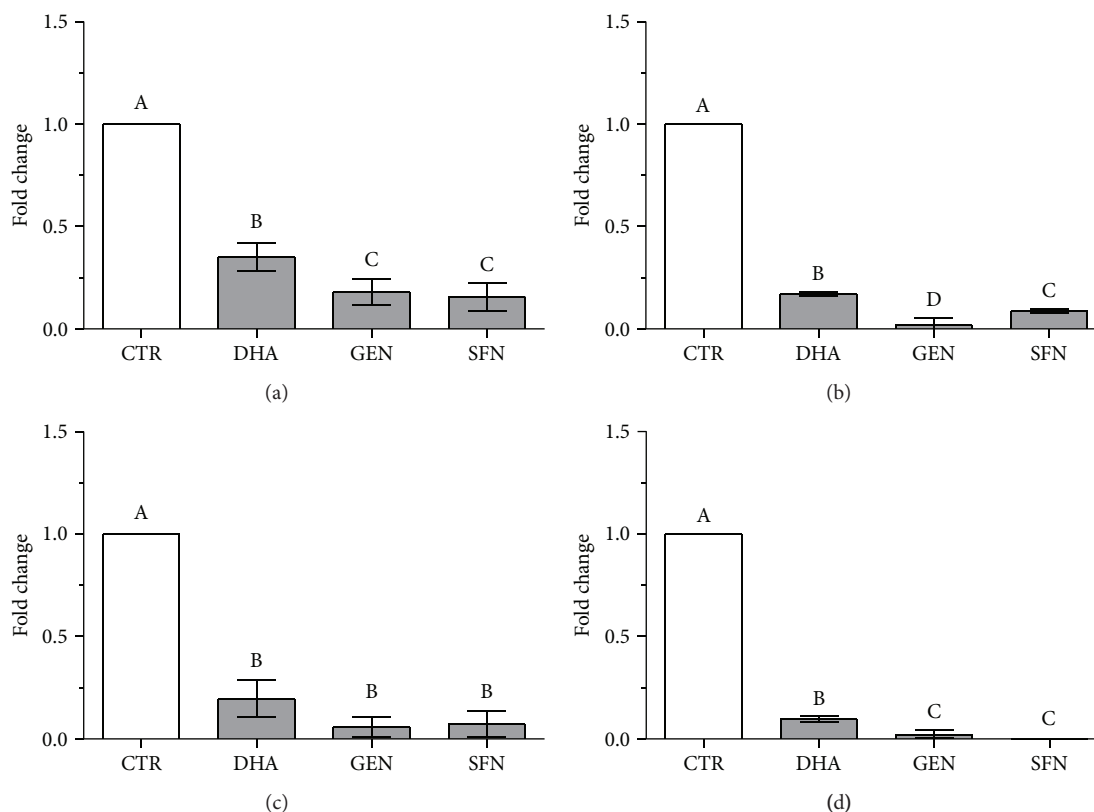
FIGURE 4: Modulatory effect of GEN, SFN, and DHA on (a) PPARγ1, (b) PPARγ2, (c) C/EBPα, and (d) GLUT4 mRNA expression. Data are expressed as the mean fold change relative to the unsupplemented control cells (CTR) at T4, normalized to one. Statistical analysis was by one-way ANOVA ($p < 0.001$ for all panels) followed by Tukey's HSD test. The expression is significantly different between groups marked with different letters (at least $p < 0.05$).

Both isoforms are strongly induced during preadipocyte differentiation [25], and our data confirm that PPARγ1 induction foreruns PPARγ2 induction [31].

C/EBPβ and C/EBPδ are overexpressed in the earlier phases of differentiation and have been shown to play a role in PPARγ induction [30]. C/EBPα is involved in the maintenance of the terminally differentiated adipocyte phenotypes [28, 32, 33]. In agreement, we observed a lower C/EBPα expression at T1 and T2 than at T3 and T4.

In adipocytes, C/EBPα regulates the expression of the gene encoding for GLUT4, the major insulin-responsive glucose transporter in adipose tissue as well as in skeletal and

cardiac muscles [34]. Accordingly, in the present study, GLUT4 expression paralleled C/EBPα expression.

Overall, our results confirm that differentiation of 3T3-L1 cells includes distinguishable multiple stages [35, 36].

Our results evidence that all tested bioactives efficiently block adipocyte differentiation. At T4, the expression of all the tested genes was significantly lower in supplemented cells than in unsupplemented ones and comparable to the expression level observed in unsupplemented cells at the first stages of differentiation.

The antiadipogenic effect of DHA, GEN, and SFN has been already reported in previous earlier studies [16–19]. Our study is not simply a confirmation that the tested bioactives act mainly through modification of the adipocyte life cycle [8], but mainly a representation of the first study comparing the effectiveness of DHA, GEN, and SFN in the same experimental conditions. Although GEN and SFN appeared effective at lower concentrations than DHA did, it is worth noting that *in vivo* the latter is absorbed and delivered to peripheral cells in its parent form. GEN and SFN are extensively metabolized, and they are detectable at very low concentrations in the bloodstream [37–39]. On the contrary, the DHA concentration used in this study for cell supplementation is easily reachable *in vivo* in the human plasma [40–42].

5. Conclusions

Our results represent an additional step in the evaluation of the antiadipogenic effects of three natural bioactive molecules, DHA, GEN, and SFN. Although *in vitro* all tested bioactive compounds appeared to be putative contributors to the prevention and treatment of obesity, their *in vivo* metabolism suggests that mainly DHA could potentially be used for the formulation of new functional food products devoted to a new dietetic natural strategy for overweight counteraction.

Further investigations are needed to verify whether the antiadipogenic properties evidenced *in vitro* do translate into *in vivo* efficacy in humans and to sort out the pathway(s) responsible for the beneficial effects. Moreover, the compounds here considered have been studied as discrete molecules and not as part of a food, ignoring both the matrix effect and the eventual synergistic or enhanced activities between the selected compounds and other food components or other bioactive molecules [43]. This issue also deserves future attention.

Disclosure

Veronica Valli's current address is Sociedad Española de Colorantes Naturales y Afines (SECNA), Polígono 33, Parcela 254, El Muladar, 46370 Chiva, Valencia, Spain.

Conflicts of Interest

The authors declare no conflict of interest.

Authors' Contributions

Veronica Valli participated in the study design and conducted all the experiments; Katharina Heilmann gave a substantial contribution in performing qPCR assays; Francesca Danesi performed the gene expression data normalization and carried out the statistical analysis; Alessandra Bordoni is the coordinator of the Pathway-27 European project and supervised the study; and Clarissa Gerhäuser conceived, designed, and supervised the experiments and wrote the manuscript together with Veronica Valli and Alessandra Bordoni. All authors contributed actively to the revision of the manuscript.

Acknowledgments

References

[1] J. M. Friedman, "Obesity in the new millennium," *Nature*, vol. 404, no. 6778, pp. 632–634, 2000.

[2] B. Vandanmagsar, Y. H. Youm, A. Ravussin et al., "The NLRP3 inflammasome instigates obesity-induced inflammation and insulin resistance," *Nature Medicine*, vol. 17, no. 2, pp. 179–188, 2011.

[3] S. Rayalam, J. Y. Yang, M. A. Della-Fera, H. J. Park, S. Ambati, and C. A. Baile, "Anti-obesity effects of xanthohumol plus guggulsterone in 3T3-L1 adipocytes," *Journal of Medicinal Food*, vol. 12, no. 4, pp. 846–853, 2009.

[4] G. A. Bray and L. A. Tartaglia, "Medicinal strategies in the treatment of obesity," *Nature*, vol. 404, no. 6778, pp. 672–677, 2000.

[5] J. T. Hwang, S. H. Kim, M. S. Lee et al., "Anti-obesity effects of ginsenoside Rh2 are associated with the activation of AMPK signaling pathway in 3T3-L1 adipocyte," *Biochemical and Biophysical Research Communications*, vol. 364, no. 4, pp. 1002–1008, 2007.

[6] M. González-Castejón and A. Rodriguez-Casado, "Dietary phytochemicals and their potential effects on obesity: a review," *Pharmacological Research*, vol. 64, no. 5, pp. 438–455, 2011.

[7] C. Andersen, S. Rayalam, M. A. Della-Fera, and C. A. Baile, "Phytochemicals and adipogenesis," *BioFactors*, vol. 36, no. 6, pp. 415–422, 2010.

[8] D. Moseti, A. Regassa, and W. K. Kim, "Molecular regulation of adipogenesis and potential anti-adipogenic bioactive molecules," *International Journal of Molecular Sciences*, vol. 17, no. 1, article 124, 2016.

[9] C. A. Baile, J. Y. Yang, S. Rayalam et al., "Effect of resveratrol on fat mobilization," *Annals of the New York Academy of Sciences*, vol. 1215, no. 1, pp. 40–47, 2011.

[10] J. Y. Yang, M. A. Della-Fera, S. Rayalam et al., "Enhanced inhibition of adipogenesis and induction of apoptosis in 3T3-L1 adipocytes with combinations of resveratrol and quercetin," *Life Sciences*, vol. 82, no. 19-20, pp. 1032–1039, 2008.

[11] S. Lorente-Cebrián, A. G. Costa, S. Navas-Carretero, M. Zabala, J. A. Martínez, and M. J. Moreno-Aliaga, "Role of omega-3 fatty acids in obesity, metabolic syndrome, and cardiovascular diseases: a review of the evidence," *Journal of Physiology and Biochemistry*, vol. 69, no. 3, pp. 633–651, 2013.

[12] K. Polkowski and A. P. Mazurek, "Biological properties of genistein. A review of *in vitro* and *in vivo* data," *Acta Poloniae Pharmaceutica*, vol. 57, no. 2, pp. 135–155, 2000.

[13] D. C. Vitale, C. Piazza, B. Melilli, F. Drago, and S. Salomone, "Isoflavones: estrogenic activity, biological effect and bioavailability," *European Journal of Drug Metabolism and Pharmacokinetics*, vol. 38, no. 1, pp. 15–25, 2013.

[14] C. T. Yeh and G. C. Yen, "Chemopreventive functions of sulforaphane: a potent inducer of antioxidant enzymes and apoptosis," *Journal of Functional Foods*, vol. 1, no. 1, pp. 23–32, 2009.

[15] A. T. Dinkova-Kostova and R. V. Kostov, "Glucosinolates and isothiocyanates in health and disease," *Trends in Molecular Medicine*, vol. 18, no. 6, pp. 337–347, 2012.

[16] A. S. Wang, C. W. Xu, H. Y. Xie et al., "DHA induces mitochondria-mediated 3T3-L1 adipocyte apoptosis by down-regulation of Akt and ERK," *Journal of Functional Foods*, vol. 21, pp. 517–524, 2016.

[17] J. H. Lee, M. H. Moon, J. K. Jeong et al., "Sulforaphane induced adipolysis via hormone sensitive lipase activation, regulated by AMPK signaling pathway," *Biochemical and Biophysical Research Communications*, vol. 426, no. 4, pp. 492–497, 2012.

[18] E. J. Choi, J. Y. Jung, and G. H. Kim, "Genistein inhibits the proliferation and differentiation of MCF-7 and 3T3-L1 cells via the regulation of ERα expression and induction of apoptosis," *Experimental and Therapeutic Medicine*, vol. 8, no. 2, pp. 454–458, 2014.

[19] G. Murali, C. V. Desouza, M. E. Clevenger, R. Ramalingam, and V. Saraswathi, "Differential effects of eicosapentaenoic acid and docosahexaenoic acid in promoting the differentiation of 3T3-L1 preadipocytes," *Prostaglandins, Leukotrienes, and Essential Fatty Acids*, vol. 90, no. 1, pp. 13–21, 2014.

[20] K. Iwashita, K. Yamaki, and T. Tsushida, "Effect of flavonoids on the differentiation of 3T3-L1 adipocytes," *Food Science and Technology Research*, vol. 7, no. 2, pp. 154–160, 2001.

[21] D. Prusty, B. H. Park, K. E. Davis, and S. R. Farmer, "Activation of MEK/ERK signaling promotes adipogenesis by enhancing peroxisome proliferator-activated receptor γ (PPARγ) and C/EBPα gene expression during the differentiation of 3T3-L1 preadipocytes," *Journal of Biological Chemistry*, vol. 277, no. 48, pp. 46226–46232, 2002.

[22] J. M. Ntambi and K. Young-Cheul, "Adipocyte differentiation and gene expression," *The Journal of Nutrition*, vol. 130, no. 12, pp. 3122S–3126S, 2000.

[23] C. E. Lowe, S. O'Rahilly, and J. J. Rochford, "Adipogenesis at a glance," *Journal of Cell Science*, vol. 124, no. 16, pp. 2681–2686, 2011.

[24] M. Rydén, A. Dicker, C. Götherström et al., "Functional characterization of human mesenchymal stem cell-derived adipocytes," *Biochemical and Biophysical Research Communications*, vol. 311, no. 2, pp. 391–397, 2003.

[25] V. Ghini, M. Di Nunzio, L. Tenori et al., "Evidence of a DHA signature in the lipidome and metabolome of human hepatocytes," *International Journal of Molecular Sciences*, vol. 18, no. 2, article 359, 2017.

[26] P. Trayhurn, C. Bing, and I. S. Wood, "Adipose tissue and adipokines – energy regulation from the human perspective," *The Journal of Nutrition*, vol. 136, no. 7, pp. 1935S–1939S, 2006.

[27] K. D. Bruce and M. A. Hanson, "The developmental origins, mechanisms, and implications of metabolic syndrome," *The Journal of Nutrition*, vol. 140, no. 3, pp. 648–652, 2010.

[28] H. X. Li, L. Xiao, C. Wang, J. L. Gao, and Y. G. Zhai, "Epigenetic regulation of adipocyte differentiation and adipogenesis," *Journal of Zhejiang University Science B*, vol. 11, no. 10, pp. 784–791, 2010.

[29] S. R. Farmer, "Transcriptional control of adipocyte formation," *Cell Metabolism*, vol. 4, no. 4, pp. 263–273, 2006.

[30] E. D. Rosen, C.-H. Hsu, X. Wang et al., "C/EBPα induces adipogenesis through PPARγ: a unified pathway," *Genes & Development*, vol. 16, no. 1, pp. 22–26, 2002.

[31] Y.-W. Cho, S. Hong, Q. Jin et al., "Histone methylation regulator PTIP is required for *PPARγ* and *C/EBPα* expression and adipogenesis," *Cell Metabolism*, vol. 10, no. 1, pp. 27–39, 2009.

[32] J. K. Hamm, A. K. el Jack, P. F. Pilch, and S. R. Farmer, "Role of PPARγ in regulating adipocyte differentiation and insulin-responsive glucose uptake," *Annals of the New York Academy of Sciences*, vol. 892, no. 1 THE METABOLIC, pp. 134–145, 1999.

[33] T. C. Otto and M. D. Lane, "Adipose development: from stem cell to adipocyte," *Critical Reviews in Biochemistry and Molecular Biology*, vol. 40, no. 4, pp. 229–242, 2005.

[34] N. Yokomori, M. Tawata, and T. Onaya, "DNA demethylation during the differentiation of 3T3-L1 cells affects the expression of the mouse GLUT4 gene," *Diabetes*, vol. 48, no. 4, pp. 685–690, 1999.

[35] H. Sakamoto, Y. Kogo, J. Ohgane et al., "Sequential changes in genome-wide DNA methylation status during adipocyte differentiation," *Biochemical and Biophysical Research Communications*, vol. 366, no. 2, pp. 360–366, 2008.

[36] Q. Q. Tang, T. C. Otto, and M. D. Lane, "Mitotic clonal expansion: a synchronous process required for adipogenesis," *Proceedings of the National Academy of Sciences of the United States of America*, vol. 100, no. 1, pp. 44–49, 2003.

[37] A. V. Gasper, A. Al-Janobi, J. A. Smith et al., "Glutathione S-transferase M1 polymorphism and metabolism of sulforaphane from standard and high-glucosinolate broccoli," *The American Journal of Clinical Nutrition*, vol. 82, no. 6, pp. 1283–1291, 2005.

[38] K. Hosoda, T. Furuta, and K. Ishii, "Metabolism and disposition of isoflavone conjugated metabolites in humans after ingestion of kinako," *Drug Metabolism and Disposition*, vol. 39, no. 9, pp. 1762–1767, 2011.

[39] Z. Yang, K. Kulkarni, W. Zhu, and M. Hu, "Bioavailability and pharmacokinetics of genistein: mechanistic studies on its ADME," *Anti-Cancer Agents in Medicinal Chemistry*, vol. 12, no. 10, pp. 1264–1280, 2012.

[40] J. J. Jans, M. G. de Sain-van der Velden, P. M. van Hasselt et al., "Supplementation with a powdered blend of PUFAs normalizes DHA and AA levels in patients with PKU," *Molecular Genetics and Metabolism*, vol. 109, no. 2, pp. 121–124, 2013.

[41] J. J. Lara, M. Economou, A. M. Wallace et al., "Benefits of salmon eating on traditional and novel vascular risk factors in young, non-obese healthy subjects," *Atherosclerosis*, vol. 193, no. 1, pp. 213–221, 2007.

[42] M. Di Nunzio, V. Valli, L. Tomas-Cobos, L. Murgui-Bosch, F. Danesi, and A. Bordoni, "Is cytotoxicity a determinant of the different in vitro and in vivo effects of bioactives?," *BMC Complementary and Alternative Medicine*, vol. 17, no. 1, article 453, 2017.

[43] F. Danesi, M. Govoni, L. F. D'Antuono, and A. Bordoni, "The molecular mechanism of the cholesterol-lowering effect of dill and kale: the influence of the food matrix components," *Electrophoresis*, vol. 37, no. 13, pp. 1805–1813, 2016.

Research Article

Biotransformation of *Dioscorea nipponica* by Rat Intestinal Microflora and Cardioprotective Effects of Diosgenin

Jia-Fu Feng,[1] Yi-Na Tang,[2,3] Hong Ji,[4] Zhan-Gang Xiao,[5] Lin Zhu,[2,6] and Tao Yi[2,7]

[1]*Department of Pharmaceutical Science, Leshan Vocational & Technical College, Leshan 614000, China*
[2]*School of Chinese Medicine, Hong Kong Baptist University, Hong Kong Special Administrative Region, China*
[3]*Sichuan Academy of Chinese Medicine Sciences, Chengdu 610041, China*
[4]*School of Pharmaceutical Science, Guangzhou Medical University, Guangzhou 511436, China*
[5]*Laboratory of Molecular Pharmacology, Department of Pharmacology, School of Pharmacy, Southwest Medical University, Luzhou, Sichuan 646000, China*
[6]*Shenzhen Research Institute, The Chinese University of Hong Kong, Shenzhen 518057, China*
[7]*Institute of Research and Continuing Education (Shenzhen), Hong Kong Baptist University, Shenzhen 518057, China*

Correspondence should be addressed to Lin Zhu; zhulin@hkbu.edu.hk and Tao Yi; yitao@hkbu.edu.hk

Studying the biotransformation of natural products by intestinal microflora is an important approach to understanding how and why some medicines—particularly natural medicines—work. In many cases, the active components are generated by metabolic activation. This is critical for drug research and development. As a means to explore the therapeutic mechanism of *Dioscorea nipponica* (DN), a medicinal plant used to treat myocardial ischemia (MI), metabolites generated by intestinal microflora from DN were identified, and the cardioprotective efficacy of these metabolites was evaluated. Our results demonstrate that diosgenin is the main metabolite produced by rat intestinal microflora from DN. Further, our results show that diosgenin protects the myocardium against ischemic insult through increasing enzymatic and nonenzymatic antioxidant levels *in vivo* and by decreasing oxidative stress damage. These mechanisms explain the clinical efficacy of DN as an anti-MI drug.

1. Introduction

Ischemic heart disease (IHD) is a significant threat to human health, leading to high morbidity and mortality in the Western world, even in China. It is estimated by the World Health Organization that IHD will be the leading cause of death in the world in the coming decades [1]. Recently, there has been a growing interest in establishing the therapeutic potentials of medicinal plants against IHD. For instance, total peony glycosides from Radix Paeoniae rubrae and cinnamic acid and cinnamic aldehyde from *Cinnamomum cassia* have been evaluated for their protective effect against isoprenaline- (ISO-) induced myocardial ischemia in rats [2, 3]. In particular, it is noteworthy that bioactive steroidal saponins from the medicinal plant *Dioscorea nipponica* (DN) have been successfully developed as effective herbal medicines by

the pharmaceutical industry for treating IHD. These herbal medicines developed from DN have been in use since the 1970s; they include "Polysponin" approved by the former Soviet Union's Ministry of Health, and Diosconin Tablet and Di'ao Xinxuekang Capsule produced in China and indicated for myocardial ischemia or angina pectoris.

In the previous study, authors of the present report established a mixed microscopic method for differentiating DN from several *Dioscorea* species in order to ensure the authentic origin of DN during herb collection [4] and later demonstrated that major constituents of DN include *Dioscorea* saponins but contained no free diosgenin [5, 6] and that DN mediates a cardioprotective effect [7]. These findings notwithstanding, the active components and therapeutic mechanism of DN have not been fully characterized. The constituents in DN in their native forms as expressed by

plant tissues may be prodrugs; the metabolites, of which, mediate therapeutic effects. Thus, further research is to better characterize their bioactive properties. Such work is anticipated to yield improved insight into clinical use of DN. Our recent research further showed that diosgenin, as a main metabolite from DN, was found and quantified in the plasma from the experimental rat group orally receiving DN [8]. Thus, we hypothesized that diosgenin is a bioactive metabolite related to the antimyocardial ischemia (MI) activity of DN. Diosgenin exerts diverse bioactivities, but most of its pharmacological actions are related to the management of cardiovascular disorders, such as lowering plasma total cholesterol and antithrombotic activity [9]. It is reported that *Dioscorea bulbifera* extract, which is similar to the DN extract that both are rich in diosgenin, improves vascular function by superoxide dismutase (SOD) and catalase (CAT) activity. Thus, it is worthwhile further exploring the anti-MI activity of diosgenin [10].

Recently, identification of metabolites involved in the biotransformation of phytochemicals by intestinal microflora has been suggested as a potentially effective means to determine which compounds are active in living systems and to gain a better understanding of how herbs affect biological processes [11, 12]. To verify our hypothesis, this follow-up study aimed, first, to determine if diosgenin was in fact a metabolite of DN through organ-specific biotransformation by intestinal microflora and, second, to validate the cardioprotective effects of the screened diosgenin using an ISO-induced myocardial ischemia model in rats. The findings of the present study provide a basis for understanding the metabolism of DN, including the identity and mode of action of its active components. The present research supports the use of DN and diosgenin in the clinical management of IHD.

2. Materials and Methods

2.1. Chemicals and Reagents. General anaerobic medium broth (GAM broth), vitamin K1, and hematin chloride were purchased from Shanghai Kayon Biological Technology Co. Ltd. (Shanghai, China). Analytical grade ethanol purchased from the Merck (Darmstadt, Germany) was used for the extraction of DN samples. Water was purified using a Milli-Q water system (Millipore; Bedford, MA, USA). Acetonitrile (RCI Lab-Scan, Bangkok, Thailand) and methanol (RCI Lab-Scan, Bangkok, Thailand) were used as the mobile phase for analysis. Formic acid (Sigma-Aldrich, USA) was added to the mobile phase for analysis. Isoprenaline was purchased from Sigma (St. Louis, USA). Test kits for SOD, CAT, GPx, T-AOC, and MDA were all purchased from Nanjing Jiancheng Biotechnology Institute (Nanjing, China). Other reagents were of analytical purity.

Standards (purity 98%) of protodioscin, dioscin, gracillin, diosgenin, protogracillin, and polyphyllin V were purchased from Phytomarker Ltd., Tianjin. Pseudoprotodioscin was provided by National Institute for Food and Drug Control (Beijing, China). The chemical structures of standards are shown in Figure 1.

2.2. Preparation of DN Extract. The rhizomes of DN were collected from the cultivation base in the city of Lingbao in Henan Province, China. All crude drugs were of high quality and authenticated by Dr. Tao Yi, School of Chinese Medicine, Hong Kong Baptist University. Corresponding voucher specimens (number DN-01) were deposited in the Chinese Medicines Center, Hong Kong Baptist University.

The DN samples were dried at 60°C and then pulverized into powder. The powder of DN (200 g) was extracted in an ultrasonic bath with 1000 mL 80% ethanol at room temperature for 1 h. The operation was repeated twice. The combined extracts were evaporated to remove ethanol at reduced pressure in a rotary evaporator (50°C) and then were lyophilized with a freeze-drying system. DN extract (26.1 g, yield 13.05%, w/w) was thus obtained. The DN extract of 0.1 g was diluted in 10 mL sterile water, filtered through a 0.22 μm pore-sized filter (Millipore, type GV). The filtrate was collected in a sterile tube. These tubes were used as *in vitro* biotransformation vessels. The dried extracts and diosgenin were suspended in 1% (w/v) aqueous carboxyl methylcellulose for administration to animals.

2.3. Preparation of Rat Fecal Samples. Fresh rat feces were immediately collected from ten healthy male Sprague Dawley rats (220–250 g). Samples were collected and mixed, on site, on the day of the experiment and were used immediately. Fecal slurries were prepared by mixing fresh feces samples with autoclaved PBS (0.1 M, pH 7.2) to yield 10% (w/v) suspensions. The fecal suspensions were filtered through two layers of gauze. The filtered suspensions were then used to inoculate the *in vitro* biotransformation vessels.

2.4. In Vitro Biotransformation of DN Extract by Rat Intestinal Microflora. A 30 g GAM broth was dissolved in 1000 mL water (70°C), filtered, while hot, treated with antibacteria process with high pressure (0.15 MPa) and temperature (121°C) for 20 min, and cooled to 45°C. The GAM broth solution was then transferred to an anaerobic chamber (37°C, anaerobic condition), and 1 mg vitamin K1 and 6 mg hematin chloride were dissolved in the solution. Then biotransformation vessels were sterilized and filled with 30 mL of GAM broth solution.

Vessels were inoculated with 3 mL of fecal suspension (10%, w/v), and then 1 mL of DN extract was added. *In vitro* biotransformation was run under anaerobic conditions for a period of 48 h. Two different control experiments were conducted: (i) incubations of the intestinal microflora in medium lacking the DN extract to monitor metabolites arising from basal metabolism and (ii) incubations of the DN extract in medium without intestinal microflora to monitor changes due to the purely chemical transformation of precursor compounds of the substrate.

The biotransformation mixtures were then prepared according to the method described in the literature [10]. Briefly, the biotransformation mixtures were extracted with 50 mL ethyl acetate three times. The remaining residues were reextracted three times with 50 mL water-saturated n-butanol. The combined n-butanol layers were washed with water three times. Then, the ethyl acetate and n-butanol
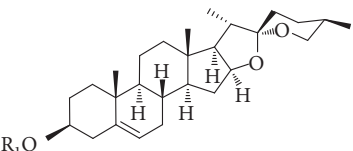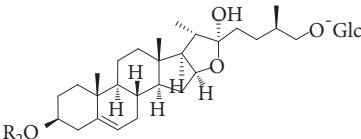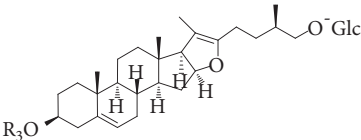
Skeleton	R	Chemical name	Molecular formula
	R₁		
	-H	Diosgenin (**8**)	$C_{27}H_{42}O_3$
	-Glc(4←1)-Rha |(2←1) Rha	Dioscin (**5**)	$C_{45}H_{72}O_{16}$
	-Glc(3←1)-Glc |(2←1) Rha	Gracillin (**6**)	$C_{45}H_{72}O_{17}$
	-Glc(2←1)-Rha	Polyphyllin V (**7**)	$C_{39}H_{62}O_{12}$
	R₂		
	-Glc(4←1)-Rha |(2←1) Rha	Protodioscin (**1**)	$C_{51}H_{84}O_{22}$
	-Glc(3←1)-Glc |(2←1) Rha	Protogracillin (**2**)	$C_{51}H_{84}O_{23}$
	R₃		
	-Glc(4←1)-Rha |(2←1) Rha	Pseudoprotodioscin (**3**)	$C_{51}H_{82}O_{21}$
	-Glc(3←1)-Glc |(2←1) Rha	Pseudoprotogracillin (**4**)	$C_{51}H_{82}O_{22}$

Figure 1: Chemical structures of constituents identified in *Dioscorea nipponica*.

layers were mixed until homogeneous, concentrated under vacuum, and then diluted to the desired volume with methanol. All solutions were centrifuged at $13,000 \times g$ for 10 min before being injected for ultra-performance liquid chromatography-mass spectrometry (UPLC-MS) analysis.

2.5. UPLC-MS Analysis. An Agilent 1290 series UPLC system (Agilent Technologies, Santa Clara, CA, USA) equipped with a binary pump, an autosampler, and a thermostatically controlled column compartment was used for the chromatographic analysis. A Waters ACQUITY™ BEH C18 column (100×2.1 mm, $1.7\,\mu$m; Milford, MA, USA) was used for sample separation at 40°C. The mobile phase consisted of 0.1% formic acid in water (A) and 0.1% formic acid in acetonitrile (B) using a gradient program of 0–2 min, 20% B; 2–12 min, 20–28% B; 12–20 min, 28–45% B; 20–35 min, 45–48% B; and 35–46 min, 48–75% B. The sample volume injected was $2\,\mu$L, and the solvent flow rate was set at 0.4 mL/min. For mass spectrometric determination, the UPLC system was hyphenated with an ultrahigh definition accurate mass quadrupole time-of-flight mass spectrometry (MS) system (Agilent Technologies G6540A) by a multimode ionization source (G1978-65339) interface. The conditions of MS analysis were optimized as follows: drying gas (N_2) flow rate, 8.0 L/min; drying gas temperature, 300°C; nebulizer, 45 psi; capillary, 2500 V; and fragmentor voltage, 150 V. Mass spectra were recorded across the range m/z 100–1700 in both positive and negative modes. All operations and data analysis were controlled by Agilent MassHunter Workstation software version B.04.00.

2.6. Animals and Acute Myocardial Ischemia Induced by ISO. Male Sprague Dawley rats weighing 150–200 g were purchased from the Laboratory Animal Services Center, the Chinese University of Hong Kong, Hong Kong. All animals were housed at a room temperature of 23 ± 1°C with a 12 h light/dark cycle. A standard rodent diet and water were provided ad libitum. All experimental protocols were approved by the Committee on the Use of Human & Animal Subjects in Teaching and Research of Hong Kong Baptist University, in accordance with the Animal Ordinance (Department of Health, Hong Kong).

A total of 42 rats were randomly divided into 7 groups: (1) normal control (0.5% w/v aqueous CMC-Na, i.g.); (2) model group (ISO injection only); (3) positive group (propranolol, 10 mg/kg i.g. for 3 days after ISO injection); (4–6) diosgenin treatment groups. For the diosgenin groups, diosgenin was administered at rates of 20, 40, or 80 mg/kg for 3 days after ISO injection. Dosage was determined from our previous study [7]; (7) DN treatment group was administered with DN extract at 500 mg/kg for 3 days after ISO injection. Diosgenin, DN extract, and propranolol were administered once daily except on the days on which ISO injection was given.

Animals were injected with ISO (1 mg/kg, s.c.) to induce experimental MI twice at an interval of 8 hours on the first day. On the last day of experiment (4th day), the animals were sacrificed. After the rats were anesthetized with diethyl ether, then the blood samples were collected from the femoral arteries of rats. Serum was saved at −80°C following centrifugation at 4°C at 4000 rpm for 20 min.

2.7. Histological Examination of Myocardium.
Immediately after the sacrifice of the rats, the hearts were removed, washed with iced normal saline, fixed in 10% formalin, and decalcified with formic acid (31.5% formic acid and 13% sodium citrate). The hearts were embedded in paraffin for sectioning by standard histological methods [13]. Sections (4 μm, Leica RM2125, Germany) from the left ventricle were stained with hematoxylin and eosin (H&E) and examined by light microscopy (Leica DMR, Germany) at 200x magnification.

2.8. Assays for Biological Activities and Statistical Analysis.
Activities of SOD, GPx, CAT, T-AOC, and MDA were measured using kits according to the manufacturers' instructions. Values obtained from the experiments were expressed as the means ± standard deviation (SD). The statistical significance of the differences was assessed by ANOVA followed by post hoc test with LSD method [14, 15]. P values less than 0.05 were considered statistically significant.

3. Results and Discussion

3.1. Choice of Ion Source.
Electrospray ionization (ESI) is a soft ionization technique. It is especially useful in producing ions from macromolecules because it overcomes the propensity of these molecules to fragment when ionized. Atmospheric pressure chemical ionization (APCI) is an ionization method used in mass spectrometry which utilizes gas-phase ion-molecule reactions at atmospheric pressure. ESI is today the most widely used ionization technique in chemical and biochemical analyses [16, 17]. However, some analytes (e.g., *Dioscorea* saponin aglycones), for structural and polar reasons, cannot produce enough strong ions with ESI; in these cases, APCI can be used to increase the ion yield. Therefore, in our previous study, ESI and APCI were used to detect saponin glycosides and saponin aglycones, respectively [6]. Due to the need to use different ion sources, each sample had to be analyzed twice, and analysis time was twice as long.

To solve this problem and save time, an ESI/APCI multimode ionization source was used for LC-MS analysis in the present study. The ESI/APCI multimode source is unique in that it incorporates both ESI and APCI into a single ion source, and it can simultaneously generate ions by ESI and APCI. The main advantages of the multimode source include eliminating the time required to switch ion sources on an instrument and eliminating the need to run samples twice to improve lab productivity [18]. Compared to the previous study, saponin glycosides and saponin aglycones both were ionized and identified in a single run with the help of multimode ionization source. As a result, we find a newly generated peak 8, which corresponds to diosgenin, from the

chromatogram of the DN extract incubated with rat intestinal microflora (Figure 2(d)).

3.2. Detection of Diosgenin as a Metabolite of DN Extract.
The effect of intestinal microflora on drug metabolism has received increasing attention in recent years. Anaerobic bacteria present in the small intestines are quite diverse in species, and different species produce enzymes which are different in functions; it is these enzymes that are also responsible for drug biotransformation in organisms. Incubation of test drugs, particularly phytochemicals, with fresh fecal specimen is a common means for investigating this kind of biotransformation [11, 12].

In the present study, DN extract was tested by this method; the resulting metabolic profile is shown in Figure 2(d). Based on the comparison of samples with standard compounds, seven peaks were unambiguously identified as protodioscin (1), protogracillin (2), pseudoprotodioscin (3), dioscin (5), gracillin (6), polyphyllin V (7), and diosgenin (8) and peak 4 was tentatively identified as pseudoprotogracillin (4) by comparing their m/z values and MS spectra with the data in the literature [8]. Compared with the identified peaks in Figure 2(a), the new generated peak 8 in Figure 2(d) was attributed to diosgenin. This finding confirmed our hypothesis that intestinal bacteria produce diosgenin from DN extract [8].

3.3. Effects of Diosgenin on Myocardial Histology.
Light microscopy of heart tissue sections from normal control rat myocardium showed obvious integrity of myocardial membrane, a normal myofibrillar structure with striations, a branched appearance, and continuity with adjacent myofibrils (Figure 3(a)). Tissue from the rat-given-ISO group revealed loss of transverse striations, marked myocardial cell swelling, large numbers of infiltrating inflammatory cells, and cardiac necrosis (Figure 3(b)). Tissue sections from the rat-given-propranolol-POS group presented approximately normal myofibrillar structure with clear striations and presence of a few inflammatory cells (Figure 3(c)). Low dosage of diosgenin-treated groups showed diminished myocardial cell swelling, unclear transverse striations, and reduced inflammatory cell infiltration compared to the ISO group (Figure 3(d)). Tissues from medium dosage of diosgenin-treated groups revealed less severe histological damage, such as normal myocardial arrangement, clear transverse striations, and few invasive inflammatory cells (Figure 3(e)). Groups treated with high dosage of diosgenin and DN extract exhibited normal, well-preserved cardiac muscle cell histology with no significant damage (Figures 3(f) and 3(g)). These findings demonstrated that diosgenin and DN extract could protect myocardial tissues from pathological damage that would have otherwise occurred from the experimental treatments.

3.4. Effects of Diosgenin on SOD, CAT, GPx, T-AOC, and MDA Serum Levels.
It is widely accepted that isoprenaline (ISO) injection can readily induce acute MI in rats; it is also widely accepted that antioxidant activity is one of the key mechanisms of anti-MI efficacy [2, 3, 19]. Therefore, it is
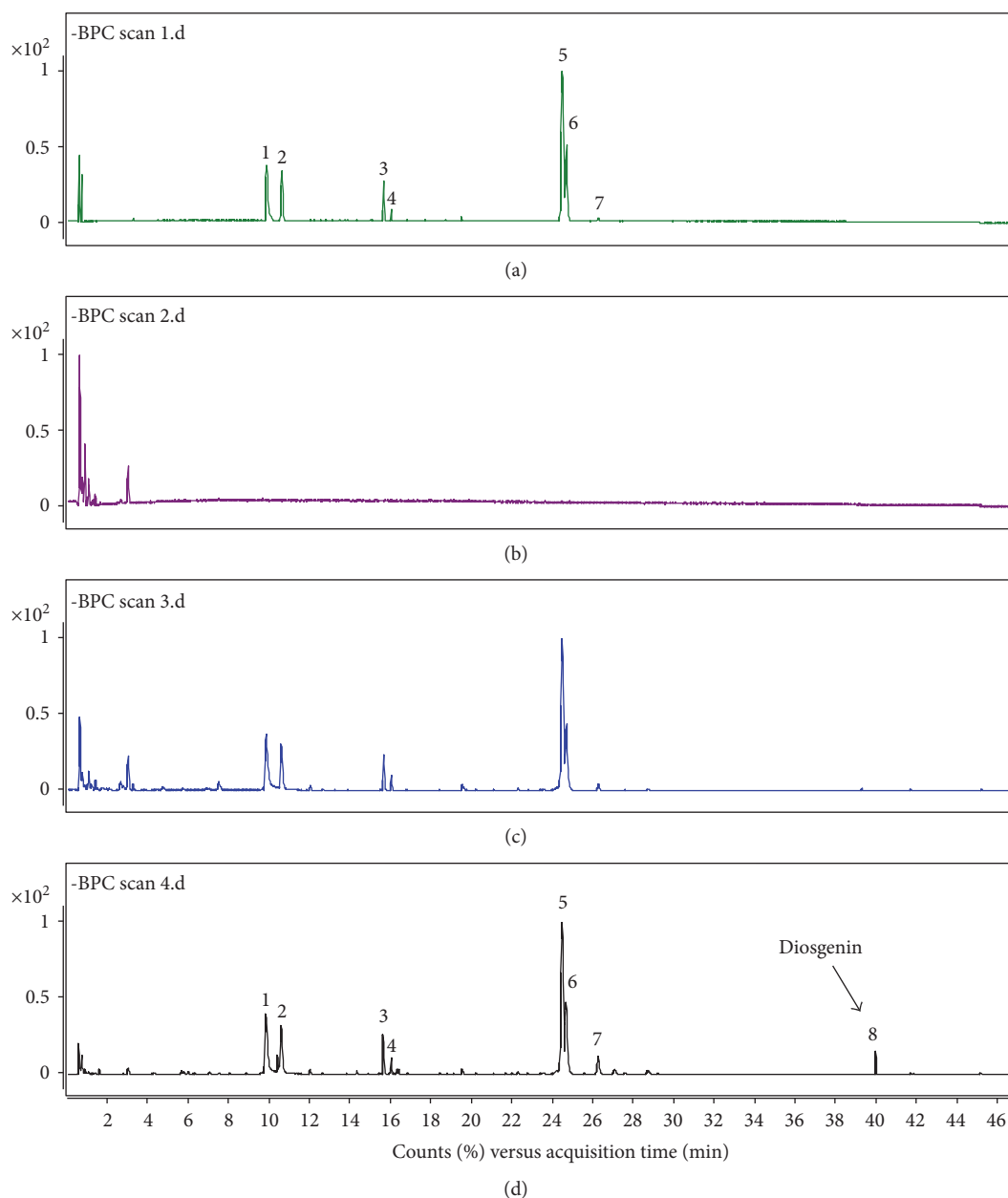
FIGURE 2: Base peak chromatograms (BPC) of *Dioscorea nipponica* (a), control I using intestinal microflora and medium (b), control II using *D. nipponica* extract and medium (c), *D. nipponica* extract after biotransformed by intestinal microflora and medium (d) by LC–Q-TOF/MS in negative ion mode (1 protodioscin, 2 protogracillin, 3 pseudoprotodioscin, 4 pseudoprotogracillin, 5 dioscin, 6 gracillin, 7 polyphyllin V, and 8 diosgenin).

reasonable to use the ISO model to compare the therapeutic effect of diosgenin with respect to antioxidant activity.

Oxidative stress plays an essential role in the pathogenesis of MI injury. One cause is reactive oxygen species (ROS) resulting from mitochondrial dysfunction via the electron transport chain during MI. The major ROS, such as hydrogen peroxide (H_2O_2), superoxide anion (O_2^-), and hydroxyl radicals (OH·), are generated during ischemia and particularly during reperfusion [19–21]. However, these potentially deleterious ROS are controlled by external or exogenous antioxidative defense systems which eliminate prooxidants and scavenge free radicals. The most well-known endogenous mitochondrial antioxidant enzyme is SOD, which dismutates superoxide to H_2O_2. Other endogenous antioxidant enzymes include catalase and glutathione peroxidase. Exogenous antioxidants are mainly derived from food and herbs. Numerous types of bioactive phytochemicals, such as polyphenolics, glycosides, and steroids, belonging to exogenous antioxidants, have gained attraction in clinical as well as research areas [22–25]. According to published reports describing anti-MI activity of herbal medicine [3, 17, 18], five indices related to the antioxidant activity in the MI model are usually monitored to evaluate the protective effect against ISO-induced injury

(a)   (b)   (c)   (d)

(e)   (f)   (g)
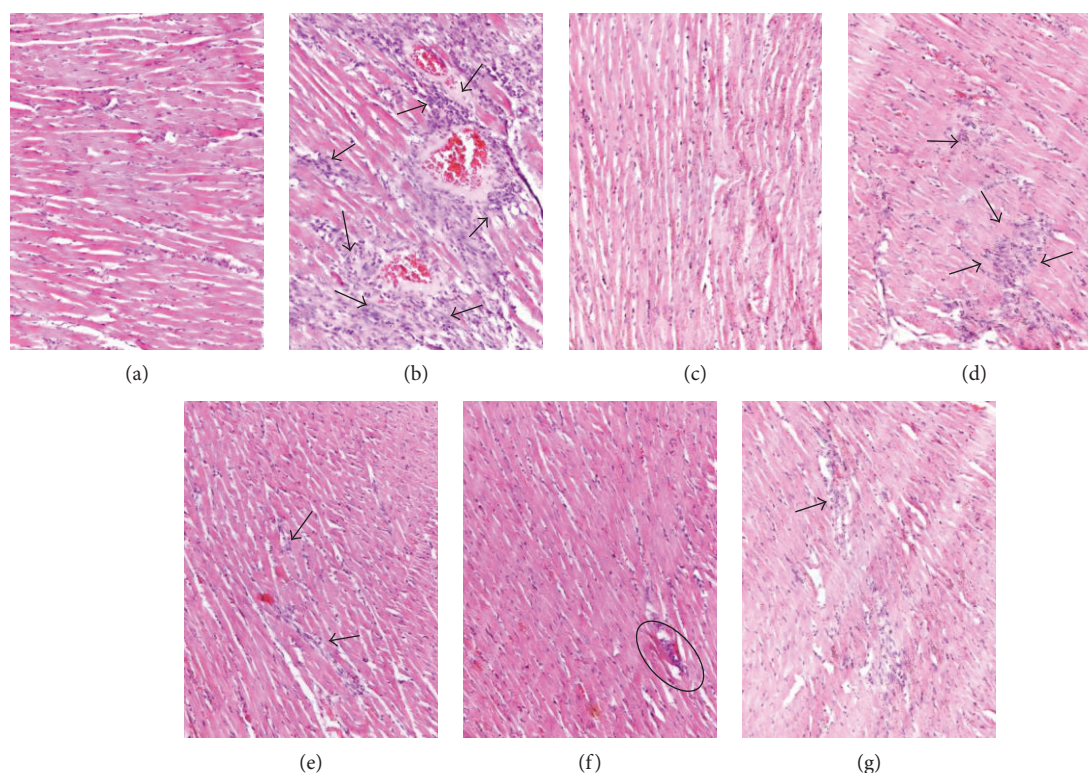
FIGURE 3: Histopathological changes of myocardial tissue (H&E, ×200). (a) Normal control group showing normal myocardial histology, clear transverse striations, and no inflammatory cell infiltration; (b) ISO group showing swelling of obvious myocardial cells, degeneration, loss of transverse striations, and large numbers of invasive inflammatory cells; (c) POS group (propranolol, 10 mg/kg) showing normal myocardial arrangement, clear transverse striations, and slight inflammatory cell infiltration; (d) diosgenin (40 mg/kg) showing myocardial cell swelling, degeneration, unclear horizontal striations, and large numbers of inflammatory cells; (e) diosgenin (60 mg/kg) showing diminished myocardial cell swelling, unclear horizontal striations, and reduced inflammatory cell infiltration; (f) diosgenin (80 mg/kg) showing normal myocardial arrangement, clear transverse striations, and little few inflammatory cells; (g) DN extract (500 mg/kg) showing normal myocardial arrangement, clear transverse striations, and few invasive inflammatory cells.

in cardiomyocytes. These are an indicator of lipid peroxidation, namely, malondialdehyde (MDA); three enzymatic antioxidants, namely, total superoxide dismutases (SOD), catalase (CAT), and glutathione peroxidase (GPx); and an indicator of both nonenzymatic and enzymatic antioxidants, namely, total antioxidant capacity (T-AOC) [26–28]. Therefore, following the widely accepted international rule, SOD, CAT, GPx, T-AOC, and MDA were chosen to assess the anti-MI activity of diosgenin identified in the biotransformation study described above.

Compared with the normal control group, SOD, CAT, GPx, and T-AOC levels in the ISO group decreased significantly ($^{\#\#}P < 0.01$), while MDA levels increased significantly ($^{\#\#}P < 0.01$) (Figures 4(a), 4(b), 4(c), 4(d), and 4(e)). This meant that our modeling by ISO injection was successful.

Groups administered with different dosages of diosgenin and DN extract exhibited varying degrees of antioxidant activity, as revealed by these five markers (Figures 4(a), 4(b), 4(c), 4(d), and 4(e)). Pathological levels of SOD, CAT, GPx, T-AOC, and MDA in experimental MI rats were almost normalized by diosgenin and DN extract treatments compared with those in the ISO group ($^{**}P < 0.01$ or $^{*}P < 0.05$), except the SOD, GPx, T-AOC, and MDA serum levels in the low dosage diosgenin-treatment groups. These

findings suggest that the anti-MI mechanism of diosgenin is related not only to more varieties of enzymatic antioxidant but also to nonenzymatic antioxidants.

Diosgenin administered orally at doses of 20, 40, and 80 mg/kg showed significant dose-dependent increment of the SOD, GPx, and T-AOC serum levels and dose-dependent reduction of the MDA serum levels. The peak treatment effects of diosgenin (78.9% and 77.3%) were recorded with the dose of 80 mg/kg in the SOD level and GPx level, which were higher than those of propranolol with the dose of 10 mg/kg (57.9% and 70.5%), compared with the ISO model group. These results demonstrate that diosgenin has distinct antioxidant properties *in vivo*. Given their known benefits, these antioxidant properties may be responsible for the therapeutic effects of DN in the treatment of MI.

Reduction in oxidative stress caused by ischemia-reperfusion injury is clearly an appropriate countermeasure to the major challenges associated with ischemia. It is worth noting that the antioxidant is not a panacea. A recent study reported that administration of 30 mg/kg/day β-carotene could significantly improve heart function of the isolated ischemic/reperfused (I/R) rat hearts through enhancing antioxidant capacity. However, increasing β-carotene dosage
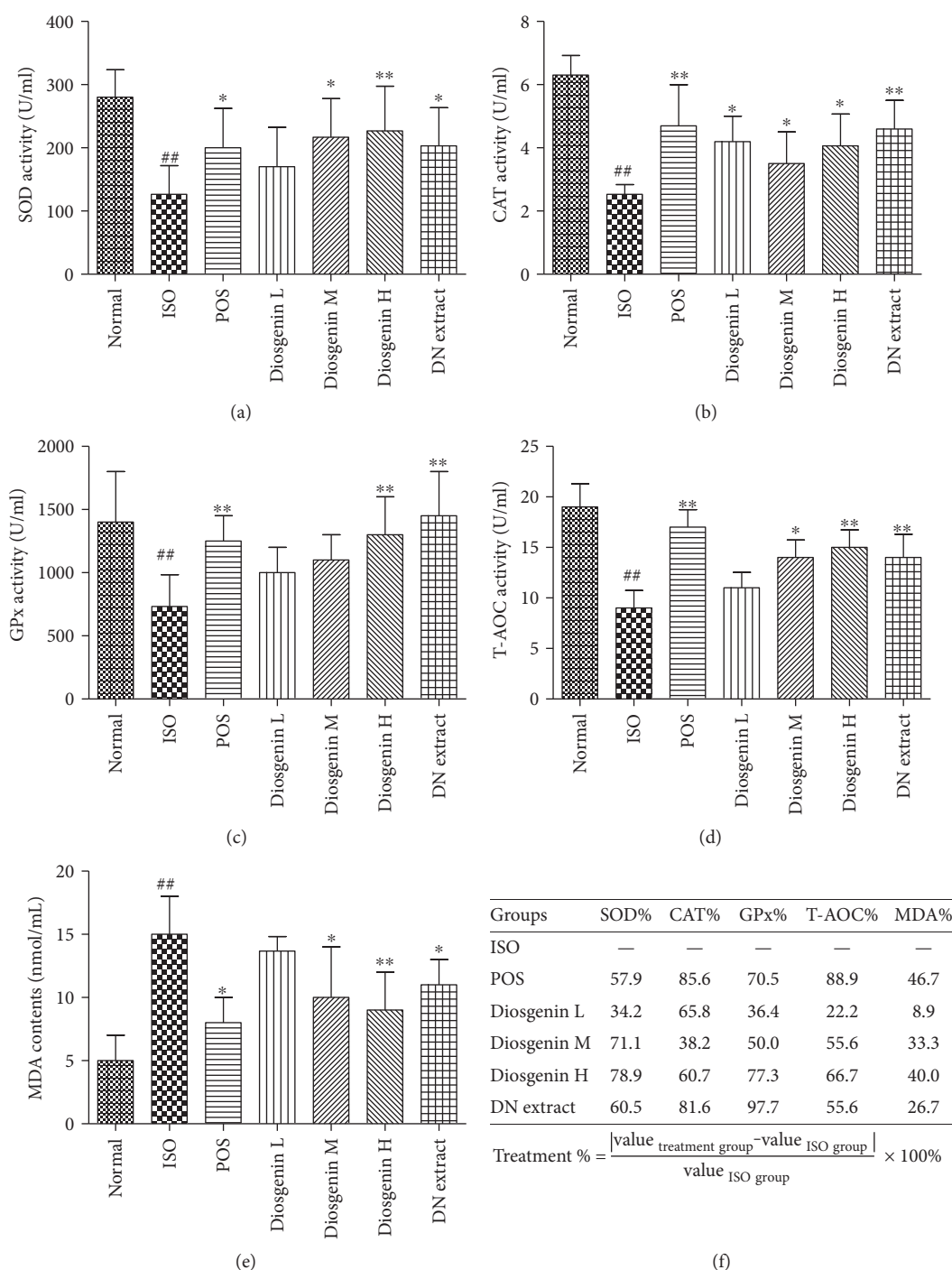
FIGURE 4: Effects of diosgenin and *Dioscorea nipponica* extract on acute experimental myocardial ischemia and treatment percentage. (i) (a–e) SOD, CAT, GPx, T-AOC, and MDA serum levels. (ii) (f) Treatment percentage of assay markers for each treatment group. Normal: normal control; ISO: model group only injected with isoprenaline; POS: positive control (propranolol, 10 mg/kg); Diosgenin L, Diosgenin M, and Diosgenin H: orally given diosgenin 20, 40, and 80 mg/kg of low, medium and high dose, respectively, after ISO injection; DN extract: orally given *Dioscorea nipponica* extract (500 mg/kg), after ISO injection. Data are expressed as mean ± SD ($n = 6$). $^{\#\#}P < 0.01$ versus normal control; $^{*}P < 0.05$, $^{**}P < 0.01$ versus ISO group.

did not add any cardiovascular benefits. Moreover, the agent may mediate and, indeed, may exacerbate existing I/R pathological mechanisms [29]. Antioxidants play a role of double-edged sword in the occurrence and development of diseases.

4. Conclusion

The present study identified the metabolites from DN through analysis of organ-specific biotransformation and validated the cardioprotective effects of the screened

metabolites using an isoprenaline-induced myocardial ische-
mia rat model. The findings of the present study provide evi-
dence that, first, diosgenin is generated from DN by intestinal
microflora; second, diosgenin can protect the myocardium
against ischemic insult in a dose-dependent manner, almost
comparable to the effect of DN extract; and, third, DN's
protective effect can be attributed to the increase of enzy-
matic and nonenzymatic antioxidants (SOD, CAT, GPx,
and T-AOC) *in vivo* and to a decrease in lipid peroxidation.
These phenomena help explain the clinical efficacy of DN
as an anti-MI drug.

Conflicts of Interest

The authors declare that they have no conflict of interests.

Authors' Contributions

Jia-Fu Feng and Yi-Na Tang contributed equally to this work,
conducted the experiment, interpreted the data, and wrote
the manuscript. Lin Zhu and Tao Yi conceived the idea and
designed the project. Hong Ji and Zhan-Gang Xiao reviewed
and revised the manuscript. All the authors approved the
version to be published.

Acknowledgments

References

[1] G. H. Yang, Y. Wang, Y. X. Zeng et al., "Rapid health transition
    in China, 1990–2010: findings from the global burden of
    disease study 2010," *The Lancet*, vol. 381, no. 9882,
    pp. 1987–2015, 2013.

[2] J. G. Long, M. L. Gao, Y. Kong et al., "Cardioprotective effect of
    total paeony glycosides against isoprenaline-induced myocar-
    dial ischemia in rats," *Phytomedicine*, vol. 19, no. 8-9,
    pp. 672–676, 2012.

[3] F. Song, H. Li, J. Y. Sun, and S. W. Wang, "Protective effects of
    cinnamic acid and cinnamic aldehyde on isoproterenol-
    induced acute myocardial ischemia in rats," *Journal of Ethno-
    pharmacology*, vol. 150, no. 1, pp. 125–130, 2013.

[4] Y. N. Tang, X. C. He, Q. L. Chen et al., "A mixed microscopic
    method for differentiating seven species of "Bixie"-related
    Chinese Materia Medica," *Microscopy Research and Tech-
    nique*, vol. 77, no. 1, pp. 57–70, 2014.

[5] T. Yi, L. L. Fan, H. L. Chen et al., "Comparative analysis of
    diosgenin in *Dioscorea* species and related medicinal plants
    by UPLC-DAD-MS," *BMC Biochemistry*, vol. 15, no. 1, p. 19,
    2014.

[6] Y. N. Tang, T. Yi, H. M. Chen, Z. Z. Zhao, and H. B. Chen,
    "Quantitative comparison of multiple components in

Dioscorea nipponica and *D. panthaica* by ultra-performance
    liquid chromatography coupled with quadrupole time-of-
    flight mass spectrometry," *Phytochemical Analysis*, vol. 24,
    no. 4, pp. 413–422, 2013.

[7] Y. N. Tang, X. C. He, M. Ye et al., "Cardioprotective effect of
    total saponins from three medicinal species of *Dioscorea*
    against isoprenaline-induced myocardial ischemia," *Journal
    of Ethnopharmacology*, vol. 175, pp. 451–455, 2015.

[8] Y. N. Tang, Y. X. Pang, X. C. He et al., "UPLC-QTOF-MS
    identification of metabolites in rat biosamples after oral
    administration of *Dioscorea* saponins: a comparative study,"
    Journal of Ethnopharmacology, vol. 165, pp. 127–140, 2015.

[9] H. R. Vasanthi, N. ShriShriMal, and D. K. Das, "Phytochemi-
    cals from plants to combat cardiovascular disease," *Current
    Medicinal Chemistry*, vol. 19, no. 14, pp. 2242–2251, 2012.

[10] H. R. Vasanthi, S. Mukherjee, D. Ray, I. Lekli, and D. K. Das,
    "Protective role of air potato (*Dioscorea bulbifera*) of yam
    family in myocardial ischemic reperfusion injury," *Food &
    Function*, vol. 1, no. 3, pp. 278–283, 2010.

[11] J. Y. Wan, P. Liu, H. Y. Wang et al., "Biotransformation and
    metabolic profile of American ginseng saponins with human
    intestinal microflora by liquid chromatography quadrupole
    time-of-flight mass spectrometry," *Journal of Chromatography
    A*, vol. 1286, pp. 83–92, 2013.

[12] H. Y. Wang, H. Y. Hua, X. Y. Liu, J. H. Liu, and B. Y. Yu,
    "*In vitro* biotransformation of red ginseng extract by human
    intestinal microflora: metabolites identification and meta-
    bolic profile elucidation using LC-Q-TOF/MS," *Journal of
    Pharmaceutical and Biomedical Analysis*, vol. 98, pp. 296–
    306, 2014.

[13] C. Kishimoto, H. Takada, H. Kawamata, M. Umatake, and H.
    Ochiai, "Immunoglobulin treatment prevents congestive heart
    failure in murine encephalomyocarditis viral myocarditis
    associated with reduction of inflammatory cytokines," *Journal
    of Pharmacology and Experimental Therapeutics*, vol. 299,
    no. 2, pp. 645–651, 2001.

[14] G. Saravanan, P. Ponmurugan, M. Sathiyavathi, S.
    Vadivukkarasi, and S. Sengottuvelu, "Cardioprotective activity
    of Amaranthus viridis Linn: effect on serum marker enzymes,
    cardiac troponin and antioxidant system in experimental
    myocardial infarcted rats," *International Journal of Cardiol-
    ogy*, vol. 165, no. 3, pp. 494–498, 2013.

[15] G. Szűcs, Z. Murlasits, S. Török et al., "Cardioprotection by
    farnesol: role of the mevalonate pathway," *Cardiovascular
    Drugs and Therapy*, vol. 27, no. 4, pp. 269–277, 2013.

[16] M. Himmelsbach, W. Buchberger, and E. Reingruber, "Deter-
    mination of polymer additives by liquid chromatography
    coupled with mass spectrometry. A comparison of atmo-
    spheric pressure photoionization (APPI), atmospheric pres-
    sure chemical ionization (APCI), and electrospray ionization
    (ESI)," *Polymer Degradation and Stability*, vol. 94, no. 8,
    pp. 1213–1219, 2009.

[17] T. Ghislain, P. Faure, and R. Michels, "Detection and monitor-
    ing of PAH and Oxy-PAHs by high resolution mass spectrom-
    etry: comparison of ESI, APCI and APPI source detection,"
    Journal of the American Society for Mass Spectrometry,
    vol. 23, no. 3, pp. 530–536, 2012.

[18] L. C. Short, K. A. Hanold, S. S. Cai, and J. A. Syage, "Electro-
    spray ionization/atmospheric pressure photoionization multi-
    mode source for low-flow liquid chromatography/mass
    spectrometric analysis," *Rapid Communications in Mass
    Spectrometry*, vol. 21, no. 10, pp. 1561–1566, 2007.

[19] D. Cokkinos, C. Pantos, G. Heusch, and H. Taegtmeyer, *Myocardial Ischemia Basic Concepts, in: Myocardial Ischemia: From Mechanisms to Therapeutic Potentials*, Springer Science + Business Media, Inc, Boston, USA, 2006.

[20] D. Zhao, J. Yang, and L. Yang, "Insights for oxidative stress and mTOR signaling in myocardial ischemia/reperfusion injury under diabetes," *Oxidative Medicine and Cellular Longevity*, vol. 2017, Article ID 6437467, 12 pages, 2017.

[21] G. A. Kurian, R. Rajagopal, S. Vedantham, and M. Rajesh, "The role of oxidative stress in myocardial ischemia and reperfusion injury and remodeling: revisited," *Oxidative Medicine and Cellular Longevity*, vol. 2016, Article ID 1656450, 14 pages, 2016.

[22] J. W. Walters, D. Amos, K. Ray, and N. Santanam, "Mitochondrial redox status as a target for cardiovascular disease," *Current Opinion in Pharmacology*, vol. 27, pp. 50–55, 2016.

[23] K. Schwarz, N. Siddiqi, S. Singh, C. J. Neil, D. K. Dawson, and M. P. Frenneaux, "The breathing heart—mitochondrial respiratory chain dysfunction in cardiac disease," *International Journal of Cardiology*, vol. 171, no. 2, pp. 134–143, 2014.

[24] S. Noori, "An overview of oxidative stress and antioxidant defensive system," *Scientific Reports*, vol. 1, p. 413, 2012.

[25] X. R. Guan, L. Zhu, Z. G. Xiao, Y. L. Zhang, H. B. Chen, and T. Yi, "Bioactivity, toxicity and detoxification assessment of *Dioscorea bulbifera* L.: a comprehensive review," *Phytochemistry Reviews*, vol. 16, no. 3, pp. 573–601, 2017.

[26] K. Y. Ning, Y. K. Li, H. L. Gao, and L. D. Li, "Therapeutic effects of methyl protodioscin for myocardial infarction in rats," *Traditional Chinese Drug Research & Clinical Pharmacology*, vol. 19, no. 1, pp. 1–3, 2008.

[27] L. F. Wang, Y. Q. Zhao, W. Z. Gao, J. S. Lou, and Y. Kang, "*Dioscorea* saponins increased antioxidative ability of myocardium after ischemia-perfusion injury in rat," *Pharmacology and Clinics of Chinese Materia Medica*, vol. 25, no. 5, pp. 44–46, 2009.

[28] T. J. Wang, R. C. Choi, J. Li et al., "Trillin, a steroidal saponin isolated from the rhizomes of *Dioscorea nipponica*, exerts protective effects against hyperlipidemia and oxidative stress," *Journal of Ethnopharmacology*, vol. 139, no. 1, pp. 214–220, 2012.

[29] E. Csepanyi, A. Czompa, D. Haines et al., "Cardiovascular effects of low versus high-dose beta-carotene in a rat model," *Pharmacological Research*, vol. 100, pp. 148–156, 2015.

Review Article

Cellular and Molecular Mechanisms of Diabetic Atherosclerosis: Herbal Medicines as a Potential Therapeutic Approach

Jinfan Tian,[1] Yanfei Liu,[2] Yue Liu,[3] Keji Chen,[3] and Shuzheng Lyu[1]

[1]*Department of Cardiology, Beijing Anzhen Hospital, Capital Medical University, Beijing 100029, China*
[2]*Graduate School, Beijing University of Chinese Medicine, Beijing 100029, China*
[3]*Cardiovascular Disease Centre, Xiyuan Hospital, China Academy of Chinese Medical Sciences, Beijing 100091, China*

Correspondence should be addressed to Yue Liu; liuyueheart@hotmail.com and Shuzheng Lyu; shuzheng@medmail.com.cn

An increasing number of patients diagnosed with diabetes mellitus eventually develop severe coronary atherosclerosis disease. Both type 1 and type 2 diabetes mellitus increase the risk of cardiovascular disease associated with atherosclerosis. The cellular and molecular mechanisms affecting the incidence of diabetic atherosclerosis are still unclear, as are appropriate strategies for the prevention and treatment of diabetic atherosclerosis. In this review, we discuss progress in the study of herbs as potential therapeutic agents for diabetic atherosclerosis.

1. Introduction

Cardiovascular diseases (CVDs), including atherosclerosis, are important complications of diabetes and the leading causes of mortality in patients with diabetes. Systemic factors accompanying diabetes, such as dyslipidaemia and hypertension, are thought to affect the development of diabetic vascular diseases. In addition, insulin resistance and excess production of advanced glycosylation end products (AGEs) contribute to disorders of lipid metabolism, oxidative stress, endothelial dysfunction, monocyte recruitment, foam cell formation, phenotype changes in vascular smooth muscle cells (VSMCs), and thrombosis formation [1]. In addition, diabetes and atherosclerosis exhibit common pathologies, although the underlying mechanisms are still being explored.

Botanical and natural drugs have a long, documented history in treating diabetes and vascular diseases. The vascular-protective properties of herb medicines include their ability to scavenge free radicals, inhibit apoptosis, and reduce inflammation and platelet aggregation [2]. Most recently, Li et al. [3] uncovered the antidiabetes effect of artemisinins, and the mechanism involves driving the in vivo conversion of pancreatic cells into functional β-like cells by enhancing GABA signalling. Furthermore, owing to the multitarget

effects and comprehensive sources of herbal medicines, it remains of utmost importance to improve our understanding of their potential use in the treatment of diabetes and diabetic atherosclerosis despite their reported side effects. Since diabetic atherosclerosis is a multifactorial disease, in this review, we first discuss the cellular and molecular mechanisms for the pathogenesis of diabetic atherosclerosis and then the progress in the study of herbs as potential therapeutic agents for diabetic atherosclerosis.

2. Cell Types Involved in Diabetic Atherosclerosis

2.1. Myeloid Cells. Diabetes and atherosclerosis are chronic inflammatory conditions. Myeloid cells (neutrophils, monocytes, and macrophages) are involved in both atherosclerosis and diabetes. The migration of circulating monocytes into the vessel wall is critical for the development of diabetic atherosclerosis. Moreover, intercellular cell adhesion molecule-1(ICAM-1), chemoattractant protein-1(MCP-1), and macrophage migration inhibitory factor (MIF), which regulate the adhesion of monocytes, are dysregulated in hyperglycemia-induced atherosclerosis in animal models. Increased foam cells derived from macrophages promote

the acceleration of atherosclerotic lesions in diabetic ApoE$^{-/-}$ mice [4, 5]. A more inflammatory monocyte/macrophage phenotype with secretion of higher levels of proinflammatory cytokines was detected in both animal models and patients with diabetes mellitus [6]. Increases in long-chain acyl-COA synthetase 1 (ACSL1), toll-like receptor (TLR) 2, and TLR4 contribute to the increased inflammatory monocyte/ macrophage phenotype in the context of diabetes [6]. Neutrophil infiltration also has a role in diabetic atherosclerosis. In addition, T-cell function is closely related to atherosclerosis in the diabetic environment, and inflammatory monocytes have been shown to activate Th17 cells under diabetic conditions [7].

2.2. Endothelial Cells.
Endothelial dysfunction due to inflammation and oxidative stress is a crucial characteristic in diabetes mellitus-linked atherosclerosis. Endothelial dysfunction is associated with decreased nitric oxide (NO) availability, either through loss of NO production or NO biological activity [8, 9]. The excess generation of free oxygen radicals leads to apoptosis in endothelial cells [9]. In hyperglycemia, chronic inflammation increases vascular permeability, promotes the generation of adhesion molecules and chemokines, and stimulates accumulation of monocytes in the artery wall. The interleukin-1 (IL-1) antagonist anakinra improves endothelial dysfunction in diabetic animals via attenuation of the proinflammatory enzymes cyclooxygenase (COX) and inducible nitric oxide synthase (iNOS) triggered by diabetes in the vascular wall [10, 11].

2.3. Smooth Muscle Cells.
Proliferation and accumulation of smooth muscle cells are detected in both type 1 and type 2 diabetes mellitus. However, it is still unclear whether changes in smooth muscle cells are a result of the diabetic environment directly or are caused by endothelial injury and macrophage recruitment. According to a report by Chen et al. [12], various concentrations of glucose (5.6, 11.1, 16.7, and 22.2 mM) increase the proliferation of vascular smooth muscle cells (VSMCs) in a concentration-dependent manner after 48 h of incubation. Another study showed that after initial injury, growth factors and cytokines released by endothelial cells, inflammatory cells, and platelets promote changes in VSMC phenotypes, thereby enhancing VSMC proliferation and migration [13]. Additionally, aortic smooth muscle cells isolated from NOX$^{-/-}$ApoE$^-$ mice exhibit a dedifferentiated phenotype, including loss of contractile gene expression [14].

2.4. Platelets.
Accumulating evidence has shown that platelet hyperreactivity is a crucial cause of diabetic atherosclerosis in both animal models and diabetic patients. Enhanced platelet aggregation and synthesis of thromboxane A2 were detected within days of streptozotocin- (STZ-) dependent induction of diabetes in a rat model [15]. Platelets from patients with diabetes have been shown to have decreased sensitivity to antiaggregation agents, such as prostacyclin (PGI2) and NO [16]. Glycated low-density lipoprotein- (GlyLDL-) and hyperinsulinemia-induced impairment of calcium homeostasis, activation of protein kinase C (PKC), increased generation

of reactive oxygen species (ROS), and decreased NO bioactivity result in hyperactivation of platelets [17]. According to a report by Wang et al., a significant correlation between plasma CTRP9 concentrations (a novel adiponectin paralog) and platelet aggregation amplitude was observed in high-fat diet-induced diabetic C57BL/6J mice. Enhancing CTRP9 production and/or exogenous supplementation of CTRP9 may protect against diabetic cardiovascular injury via inhibition of abnormal platelet activity [18].

3. Molecules or Signal Transduction Pathways

3.1. Molecules

3.1.1. AGEs.
The detrimental effects of hyperglycemia can be attributed to the biochemical consequences of intracellular metabolism associated with excess glucose, including nonenzymatic glycation with formation of AGEs [1]. AGEs are heterogeneous compounds that interact with the arterial wall through receptors for AGE (RAGEs). Formation of GlyLDLs and other AGEs induces uptake of proatherogenic lipids by cultured aortic SMCs [19] and stimulation of RAGE and scavenger-receptor expression in macrophages [20]. Schmidt et al. found that the interactions between AGEs and RAGEs enhance the adhesion of monocytes to endothelial cells via stimulating the expression of nuclear factor-κB (NF-κB-) dependent proinflammatory and prothrombotic molecules [21]. Consequently, the AGE/RAGE axis contributes to diabetic atherosclerosis by attracting monocytes to the vascular intima, increasing oxidative stress, inducing endothelial dysfunction, and promoting vascular wall remodeling [22, 23]. Menini et al. have shown that d-carnosine-octylester- (DCO-) attenuated AGE formation is related to its reactive carbonyl species- (RCS-) quenching activity [24]. Moreover, they also revealed that DCO treatment attenuated lesion size, necrotic area, and apoptotic cells in diabetic ApoE-null mice. These protection effects were more effectively achieved by early treatment (60 mg/kg body weight, from weeks 1 to 11, DCO early) than by late treatment (60 mg/kg body weight, from weeks 9 to 19, DCO late) [25]. Zhu et al. [26] demonstrated that immunized diabetic ApoE$^{-/-}$ and low-density lipoprotein (LDL) receptor knockout (LDLR)$^{-/-}$ mice with AGE-LDL significantly reduced atherosclerosis, indicating that vaccination with AGE-LDL may offer a novel approach for the treatment of atherosclerosis in patients with diabetes. Inhibition of RAGE using murine-soluble RAGE (sRAGE) attenuates atherosclerotic lesions in STZ-induced diabetic ApoE$^{-/-}$ mice and ApoE$^{-/-}$/db/db mice [27]. These findings further supported the roles of AGE and RAGE in the macrovascular complications of diabetes, and blockade of RAGE may be a potential therapeutic strategy in diabetic atherosclerosis.

3.1.2. ACSL1.
A recent study showed that monocytes and macrophages expressed increased levels of ACSL1 (an enzyme that catalyzes the thioesterification of fatty acids) in both diabetic mouse models and human subjects [6]. ACSL1 is markedly induced by the TLR4 ligand lipopolysaccharide (LPS) in isolated macrophages, suggesting that ACSL1 may

TABLE 1: MicroRNA involved in diabetic atherosclerosis.

miR type	Animal model	Mechanism	Target gene	Reference
miR33	STZ-induced diabetic Ldlr−/− mice	Increased macrophages and lipid content	ABCA1	[37]
miR 125b	Type 2 diabetic db/db mice	Increased inflammatory gene expression	SUV39H1	[38]
miR 200	Type 2 diabetic db/db mice	Increased inflammatory gene expression	Zeb1	[39]
miR 504	Type 2 diabetic db/db mice	Vascular smooth muscle phenotype change	Grb10	[40]
miR138	Type 2 diabetic db/db mice	Vascular smooth muscle phenotype change	SIRT1	[41]

ABCA1: ATP-binding cassette transporter A1; SIRT1: silent information regulator 1.

be a downstream effector of TLR4 cascade in macrophages [28]. Myeloid-specific ACSL1 deficiency results in a specific reduction in 20:4-COA levels and completely prevents the increased release of prostaglandin E2 (PGE2) and increased inflammatory phenotype in monocytes and macrophages from diabetic mice, suggesting that the inflammatory phenotype is associated with increased expression of ACSL1. In addition, increased chemokine (C-C motif) ligand 2 (CCL2) secretion from macrophages in diabetic mice is completely prevented by ACSL1 deficiency, supporting that monocyte recruitment is reduced by ACSL1 deficiency [6]. Kanter et al. [29] demonstrated that ACSL1 could directly influence ATP-binding cassette transporter A1 (ABCA1) levels and cholesterol efflux in mouse macrophages. Mouse macrophages deficient in ACSL1 displayed increased ABCA1 levels and increased apolipoprotein A-I-dependent cholesterol efflux in the presence of unsaturated fatty acids compared with those of wild-type mouse macrophages. Conversely, overexpression of ACS1 led to reduced ABCA1 levels and reduced cholesterol efflux in the presence of unsaturated fatty acids. Taken together, the reduced levels of cholesterol efflux and expression of ABCA1 in mouse macrophages in the context of diabetes and elevated fatty load were partly mediated by ACSL1.

3.1.3. Paraoxonase (PON1).
In the state of high oxidative stress, such as STZ-induced diabetes, serum PON1 and arylesterase activities were reduced [30, 31]. Decreased serum PON activity is related to glycation and glycol oxidation of high-density lipoprotein (HDL) in the hyperglycemic state, thus leading to impairment of HDL activity, such as protection of LDL from oxidation, cholesterol efflux from cells, and inhibition of monocyte migration to endothelial cells [32, 33]. Taş et al. have demonstrated that vitamin B6 supplementation enhances serum PON1 and arylesterase activities, which could be related to the potential direct effects of this vitamin on the enzyme and/or to its ability to reduce oxidative stress [34]. These results suggested that protection of PON1 from inactivation may be a potential therapeutic approach for the treatment of diabetic atherosclerosis.

3.1.4. Insulinotropic Polypeptide (GIP).
As illustrated previously, high glucose accelerates atherosclerosis and foam cell formation. GIP potently stimulates insulin release from the pancreas under conditions of normal glucose tolerance. However, under diabetic conditions, the activity of GIP is reduced [35]. Thus, GIP is thought to be involved in diabetic atherosclerosis. According to Nogi et al. [36], chronic administration of GIP in vivo attenuates macrophage-driven atherosclerotic lesions in STZ-induced diabetic ApoE−/− mice, although this effect is abolished by cofusion with a GIPR antagonist, [Pro³]GIP. GIP infusion attenuates foam cell formation in both diabetic ApoE−/− mice and db/db mice. In vitro treatment with GIP (1 nM) reduces foam cell formation by 15% in macrophages from diabetic ApoE−/− mice.

3.1.5. MicroRNA (miRNA).
miRNA is a class of conserved 19–25-nucleotide noncoding RNAs that regulate gene expression posttranscriptionally. Recently, researchers have demonstrated that miRNAs play important roles in diabetes and related complications (Table 1). According to a study by Distel et al., treatment of STZ-induced diabetic LDLR−/− mice with anti-miR-33 decreases plaque macrophage content and inflammatory gene expression in diabetic LDLR−/− mice, accompanied by upregulation of ABCA1, which mediates cholesterol efflux from macrophages in the plaque [37]. Villeneuve et al. [38] first demonstrated the role of miR-125b in vascular complications of diabetes. They verified that miR-125b, which targets SUV39H1, led to increased levels of inflammatory genes, such as IL-6 and MCP-1. miR-125b mimic significantly increased monocyte binding to smooth muscle cells in db/db mice. According to a study by Reddy et al. [39], the expression levels of miR-200b and miR-200c were increased, whereas Zeb1 protein levels were decreased in VSMCs and aortas from db/db mice relative to those in control db/+mice. Transfection with miR-200 mimic downregulated Zeb1, upregulated the inflammatory genes COX-2 and MCP-1, and promoted monocyte binding in db/+ VSMCs. Both miR mimics and Zeb1 siRNA increased the proinflammatory response in db/db VSMCs. In contrast, miR-200 inhibitors reversed the enhanced monocyte binding of db/db VSMCs. Moreover, miR-504 significantly upregulated in db/db VSMCs compared with that in db/+VSMCs [40]. miR-504 may enhance extracellular regulated protein kinase 1/2 (ERK1/2) activation by targeting Grb10 and thereby contribute to changes in the VSMC phenotype. According to Xu et al. [41], higher miR-138 levels and reduced expression of silent information regulator 1 (SIRT1) were observed in SMCs isolated from db/db mice. Additionally, miR-138 promotes smooth muscle cell proliferation and migration in db/db mice through downregulation of SIRT1, whereas transfection with miR-138 inhibitor reverses these effects.

3.1.6. Tribbles Homolog 3 (TRIB3).
The expression of TRIB3, a protein made up of 358 amino acids, is increased in patients
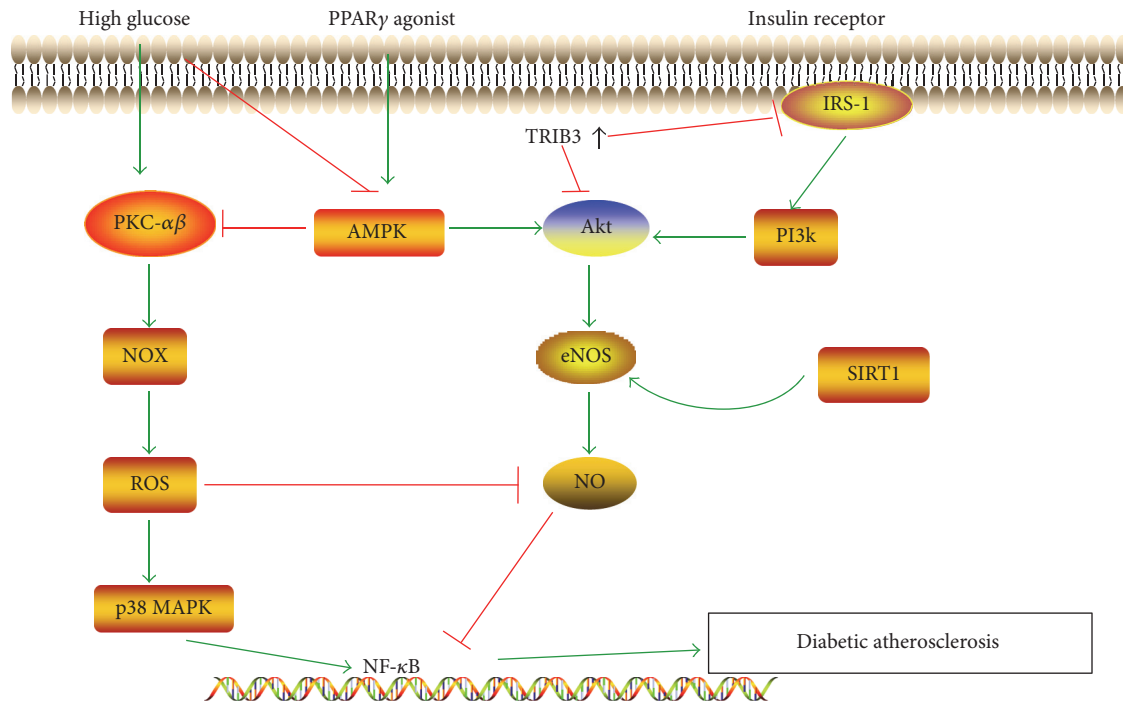
FIGURE 1: The NF-κB signalling pathway is involved in the diabetic atherosclerosis. Decreased NO produced by eNOS is associated with diabetic atherosclerosis. PI3K and AMPK are upstream of Akt and eNOS. Under hyperglycemic conditions, PKC activates NOX, the major source of reactive ROS production, leading to the activation of p38 MAPK and NF-κB and decrease in NO bioavailability. AMPK suppression in the context of high glucose contributes to the downregulation of the Akt/NO cascade. Increased levels of TRIB3 inhibit the phosphorylation of Akt directly or by reducing activation of PI3K/Akt. SIRT1 stimulates NO production by deacetylating eNOS at lysine residues or by upregulating AMPK. PPARγ agonists activate AMPK, which in turn increases the bioactivity of eNOS and prevents PKC-activated NOX caused by high glucose. PKC: protein kinase; NOX: NADPH oxidase; TRIB3: Tribbles homolog 3; ROS: reactive oxygen species; p38 MAPK: p38 mitogen-activated protein kinase; PI3K: phosphatidylinositol 3-kinase; AMPK: AMP-activated protein kinase; eNOS: endothelial NO synthase; IRS-1: insulin receptor substrate 1; SIRT1: silent information regulator 1; PPARγ: peroxisome proliferator-activated receptor γ.

and animals with type 2 diabetes [42]. Endoplasmic reticulum stress, an important feature of diabetes, has also been shown to increase TRIB3 expression, thus promoting cell death in response to endoplasmic reticulum stress [43].TRIB3 impairs insulin metabolic signalling by increasing serine phosphorylation of insulin receptor substrate 1 (IRS-1), reducing activation of phosphatidylinositol 3-kinase (PI3K)/Akt [44], or directly inhibiting the phosphorylation of Akt [45, 46].

Several mechanisms are involved in TRIB3-dependent promotion of atherosclerotic lesions. TRIB3 impairs IRS-1/Akt signalling in endothelial cells mediated by insulin [47], leading to reduced endothelial nitric oxide synthase (eNOS) and NO bioavailability [46], which is associated with endothelial dysfunction and increased leukocyte adhesion to endothelial cells, important steps for atherosclerotic lesion formation (Figure 1) [9]. In addition, TRIB3 is involved in lipid metabolism and macrophage apoptosis, an important feature for vulnerable plaques [48, 49]. According to a study by Wang et al. [49], silencing of TRIB3 in STZ plus diet-induced diabetic ApoE$^{-/-}$/LDLR$^{-/-}$ mice significantly decreases insulin resistance and blood glucose and reduces the numbers of apoptotic cells and macrophages in atherosclerotic lesions. Consequently, silencing of TRIB3 attenuates

the atherosclerosis burden and promotes plaque stability in diabetic mice. Thus, TRIB3 is a promising target for the treatment of diabetic atherosclerosis.

3.2. Signalling Pathways

3.2.1. The Janus Kinase (JAK)/Signal Transducers and Activators of Transcription (STAT) Cascade.
JAK/STAT is an essential intracellular pathway that regulates leukocyte recruitment, foam cell formation, and proliferation and migration of VSMCs, which are important features in atherosclerosis [50–52]. STAT isoforms have been found in the atherosclerotic lesions in both humans and animal models [53, 54]. STAT signalling cascade contributes to the macrophage apoptosis in advanced atherosclerotic plaque [55]. Inhibition of JAK2, STAT1, and STAT3 reduces lesion size and neointimal hyperplasia [56, 57]. Moreover, JAK/STAT is also a pivotal inflammatory mechanism through which hyperglycemia contributes to the pathogenesis of diabetes mellitus and its vascular complications [58–60]. High glucose stimulates endothelial IL-6 secretion via redox-dependent mechanisms, which may consequently induce STAT3 activation and ICAM-1 expression; the specific STAT3 inhibitor SI-201 (20 μM) suppresses high glucose-induced ICAM expression

in cultured human umbilical vein endothelial cells (HUVECs) [61]. The suppressor of cytokine signalling (SOCS) family regulates JAK/STAT signalling through STAT binding, kinase inhibition, targeting for proteasomal degradation, or direct suppression of JAK tyrosine kinase activity [62, 63]. According to a report by Recio et al. [64], SOCS1 peptide inhibits STAT1/STAT3 activation and target gene expression in VSMCs and macrophages and blocks the migration and adhesion of macrophages in vitro. Their results showed that intraperitoneal injection of SOCS1 into STZ-induced diabetic ApoE$^{-/-}$ mice (ages 8 and 22 weeks) for 6–10 weeks suppressed STAT1/STAT3 activation in atherosclerotic plaques and significantly attenuated lesion size for both early and advanced lesions. The accumulation of lipids, macrophages, and T lymphocytes was decreased following treatment with SOCS1 peptide, whereas collagen and smooth muscle cell content were significantly increased. Thus, the SOCS/JAK/STAT cascade was a key molecular mechanism through which diabetes promoted atherosclerotic plaque formation, and SOCS1 endogenous protein may be a feasible target for modulating inflammation-related complications of diabetes mellitus. Approaches to supplement SOC1 or mimic native SOCS1 function may have therapeutic effects on accelerated atherosclerosis in diabetes.

3.2.2. The eNOS/NO Pathway. NO produced by eNOS is an important vasodilator that possesses multiple antiatherosclerotic properties. eNOS-derived NO has been shown to inhibit platelet aggregation, block vascular inflammation by inhibiting the activation of NF-κB [65], and suppress VSMC proliferation. As illustrated previously, decreased bioactivity of NO is associated with exposure of endothelial cells to high-glucose concentration [9]. High-glucose levels block endothelial injury repair by circulating endothelial progenitor cells (EPCs) through decreasing eNOS/NO bioavailability [9, 66, 67]. According to a study by Sun et al. [68], the Akt kinase inhibitor (GSK690693) inhibited Akt and eNOS phosphorylation, suggesting that Akt may be necessary to activate eNOS. The PI3K inhibitor LY-29402 inhibits vaspin-induced eNOS and Akt phosphorylation, suggesting that PI3K acts upstream of Akt activation and eNOS. Additionally, vaspin induces endothelial protective effects via the PI3K/Akt/eNOS pathway. Ouchi et al. [69] showed that adiponectin-induced Akt phosphorylation, eNOS phosphorylation, and cell migration and differentiation in HUVECs were abolished when the cells were transduced with a dominant-negative form of AMP-activated protein kinase (AMPK). However, AMPK phosphorylation was not affected by dominant-negative transduction in HUVECs, suggesting that AMPK acts upstream of Akt in the Akt/eNOS/NO pathway to regulate endothelial function under conditions of hyperglycemia. SIRT1 is a class III histone deacetylase that has been shown to stimulate NO production by deacetylating eNOS at lysine residues [70] or by mediating the activation of AMPK [71]. Yang et al. [70] found that SIRT1 had a positive role in improving the expression of eNOS impaired by high glucose, and the low level of NO in endothelial cells cultured in the presence of high glucose may be partly related to the decreased expression of SIRT1 (Figure 1).

3.2.3. The Mitogen-Activated Protein Kinase (MAPK) Pathway. The MAPK pathway, including p38 MAPK, ERK, and c-Jun N-terminal kinase (JNK) branches, is involved in vascular inflammation. ERKs are typically initiated by Ras, which can be stimulated by inflammatory cytokines from high-glucose injured endothelial cells, leading to the proliferation of SMCs [72–75]. p38 MAPK activation is associated with diabetes and its complications, and the detrimental effects of high glucose can be blocked by coincubation with a p38 MAPK inhibitor [67]. Moreover, p38 MAPK has been shown to be involved in diabetic atherosclerosis. Hyperglycemic culture conditions accelerate the onset of EPC senescence, leading to impairment of endothelial repair, potentially through the activity of the p38 MAPK pathway [76]. Microparticles (MPs), which are submicron membrane vesicles (0.1–1 μm) shed from the plasma membrane of activated or apoptotic cells, are significantly increased in the presence of high-glucose levels. According to a study by Jansen et al. [77], p38 MAPK is activated to phospho-p38MAPK within 30 min when human coronary endothelial cells (HCAECs) are treated with "injured" EMP (iEMP, MPs derived from glucose-treated HCAECs), whereas there is no change following treatment with normal endothelial cell-derived MPs (EMPs). iEMP-induced expression of ICAM-1 and VCAM-1 and monocyte adhesion to HCAECs were significantly reduced by pretreatment of HCAECs with the p38MAPK inhibitor SB-203580 (1 μm). Consequently, these results showed that p38MAPK was involved in iEMP-induced endothelial dysfunction and monocyte adhesion. Further studies have shown that iEMP increases ROS production through NADPH oxidase (NOX) activation in endothelial cells, thus leading to activation of p38 MAPK. The p38 MAPK signalling pathway in diabetic atherosclerosis is illustrated in Figure 1.

3.2.4. The Protein Kinase (PKC) Pathway. High concentrations of glucose and nonesterified fatty acids result in activation of PKC. Active PKC is involved in vascular inflammation through the generation of proinflammatory cytokines and chemokines. PKC activates NOX, the major source of ROS production in high-glucose stress, thus leading to the activation of signalling pathways such as ERK, p38 MAPK, and NF-κB and decreased NO bioavailability (Figure 1) [78, 79]. ROS not only activate p38 MAPK but also act as an agonist to activate the nucleotide-binding domain-like receptor 3 (NLRP3) inflammasome, further disrupting endothelial function. These effects could be prevented by AMPK [80]. Durpès et al. [78] showed that PKCβ decreases the expression of IL-18-binding protein (IL-18BP), a molecule involved in a negative feedback mechanism in response to elevated IL-18 production, thus enhancing the production of cytokines and cellular adhesion molecules, which promote atherosclerotic plaque formation and instability in STZ-induced diabetic ApoE$^{-/-}$ mice. Kong et al. [81] found that activated plasma membrane-bound PKCβ is elevated in the aortas of low-dose STZ-induced hyperglycemic ApoE$^{-/-}$ mice and that pharmacological inhibition of PKCβ attenuates atherosclerotic lesions in hyperglycemic ApoE$^{-/-}$ mice. Deficiency of PKCβ blocks the upregulation of Egr-1, ERK1/2, and

JNK and results in diminished lesional macrophages and CD11c-expressing cells in diabetic ApoE$^{-/-}$ mice. In vitro, inhibitors of PKCβ and ERK1/2 significantly decrease high glucose-induced expression of CD11c, CCL2, and IL-1β in U937 macrophages. These studies suggest that selective PKCβ inhibitors may have potential therapeutic effects in diabetes-associated atherosclerosis.

3.2.5. The Peroxisome Proliferator-Activated Receptor (PPAR)γ Signalling Pathway.

Accumulating evidence has shown that PPARγ has protective effects in both diabetes and atherosclerosis. In a combined diabetes/atherosclerosis mouse model, PPARγ agonists were found to exert anti-atherogenic effects independent of a reduction in insulin resistance and plasma glucose [82], indicating that attenuation of insulin resistance is not the only mechanism through which PPARγ functions as an antiatherognic agent. PPARγ agonists activate AMPK, which in turn increases the bioactivity of eNOS and prevents PKC-activated NOX caused by high glucose [80, 83]. Pioglitazone downregulates RAGE expression and inhibits ROS production and NF-κB activation via PPARγ activation, which may prevent the inflammatory effects of the AGE/RAGE system in diabetes [84]. Recent studies have shown that pioglitazone attenuates platelet-derived growth factor (PDGF)-induced VSMC proliferation through AMPK-dependent and -independent inhibition of mammalian target of rapamycin (mTOR)/p70S6K and ERK signalling [85]. Furthermore, PPARγ agonists have been reported to promote cholesterol efflux from macrophages via upregulation of ABCA1 expression [86, 87]. The PPARγ signalling pathway in antiatherosclerosis under hyperglycemic conditions is illustrated in Figure 1.

3.2.6. The Nuclear Factor of Activated T Cells (NFAT) Signalling Pathway.

NFAT proteins are a family of Ca^{2+}/calcineurin-dependent transcription factors first characterized in T lymphocytes as inducers of cytokine gene expression. There are four well-characterized members of the NFAT family, which function in VSMC proliferation in the context of atherosclerosis and hypertension and have roles in glucose and insulin homeostasis [88]. According to a study by Nilsson et al., in intact cerebral arteries, raising the extracellular glucose concentration from 11.5 mM (control) to 20 mM [HG] for 30 min significantly increases NFAT nuclear accumulation, accompanied by enhanced transcriptional activity. UTP and UDP mediate glucose-induced NFAT activation via P2Y receptors. High-glucose concentrations downregulate glycogen synthase kinase 3 (GSK) β and JNK activity, leading to decreased export of NFATc3 from the nucleus and enhanced robust NFATc3 nuclear accumulation, representing another mechanism for glucose-induced NFAT activation [89]. NFATc3 is activated by hyperglycemia, thereby inducing the expression of osteopontin (OPN), a cytokine that promotes diabetic atherosclerosis [90]. Zetterqvist et al. demonstrated a link between NFAT activation and diabetic atherosclerosis using STZ-induced diabetic ApoE$^{-/-}$ mice. In vivo treatment with the NFAT inhibitor A285222 (0.29 mg/kg/day i.p.) for 4 weeks prevented diabetes-associated atherosclerosis lesions in the aortic arch independent of blood glucose lowering, accompanied by decreased expression of IL-6, OPN, MCP-1, and ICAM-1 and the macrophage markers CD68 and tissue factor (TF) in the aortic arch. These findings revealed that the NFAT signalling pathway may be a promising target for the treatment of diabetes-associated atherosclerosis [91].

3.2.7. The Nrf2 Signalling Pathway.

Ungvari et al. demonstrated the vasoprotective role of Nrf2 in diabetes using Nrf2$^{-/-}$ mice. They showed that the expression of Nrf2 downstream genes was significantly upregulated in diabetic Nrf2$^{+/+}$ mice, but not in diabetic Nrf2$^{-/-}$ mice [92]. Under normal conditions, Nrf2 constitutively interacts with keap1, a negative regulator, for ubiquitination and degradation in the cytosol. Under high-glucose stress, Nrf2 is released from keap1 and translocates to the nucleus and subsequently binds to antioxidant-responsive elements (ARE); this results in increased transcription of genes such as NADPH: quinine oxidoreductase 1 (NQO1), heme oxygenase-1 (HO-1), superoxide dismutase (SOD), and catalase (CAT). These antioxidant enzymes decrease the levels of ROS, thus attenuating diabetic atherosclerosis (Figure 2) [93]. These results suggest that Nrf2 activators may have efficacy in the management of diabetic atherosclerosis.

4. Herbal Medicines: Promising Therapeutic Agents for the Management of Diabetic Atherosclerosis

4.1. Ginkgo biloba.

Ginkgo biloba is a dioecious tree with a history of use in traditional Chinese medicine and has many pharmacologic effects. Ginkgo has vascular protection functions due to its antioxidant effects, free radical scavenging activity, stabilization of membranes, and inhibition of platelet-activating factor. Ginkgo biloba extract (GBE), produced from Ginkgo biloba leaves, is commonly used in dietary supplements for aliments and has shown excellent clinical effects in many cases. GBE contains terpenoids, flavonoids, alkylphenols, polyprenols, and organic acids. Terpenoids (including ginkgolides and biobalide) and flavonoids are the two major groups of active substances in Ginkgo leaves. The basic structures of ginkgolides, biobalides, and Ginkgo biloba flavonol aglycones are shown in Figures 3(a), 3(b), 3(c).

There have been several reports showing that EGB761, a standard GBE, improves glucose homeostasis, possibly because of increased plasma insulin levels, via protection of pancreatic β-cells and/or stimulation of insulin secretion. Cheng et al. reported that GBE (100, 200, and 300 mg/kg) administered orally once a day for 30 days caused a significant dose- and time-dependent reduction in blood glucose levels in diabetic rats. In their study, GBE increased the activities of SOD, CAT, and glutathione peroxidase (GSH-Px) in diabetic rats and resulted in protection of pancreatic β-cells [94]. In addition, several reports have shown that GBE lowers blood glucose by improving insulin resistance [95–97]. Thus, GBE may attenuate atherosclerosis in the context of diabetes. According to a study by Lim et al. [98], neointimal formation
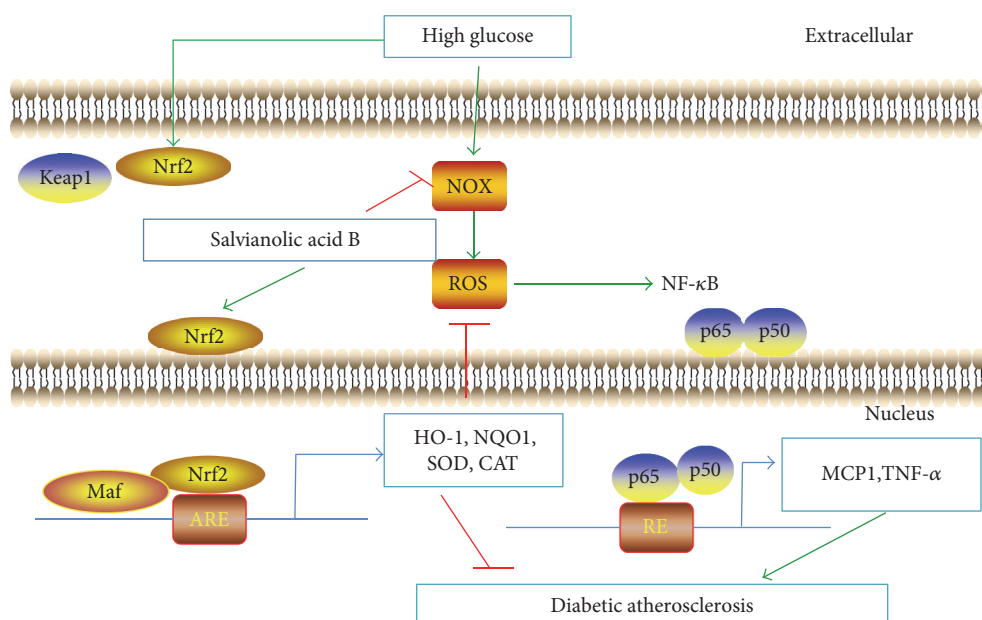
FIGURE 2: Salvianolic acid B protects against diabetic atherosclerosis via the Nrf2 signalling pathway. Under normal conditions, Nrf2 constitutively binds to keap1, a negative regulator in the cytosol. Under high-glucose stress, Nrf2 is released from keap1 and translocates to the nucleus, enhancing the transcriptional activity of NADPH: quinine oxidoreductase 1 (NQO1), heme oxygenase-1 (HO-1), superoxide dismutase (SOD), and catalase (CAT). These antioxidant enzymes decrease the levels of ROS. Salvianolic acid B is capable of upregulating Nrf2 activity or inhibiting NOX generation directly. ARE: antioxidant-responsive element; HO-1: heme oxygenase-1; NQO1: quinine oxidoreductase 1; SOD: superoxide dismutase; CAT: catalase.

in balloon-injured carotid arteries is significantly reduced when insulin-resistant rats are treated with EGb761 (100 or 200 mg/kg/day) for 6 weeks, resulting in reduced proliferation and migration of VSMCs. EGb761 (50–200 μg/mL) decreases the proliferation of rat aortic SMCs in a concentration-dependent manner in vitro. In addition, EGb761 at both 100 and 200 μg/mL suppresses the expression of ICAM and VCAM in HUVECs. Zhao et al. [99] found that GBE improves SOD activity and reduces the rate of apoptosis of EPCs within the peripheral blood of diabetic patients in a dose-dependent manner. According to Tsai et al. [100], GBE inhibits high glucose-induced ROS generation, adhesion molecule expression, and monocyte adhesiveness in human aortic endothelial cells (HAECs) via the Akt/eNOS and p38 MAPK pathways. Another study showed that Ginkgolide A at 10, 15, and 20 μM inhibits high glucose-induced IL-4, IL-6, and IL-3 expression in HUVECs. Ginkgolide A attenuates vascular inflammation by regulating the STAT3-mediated pathway [61]. According to a study by Wang et al. [101], treatment with the rutin (30 and 100 μM) significantly restores NO production by decreasing NOX4 mRNA and protein levels and reducing the generation of ROS in HUVECs under high-glucose conditions. Furthermore, rutin at doses of 35 and 70 mg/kg improves endothelium function by restoring impaired NO generation from glucose-triggered endothelial cells and ameliorating the endothelial contraction and relaxation response in thoracic aortas of rats with a high-glucose diet. The potential mechanism for GBE in the treatment of diabetic atherosclerosis is shown in Figure 4.

4.2. Tetramethylpyrazine (TMP).

TMP is a biologically active compound isolated from rhizomes of *Ligusticum chuanxiong*, a traditional Chinese medicine (Figure 3(d)). Several studies have shown that TMP exerts antiatherosclerosis effects through promotion of endothelial protection, inhibition of VSMC proliferation, reduction of oxidative stress, and suppression of inflammation and apoptosis. The link between TMP and NO generation has been verified by several researchers. For example, Lv et al. [102] demonstrated that TMP pretreatment in vivo enhances Akt and eNOS phosphorylation. Additionally, Xu et al. reported that Qiong Huo Yi Hao (QHYH), which consists of several herbals based on the "clearing heat and detoxifying" principle of traditional Chinese Medicine, is a potent antioxidant acting to scavenge superoxide anions in endothelial cells treated with high concentrations of glucose [103]. TMP, an active compound in QHYH, has been shown to be the strongest component of QHYH in the prevention of ROS production, functioning to block Akt/eNOS phosphorylation and reduce NO generation in endothelial cells treated with high concentrations of glucose [104]. Xu et al. further demonstrated that TMP ameliorates high glucose-induced endothelial dysfunction by increasing mitochondrial biogenesis through reversing high glucose-induced suppression of SIRTI1 [105]. These findings provide evidence for the endothelial protection function of TMP in the context of hyperglycemia. Studies have shown that TMP can suppress the proliferation of VSMCs [106], and the ERK and p38MAPK pathways may be involved in this process [107]. Additionally, TMP can block LPS-induced IL-8 overexpression in HUVECs at both protein and mRNA levels,

(a) Bilobalide

(b) Ginkgolide

(c) *Ginkgo biloba* flavonol aglycones

(d) Tetramethylpyrazine

(e) Salvianolic acid B
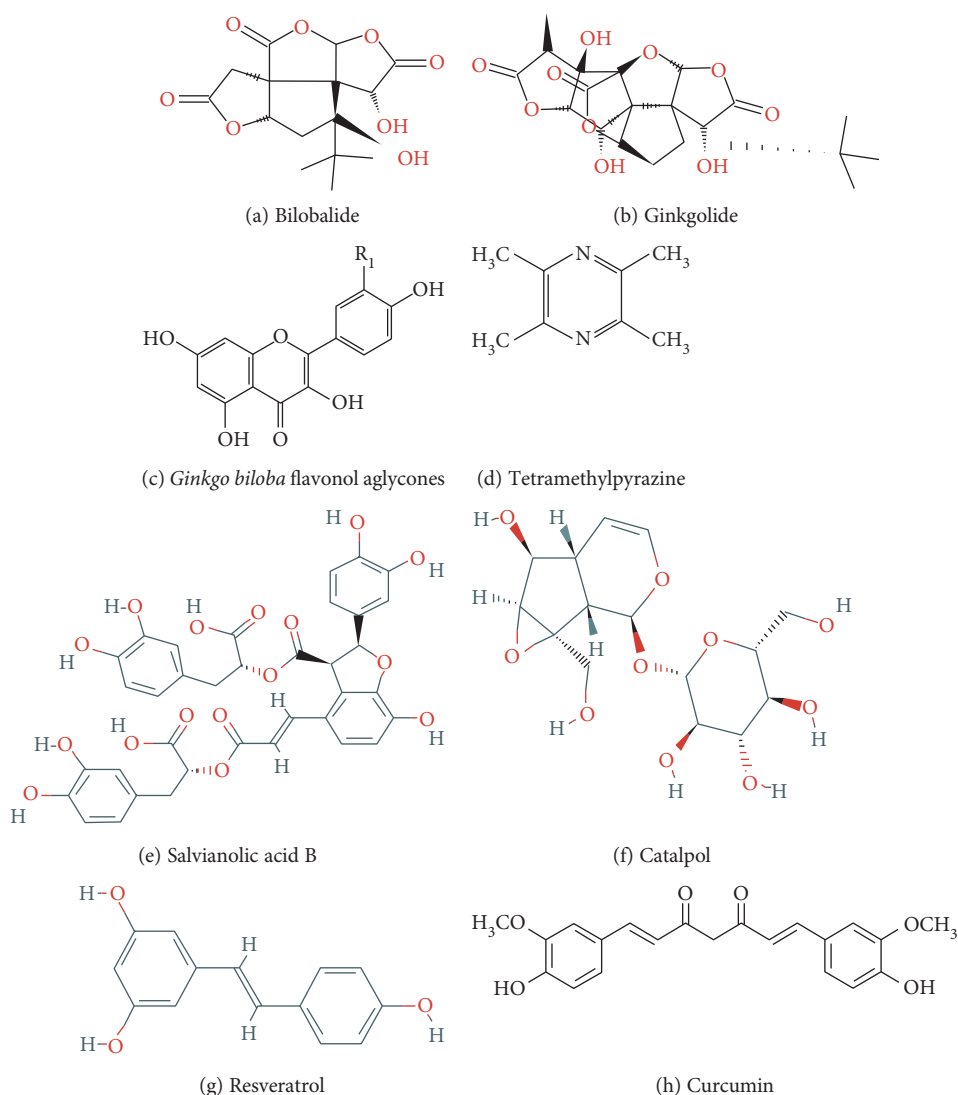
(f) Catalpol

(g) Resveratrol

(h) Curcumin

FIGURE 3: Molecular structure of the compounds described in this review.

which could be attributed to inhibition of the ERK and p38MAPK pathways and the inactivation of NF-κB [108]. The antiapoptotic function of TMP can be attributed to the inhibition of JAK/STAT signal transduction [109].

Importantly, Lee et al. [110] investigated the effects of TMP on lipid peroxidation in STZ-induced diabetic mice. The results showed that TMP dose dependently inhibited glucose concentrations, blood urea nitrogen elevation, and the degree of lipoperoxidation. Thus, TMP may be an effective agent for the treatment of diabetes and related vascular complication. The mechanisms through which TMP protects against diabetes are shown in Figure 5.

4.3. Danggui. Danggui-Buxue-Tang (DBT) is a well-known traditional formula. Zhang et al. [111] found that oral administration of DBT (3 or 6 g/kg/day for 4 weeks) decreased the concentrations of c-reactive protein and tumour necrosis factor-α and resulted in higher survival rates and lower body weight loss in diabetic GK rats; the diabetic atherosclerosis

rats were induced by NO inhibition (I-NAME in drinking water, 1 mg/mL) plus a high-fat diet. They also investigated the effects of DBT on blood lipids and the expression of genes related to foam cell formation during the early stage of atherosclerosis in diabetic GK rats. The results demonstrated that DBT could regulate blood lipids and inhibit the expression of *MCP*, *ICAM-1*, and *CD36* genes in the aorta [112]. Galgeun-dang-gwi-tang (GGDGT), a Korean herbal medicine, has traditionally been prescribed for the treatment of diabetes. In a study by Lee et al. [113], lipid metabolism and insulin resistance were shown to be improved by GGDGT in ApoE$^{-/-}$ mice fed with a Western diet. Immunohistochemical staining showed that GGDGT suppressed ICAM expression, whereas the expression of eNOS and IRS-1 was restored by GGDGT in the thoracic aorta and skeletal muscle. GGDGT attenuates endothelial dysfunction via improvement of the NO-cylic guanosine monophosphate signalling pathway and promotes insulin sensitivity in diabetic atherosclerosis.
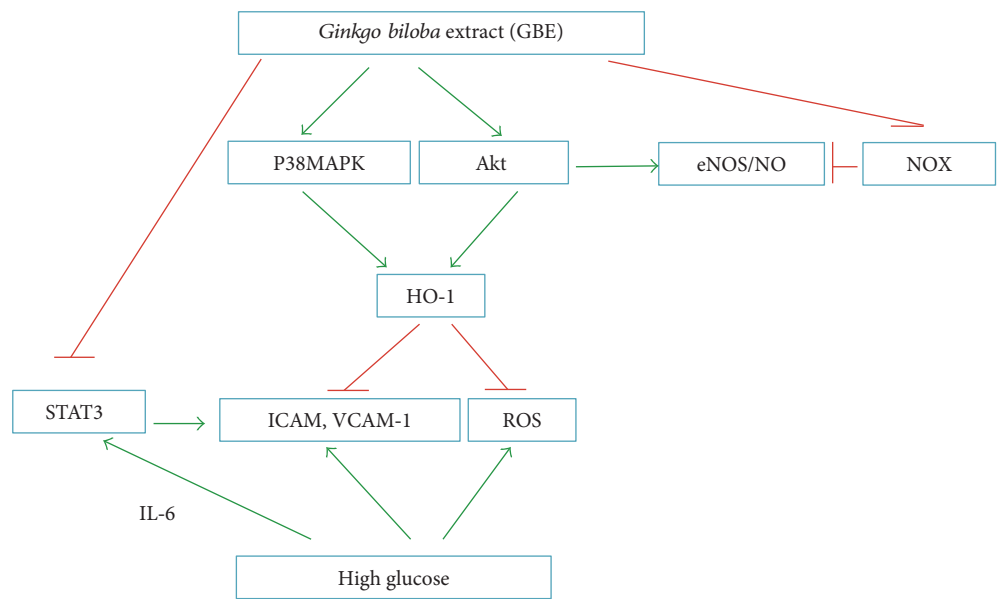
FIGURE 4: Mechanism for GBE antiatherosclerosis under diabetic conditions. STAT: signal transducer and activator of transcription; ICAM: intercellular cell adhesion molecule-1; VCAM-1: vascular cell adhesion molecule 1.
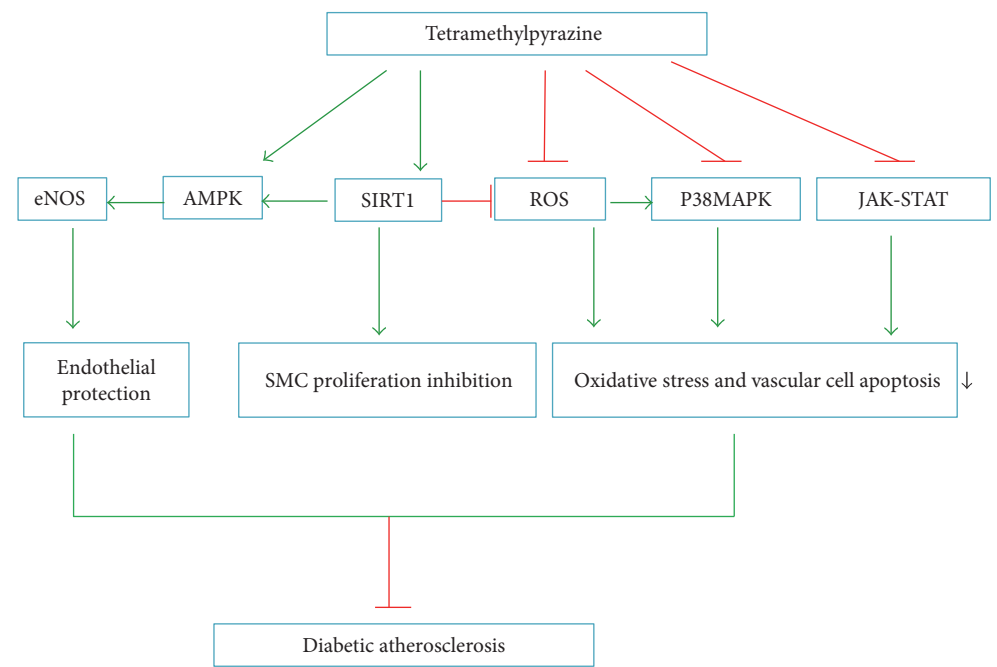
FIGURE 5: Mechanism through which tetramethylpyrazine protects against diabetic atherosclerosis.

4.4. *Salvia miltiorrhiza* (Danshen) and Salvianolic Acid. *Salvia miltiorrhiza* (Danshen), a traditional Chinese herbal medicine, is commonly used for the prevention and treatment of cardiovascular disease. Salvianolic acid B is the most abundant water-soluble compound extracted from Danshen (Figure 3(e)). Inhibition of inflammation, improvement of antioxidative effects, regulation of leukocyte endothelial adhesion, and modulation of NO production in endothelial cells are involved in the cardiovascular protection

mechanism for Danshen and its bioactive compounds [114, 115]. Danshen extract and purified salvianolic acid B exert anti-inflammatory effects by inhibiting iNOS expression and NO production induced by LPS in RAW267.4 macrophages by inducing Nrf2-mediated HO-1 expression [114, 116]. Lee et al. [117] also demonstrated that salvianolic acid B inhibits platelet-derived growth factor-induced neointimal hyperplasia in arteries through induction of Nrf2-dependent HO-1. In addition, salvianolic acid B increases NO

FIGURE 6: Antiatherosclerotic mechanism of resveratrol under diabetic conditions. RAGE: advanced glycosylation end product receptor.

production in the endothelium of isolated mouse aortas via inhibition of arginase activity [114]. According to Raoufi et al., administration of salvianolic acid B at doses of 20 or 40 mg/kg/day (i.p.) for 3 weeks significantly decreases serum gluco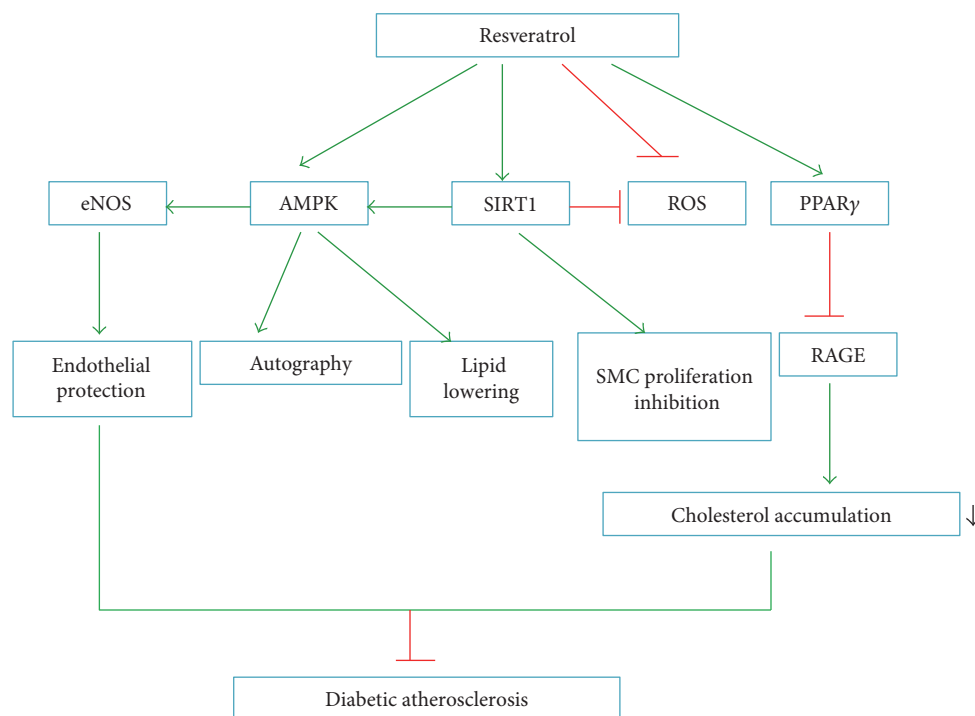se and improves oral glucose tolerance test (OGTT) in STZ-induced diabetic rats via attenuation of oxidative stress and apoptosis and augmentation of the antioxidant system [118]. The vascular endothelial protective function of *Salvia miltiorrhiza* and salvianolic acid B under high-glucose conditions has been verified both in vitro and in vivo. According to Qian et al. [119], *Salvia miltiorrhiza* (10 μg/mL) significantly decreases vascular endothelial ROS formation in human microvascular endothelial cells exposed to 30 mM glucose. Ren et al. [120] demonstrated that salvianolic acid B significantly restores eNOS in STZ-induced diabetic rats and decreases the levels of NOX and endothelial cell apoptosis. The mechanism through which salvianolic acid B protects against diabetic atherosclerosis is shown in Figure 2.

4.5. Catalpol. Catalpol is the most abundant bioactive component in the roots of *Rehmannia glutinosa* (Figure 3(f)). Catalpol ameliorates plasma glucose in STZ-induced diabetic rats [121], and total cholesterol, triglycerides, and LDL cholesterol are reduced, whereas HDL cholesterol is elevated when the rats fed with high-cholesterol chow are treated with catalpol [122]. Additionally, atherosclerotic lesions and inflammatory markers are markedly reduced in the catalpol group, and catalpol attenuates atherosclerotic lesions and delays the progression of atherosclerosis in alloxan-induced diabetic rabbits. These protective effects are associated with regulation of glucose insulin homeostasis and inhibition of oxidative stress and inflammation [123].

4.6. Resveratrol. Resveratrol (*trans*-3,5,4′-trihydroxystilbene) is a natural polyphenol phytoalexin (Figure 3(g)) with various biological effects. The beneficial cardiovascular effects of this drug are attributable to its anti-inflammatory, antioxidative stress, endothelial protection, antiplatelet, and insulin-sensitizing effects [124]. Resveratrol increases NO bioavailability by regulating SIRT1, AMPK, and ROS. According to a study by Yang et al. [125], resveratrol restores the NO bioavailability impaired by high glucose in human endothelial cells in a SIRT1-dependent manner. Other studies have shown that resveratrol downregulates NF-κB induced by high glucose in smooth muscle cells and decreases the proliferation and migration of smooth muscle cells, a function similar to *miR-138* inhibitors, which result in upregulation of SIRT1 [41]. Zhang et al. [126] demonstrated that resveratrol prevents impairment of the effects of AGEs on macrophage lipid homeostasis partially by suppressing RAGEs via PPARγ activation, thus providing new insights into the protective roles of resveratrol against diabetic atherosclerosis. Furthermore, resveratrol lowers lipid levels and decreases hepatic lipid accumulation by stimulation of AMPK dependent on SIRT1 activity. These findings suggest that resveratrol may have potential therapeutic effects through regulation of dyslipidaemia-associated atherosclerosis in diabetes by targeting SIRTI/AMPK signalling [127, 128]. The underlying antiatherosclerotic mechanisms of resveratrol in the context of diabetes are illustrated in Figure 6.

4.7. Curcumin. Curcumin (diferuloylmethane) is a constituent of turmeric (*Curcuma longa*) spice. Decreased serum LDL levels and increased serum HDL levels were observed after patients with atherosclerosis were administered 10 mg

TABLE 2: Fundamental application of herb in diabetic atherosclerosis.

Drug	Dosage	Administration	Model	Reference
			In vitro studies	
GBE	100 μg/mL	Incubation 18 h	HAECs cultured in high glucose	[100]
Ginkgolide A	10, 15, 20 μM	Preincubation 30 min	HUVECs cultured in high glucose	[61]
Rutin	30, 100 μM	Preincubation 30 min	HUVECs cultured in high glucose	[101]
TMP	10 μM	Incubation 48 h	bEnd.3 and HUVECs cultured in high glucose	[104]
TMP	30 μmol/L	Incubation 48 h	bEnd.3 and HUVECs cultured in high glucose	[105]
Salvia miltiorrhiza	10 μg/mL	Incubation 48 h	HMECs cultured in high glucose	[119]
Resveratrol	1 μmol/L	Preincubation 24 h	HUVECs cultured in high glucose	[70, 125]
			In vivo studies	
EGb761	100, 200 mg/kg/d	p.o. 6 weeks	Obesity and insulin-resistant rats	[98]
Rutin	35, 70 mg/kg/d	p.o. 12 weeks	SD rats fed with high glucose	[101]
TMP	10, 25, 50 mg/kg	i.p. 2 weeks	STZ-induced diabetic mice	[110]
DBT	3, 6 g/kg/d	p.o. 4 weeks	Nitric oxide inhibition plus high-fat diet-fed rats	[111]
DBT	3, 6 g/kg/d	p.o. 4 weeks	Nitric oxide inhibition plus high-fat diet rats	[112]
GGDGT	200 mg/kg/d	p.o. 12 weeks	Western diet-fed ApoE−/− mice	[113]
Salvianolic acid B	80, 160 mg/kg/d	p.o. 6 weeks	STZ-induced diabetic atherosclerosis	[120]
Catalpol	5 mg/kg/d	p.o. 12 weeks	Hyperlipidemic diet plus alloxan diabetic-induced rabbit	[123]

HUVECs: human umbilical vein endothelial cells; HACEs: human aortic endothelial cells; bEnd.3: murine brain microvascular cell line; HMECs: microvascular endothelial cells; DBT: Danggui-Buxue-Tang; GGDGT: Galgeun-dang-gwi-tang; STZ: streptozotocin.

curcumin twice daily for 28 days [129]. Usharani et al. [130] showed that administration of a standardized preparation of curcuminoids (NCB-02, two capsules containing 150 mg curcumin, twice daily) for 8 weeks significantly improved the endothelial function of patients with type 2 diabetes mellitus. Curcumin also blocks oxidative stress and inflammation by modulating PPARγ and Nrf2 activity [131]. Zheng et al. showed that the curcumin analogue L3 alleviates dyslipidaemia and hyperglycemia and reduces oxidative stress in diabetic mice induced by STZ and a high-fat diet. Additionally, L3 effectively decreases lectin-like oxidized low-density lipoprotein receptor-1 expression in the aortic arch. These results suggested that curcumin ameliorates diabetic atherosclerosis through multiple mechanisms [132].

5. Future Perspectives

Insulin resistance and hyperglycemia are associated with diabetic atherosclerosis, and endothelial dysfunction, vascular inflammation, myeloid cell recruitment, oxidative stress, VSMC phenotype changes, and platelet hyperreactivity all contribute to diabetic atherosclerosis. As reported recently, crosstalk between macrophage polarization and autophagy may be involved in diabetes and related atherosclerosis complications [133, 134]. Extensive preclinical studies have identified the molecule targets and herbs that act on these targets as potential therapeutic agents for the management of diabetic atherosclerosis (see Table 2). However, currently, most clinical studies have small sample sizes and are not performed using a randomised design. The lack of high-quality clinical trials hampers the application of herbal medicines in patients with diabetic atherosclerosis. Therefore, more rigorous clinical trials of herbs on diabetic atherosclerosis, with large sample sizes and a randomised, controlled design, are

needed. Furthermore, detection of new molecules and signalling cascades that regulate diabetes and atherosclerosis will help to improve treatment approaches owing to the multifaceted characteristics of diabetic atherosclerosis. Investigation of the mechanisms of multitargeted effects of herbs will also help to establish novel drugs for the treatment of diabetes and diabetic atherosclerosis. In the future, the combination of herb with western medicine may also facilitate the treatment of diabetic atherosclerosis. Thus, further studies on drug interactions and safety are needed.

Conflicts of Interest

The authors have no conflict of interest to declare.

Authors' Contributions

Yue Liu conceived the topic and helped in drafting the paper. Shuzheng Lyu helped in revising the manuscript. Jinfan Tian searched the literature and wrote the manuscript together with Yanfei Liu, and they are co-first authors. Keji Chen helped in drafting the manuscript. All authors read and approved the final manuscript.

Acknowledgments

References

[1] M. Haneda, D. Koya, M. Isono, and R. Kikkawa, "Overview of glucose signaling in mesangial cells in diabetic nephropathy," *Journal of the American Society of Nephrology*, vol. 14, no. 5, pp. 1374–1382, 2003.

[2] C. Liu and Y. Huang, "Chinese herbal medicine on cardiovascular diseases and the mechanisms of action," *Frontiers in Pharmacology*, vol. 7, p. 469, 2016.

[3] J. Li, T. Casteels, T. Frogne et al., "Artemisinins target GABAA receptor signaling and impair alpha cell identity," *Cell*, vol. 168, no. 1-2, pp. 86–100, 2017.

[4] L. A. Johnson, H. S. Kim, M. J. Knudson, C. T. Nipp, X. Yi, and N. Maeda, "Diabetic atherosclerosis in APOE*4 mice: synergy between lipoprotein metabolism and vascular inflammation," *Journal of Lipid Research*, vol. 54, no. 2, pp. 386–396, 2013.

[5] H. Sun, X. Zhang, L. Zhao et al., "Attenuation of atherosclerotic lesions in diabetic apolipoprotein E-deficient mice using gene silencing of macrophage migration inhibitory factor," *Journal of Cellular and Molecular Medicine*, vol. 19, no. 4, pp. 836–849, 2015.

[6] J. E. Kanter, F. Kramer, S. Barnhart et al., "Diabetes promotes an inflammatory macrophage phenotype and atherosclerosis through acyl-CoA synthetase 1," *Proceedings of the National Academy of Sciences of the United States of America*, vol. 109, no. 12, pp. E715–E724, 2012.

[7] E. M. Bradshaw, K. Raddassi, W. Elyaman et al., "Monocytes from patients with type 1 diabetes spontaneously secrete proinflammatory cytokines inducing Th17 cells," *Journal of Immunology*, vol. 183, no. 7, pp. 4432–4439, 2009.

[8] G. M. Pieper, P. Langenstroer, and W. Siebeneich, "Diabetic-induced endothelial dysfunction in rat aorta: role of hydroxyl radicals," *Cardiovascular Research*, vol. 34, no. 1, pp. 145–156, 1997.

[9] I. A. van den Oever, H. G. Raterman, M. T. Nurmohamed, and S. Simsek, "Endothelial dysfunction, inflammation, and apoptosis in diabetes mellitus," *Mediators of Inflammation*, vol. 2010, Article ID 792393, 15 pages, 2010.

[10] M. Y. Donath and T. Mandrup-Poulsen, "The use of interleukin-1-receptor antagonists in the treatment of diabetes mellitus," *Nature Clinical Practice. Endocrinology & Metabolism*, vol. 4, no. 5, pp. 240-241, 2008.

[11] S. Vallejo, E. Palacios, T. Romacho, L. Villalobos, C. Peiró, and C. F. Sánchez-Ferrer, "The interleukin-1 receptor antagonist anakinra improves endothelial dysfunction in streptozotocin-induced diabetic rats," *Cardiovascular Diabetology*, vol. 13, p. 158, 2014.

[12] G. P. Chen, X. Q. Zhang, T. Wu, L. Li, J. Han, and C. Q. Du, "Alteration of mevalonate pathway in proliferated vascular smooth muscle from diabetic mice: possible role in high-glucose-induced atherogenic process," *Journal of Diabetes Research*, vol. 2015, Article ID 379287, 11 pages, 2015.

[13] G. Orasanu and J. Plutzky, "The pathologic continuum of diabetic vascular disease," *Journal of the American College of Cardiology*, vol. 53, Supplement 5, pp. S35–S42, 2009.

[14] E. Di Marco, S. P. Gray, K. Kennedy et al., "NOX4-derived reactive oxygen species limit fibrosis and inhibit proliferation of vascular smooth muscle cells in diabetic atherosclerosis," *Free Radical Biology & Medicine*, vol. 97, pp. 556–567, 2016.

[15] J. M. Gerrard, M. J. Stuart, G. H. Rao et al., "Alteration in the balance of prostaglandin and thromboxane synthesis in diabetic rats," *The Journal of Laboratory and Clinical Medicine*, vol. 95, no. 6, pp. 950–958, 1980.

[16] P. A. Modesti, A. Fortini, G. F. Gensini, D. Vanni, D. Prisco, and R. Abbate, "Human prostacyclin platelet receptors in diabetes mellitus," *Thrombosis Research*, vol. 63, no. 5, pp. 541–548, 1991.

[17] P. Ferroni, S. Basili, A. Falco, and G. Davì, "Platelet activation in type 2 diabetes mellitus," *Journal of Thrombosis and Haemostasis*, vol. 2, no. 8, pp. 1282–1291, 2004.

[18] W. Wang, W. B. Lau, Y. Wang, X. Ma, and R. Li, "Reduction of CTRP9, a novel anti-platelet adipokine, contributes to abnormal platelet activity in diabetic animals," *Cardiovascular Diabetology*, vol. 15, p. 6, 2016.

[19] I. A. Sobenin, V. V. Tertov, A. N. Orekhov, and V. N. Smirnov, "Synergetic effect of desialylated and glycated low density lipoproteins on cholesterol accumulation in cultured smooth muscle intimal cells," *Atherosclerosis*, vol. 89, no. 2-3, pp. 151–154, 1991.

[20] N. Younis, R. Sharma, H. Soran, V. Charlton-Menys, M. Elseweidy, and P. N. Durrington, "Glycation as an atherogenic modification of LDL," *Current Opinion in Lipidology*, vol. 19, no. 4, pp. 378–384, 2008.

[21] A. M. Schmidt, O. Hori, J. X. Chen et al., "Advanced glycation endproducts interacting with their endothelial receptor induce expression of vascular cell adhesion molecule-1 (VCAM-1) in cultured human endothelial cells and in mice. A potential mechanism for the accelerated vasculopathy of diabetes," *The Journal of Clinical Investigation*, vol. 96, no. 3, pp. 1395–1403, 1995.

[22] S. Del Turco and G. Basta, "An update on advanced glycation endproducts and atherosclerosis," *BioFactors*, vol. 38, no. 4, pp. 266–274, 2012.

[23] K. Fukami, S. Yamagishi, and S. Okuda, "Role of AGEs-RAGE system in cardiovascular disease," *Current Pharmaceutical Design*, vol. 20, no. 14, pp. 2395–2402, 2014.

[24] S. Menini, C. Iacobini, C. Ricci et al., "D-carnosine octylester attenuates atherosclerosis and renal disease in ApoE null mice fed a Western diet through reduction of carbonyl stress and inflammation," *British Journal of Pharmacology*, vol. 166, no. 4, pp. 1344–1356, 2012.

[25] S. Menini, C. Iacobini, C. Ricci, C. Blasetti Fantauzzi, and G. Pugliese, "Protection from diabetes-induced atherosclerosis and renal disease by D-carnosine-octylester: effects of early vs late inhibition of advanced glycation end-products in Apoe-null mice," *Diabetologia*, vol. 58, no. 4, pp. 845–853, 2015.

[26] L. Zhu, Z. He, F. Wu et al., "Immunization with advanced glycation end products modified low density lipoprotein inhibits atherosclerosis progression in diabetic apoE and LDLR null mice," *Cardiovascular Diabetology*, vol. 13, p. 151, 2014.

[27] Y. Naka, L. G. Bucciarelli, T. Wendt et al., "RAGE axis: animal models and novel insights into the vascular complications of diabetes," *Arteriosclerosis, Thrombosis, and Vascular Biology*, vol. 24, no. 8, pp. 1342–1349, 2004.

[28] K. B. Rubinow, V. Z. Wall, J. Nelson et al., "Acyl-CoA synthetase 1 is induced by Gram-negative bacteria and lipopolysaccharide and is required for phospholipid turnover in stimulated macrophages," *The Journal of Biological Chemistry*, vol. 288, no. 14, pp. 9957–9970, 2013.

[29] J. E. Kanter, C. Tang, J. F. Oram, and K. E. Bornfeldt, "Acyl-CoA synthetase 1 is required for oleate and linoleate mediated inhibition of cholesterol efflux through ATP-binding cassette transporter A1 in macrophages," *Biochimica et Biophysica Acta (BBA) - Molecular and Cell Biology of Lipids*, vol. 1821, no. 3, pp. 358–364, 2012.

[30] M. Pan, A. I. Cederbaum, Y. L. Zhang, H. N. Ginsberg, K. J. Williams, and E. A. Fisher, "Lipid peroxidation and oxidant stress regulate hepatic apolipoprotein B degradation and VLDL production," *The Journal of Clinical Investigation*, vol. 113, no. 9, pp. 1277–1287, 2004.

[31] M. Wegner, M. Pioruńska-Stolzmann, A. Araszkiewicz, D. Zozulińska-Ziółkiewicz, and B. Wierusz-Wysocka, "Evaluation of paraoxonase 1 arylesterase activity and lipid peroxide levels in patients with type 1 diabetes," *Polskie Archiwum Medycyny Wewnętrznej*, vol. 121, no. 12, pp. 448–454, 2011.

[32] D. K. Spady, "Reverse cholesterol transport and atherosclerosis regression," *Circulation*, vol. 100, no. 6, pp. 576–578, 1999.

[33] S. R. Zatalia and H. Sanusi, "The role of antioxidants in the pathophysiology, complications, and management of diabetes mellitus," *Acta Medica Indonesiana*, vol. 45, no. 2, pp. 141–147, 2013.

[34] S. Taş, E. Sarandöl, and M. Dirican, "Vitamin B6 supplementation improves oxidative stress and enhances serum paraoxonase/arylesterase activities in streptozotocin-induced diabetic rats," *The Scientific World Journal*, vol. 2014, Article ID 351598, 7 pages, 2014.

[35] M. A. Nauck, M. M. Heimesaat, C. Orskov, J. J. Holst, R. Ebert, and W. Creutzfeldt, "Preserved incretin activity of glucagon-like peptide 1 [7-36 amide] but not of synthetic human gastric inhibitory polypeptide in patients with type-2 diabetes mellitus," *The Journal of Clinical Investigation*, vol. 91, no. 1, pp. 301–307, 1993.

[36] Y. Nogi, M. Nagashima, M. Terasaki, K. Nohtomi, T. Watanabe, and T. Hirano, "Glucose-dependent insulinotropic polypeptide prevents the progression of macrophage-driven atherosclerosis in diabetic apolipoprotein E-null mice," *PLoS One*, vol. 7, no. 4, article e35683, 2012.

[37] E. Distel, T. J. Barrett, K. Chung et al., "miR33 inhibition overcomes deleterious effects of diabetes mellitus on atherosclerosis plaque regression in mice," *Circulation Research*, vol. 115, no. 9, pp. 759–769, 2014.

[38] L. M. Villeneuve, M. Kato, M. A. Reddy, M. Wang, L. Lanting, and R. Natarajan, "Enhanced levels of microRNA-125b in vascular smooth muscle cells of diabetic db/db mice lead to increased inflammatory gene expression by targeting the histone methyltransferase Suv39h1," *Diabetes*, vol. 59, no. 11, pp. 2904–2915, 2010.

[39] M. A. Reddy, W. Jin, L. Villeneuve et al., "Pro-inflammatory role of microrna-200 in vascular smooth muscle cells from diabetic mice," *Arteriosclerosis, Thrombosis, and Vascular Biology*, vol. 32, no. 3, pp. 721–729, 2012.

[40] M. A. Reddy, S. Das, C. Zhuo et al., "Regulation of vascular smooth muscle cell dysfunction under diabetic conditions by miR-504," *Arteriosclerosis, Thrombosis, and Vascular Biology*, vol. 36, no. 5, pp. 864–873, 2016.

[41] J. Xu, L. Li, H. F. Yun, and Y. S. Han, "MiR-138 promotes smooth muscle cells proliferation and migration in db/db mice through down-regulation of SIRT1," *Biochemical and Biophysical Research Communications*, vol. 463, no. 4, pp. 1159–1164, 2015.

[42] H. Oberkofler, A. Pfeifenberger, S. Soyal et al., "Aberrant hepatic TRIB3 gene expression in insulin-resistant obese humans," *Diabetologia*, vol. 53, no. 9, pp. 1971–1975, 2010.

[43] N. Ohoka, S. Yoshii, T. Hattori, K. Onozaki, and H. Hayashi, "TRB3, a novel ER stress-inducible gene, is induced via ATF4-CHOP pathway and is involved in cell death," *The EMBO Journal*, vol. 24, no. 6, pp. 1243–1255, 2005.

[44] J. Liu, X. Wu, J. L. Franklin et al., "Mammalian Tribbles homolog 3 impairs insulin action in skeletal muscle: role in glucose-induced insulin resistance," *American Journal of Physiology. Endocrinology and Metabolism*, vol. 298, no. 3, pp. E565–E576, 2010.

[45] K. Du, S. Herzig, R. N. Kulkarni, and M. Montminy, "TRB3: a tribbles homolog that inhibits Akt/PKB activation by insulin in liver," *Science*, vol. 300, no. 5625, pp. 1574–1577, 2003.

[46] J. R. Sowers, "Role of TRIB3 in diabetic and overnutrition-induced atherosclerosis," *Diabetes*, vol. 61, no. 2, pp. 265-266, 2012.

[47] A. Whaley-Connell and J. R. Sowers, "Indices of obesity and cardiometabolic risk," *Hypertension*, vol. 58, no. 6, pp. 991–993, 2011.

[48] L. Qi, J. E. Heredia, J. Y. Altarejos et al., "TRB3 links the E3 ubiquitin ligase COP1 to lipid metabolism," *Science*, vol. 312, no. 5781, pp. 1763–1766, 2006.

[49] Z. H. Wang, Y. Y. Shang, S. Zhang et al., "Silence of TRIB3 suppresses atherosclerosis and stabilizes plaques in diabetic ApoE$^{-/-}$/LDL receptor$^{-/-}$ mice," *Diabetes*, vol. 61, no. 2, pp. 463–473, 2012.

[50] G. Miklossy, T. S. Hilliard, and J. Turkson, "Therapeutic modulators of STAT signalling for human diseases," *Nature Reviews. Drug Discovery*, vol. 12, no. 8, pp. 611–629, 2013.

[51] M. B. Marrero, "Introduction to JAK/STAT signaling and the vasculature," *Vascular Pharmacology*, vol. 43, no. 5, pp. 307–309, 2005.

[52] T. Tamiya, I. Kashiwagi, R. Takahashi, H. Yasukawa, and A. Yoshimura, "Suppressors of cytokine signaling (SOCS) proteins and JAK/STAT pathways: regulation of T-cell inflammation by SOCS1 and SOCS3," *Arteriosclerosis, Thrombosis, and Vascular Biology*, vol. 31, no. 5, pp. 980–985, 2011.

[53] S. Agrawal, M. Febbraio, E. Podrez, M. K. Cathcart, G. R. Stark, and G. M. Chisolm, "Signal transducer and activator of transcription 1 is required for optimal foam cell formation and atherosclerotic lesion development," *Circulation*, vol. 115, no. 23, pp. 2939–2947, 2007.

[54] N. M. Gharavi, J. A. Alva, K. P. Mouillesseaux et al., "Role of the Jak/STAT pathway in the regulation of interleukin-8 transcription by oxidized phospholipids in vitro and in atherosclerosis in vivo," *The Journal of Biological Chemistry*, vol. 282, no. 43, pp. 31460–31468, 2007.

[55] W. S. Lim, J. M. Timmins, T. A. Seimon et al., "Signal transducer and activator of transcription-1 is critical for apoptosis in macrophages subjected to endoplasmic reticulum stress in vitro and in advanced atherosclerotic lesions in vivo," *Circulation*, vol. 117, no. 7, pp. 940–951, 2008.

[56] D. Torella, A. Curcio, C. Gasparri et al., "Fludarabine prevents smooth muscle proliferation in vitro and neointimal hyperplasia in vivo through specific inhibition of STAT-1 activation," *American Journal of Physiology. Heart and Circulatory Physiology*, vol. 292, no. 6, pp. H2935–H2943, 2007.

[57] J. M. Daniel, J. Dutzmann, W. Bielenberg et al., "Inhibition of STAT3 signaling prevents vascular smooth muscle cell proliferation and neointima formation," *Basic Research in Cardiology*, vol. 107, no. 3, p. 261, 2012.

[58] M. B. Marrero, A. K. Banes-Berceli, D. M. Stern, and D. C. Eaton, "Role of the JAK/STAT signaling pathway in diabetic nephropathy," *American Journal of Physiology. Renal Physiology*, vol. 290, no. 4, pp. F762–F768, 2006.

[59] J. Hu, X. Fan, X. Meng, Y. Wang, Q. Liang, and G. Luo, "Evidence for the involvement of JAK/STAT/SOCS pathway in the mechanism of Tangshen formula-treated diabetic nephropathy," *Planta Medica*, vol. 80, no. 8-9, pp. 614–621, 2014.

[60] D. Suchy, K. Łabuzek, G. Machnik, M. Kozłowski, and B. Okopień, "SOCS and diabetes—ups and downs of a turbulent relationship," *Cell Biochemistry and Function*, vol. 31, no. 3, pp. 181–195, 2013.

[61] Q. Zhao, C. Gao, and Z. Cui, "Ginkgolide A reduces inflammatory response in high-glucose-stimulated human umbilical vein endothelial cells through STAT3-mediated pathway," *International Immunopharmacology*, vol. 25, no. 2, pp. 242–248, 2015.

[62] A. Yoshimura, T. Naka, and M. Kubo, "SOCS proteins, cytokine signalling and immune regulation," *Nature Reviews. Immunology*, vol. 7, no. 6, pp. 454–465, 2007.

[63] H. Kiu and S. E. Nicholson, "Biology and significance of the JAK/STAT signalling pathways," *Growth Factors*, vol. 30, no. 2, pp. 88–106, 2012.

[64] C. Recio, A. Oguiza, I. Lazaro, B. Mallavia, J. Egido, and C. Gomez-Guerrero, "Suppressor of cytokine signaling 1-derived peptide inhibits Janus kinase/signal transducers and activators of transcription pathway and improves inflammation and atherosclerosis in diabetic mice," *Arteriosclerosis, Thrombosis, and Vascular Biology*, vol. 34, no. 9, pp. 1953–1960, 2014.

[65] H. B. Peng, P. Libby, and J. K. Liao, "Induction and stabilization of I kappa B alpha by nitric oxide mediates inhibition of NF-kappa B," *The Journal of Biological Chemistry*, vol. 270, no. 23, pp. 14214–14219, 1995.

[66] G. P. Fadini, M. Miorin, M. Facco et al., "Circulating endothelial progenitor cells are reduced in peripheral vascular complications of type 2 diabetes mellitus," *Journal of the American College of Cardiology*, vol. 45, no. 9, pp. 1449–1457, 2005.

[67] Y. H. Chen, S. J. Lin, F. Y. Lin et al., "High glucose impairs early and late endothelial progenitor cells by modifying nitric oxide-related but not oxidative stress-mediated mechanisms," *Diabetes*, vol. 56, no. 6, pp. 1559–1568, 2007.

[68] N. Sun, H. Wang, and L. Wang, "Vaspin alleviates dysfunction of endothelial progenitor cells induced by high glucose via PI3K/Akt/eNOS pathway," *International Journal of Clinical and Experimental Pathology*, vol. 8, no. 1, pp. 482–489, 2015.

[69] N. Ouchi, H. Kobayashi, S. Kihara et al., "Adiponectin stimulates angiogenesis by promoting cross-talk between AMP-activated protein kinase and Akt signaling in endothelial cells," *The Journal of Biological Chemistry*, vol. 279, no. 2, pp. 1304–1309, 2004.

[70] J. Yang, N. Wang, Y. Zhu, and P. Feng, "Roles of SIRT1 in high glucose-induced endothelial impairment: association with diabetic atherosclerosis," *Archives of Medical Research*, vol. 42, no. 5, pp. 354–360, 2011.

[71] N. L. Price, A. P. Gomes, A. J. Ling et al., "SIRT1 is required for AMPK activation and the beneficial effects of resveratrol on mitochondrial function," *Cell Metabolism*, vol. 15, no. 5, pp. 675–690, 2012.

[72] J. Chen, M. Dai, and Y. Wang, "Paeonol inhibits proliferation of vascular smooth muscle cells stimulated by high glucose via Ras-Raf-ERK1/2 signaling pathway in coculture model," *Evidence-Based Complementary and Alternative Medicine*, vol. 2014, Article ID 484269, 9 pages, 2014.

[73] Y. Mebratu and Y. Tesfaigzi, "How ERK1/2 activation controls cell proliferation and cell death: is subcellular localization the answer?" *Cell Cycle*, vol. 8, no. 8, pp. 1168–1175, 2009.

[74] Y. Zhao, J. Liu, L. Li, L. Liu, and L. Wu, "Role of Ras/PKCzeta/MEK/ERK1/2 signaling pathway in angiotensin II-induced vascular smooth muscle cell proliferation," *Regulatory Peptides*, vol. 128, no. 1, pp. 43–50, 2005.

[75] D. Popov, M. Nemecz, M. Dumitrescu, A. Georgescu, and F. D. Böhmer, "Long-term high glucose concentration influences Akt, ERK1/2, and PTP1B protein expression in human aortic smooth muscle cells," *Biochemical and Biophysical Research Communications*, vol. 388, no. 1, pp. 51–55, 2009.

[76] S. Kuki, T. Imanishi, K. Kobayashi, Y. Matsuo, M. Obana, and T. Akasaka, "Hyperglycemia accelerated endothelial progenitor cell senescence via the activation of p38 mitogen-activated protein kinase," *Circulation Journal*, vol. 70, no. 8, pp. 1076–1081, 2006.

[77] F. Jansen, X. Yang, B. S. Franklin et al., "High glucose condition increases NADPH oxidase activity in endothelial microparticles that promote vascular inflammation," *Cardiovascular Research*, vol. 98, no. 1, pp. 94–106, 2013.

[78] M. C. Durpès, C. Morin, J. Paquin-Veillet et al., "PKC-beta activation inhibits IL-18-binding protein causing endothelial dysfunction and diabetic atherosclerosis," *Cardiovascular Research*, vol. 106, no. 2, pp. 303–313, 2015.

[79] P. Geraldes and G. L. King, "Activation of protein kinase C isoforms and its impact on diabetic complications," *Circulation Research*, vol. 106, no. 8, pp. 1319–1331, 2010.

[80] G. Ceolotto, A. Gallo, I. Papparella et al., "Rosiglitazone reduces glucose-induced oxidative stress mediated by NAD (P) H oxidase via AMPK-dependent mechanism," *Arteriosclerosis, Thrombosis, and Vascular Biology*, vol. 27, no. 12, pp. 2627–2633, 2007.

[81] L. Kong, X. Shen, L. Lin et al., "PKCbeta promotes vascular inflammation and acceleration of atherosclerosis in diabetic ApoE null mice," *Arteriosclerosis, Thrombosis, and Vascular Biology*, vol. 33, no. 8, pp. 1779–1787, 2013.

[82] Z. Levi, A. Shaish, N. Yacov et al., "Rosiglitazone (PPAR-gamma-agonist) attenuates atherogenesis with no effect on hyperglycaemia in a combined diabetes-atherosclerosis mouse model," *Diabetes, Obesity & Metabolism*, vol. 5, no. 1, pp. 45–50, 2003.

[83] Z. Bagi, A. Koller, and G. Kaley, "PPARgamma activation, by reducing oxidative stress, increases NO bioavailability in coronary arterioles of mice with type 2 diabetes," *American Journal of Physiology. Heart and Circulatory Physiology*, vol. 286, no. 2, pp. H742–H748, 2004.

[84] B. B. Di, H. W. Li, W. P. Li, X. H. Shen, Z. J. Sun, and X. Wu, "Pioglitazone inhibits high glucose-induced expression of receptor for advanced glycation end products in coronary artery smooth muscle cells," *Molecular Medicine Reports*, vol. 11, no. 4, pp. 2601–2607, 2015.

[85] I. Osman and L. Segar, "Pioglitazone, a PPARgamma agonist, attenuates PDGF-induced vascular smooth muscle cell proliferation through AMPK-dependent and AMPK-independent inhibition of mTOR/p70S6K and ERK signaling," *Biochemical Pharmacology*, vol. 101, pp. 54–70, 2016.

[86] G. Chinetti, S. Lestavel, V. Bocher et al., "PPAR-alpha and PPAR-gamma activators induce cholesterol removal from human macrophage foam cells through stimulation of the ABCA1 pathway," *Nature Medicine*, vol. 7, no. 1, pp. 53–58, 2001.

[87] K. J. Moore, E. D. Rosen, M. L. Fitzgerald et al., "The role of PPAR-gamma in macrophage differentiation and cholesterol uptake," *Nature Medicine*, vol. 7, no. 1, pp. 41–47, 2001.

[88] G. C. Amberg, C. F. Rossow, M. F. Navedo, and L. F. Santana, "NFATc3 regulates Kv2.1 expression in arterial smooth muscle," *The Journal of Biological Chemistry*, vol. 279, no. 45, pp. 47326–47334, 2004.

[89] J. Nilsson, L. M. Nilsson, Y. W. Chen, J. D. Molkentin, D. Erlinge, and M. F. Gomez, "High glucose activates nuclear factor of activated T cells in native vascular smooth muscle," *Arteriosclerosis, Thrombosis, and Vascular Biology*, vol. 26, no. 4, pp. 794–800, 2006.

[90] L. M. Nilsson-Berglund, A. V. Zetterqvist, J. Nilsson-Ohman et al., "Nuclear factor of activated T cells regulates osteopontin expression in arterial smooth muscle in response to diabetes-induced hyperglycemia," *Arteriosclerosis, Thrombosis, and Vascular Biology*, vol. 30, no. 2, pp. 218–224, 2010.

[91] A. V. Zetterqvist, L. M. Berglund, F. Blanco et al., "Inhibition of nuclear factor of activated T-cells (NFAT) suppresses accelerated atherosclerosis in diabetic mice," *PLoS One*, vol. 8, no. 6, article e65020, 2014.

[92] Z. Ungvari, L. Bailey-Downs, T. Gautam et al., "Adaptive induction of NF-E2-related factor-2-driven antioxidant genes in endothelial cells in response to hyperglycemia," *American Journal of Physiology. Heart and Circulatory Physiology*, vol. 300, no. 4, pp. H1133–H1140, 2011.

[93] S. M. Tan and J. B. Haande, "Combating oxidative stress in diabetic complications with Nrf2 activators: how much is too much?" *Redox Report*, vol. 19, no. 3, pp. 107–117, 2014.

[94] D. Cheng, B. Liang, and Y. Li, "Antihyperglycemic effect of *Ginkgo biloba* extract in streptozotocin-induced diabetes in rats," *BioMed Research International*, vol. 2013, Article ID 162724, 7 pages, 2013.

[95] G. Liu, M. Grifman, J. Macdonald, P. Moller, F. Wong-Staal, and Q. X. Li, "Isoginkgetin enhances adiponectin secretion from differentiated adiposarcoma cells via a novel pathway involving AMP-activated protein kinase," *The Journal of Endocrinology*, vol. 194, no. 3, pp. 569–578, 2007.

[96] L. Zhou, Q. Meng, T. Qian, and Z. Yang, "*Ginkgo biloba* extract enhances glucose tolerance in hyperinsulinism-induced hepatic cells," *Journal of Natural Medicines*, vol. 65, no. 1, pp. 50–56, 2011.

[97] X. Li, Y. Hu, Y. Fu, Y. Ying, and G. Chen, "Effect of Ginkgo biloba extract on glucose uptake of diaphragm in diabetic rats," *Zhongguo Zhong Yao Za Zhi*, vol. 35, no. 3, pp. 356–359, 2010, [Article in Chinese].

[98] S. Lim, J. W. Yoon, S. M. Kang et al., "EGb761, a Ginkgo biloba extract, is effective against atherosclerosis in vitro, and in a rat model of type 2 diabetes," *PLoS One*, vol. 6, no. 6, article e20301, 2011.

[99] M. Zhao, X. X. Wang, and W. H. Wan, "Effects of the ginkgo biloba extract on the superoxide dismutase activity and apoptosis of endothelial progenitor cells from diabetic peripheral blood," *Genetics and Molecular Research*, vol. 13, no. 1, pp. 220–227, 2014.

[100] H. Y. Tsai, P. H. Huang, F. Y. Lin, J. S. Chen, S. J. Lin, and J. W. Chen, "*Ginkgo biloba* extract reduces high-glucose-induced endothelial reactive oxygen species generation and cell adhesion molecule expression by enhancing HO-1 expression via Akt/eNOS and p38 MAP kinase pathways," *European Journal of Pharmaceutical Sciences*, vol. 48, no. 4-5, pp. 803–811, 2013.

[101] W. Wang, Q. H. Wu, Y. Sui, Y. Wang, and X. Qiu, "Rutin protects endothelial dysfunction by disturbing Nox4 and ROS-sensitive NLRP3 inflammasome," *Biomedicine & Pharmacotherapy*, vol. 86, pp. 32–40, 2016.

[102] L. Lv, S. S. Jiang, J. Xu, J. B. Gong, and Y. Cheng, "Protective effect of ligustrazine against myocardial ischaemia reperfusion in rats: the role of endothelial nitric oxide synthase," *Clinical and Experimental Pharmacology & Physiology*, vol. 39, no. 1, pp. 20–27, 2012.

[103] Q. Xu, B. Zhang, X. M. Li, and X. Gao, "Traditional Chinese medicine formula Qing Huo Yi Hao as superoxide anion scavenger in high glucose-treated endothelial cells," *Acta Pharmacologica Sinica*, vol. 33, no. 4, pp. 496–502, 2012.

[104] Y. Kang, M. Hu, Y. Zhu, X. Gao, and M. W. Wang, "Antioxidative effect of the herbal remedy Qin Huo Yi Hao and its active component tetramethylpyrazine on high glucose-treated endothelial cells," *Life Sciences*, vol. 84, no. 13-14, pp. 428–436, 2009.

[105] Q. Xu, P. Xia, X. Li, W. Wang, Z. Liu, and X. Gao, "Tetramethylpyrazine ameliorates high glucose-induced endothelial dysfunction by increasing mitochondrial biogenesis," *PLoS One*, vol. 9, no. 2, article e88243, 2014.

[106] S. Li, J. H. Wang, and S. L. Chen, "Inhibitory effect of ligustrazine on proliferation of rabbit vascular smooth muscle cells after arterial injury," *Zhongguo Yao Li Xue Bao*, vol. 20, no. 10, pp. 917–922, 1999.

[107] L. Yu, X. Huang, K. Huang, C. Gui, Q. Huang, and B. Wei, "Ligustrazine attenuates the platelet-derived growth factor-BB-induced proliferation and migration of vascular smooth muscle cells by interrupting extracellular signal-regulated kinase and P38 mitogen-activated protein kinase pathways," *Molecular Medicine Reports*, vol. 12, no. 1, pp. 705–711, 2015.

[108] X. Y. Li, J. L. He, H. T. Liu, W. M. Li, and C. Yu, "Tetramethylpyrazine suppresses interleukin-8 expression in LPS-stimulated human umbilical vein endothelial cell by blocking ERK, p38 and nuclear factor-kappaB signaling pathways," *Journal of Ethnopharmacology*, vol. 125, no. 1, pp. 83–89, 2009.

[109] M. H. Gao, L. Zhang, B. Li, S. R. Ren, and B. Zhang, "Effect of tetramethylpyrazine on JAK-STAT signal transduction in cardiomyocyte hypertrophy," *Xi Bao Yu Fen Zi Mian Yi Xue Za Zhi*, vol. 27, no. 5, pp. 519–521, 524, 2011, [Article in Chinese].

[110] L. M. Lee, C. F. Liu, and P. P. Yang, "Effect of tetramethylpyrazine on lipid peroxidation in streptozotocin-induced diabetic mice," *The American Journal of Chinese Medicine*, vol. 30, no. 4, pp. 601–608, 2002.

[111] H. Zhang, S. Chen, X. Deng, X. Yang, and X. Huang, "Danggui-Buxue-Tang decoction has an anti-inflammatory

effect in diabetic atherosclerosis rat model," *Diabetes Research and Clinical Practice*, vol. 74, no. 2, pp. 194–196, 2006.

[112] H. Zhang, S. Chen, X. Deng, X. Yang, and X. Huang, "The effects of Danggui-Buxue-Tang on blood lipid and expression of genes related to foam cell formation in the early stage of atherosclerosis in diabetic GK rats," *Diabetes Research and Clinical Practice*, vol. 77, no. 3, pp. 479–481, 2007.

[113] S. M. Lee, Y. J. Lee, J. H. Choi et al., "Gal-geun-dang-gwi-tang improves diabetic vascular complication in apolipoprotein E KO mice fed a western diet," *BMC Complementary and Alternative Medicine*, vol. 14, p. 453, 2014.

[114] Y. Joe, M. Zheng, H. J. Kim et al., "Salvianolic acid B exerts vasoprotective effects through the modulation of heme oxygenase-1 and arginase activities," *The Journal of Pharmacology and Experimental Therapeutics*, vol. 341, no. 3, pp. 850–858, 2012.

[115] J. H. Ho and C. Y. Hong, "Salvianolic acids: small compounds with multiple mechanisms for cardiovascular protection," *Journal of Biomedical Science*, vol. 18, p. 30, 2011.

[116] S. E. Lee, S. I. Jeong, H. Yang et al., "Extract of Salvia miltiorrhiza (Danshen) induces Nrf2-mediated heme oxygenase-1 expression as a cytoprotective action in RAW 264.7 macrophages," *Journal of Ethnopharmacology*, vol. 139, no. 2, pp. 541–548, 2012.

[117] H. J. Lee, M. Seo, and E. J. Lee, "Salvianolic acid B inhibits atherogenesis of vascular cells through induction of Nrf2-dependent heme oxygenase-1," *Current Medicinal Chemistry*, vol. 21, no. 26, pp. 3095–3106, 2014.

[118] S. Raoufi, T. Baluchnejadmojarad, M. Roghani, T. Ghazanfari, F. Khojasteh, and M. Mansouri, "Antidiabetic potential of salvianolic acid B in multiple low-dose streptozotocin-induced diabetes," *Pharmaceutical Biology*, vol. 53, no. 12, pp. 1803–1809, 2015.

[119] S. Qian, D. Huo, S. Wang, and Q. Qian, "Inhibition of glucose-induced vascular endothelial growth factor expression by Salvia miltiorrhiza hydrophilic extract in human microvascular endothelial cells: evidence for mitochondrial oxidative stress," *Journal of Ethnopharmacology*, vol. 137, no. 2, pp. 985–991, 2011.

[120] Y. Ren, S. Tao, S. Zheng et al., "Salvianolic acid B improves vascular endothelial function in diabetic rats with blood glucose fluctuations via suppression of endothelial cell apoptosis," *European Journal of Pharmacology*, vol. 791, pp. 308–315, 2016.

[121] J. P. Shieh, K. C. Cheng, H. H. Chung, Y. F. Kerh, C. H. Yeh, and J. T. Cheng, "Plasma glucose lowering mechanisms of catalpol, an active principle from roots of Rehmannia glutinosa, in streptozotocin-induced diabetic rats," *Journal of Agricultural and Food Chemistry*, vol. 59, no. 8, pp. 3747–3753, 2011.

[122] J. Y. Liu and D. J. Zhang, "Amelioration by catalpol of atherosclerotic lesions in hypercholesterolemic rabbits," *Planta Medica*, vol. 81, no. 3, pp. 175–184, 2015.

[123] J. Y. Liu, C. Z. Zheng, X. P. Hao, D. J. Zhang, A. W. Mao, and P. Yuan, "Catalpol ameliorates diabetic atherosclerosis in diabetic rabbits," *American Journal of Translational Research*, vol. 8, no. 10, pp. 4278–4288, 2016.

[124] B. N. Zordoky, I. M. Robertson, and J. R. Dyck, "Preclinical and clinical evidence for the role of resveratrol in the treatment of cardiovascular diseases," *Biochimica et Biophysica Acta (BBA) - Molecular Basis of Disease*, vol. 1852, no. 6, pp. 1155–1177, 2015.

[125] J. Yang, N. Wang, J. Li, J. Zhang, and P. Feng, "Effects of resveratrol on NO secretion stimulated by insulin and its dependence on SIRT1 in high glucose cultured endothelial cells," *Endocrine*, vol. 37, no. 2, pp. 365–372, 2010.

[126] Y. Zhang, Z. Luo, L. Ma, Q. Xu, Q. Yang, and L. Si, "Resveratrol prevents the impairment of advanced glycosylation end products (AGE) on macrophage lipid homeostasis by suppressing the receptor for AGE via peroxisome proliferator-activated receptor gamma activation," *International Journal of Molecular Medicine*, vol. 25, no. 5, pp. 729–734, 2010.

[127] X. Hou, S. Xu, K. A. Maitland-Toolan et al., "SIRT1 regulates hepatocyte lipid metabolism through activating AMP-activated protein kinase," *The Journal of Biological Chemistry*, vol. 283, no. 29, pp. 20015–20026, 2008.

[128] M. Zang, S. Xu, K. A. Maitland-Toolan et al., "Polyphenols stimulate AMP-activated protein kinase, lower lipids, and inhibit accelerated atherosclerosis in diabetic LDL receptor-deficient mice," *Diabetes*, vol. 55, no. 8, pp. 2180–2191, 2006.

[129] A. Ramirez Boscá, A. Soler, M. A. Carrión-Gutiérrez et al., "An hydroalcoholic extract of Curcuma longa lowers the abnormally high values of human-plasma fibrinogen," *Mechanisms of Ageing and Development*, vol. 114, no. 3, pp. 207–210, 2000.

[130] P. Usharani, A. A. Mateen, M. U. Naidu, Y. S. Raju, and N. Chandra, "Effect of NCB-02, atorvastatin and placebo on endothelial function, oxidative stress and inflammatory markers in patients with type 2 diabetes mellitus: a randomized, parallel-group, placebo-controlled, 8-week study," *Drugs in R & D*, vol. 9, no. 4, pp. 243–250, 2008.

[131] J. M. Zingg, S. T. Hasan, and M. Meydani, "Molecular mechanisms of hypolipidemic effects of curcumin," *BioFactors*, vol. 39, no. 1, pp. 101–121, 2013.

[132] B. Zheng, L. Yang, C. Wen et al., "Curcumin analog L3 alleviates diabetic atherosclerosis by multiple effects," *European Journal of Pharmacology*, vol. 775, pp. 22–34, 2016.

[133] M. Ouimet, "Autophagy in obesity and atherosclerosis: interrelationships between cholesterol homeostasis, lipoprotein metabolism and autophagy in macrophages and other systems," *Biochimica et Biophysica Acta (BBA) - Molecular and Cell Biology of Lipids*, vol. 1831, no. 6, pp. 1124–1133, 2013.

[134] F. Tian, B. L. Yu, and J. R. Hu, "mTOR mediates the crosstalk of macrophage polarization and autophagy in atherosclerosis," *International Journal of Cardiology*, vol. 177, no. 1, pp. 144-145, 2014.